The University of Nottingham
School of Physics & Astronomy

Electrical and Optical Studies of Dilute Nitride and Bismide Compound Semiconductors

GEORGE GREEN LIBRARY OF
SCIENCE AND ENGINEERING

by

MUHAMMAD SHAFI
M. Phil (Physics)

Thesis submitted to the University of Nottingham
for the degree of Doctor of Philosophy

November 2010

BEST COPY

AVAILABLE

Variable print quality

ABSTRACT

A few percent of nitrogen (N) or bimuth (Bi) incorporation in GaAs compound semiconductors have proved to lower significantly its bandgap. This unusual bandgap reduction is of interest for numerous applications such as long wave-length lasers, solar cells etc. However, the addition of these impurity atoms also introduces defect levels in the bandgap of the host materials. These can have severe implications on the material's quality, for example they can decrease the lifetime of the charge carriers and degrade the optical efficiency.

In this work, deep levels traps were investigated in silicon-doped GaAsN epitaxial layers containing N concentrations from 0.2% to 1.2% grown by molecular beam epitaxy (MBE) on n+ GaAs substrates using DLTS and high resolution Laplace DLTS techniques. In addition, a further investigation was carried out to study the effect of annealing and hydrogenation treatments on the defects present in the as-grown layers.

Several deep levels were detected in the as-grown GaAsN samples. These were identified with previously reported (Si_{Ga}-N_{As}), EL6 (Ga vacancies-related complex), $(N\text{-}As)_{As}$, EL3 (off-centre substitutional oxygen in As sites) and EL2-like (antisite As_{Ga}) defect levels.

It was found that, depending upon the N concentration, heat treatment has a different effect on the traps. For samples with N = 0.2 - 0.4 %, some defects were annihilated and no generation of new defects was observed. In the case of samples with N = 0.8 -

1.2 % the annealing results in both generation of new traps and elimination of some existing traps.

In general, it was found that hydrogenation of the as-grown GaAsN epilayers passivates most of the deep levels. However, for the samples with N = 0.8%, although hydrogen passivates some of the defects and reduce the concentration of others it also creates new defects which are suspected to be hydrogen-related complexes.

(100) and (311)B GaAsBi layers grown by molecular beam epitaxy under various arsenic overpressures have been investigated using optical and structural techniques. The optimised Bi incorporation was found to occur near stoichiometric conditions. The incorporation of Bi into the GaAsBi alloy, as determined by high resolution X-ray diffraction (HRXRD), is sizably larger in the (311)B epilayers than in (100) epilayers. HRXRD reveals 4% Bi-incorporation in (311)B and 3% in (100) GaAs orientations. The conventional optical transmission results confirmed that the bandgap of the (311)B epilayer is around 90 meV lower than that corresponding to (100) sample. This measurement provide further evidence that Bi incorporates more in (311)B than in (100) surfaces. The low temperature post-growth heat treatment of GaAsBi alloys reveals an improvement in the structural and optical properties of these materials. A substantial increase in photoluminescence signal infers a large reduction of defects.

PUBLICATIONS

1. M. Henini, J. Ibáñez, M. Schmidbauer, **M. Shafi,** S. V. Novikov, L. Turyanska, S. I. Molina, D. L. Sales, M. F. Chisholm, and J. Misiewicz, *'Molecular Beam Epitaxy of GaAsBi on(311)B GaAs Substrates'*, Appl. Phys. Lett., 91, 251909, (2007).

2. R. Kudrawiec, P. Poloczek, J. Misiewicz, **M. Shafi,** J. Ibáñez, R. H. Mari, M. Henini, M. Schmidbauer, S. V. Novikov, L. Turyanska, S. I. Molina, D. L. Sales, and M. F. Chisholm, *'Photomodulated transmittance of GaAsBi layers grown on* (100) *and (311)B GaAs substrates'*, Microelectronics Journal 40, 537, (2009).

3. **M. Shafi**, R.H. Mari, M. Henini, D. Taylor, and M. Hopkinson, *'Electrical Properties of Nitrogen-related Defects in n-type GaAsN Grown by Molecular Beam Epitaxy'*. Phys. Status Solidi C 6, No. 12, 2652 (2009).

4. R. Kudrawiec, M. Syperek, P. Poloczek, J. Misiewicz, R. H. Mari, **M. Shafi**, M. Henini, Y. Gobato, S. V. Novikov, J. Ibanez, M. Schmidbauer and S. I. Molina, *'Carrier Localization in GaAsBi Probed by Photomodulated Transmittance and Photoluminescence*, J. Appl. Phys., 106, 023518, (2009).

5. R. H. Mari, **M. Shafi**, M. Henini and D.Taylor, *'Laplace DLTS of Molecular Beam Epitaxy GaAs Grown on (100) and (211)B Substrates'*, Phys. Status Solidi C 6, No. 12, 2873 (2009).

6. J.F. Rodrigo, D.L. Sales, **M. Shafi**, M. Henini, L. Turyanska, S. Novikov, S.I. Molina, *'Effect of annealing on the structural and optical properties of (311)B GaAsBi layers'*, Applied Surface Science, 256, 5688 (2010).

7. **M. Shafi**, R.H. Mari, A. Khatab, D.Taylor and M. Henini, *'Deep level transient spectroscopy of GaAs/AlGaAs multi-quantum wells grown on (100) and (311)B GaAs substrates'*, Nanoscale Res. Lett., 5, 1948 (2010).

8. J. F. Rodrigo, E. Guerrero, D. L. Sales, A. Yáñez, P. L. Galindo, **M. Shafi**, A. Khatab, M. Henini, M. F. Chisholm, S. I. Molina, and S. V. Novikov, *'Distribution of Bismuth Atoms in GaAsBi Epilayers'*. (**Accepted** to appear in Journal of Nanoscience and Nanotechnology).

9. R.H. Mari, M. **Shafi,** D.Taylor, A. Khatab and M. Henini, *'Electrical characterisation of deep level defects in Be-doped AlGaAs grown on (100) and (311)A GaAs substrates by MBE'* (**submitted** and under review for Nanoscale Research Letters).

10. J. Ibáñez, R. Oliva, M. De la Mare, M. Schmidbauer, S. Hernández and P. Pellegrino, D. J. Scurr, R. Cusco, L. Artus, **M. Shafi,** R. H. Mari, M. Henini, Q. Zhuang, A. Godenir and A. Krier, *'Structural and optical properties of dilute InAsN grown by molecular beam epitaxy'*, J. Appl. Phys., 108, 103504 (2010).

11. **M. Shafi,** R. H. Mari, M. Henini, A. Polimeni and M. Hopkinson, *'Effects of hydrogen irradiation on deep levels in MBE Grown GaAsN'* (**Submitted** in Physica B, 2010).

CONFERENCE PRESENTATIONS

1. Oral presentation in 15th international conference on molecular beam epitaxy (MBE) held at the university of british columbia in vancouver, Canada, August 3-8, (2008), *'Structural and optical studies of GaAsBi layers grown by molecular beam epitaxy on (311)B and* (100) *GaAs substrates'*

2. Oral presentation in Semiconducting and Insulating materials Conference (SIMC –XV), held at the university of vilinius, Lithuania, June 15-19, (2009), *'Nitrogen-related defects in n-type GaAsN grown by molecular-beam epitaxy'*.

3. Poster presented in Essex meeting of COST Action MP0805 on 'Novel Gain Materilas and Devices Based on III-V-N Compounds', 24th May (2009), *'High resolution Laplace DLTS investigation of nitrogen related defects in dilute n-type GaAsN'*.

4. Poster presented in European materials research society (E-MRS 2010) spring meeting held at strasbourg, France, june 7-11 (2010), *'Effect of nitrogen on the EL2-like electron trap in n-type dilute GaAsN grown by molecular beam epitaxy'*.

ACKNOWLEDGEMENTS

First and foremost, I would like to acknowledge and express my deepest gratitude to my supervisor Prof. M. Henini for numerous opportunities he made possible to me during my PhD; from conferences to collaborations. Many thanks for always having faith in my work. I have been a very privileged student.

I would like to thank Late Prof. L. Dobaczewski, Poland for his great support to setup DLTS system, Robert Chettle for electronic support, David Taylor for his help to process Schottky diodes and Peter, who is now retired from machine shop, for his generous help to manufacture several parts for the DLTS and PL setups. I would also like to thank Yara Gobato and Lara Fernandes, Universidade Federal de São Carlos, Brazil, for their immense contributions to build PL system.

I would like to thank all of my collaborators; J. Ibáñez in Institut Jaume Almera, Spain, M. Schmidbauer in Leibniz Institute for Crystal Growth, Berlin, Germany, R. Kudrawiec, Wroclaw University of Technology, Poland, J. F. Rodrigo and D. L. Sales, Universidad de Cádiz, Spain, S. V. Novikov, and L. Turyanska, University of Nottingham, for their contributions in this work.

Many thanks to all of my friends for every thing they did for me.

Most importantly, thanks to my family for their love and support. Finally, I would like to dedicate this work to my Late father.

TABLE OF CONTENTS

CHAPTER 1: INTRODUCTION.....1
1.1 INTRODUCTION.....1
1.2 MOTIVATION.....7
1.3 SCHEME OF THE THESIS.....8
REFERENCES.....10

CHAPTER 2: THEORY AND FUNDAMENTAL CONCEPTS OF SEMICONDUCTORS.....12
2.1 SEMICONDUCTORS.....12
2.1.1 UNDOPED AND DOPED SEMICONDUCTORS.....13
2.2 CRYSTAL STRUCTURE AND PROPERTIES.....14
2.2.1 CRYSTAL STRUCTURE.....14
2.2.2 DENSITY OF STATES.....18
2.2.3 ENERGY BANDGAP.....21
2.2.4 INDIRECT AND DIRECT ENERGY BANDGAP.....21
2.2.5 TEMPERATURE DEPENDENCE OF BANDGAP.....23
2.3 HETEROSTRUCTURES.....23
2.3.1 ATOM SIZE AND ELECTRONEGATIVITY.....24
2.3.2 BAND ALIGNMENT.....24
2.3.3 LATTICE MISMATCH.....26
2.3.4 GRADED GAP SEMICONDUCTOR STRUCTURES.....28
2.3.5 VEGARD'S LAW.....28
2.4 OPTICAL PROPERTIES OF SEMICONDUCTORS.....29
2.4.1 ABSORPTION PROCESSES.....29
2.4.2 EMISSION PROCESSES.....31
2.5 DILUTE NITRIDE MATERIALS.....35
2.5.1 DEVIATION FROM VIRTUAL CRYSTAL APPROXIMATION.....36
2.5.2 THE BAND ANTICROSSING MODEL.....37
2.5.3 SOME IMPORTANT PROPERTIES OF GaAsN.....40
2.6 DILUTE BISMIDE MATERIALS.....41
2.7 BISMUTH INCORPORATION ON HIGH INDEX GaAs PLANES.....42
2.8 CHARACTERISATION METHODS.....43
REFERENCES.....44

CHAPTER 3: DEFECTS IN SEMICONDUCTORS AND THEIR PROPERTIES 47
3.1 CLASSIFICATION OF DEFECTS 47
3.1.1 POINT DEFECTS 48
3.1.1.1 COMPLEXES OF THE POINT DEFECTS 51
3.1.2 LINE DEFECTS 54
3.1.3 PLANAR DEFECTS 55
3.2 ROLE OF IMPURITIES IN SEMICONDUCTORS 56
3.3 DEFECTS AND THEIR CARRIER KINETICS 60
3.3.1 SHALLOW LEVELS: DONORS AND ACCEPTORS 60
3.3.2 DEEP LEVEL KINETICS 62
3.3.2.1 SHOCKLEY-READ-HALL THEORY 63
3.4 DEFECTS IN DILUTE NITRIDE SEMICONDUCTORS 70
3.4.1 EFFECTS OF THERMAL ANNEALING 73
3.4.2 EFFECTS OF HYDROGEN IRRADIATION 74
3.5 DEFECTS IN DILUTE BISMIDE SEMICONDUCTORS 75
3.5.1 EFFECTS OF THERMAL ANNEALING 77
REFERENCES 79

CHAPTER 4: EXPERIMENTAL TECHNIQUES 83
4.1 SCHOTTKY DIODES:
PROPERTIES AND CHARACTERISATION 83
4.1.1 ENERGY BAND DIAGRAM 83
4.1.2 SPACE CHARGE REGION 85
4.1.3 CAPACITANCE ASSOCIATED WITH SPACE CHARGE REGION 87
4.2 DEEP LEVEL TRANSIENT SPECTROSCOPY (DLTS) 88
4.2.1 CAPACITANCE TRANSIENTS 88
4.2.2 CONVENTIONAL DLTS 93
4.2.3 LAPLACE DLTS SPECTROSCOPY 96
4.2.4 DLTS APPLICATIONS 97
4.2.4.1 EMISSION RATE SIGNATURE 100
4.2.4.2 CAPTURE CROSS-SECTION MEASUREMENTS 100
4.2.4.3 TRAP CONCENTRATION 102
4.3 SYSTEM HARDWARE IMPLEMENTATION 102
4.3.1 DESCRIPTION OF SYSTEM HARDWARE 104
4.3.1.1 SIGNAL SOURCE 104
4.3.1.2 CURRENT-VOLTAGE SOURCE-METER 105
4.3.1.3 PULSE GENERATOR 105
4.3.1.4 CRYOSTAT AND TEMPERATURE CONTROLLER 106

4.3.1.5 DATA ACQUISITION BLOCK 107
4.3.1.5 COMPUTER INTERFACE 107
4.4 SYSTEM SOFTWARE 107
4.4.1 CONVENTIONAL DLTS MEASUREMENT MODE 108
4.4.1.1 TRAPVIEW VERSION 4.0 108
4.4.1.2 MULTIPLE RATE WINDOWS 109
4.4.1.3 EXPONENTIAL FITTINGH 109
4.4.2 LAPLACE TRANSIENT PROCESSING MODE 109
4.4.3 EXPERIMENTAL DATA BASE 110
4.5 PHOTOLUMINESCENCE 110
4.6 SYSTEM HARDWARE IMPLEMENTATION 113
4.6.1 DESCRIPTION OF SYSTEM HARDWARE 113
4.6.1.1 SPECTROMETER 113
4.6.1.2 LASER, LIGHT CHOPPER AND OPTICS 113
4.6.1.3 DETECTORS 115
4.6.1.4 SpectrAcq2 116
4.6.1.5 LOCK-IN AMPLIFIER 116
4.6.1.6 CRYOSTAT AND TEMPERATURE CONTROLLER 116
4.6.1.7 COMPUTER INTERFACE 117
4.6.2 SYSTEM CONTOLLING SOFTWARE 117
REFERENCES 118

CHAPTER 5: EXPERIMENTAL DETAILS 119
5.1 SAMPLES 119
5.1.1 DILUTE NITRIDE SAMPLES 119
5.1.2 DILUTE BISMIDE SAMPLES 122
5.2 MEASUREMENT DETAILS 125
5.2.1 CURRENT-VOLTAGE MEASUREMENTS 125
5.2.2 CAPACITANCE-VOLTAGE MEASUREMENTS 125
5.2.3 DLTS MEASUREMENTS 126
5.2.4 OPTICAL ABSORPTION MEASUREMENTS 126
5.2.5 PHOTOLUMINESCENCE MEASUREMENTS 127
5.2.6 HIGH RESOLUTION X-RAY DIFFRACTION MEASUREMENTS 128

CHAPTER 6: DEEP LEVELS IN GaAsN GROWN BY MOLECULAR BEAM EPITAXY 129
6.1 INTRODUCTION 129
6.2 RESULTS 130

6.2.1 CURRENT-VOLTAGE (I-V) AND CAPACITANCE-VOLTAGE (C-V) CHARACTERISTICS 130
6.2.2 DLTS MEASUREMENTS 134
6.2.3 THERMAL EMISSION RATES 137
6.2.4 CAPTURE CROSS-SECTION MEASUREMENTS 137
6.2.5 TRAP CONCENTRATION 137
6.2.6 CURRENT-VOLTAGE-TEMPERATURE (I-V-T) CHARACTERISTICS 141
6.3 DISSCUSSION 143
6.3.1 DLTS AND LDLTS ANALYSIS 143
6.3.2 CURRENT-VOLTAGE-TEMPERATURE ANALYSIS 149
6.4 CONCLUSIONS 151
REFERENCES 152

CHAPTER 7: EFFECTS OF THERMAL ANNEALING ON THE DEEP LEVELS IN GaAsN 154
7.1 INTRODUCTION 154
7.2 RESULTS 159
7.2.1 CURRENT-VOLTAGE (I-V) AND CAPACITANCE-VOLTAGE (C-V) CHARACTERISTICS 159
7.2.2 DLTS MEASUREMENTS 160
7.3 DISCUSSION 176
7.3.1 GaAsN WITH N = 0.2% 176
7.3.2 GaAsN WITH N = 0.4% 180
7.3.3 GaAsN WITH N = 0.8% 181
7.3.4 GaAsN WITH N = 1.2% 183
7.4 CONCLUSIONS 185
REFERENCES 187

CHAPTER 8: EFFECTS OF HYDROGEN IRRADIATION ON THE DEEP LEVELS IN GaAsN 190
8.1 INTRODUCTION 190
8.2 RESULTS 194
8.2.1 CURRENT-VOLTAGE (I-V) AND CAPACITANCE-VOLTAGE (C-V) CHARACTERISTICS 194
8.2.2 DLTS MEASUREMENTS 194
8.3 DISCUSSION 205
8.4 CONCLUSIONS 209
REFERENCES 210

CHAPTER 9: CHARACTERISATION OF GaAsBi EPILAYERS GROWN BY MBE ON (100) AND (311)B GaAs SUBSTRATES 212
9.1 INTRODUCTION 212
9.2 RESULTS 214
9.2.1 X-RAY DIFFRACTION MEASUREMENTS 214
9.2.2 OPTICAL TRANSMISSION MEASUREMENTS 218
9.2.3 PL SPECTRA OF AS-GROWN AND ANNEALED GaAsBi LAYERS 223
9.3 DISCUSSION 229
9.3.1 HRXRD ANALYSIS 229
9.3.2 ABSORPTION ANALYSIS 233
9.3.3 PL ANALYSIS OF AS-GROWN AND ANNEALED GaAsBi ALLOYS 234
9.4 CONCLUSIONS 237
REFERENCES 238

CHAPTER 10: SUMMARY AND CONCLUSIONS 240
10.1 DLTS AND PL TECHNIQUES 240
10.2 DEEP LEVELS IN GaAsN (N = 0 % to 1.2%) 242
10.3 ANNEALING EFFECTS ON THE DEEP LEVELS IN GaAsN 243
10.4 HYDROGENATION of GaAsN 244
10.5 OPTICAL AND STRUCTURAL CHARACTERISATION OF GaAsBi ALLOYS 245
10.6 FUTURE WORK 246

CHAPTER 1

INTRODUCTION

1.1 INTRODUCTION

The modern semiconductor materials have revolutionised the electronics industry due to their fascinating technologically important properties and their applications such as: the microwave transceivers used in cell phones; light emitting diodes (LEDs); laser diodes for data transmission, reading and recording for DVD and CD players; high efficiency solar cells; etc. The III-V compound semiconductors are one of these classes. Amongst the III-V family, GaAs is one of the most extensively studied and considered to be the most technologically important due to its superior semiconducting properties. For example, because of its direct bandgap it facilitate more efficiently the generation of light than elemental semiconductors. This property makes this material very suitable for light emitting and light detecting devices. The other very important property of GaAs is high carrier mobility which makes this material suitable for the high speed transistors. Apart from its direct bandgap and high carrier mobility, the very interesting property that makes this material, highly attractive is the formation of ternary compounds which allow tailoring the bandgap. The interest in the III-V compound semiconductors has dominated since the advent in the early 1980's of the non-equilibrium growth

techniques such as molecular beam epitaxy (MBE) which offers tremendous tailoring capabilities for device fabrication by forming compound materials from these semiconductors. Fig.1.1 shows the bandgap energy as a function of lattice constant for some selected III-V compound and elemental semiconductors. A desired bandgap variation can be engineered by alloying different III-V compounds and using growth techniques like MBE. A typical example is shown in Fig.1.1 where the lines schematically indicate the bandgap bowing due to incorporation of N and Bi into GaAs.

In the recent history of growth of the ternary compounds some of the untested elements from group-V of the periodic table have been incorporated into GaAs materials yielding some surprising and interesting results. Examples of such emerging ternary compounds are GaAsN and GaAsBi. Kondow *et al.* [1] in 1990 has incorporated a small amount of nitrogen (N <4%) into GaAs and found that the dilute nitride GaAsN exhibits a smaller band gap than that of GaAs. The GaAs energy gap decreases by approximately 0.1eV for each percent of N in the alloy. This enormous bandgap bowing is illustrated schematically in Fig. 1.1. This discovery has led to a new family of III-V semiconductors having unique properties and wide range of possible device applications like solar cells, long wavelength lasers, terahertz emitters, optical amplifiers, and temperature-insensitive semiconductor band gap [2-6].

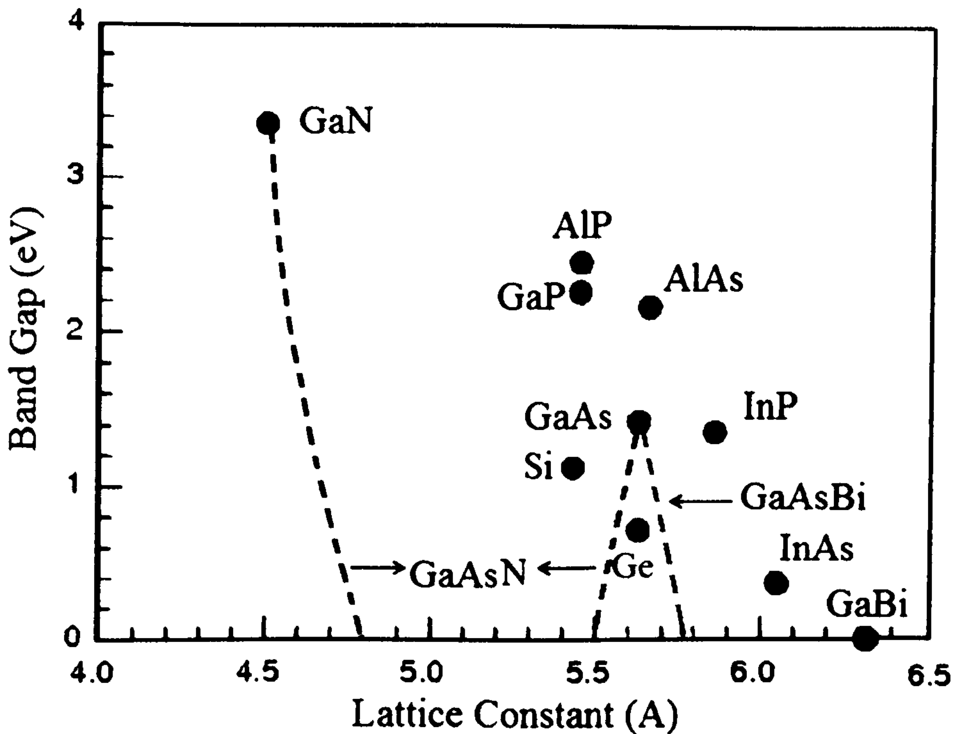

Fig.1.1 Band gap versus lattice constant for various III-V compound and elemental semiconductors [19-25]. Lines schematically indicate the bowing due to N and Bi alloying with GaAs. The lattice parameter for the metal GaBi is also indicated [14].

A potential alternative to GaAsN is the GaAsBi system. Bismuth has previously been used extensively for the growth of GaAs by liquid phase epitaxy (LPE), where it is well known to improve the properties of the layers [7]. It is known that bismuth is not incorporated at high growth temperature in large quantities into all III-V films, due to the large size of the bismuth atom [7-9]. Bismuth can be used as a surfactant during the growth of III-Vs by MBE to improve the surface morphology [8, 9]. Recently, it has been shown that it is possible to grow $GaAs_{1-x}Bi_x$ alloys at relatively low temperatures by both metal-organic chemical vapour epitaxy

(MOCVD) [10, 11] and by MBE [12, 13]. The $GaAs_{1-x}Bi_x$ alloy system has attracted significant attention due the potential to realise a temperature-insensitive semiconductor band gap [10, 11]. Photoluminescence (PL) studies of $GaAs_{1-x}Bi_x$ have shown that the temperature variation of PL peak was fairly weak (~ 0.1meV/K) compared with that of the GaAs [10]. Francoeur *et. al* [13] also reported that the band gap decreases rapidly with Bi concentration (~83meV/% Bi); they suggested that Bi modifies the band structure of GaAs significantly, because of the large bowing parameter ~5.6eV and the large valence band splitting.

In both MOCVD and MBE, to obtain $GaAs_{1-x}Bi_x$ layers the growth temperature should be lower than 400°C [12, 13], because Bi atoms surface-segregate and do not incorporate under typical MOCVD/MBE growth conditions. In MBE, the As:Ga flux ratio is very important, the ratio needs to be close to the stoichiometric value "on the brink of As shortage" [12, 14] in order to incorporate Bi efficiently.

The unusual large band gap reduction of GaAs by incorporating few percent of N and Bi is the resembling factor between the two alloys. Nitrogen and bismuth in GaAs behave as isoelectronic impurities. They replace the As atom in GaAs substitutionally. The large reduction of GaAs band gap with Bi incorporation is thought to be due to resonant interaction between the valence band maxima and 6*p* state of Bi atom [15, 16]. Whereas the large reduction in GaAs band gap with the incorporation of N is considered to be due to the interaction between the resonant empty N 2*s* antibonding state and conduction band minima [17, 18]. This shows that the situation is opposite in the case of the dilute nitrides, where the bonding N 2*p* orbitals are deep in the valence band of GaAs and not to be considered for band gap reduction. Fig. 1.2 schematically shows the band structure of the GaAsN and

GaAsBi with respect to GaAs band structure. This energetic behaviour of the N and Bi isoelectronic impurities can be explained physically by the difference in the low electronegativity of Bi and the large electronegativity of N as compared to that of As.

Semiconductor materials are known for their high sensitivity to defects, whether they are native due to crystal imperfections or due to foreign impurity incorporation. This is true regardless of the nature of the host semiconductor, elemental or compound. A very beneficial role of defects in semiconductors is the intentional incorporation of impurity atoms in order to produce n-type or p-type electrical conductivity. This type of deliberate introduction of defect states or impurity atoms in the host material is very valuable for electronic and optoelectronic devices. On the other hand foreign atoms and defects can affect the quality of the materials too. It is well established that the defect states can play an important role in the degradation of the electrical and optical properties of semiconductor materials. For example, they can reduce the lifetime of the charge carriers which is required for high speed devices, and they can act as non-radiative recombination centers that degrade the optical quality of the material required for making suitable lasers and other optoelectronic devices. Thus, it is extremely important in terms of the performance of devices to have a thorough knowledge of these defect states present in the host materials.

In this thesis two emerging and technologically important III-V semiconductors, namely dilute nitrides GaAsN and dilute bismides GaAsBi, have been studied using electrical and optical techniques. A brief summary of the work carried out is given in the following sections.

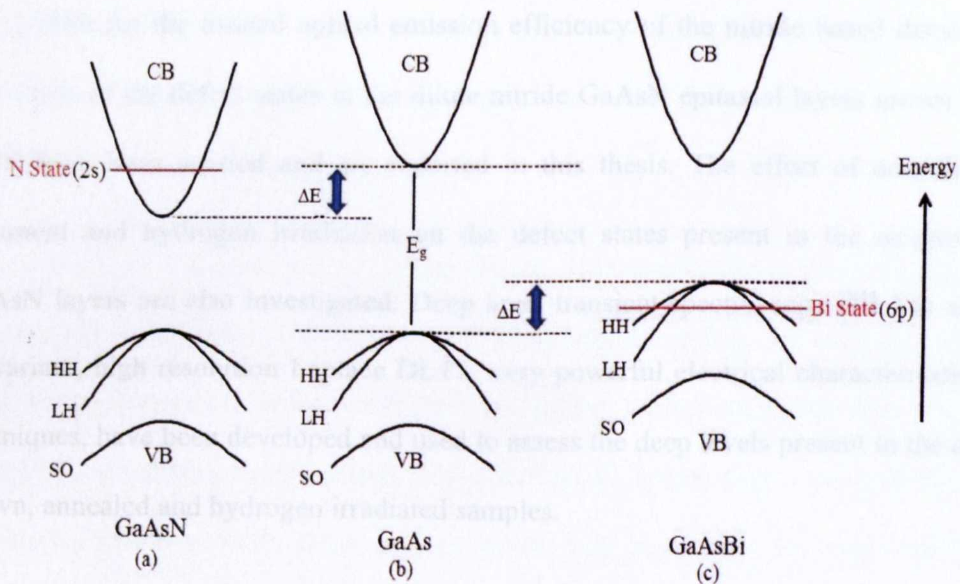

Fig.1.2 Schematic illustration of the band structure of (a) GaAsN and (c) GaAsBi with respect to (b) GaAs [26] showing conduction band (CB), heavy hole valence band (VB) (HH), light hole VB (LH) and split-off band (SO). The bandgap of GaAsN and GaAsBi is reduced due to the resonance of the N 2s state and the conduction band minimum (CBM) energy level, and the resonance of Bi 6p with the valence band maximum (VBM), respectively. [15, 18]

The covalent radii and electronegativity of As and N is 0.118nm and 0.07nm and, of 2.18 and 3.04, respectively. Due to the large size and electronegativity differences between As and N, the formation of several point defect complexes has been predicted [27-29]. These point defects and their complexes are likely to be responsible for the limited optical emission efficiency of the nitride based devices. The study of the defect states in the dilute nitride GaAsN epitaxial layers grown by MBE have been studied and are reported in this thesis. The effect of annealing treatment and hydrogen irradiation on the defect states present in the as-grown GaAsN layers are also investigated. Deep level transient spectroscopy (DLTS) and its variant, high resolution Laplace DLTS, very powerful electrical characterisation techniques, have been developed and used to assess the deep levels present in the as-grown, annealed and hydrogen irradiated samples.

The MBE growth and optical assessment of GaAsBi layers grown on non-conventional GaAs planes is reported in this thesis for the first time. The effect of the MBE growth conditions on the bismuth incorporation in both (100) and high index GaAs substrates is investigated using techniques such as high resolution x-ray diffraction, transmission spectroscopy and photoluminescence which was setup during the course of this research.

1.2 MOTIVATION

Defect states in semiconductors play an important role in the charge carrier kinetics, in the electrical and optical quality of the materials and in the performance

of the solid state devices. The motivation of this work was to study the electronic and optical properties of novel materials, namely dilute nitrides and bismides compound semiconductors. In order to carry out this investigation a DLTS and PL systems were setup.

The DLTS system has been applied for the electrical characterisation of silicon-doped $GaAs_{1-x}N_x$ (x = 0 - 1.2%) grown by MBE. The effect of annealing [anneal temperature = 500°C – 800 °C] and hydrogenation on the defects present in the as-grown layers have been also examined.

The effect of substrate orientation on the Bi incorporation in GaAsBi grown by MBE has been studied. The motivation behind this research is due to the fact that the growth of epitaxial layers on high-index planes represents a step forward in semiconductor material engineering, as it offers an additional degree of freedom to develop applications with improved properties with respect to the conventional (100)-grown devices [30-32].

1.3 SCHEME OF THE THESIS

The structure of this thesis is as follows. Chapter one gives a brief introduction to semiconductor materials studied here, experimental techniques which have been implemented and the work reported in the thesis. Chapter two describes the basic concepts of semiconductor materials such as their electrical conductivity, crystal structure, etc. The role of nitrogen and bismuth impurities in the modification of the bandgap of GaAs is also given in this chapter. Chapter three explains the theoretical background of the carrier kinetics dealing with deep levels. A brief

description about the crystal imperfections and their role in carrier trapping is also given in this chapter. Experimental techniques for electrical [DLTS and Laplace DLTS], and optical [PL spectroscopy; optical transmission spectroscopy] characterisation are illustrated in Chapter four. The hardware and software required to implement these methods are also presented. The details of the samples preparation and experimental setup are described in Chapter five. Results of electrical investigations obtained from as-grown GaAsN (N = 0 to 1.2%) layers using standard DLTS and Laplace DLTS techniques are given in Chapter six. The effect of annealing on the as-grown layers with N=0-1.2% at 500 ^{0}C, 600 ^{0}C, 700 ^{0}C and 800 ^{0}C is presented in Chapter seven. The results for the effect of the hydrogen irradiation on the deep levels in as-grown GaAsN layers containing nitrogen 0.2%, 0.4% and 0.8% are covered in Chapter eight. The effect of the MBE growth conditions on the incorporation of bismuth in GaAs grown on (100)- and (311)B-GaAs orientations and their optical and structural assessement are detailed in Chapter nine. Finally Chapter ten gives the overall conclusions of the work reported in this thesis and summarizes the results for dilute nitride and bismide -GaAs semiconductor materials.

REFERENCES

[1] M. Kondow, K. Uomi, K. Hosomi, and T. Mozume., Jpn. J. Appl. Phys., 33(8A), L1056 (1994).

[2] S. R. Kurtz, A. A. Allerman, E. D. Jones, J. M. Gee, J. J. Banas, and B. E. Hammons, Appl. Phys. Lett., 74, 729 (1999).

[3] J. Wei, F. Xia, C. Li, and S. R. Forrest, IEEE Photonics Tech. Lett., 4, 597 (2002).

[4] GDR-E-2008 THz Workshop, 25-26.09 (2008), Paris, France.

[5] P. J. A. Thijs, L. F. Tiemeijer, K. I. Kuindersma, J. J. M. Binsma, T. Van Dongem, IEEE J. Quantum Electron. 27, 1426 (1991).

[6] I. Suemune, K. Uesugi, and W. Walukiewicz, Appl. Phys. Lett., 77, 3021 (2000).

[7] V. V. Chaldyshev and S. V. Novikov in "Semiconductor Technology: Processing and Novel Fabrication Techniques", A Wiley-Interscience Publication, New York, 165. (1997).

[8] S. Tixier, M. Adamcyk, E. C. Young, J. H. Schmid and T. Tiedje, J. Cryst. Growth, 251, 449 (2003).

[9] S. V. Novikov, A. J. Winser, T. Li, R. P. Campion, I. Harrison and C.T. Foxon, J. Cryst. Growth, 247, 35 (2003).

[10] K. Oe and H. Okamoto, Jpn. J. Appl. Phys., 37, L1283 (1998).

[11] K. Oe, J. Cryst. Growth, 237, 1481 (2002).

[12] Yoshimoto M, Murata S, Chayahara A, Horino Y, Saraie J and Oe K, Jpn. J. Appl. Phys., 42 L, 1235 (2003).

[13] S. Francoeur, M. J. Seong, A. Mascarenhas, S. Tixier, M. Adamcyk and T. Tiedje, Appl. Phys. Lett., 82, 3874 (2003).

[14] S. Tixier, M. Adamcyk, T. Tiedje, S. Francoeur, A. Mascarenhas, P. Wei and F. Schiettekatte, Appl. Phys. Lett., 82, 2245 (2003).

[15] A. Janotti, S. H. Wei and S. B. Zhang, Phys. Rev. B. 65, 115203 (2002).

[16] T. Tiedje, E. C. Young and A. Mascarenhas, Int. J. Nanotechnol. 5, 963 (2008).

[17] W. Shan, W. Walukiewicz, J. W. Ager, E. E. Haller, J. F. Geisz, D. J. Friedman, J. M. Olson and S. R. Kurtz, Phys. Rev. Lett., 82,1221 (1999).

[18] S. Tixier, S. E. Webster, E. C. Young, T. Tiedje, S. Francoeur, A. Mascarenhas, P. Wei and F. Schiettekatte, Appl. Phys. Lett., 86, 112113 (2005).

[19] W. G. Bi and C. W. Tu, Appl. Phys. Lett., 70, 1608 (1997).

[20] K. Uesugi, N. Morooka and I. Suemune, Appl. Phys. Lett., 74, 1254 (1999).

[21] I. Vurgaftman, J. R. Meyer and L. R. Ram-Mohan, J. Appl. Phys., 89, 5815 (2001).

[22] H. J. Hovel and J. J. Cuomo, Appl. Phys. Lett., 20, 71 (1972).

[23] T. L. Tansley and C. P. Foley, J. Appl. Phys., 59, 3241 (1986).

[24] P. Specht, J. C. Ho, X. Xu, R. Armitage, E. R. Weber, R. Erni and C. Kisielowski, Solid State Commun. 135, 340 (2005).

[25] B. Monemar, P. P. Paskov and A. Kasic, Superlattices Microstruct., 38, 38 (2005).

[26] Jasprit Singh. 'Electronic and optoelectronic properties of semiconductor structures', Cambridge University Press. (2003).

[27] J. Li, P. Carrier, S. H. Wei, S. S. Li and J. B. Xia, Phys. Rev. Lett., 96, 035505 (2006).

[28] K. M. Yu, W. Walukiewicz, J. Wu, D. E. Mars, D. R. Chamberlin, M. A. Scarpulla, O. D. Dubon and J. F. Geisz, Nat. Mater., 1, 185 (2002).

[29] A. Janotti, P. Reunchan, S. Limpijumnong and C. G. Van de Walle, Phys. Rev. Lett., 100, 045505 (2008).

[30] M. Henini, P. J. Rodgers, P. A. Crump, B. L. Gallagher, and G. Hill, Appl. Phys. Lett., 65, 2054 (1994).

[31] A. Polimeni, M. Henini, A. Patanè, L. Eaves, P. C. Main, and G. Hill, Appl. Phys. Lett., 73, 1415 (1998).

[32] K. Y. Wang, K. W. Edmonds, L. X. Zhao, M. Sawicki, R. P. Campion, B. L. Gallagher, and C. T. Foxon, Phys. Rev. B. 72, 115207 (2005).

CHAPTER 2

THEORY AND FUNDAMENTAL CONCEPTS OF SEMICONDUCTORS

This chapter describes the basic concepts of semiconductor materials such as their electrical conductivity improvements and doping type by the addition of impurity atoms. It highlights the different structures and orientations of the crystals. Heterostructures and their properties such as lattice mismatch and band alignment are also discussed. The electronic and optical properties of semiconductors in general and parameters of III-V materials in particular are discussed. A brief introduction to dilute III-nitride materials and III- bismide materials is given which includes the role of nitrogen and bismuth impurities in the modification of the bandgap of the GaAs.

2.1 SEMICONDUCTORS

Semiconductors are the base materials for modern electronic and optical devices and play a key role in current technologies including computers, cell phones, transceivers, light emitting diodes, lasers, detectors, solar cells, optical amplifiers etc.

A semiconductor is a material whose electrical conductivity lies between a conductor and an insulator. It can be loosely defined as a material with an electrical resistivity from 10^{-2} to 10^{9} Ωcm.

There are two classes of semiconductor materials, namely elemental and compound semiconductors. Elemental semiconductors consist of a single element. For example, the well-known elemental semiconductors such as silicon (Si), germanium (Ge) and diamond (C) are from the group IV of the Mendeliev chemical table.

Materials formed by adding two or more elements from the periodic table are known as compound semiconductors. For example elements of the group III and V of the periodic table are used to make important compound semiconductors such as GaAs, InP and GaP. Other compound semiconductors include II-VI elements such as ZnS, HgCdTe. Compound semiconductors with two elements are called binary compounds and those which have three elements are known as ternary compounds such as AlGaAs and GaAsN

Semiconductor materials possess exclusive properties including negative temperature coefficient of resistance and electrical conductivity which can be controlled over several order of magnitudes by varying the temperature, adding impurities or by electrical and optical injections.

2.1.1 UNDOPED AND DOPED SEMICONDUCTORS

An undoped semiconductor, which is also called intrinsic semiconductor, is a pure material without any significant impurity that can appreciably affect its electrical behavior. In an intrinsic semiconductor the number of electrons in the conduction band is equal to the number of holes in the valence band. At zero Kelvin

temperature, they behave like insulators because the valence band is completely filled and the conduction band is completely empty so there is no flow of charge carrier to contribute to its conductivity unless a thermal excitation or photo-excitation is applied.

A doped semiconductor, which is also known as extrinsic semiconductor, is a material which has some impurity atoms that can change its electrical properties. The electrical conductivity of the extrinsic semiconductor depends upon the dopant atoms because their incorporation changes the concentration of electrons and holes at thermal equilibrium. The dominant charge carrier concentrations in doped semiconductor classify it as n-type (excess of electrons) or p-type (deficiency of electrons or excess of holes) material. For example if Si and Be atoms are introduced in GaAs, n-type and p-type conductivities can be achieved respectively. Means of obtaining n and p- type of semiconductors will be covered in Chapter 3.

2.2 CRYSTAL STRUCTURE AND PROPERTIES

All high performance semiconductor devices are based on crystalline materials. The crystal structure of the semiconductors is determined by the positions of the atoms in the crystal.

2.2.1 CRYSTAL STRUCTURE

A solid is a three dimensional arrangement of a regularly-repeated pattern of atoms. The regular pattern of atoms in a crystalline substance is known as a crystal lattice which can be seen as repetitive translations of a primitive cell. The smallest assembly of atoms that can be repeated to form the entire crystal is called a primitive cell, with a dimension of lattice constant $\boldsymbol{a}$ and sides parallel to the crystal axes.

Some important unit cells; simple cubic (sc), body-centered cubic (bcc) and face-centered cubic (fcc) are shown in Fig.2.1. In a simple cubic primitive cell, there is one host atom (lattice point) at each corner of a cubic unit cell. Body-centered cubic unit cell has one host atom at each corner and one atom in the middle of the body of the unit cell such that each atom touches eight other host atoms along the body diagonal of the cube. In the face-centered cubic structure, there is one host atom at each corner, one host atom in the center of each face, and the host atoms touch along the face diagonal.

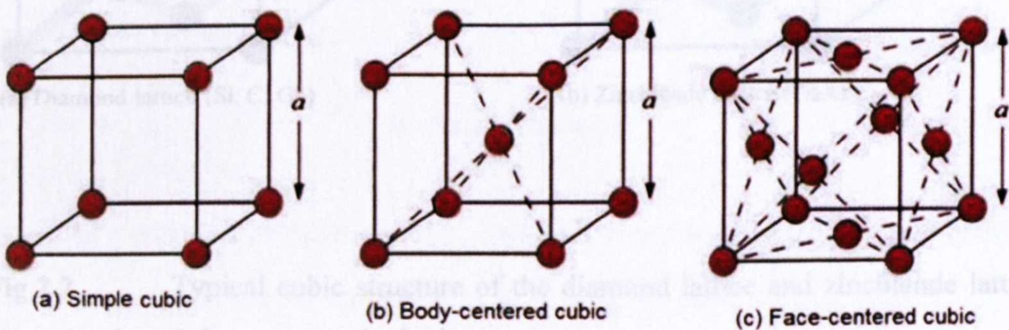

Fig.2.1 Some important primitive cells (***a*** is the lattice constant).

Several important semiconductors have diamond or zincblende lattice structures. These structures belong to the tetrahedral geometry in which each atom is surrounded by four equidistant nearest neighbors positioned at the corners of a tetrahedron. The zinc blend structure is very similar to the diamond lattice structure and can be considered as two interpenetrating face-centered cubic (fcc) lattices. However, in the diamond lattice all the sites are occupied by the same kind of atoms, whereas in the zinc blend lattice the different kind of atoms occupy alternate

positions in the lattice. For example in the diamond lattice such as Si, Ge and C has all the atoms belonging to one element are same. Whereas in a zincblende lattice, such as gallium arsenide, one sublattice is gallium and the other is arsenic. Fig. 2.2 (a, b) shows the diamond and zincblende structures.

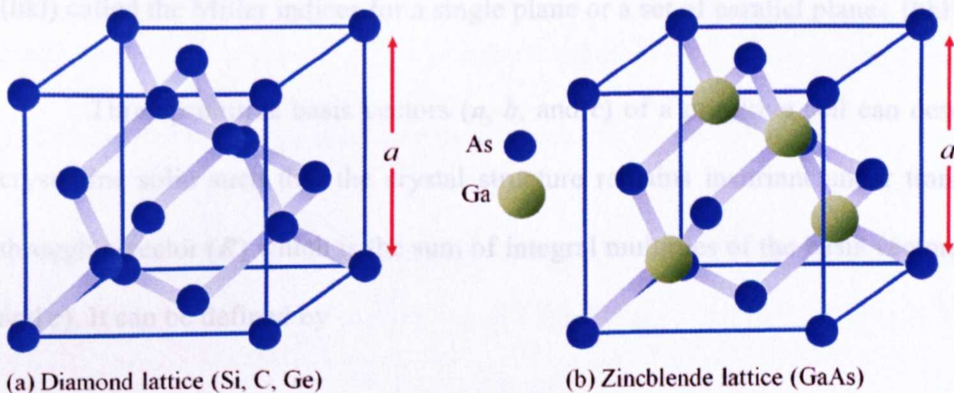

Fig.2.2 Typical cubic structure of the diamond lattice and zincblende lattice (GaAs). where '*a*' represents the lattice constant.

2.2.1.1 CRYSTAL PLANES

Since semiconductor devices are built on or near the semiconductor surface, the orientations and properties of the surface crystal planes are important. It is also essential to know the cleavage orientations of the crystal in order to cut pieces into desire sizes. For example, for single-element crystal such as Si the easiest cleavage directions are the (111) orientations. Whereas, GaAs which has a similar lattice structure but also has a slight ionic part in their atomic bonding offers easy way to cleave along (110) directions.

A convenient method of defining the various planes in a crystal is to use Miller indices. These indices are determined by first finding the intercepts of the plane with the three basis axes (x, y, z) in terms of the lattice constants (or primitive cells), and then taking the reciprocals of these numbers and reducing them to the smallest three integers having the same ratio. The result is enclosed in parentheses (hkl) called the Miller indices for a single plane or a set of parallel planes {hkl}.

Three primitive basis vectors (***a***, ***b***, and ***c***) of a primitive cell can describe a crystalline solid such that the crystal structure remains invariant under translation through a vector (***R***) which is the sum of integral multiples of the basis vectors (***a***, ***b***, and ***c***). It can be defined by

$$\boldsymbol{R} = m\boldsymbol{a} + n\boldsymbol{b} + p\boldsymbol{c}$$

where m, n and p are integers and **a, b, c** are known as the primitive vectors. For any choice of position vector **R**, the lattice looks exactly the same.

The reciprocal lattice basis vectors a^*, b^*, c^* in term of direct lattice basis vectors (a, b, c) can be defined by

$$\boldsymbol{a}^* = \boldsymbol{2\pi}\ [(\boldsymbol{b} \times \boldsymbol{c})/(\boldsymbol{a}.\boldsymbol{b} \times \boldsymbol{c})],\ \boldsymbol{b}^* = \boldsymbol{2\pi}\ [(\boldsymbol{c} \times \boldsymbol{a})/(\boldsymbol{a}.\boldsymbol{b} \times \boldsymbol{c})]$$

$$\boldsymbol{c}^* = \boldsymbol{2\pi}\ [(\boldsymbol{a} \times \boldsymbol{b})/(\boldsymbol{a}.\boldsymbol{b} \times \boldsymbol{c})]$$

such that $a^*. a = 2\pi$ and $a . b^* = 0$, and so on. where $a . b \times c = b . c \times a = c . a \times b$ is the volume enclosed by the vectors.

The position vector in the reciprocal space can be defined by

$$\boldsymbol{G} = h\boldsymbol{a}^* + k\boldsymbol{b}^* + l\boldsymbol{c}^*$$

where h, k, l are integers.

It follows the important relationship between the direct and reciprocal lattice is given by

$$G.R = 2\pi \times \text{integer}.$$

Hence, each vector of the reciprocal lattice is normal to a set of planes in the direct lattice. The volume V_c^* of a primitive cell in the reciprocal lattice is inversely proportional to that of the direct lattice V_c such that $V_c^* = \frac{(2\pi)^3}{V_c}$.

Some of the crystal planes are shown in Fig. 2.3. To calculate Miller indices, for example, of the plane shown in Fig. 2.3 (a) the intercept on the x-axis is at $x = a$ (a is lattice constant), but the surface is parallel to the y- and z-axes. There is, therefore, no intercept with these two axes and can be consider at infinity (∞) for the special case where the plane is parallel to an axis. The intercepts on the x-, y- and z-axes are thus a, ∞, ∞. The fractional intercepts are a/a, ∞/a, ∞/a i.e. 1, ∞, ∞. The reciprocal is therefore (1,0,0) and the Miller indices are 100. Similarly Miller indices for the planes shown in Fig. 2.3 (b, c and d) are 110, 111 and 210.

The (100), (110) and (111) planes are the so-called low index planes of a cubic crystal system (the "low" refers to the Miller indices being small numbers; 0 or 1 in this case). Whereas, values greater than these are called high index planes such as (210) plane depicted in Fig. 2.3 (d).

2.2.2 DENSITY OF STATES

Atoms are close enough in solids for their respective electric field to interact with each other and lead to a splitting of energy levels into a finite number of electronic states [1].

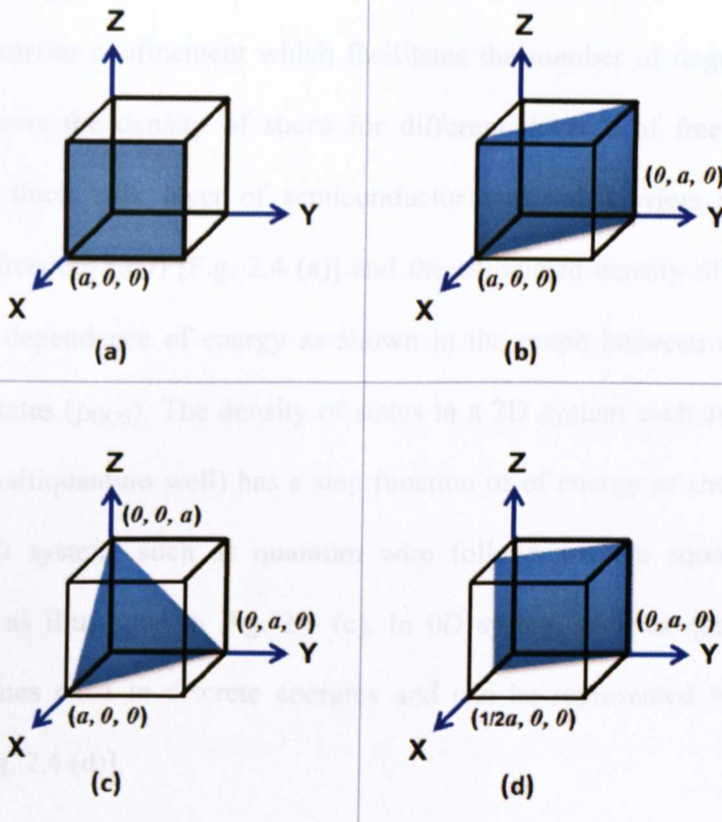

Fig.2.3 Illustration of crystal planes (a) the (100) plane, (b) the (110) plane, (c) the (111) plane and (d) the (210) plane of the cubic crystal.

Energy bands arise from their closely spaced sublevels as electrons tend to occupy all lower energy states available to them which in turn give rise to two highest energy bands known as valence and conduction bands. In the conduction phenomenon, an excited electron from the valence band can occupy a state in the conduction band by leaving behind a local positive charge (a hole) in the valence band. The density of states (ρ_{DOS}) of a system describes the number of states at each energy level that are available to be occupied. A high ρ_{DOS} at a specific energy level means that there are many states available for occupation. The density of states

(ρ_{DOS}) depends on the confinement of charge carriers and the degree of their freedom (0, 1, 2 or 3 degree of freedom). The thickness of the material is most important for the charge carrier confinement which facilitates the number of degree of freedom. Fig. 2.4 shows the density of states for different degrees of freedom. In a few micrometer thick bulk layer of semiconductor material, carriers possesses three degrees of freedom (3D) [F.g. 2.4 (a)] and the associated density of states shows a square-root dependence of energy as shown in the graph between energy (E) and density of states (ρ_{DOS}). The density of states in a 2D system such as quantum well (single or multiquantum well) has a step function of of energy as shown in Fig. 2.4 (b). The 1D system, such as quantum wire follows inverse square-root energy relationship as illustrated in Fig. 2.4 (c). In 0D system such as quantum dots, all available states exist in discrete energies and can be represented by Dirac delta-function [Fig. 2.4 (d)].

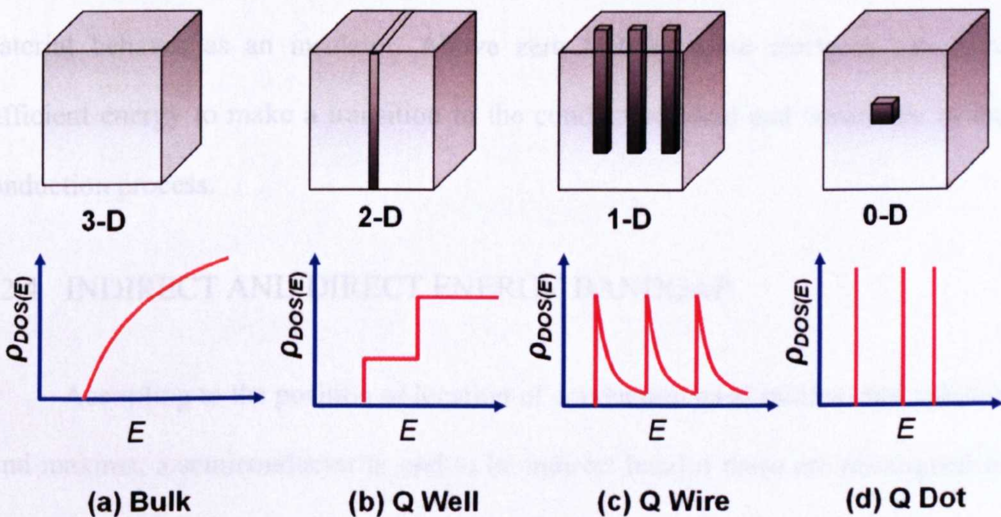

Fig.2.4 Density of states for different degrees of freedom; **(a)** Bulk(3D), **(b)** Quantum well (2D), **(c)** Quantum wire (1D) and **(d)** Quantum dot (0D).

2.2.3 ENERGY BANDGAP

The band gap of a semiconductor is usually represented by the energy-wave vector (E-k) relationship as shown in Fig.2.5. The upper and lower bands are called conduction (E_C) and valence band (E_V), respectively, and are separated by a gap where no allowed state exists. This gap between the valence band maxima and conduction band minima is called energy band gap of the material (E_g).

The shape of the conduction band and valence band at edges near $\boldsymbol{k} = 0$ is approximately parabolic and their energy is given by

$$E_C = E_g + \frac{h^2 k^2}{8\pi^2 m_e^*}, \qquad E_V = -\frac{h^2 k^2}{8\pi^2 m_h^*}$$

where h is the Plank's constant. m_e^* and m_h^* are the effective mass of electron and hole, respectively.

At zero Kelvin, all the electrons are confined to the valence band and the material behaves as an insulator. Above zero Kelvin, some electrons can have sufficient energy to make a transition to the conduction band and contribute in the conduction process.

2.2.4 INDIRECT AND DIRECT ENERGY BANDGAP

According to the position or location of conduction band minima and valence band maxima, a semiconductor is said to be indirect band if these are misaligned in the $\boldsymbol{k}$-direction. When these two bands are at the same $\boldsymbol{k}$ value or position, the semiconductor is said to be direct band gap material. Fig. 2.5 shows an example of indirect band gap such as Si and direct band gap such as GaAs.

Semiconductors with direct band gap such as GaAs allow transitions with conservation of momentum ($p=hk/2\pi$) and have higher radiative recombination probability. This property makes GaAs a very useful material for the optoelectronic applications.

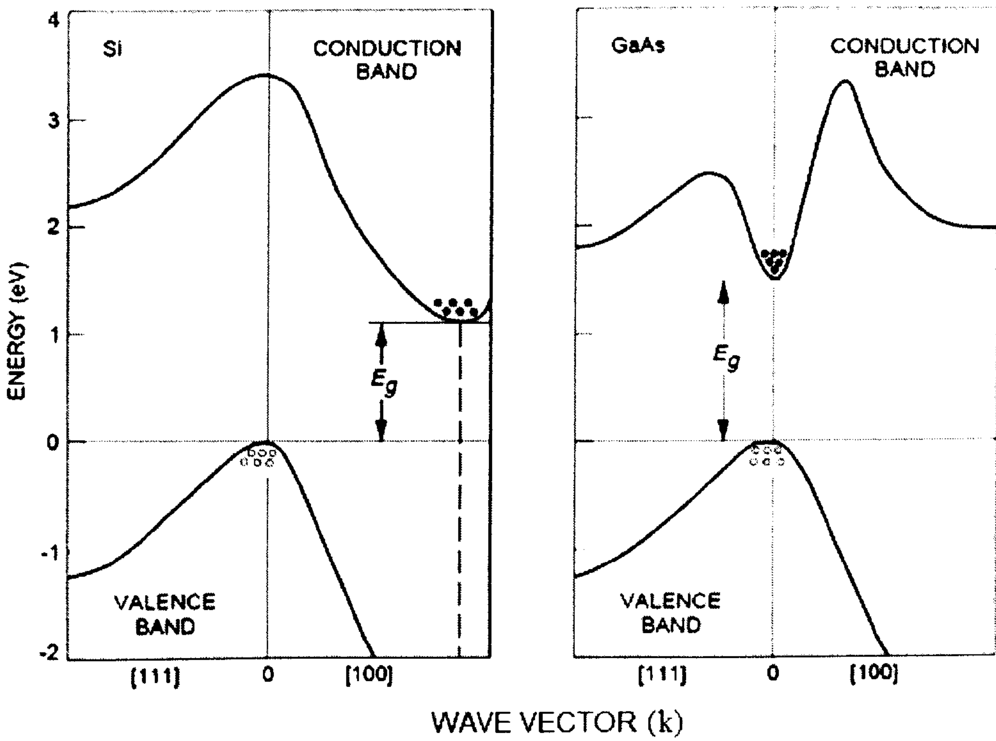

Fig.2.5 Indirect and direct band gap of Si and GaAs respectively.

2.2.5 TEMPERATURE DEPENDENCE OF BANDGAP

The bandgap of a semiconductor decreases with the increase of temperature. The reason for this reduction is the thermal energy which gives rise to atomic vibrations. When the amplitude of the atomic vibrations increases due to the increased thermal energy, the interatomic spacing also increases. This effect is quantified by the linear expansion coefficient of a material. An increased interatomic spacing decreases the potential seen by the electrons in the material, which in turn reduces the size of the energy bandgap.

The interaction between the free electron and phonons (lattice vibrations) can also affect the band gap to a smaller extent [2].

Varshni [3] has introduced an empirical relationship for the temperature dependence of energy band gap which is given by

$$E_g(T) = E_g(0) - \frac{\alpha T^2}{\beta + T}$$

Where $E_g(0)$ is the band gap energy at zero Kelvin. α and β are empirical parameters related to the material. For GaAs. α is ~0.5 meV/K and β is 220 K [4].

2.3 HETEROSTRUCTURES

A heterostructure is obtained by the junction of two dissimilar crystalline semiconductors. The constituent materials of the heterojunction have different energy band gaps, atomic size or lattice parameters.

2.3.1 ATOM SIZE AND ELECTRONEGATIVITY

'Atomic radii' describes the size of the atoms. In a heterostructure formation, the difference in the sizes of atoms belonging to two different materials can create strain in the structure. Electronegativity (χ) is the ability of an atom to attract an electron towards itself and to form a chemical bond. The concept of electronegativity (χ) was first proposed by Pauling in 1932 [5]. This is a unitless quantity and usually referred to as Pauling scale. It is generally quantified from 0.7 to 4 in the Pauling scale. Electronegativity (χ) plays a very important role in crystal structure. For a heterostructure, which is formed by two different semiconductor materials A and B, according to Pauling's theory the difference in electronegativity (χ_A- χ_B) between atoms of material A and material B is given by the relation

$$\chi_A - \chi_B = (eV)^{-1/2} \sqrt{E_D(AB) - [E_D(AA) + E_D(BB)]/2}$$

where E_D is the dissociation energy in eV between atoms of the materials AB, AA and BB. To make electronegativity (χ_A- χ_B) unitless, the factor $(eV)^{-1/2}$ was introduced. If a heterostructure has a large difference in the Pauling electonegativity then a drastic change occurs in the electronic structure.

2.3.2 BAND ALIGNMENT

Since two different energy bands are brought together in the formation of a semiconductor heterostructure, so the properties of these structures such as energy band alignment at the materials interface are of critical importance for device applications.

Three different possible alignments of the conduction and valence bands namely straddled alignment or type-I, staggered alignment or type-II and broken-gap

alignment or type-III, are shown in Fig. 2.6. In type-I bands alignments, conduction and valence band edges of a smaller gap material (B) lie in the bandgap region of a larger energy gap material (A). AlGaAs/GaAs, InGaAs/InP structures are example of such structures. In type-II heterostuctures, lowest conduction band edge lies in one type of material (A) and highest valence band edge is in the other type of material (B) such that the lowest conduction band edge is above the highest valence band edge, for example GaAsSb/GaInAs structures. In a situation where conduction band edge of one material (A) is below the valence band edge of the other material (B) is known as broken-gap or type-III band alignment (e.g. GaSb/InAs structures).

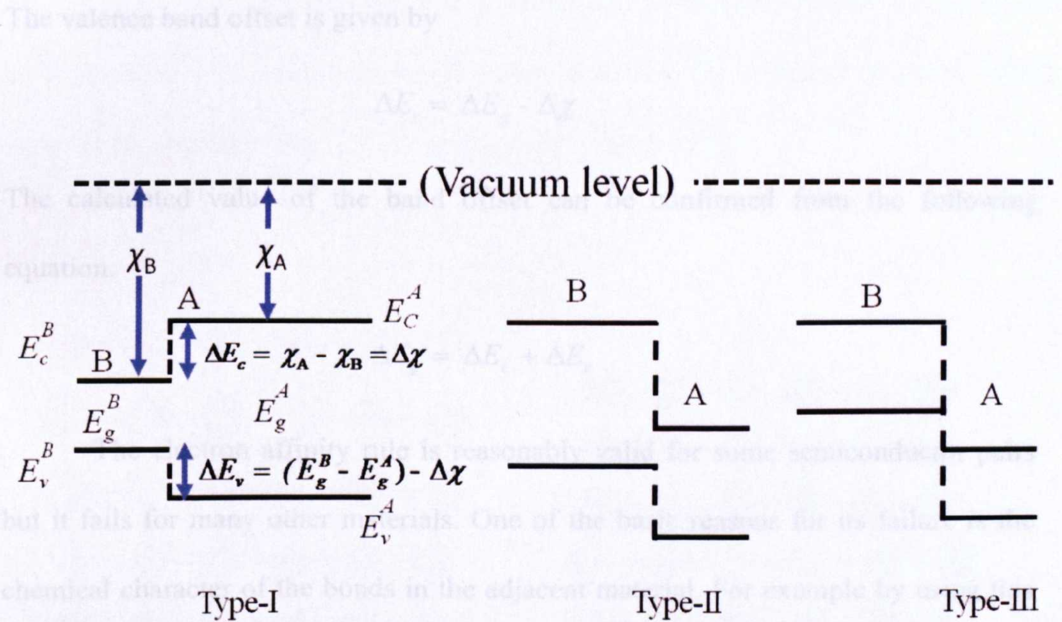

Fig.2.6 Possible energy-bands alignments in heterostructures. E_g^A , E_v^A , E_c^A and E_g^B , E_v^B, E_c^B are the bandgap, valence and conduction band edges, and χ_A, χ_B are the electron affinity of the semiconductors A and B respectively. ΔE_c and ΔE_v represent the band offsets in conduction and valence bands, respectively.

Anderson in 1962 first proposed a model to calculate band offset in an ideal semiconductor heterostructure which is also known as electron affinity rule [6]. According to this rule, the conduction band offset depends only on the electron affinity difference between the two semiconductor materials which is given by

$$\Delta E_c = \chi_A - \chi_B = \Delta\chi$$

The change in the energy gaps of the two materials is given by

$$\Delta E_g = E_g^B - E_g^A$$

The valence band offset is given by

$$\Delta E_v = \Delta E_g - \Delta\chi$$

The calculated value of the band offset can be confirmed from the following equation.

$$\Delta E_g = \Delta E_c + \Delta E_v$$

The electron affinity rule is reasonably valid for some semiconductor pairs but it fails for many other materials. One of the basic reasons for its failure is the chemical character of the bonds in the adjacent material. For example by using this rule, the theoretical value of the band offset of the AlAs/GaAs heterostructure is 230 meV while the experimental value for this is near 530 meV.

2.3.3 LATTICE MISMATCH

For a lattice-matched structure, the lattice constants or lattice parameters of the constituents of the semiconductor heterostructure are nearly the same. For example the AlGaAs/GaAs system which has s a very small mismatch of the lattice constants allows the fabrication of heterostructures with least interface

imperfections. If the lattice constants of the grown layer and substrate are not similar this leads to a lattice-mismatched structure.

The lattice-mismatch can empirically be expressed by the change in lattice constants at the interface of two materials. It is given by

$$\frac{\Delta a}{a} = \frac{a_{layer} - a_{sub}}{a_{sub}}$$

where a_{layer} and a_{sub} are the lattice constants of a fully-relaxed epilayer and substrate. When a semiconductor layer of larger lattice constant is grown on a substrate of smaller lattice constant, the structure is under compression strain and a layer grown on a substrate with relatively larger lattice constant, the structure is under tensile strain as illustrated in Fig. 2.7 (a) and 2.7 (b), respectively.

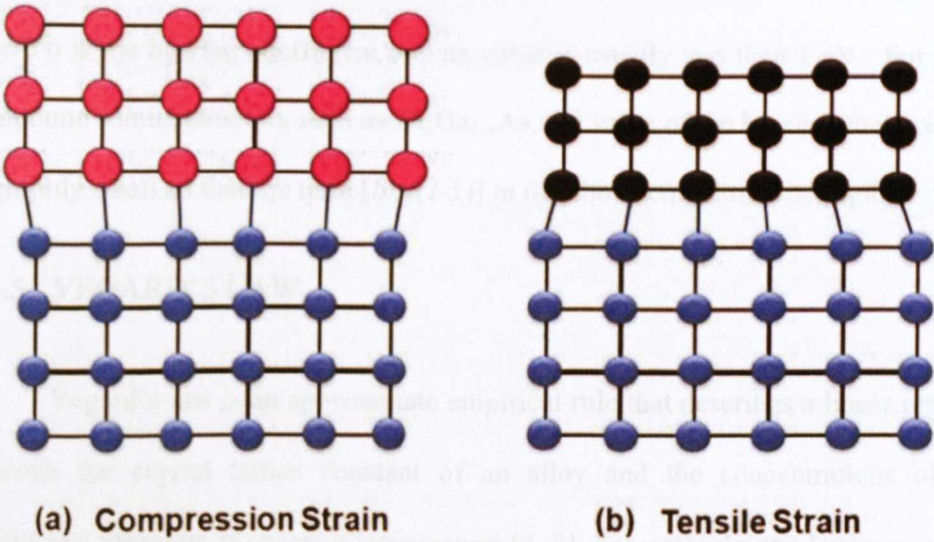

Fig.2.7 Schematic illustration of lattice mismatched structures having compressional and tensile strains

2.3.4 GRADED GAP SEMICONDUCTOR STRUCTURES

In the graded semiconductor structures, chemical composition of the semiconductor is varied and this variation may lead to a change in the alloy properties such as change in gap energy and change in lattice constant but in most of the graded structures, lattice constants do not change appreciably.

For example, in a ternary compound semiconductor material AB_xC_{1-x}, (where x is the mole fraction or chemical composition), the properties of AB_xC_{1-x} change gradually from the properties of the semiconductor AC to AB with the increase of x from 0 to1. For the case where the lattice constant behaves linearly with x and the energy gap exhibits non-linear bowing, the gap energy of the compound material AB_xC_{1-x} can be expressed as

$$E_{g,ABC}(x) = x \,.\, E_{g,AB} + (1-x)\,.\, E_{g,AC} - b\,.\,x\,.\,(1-x)$$

where b is the bowing coefficient and its value is usually less than 1 eV. For some compound semiconductors such as $Al_xGa_{1-x}As$, the value of the bowing coefficient is negligibly small so that the term $[b.x.(1-x)]$ in the above equation is negligible.

2.3.5 VEGARD'S LAW

Vegard's law is an approximate empirical rule that describes a linear relation between the crystal lattice constant of an alloy and the concentrations of the constituent elements at constant temperature [7, 8]. For example, the lattice constant of a ternary is the average of the lattice constants of component binaries. For a compound material AB_xC_{1-x}, it can be expressed as

$$a_{ABC}(x) = x \,.\, a_{AB} + (1-x)\,.\, a_{AC}$$

2.4 OPTICAL PROPERTIES OF SEMICONDUCTORS

The incidence of photons on the surface of a semiconductor material can follow different optical processes such as reflection from the material surface, transmission through the material or absorption in the material. If the photons have sufficient energy, they can excite an electron from valence band to conduction band and they may interact with lattice vibrations and electron of localized defects. As a result, the optical spectra of the semiconductor provide a rich source of information about the properties of the material.

2.4.1 ABSORPTION PROCESSES

The illumination of a semiconductor with photons of energy greater than the band gap energy generates an electron-hole pair by the optical process illustrated in Fig. 2.8. The process designated by (A) is a band-to-band transition in which an electron in the valence band absorbs a photon with enough energy and be excited to the conduction band leaving a hole behind. In the process (B) and (C), an electron can make a transition by absorbing a photon from the valence band to an empty impurity atom or from an occupied impurity atom to the conduction band. The optical absorption process (D) engages two impurity atoms for the transition.

A relatively simple method to probe the band structure of the semiconductor is the measure of its optical absorption spectra. For example if a light of intensity I_o and wave length λ is incident on a semiconductor of thickness t, a transmitted intensity I appears on the other side and is given by

$$I(\lambda,t) = [1 - R(\lambda)] I_o(\lambda) e^{-\alpha(\lambda)t}$$

where R(λ) is the reflection coefficient at the interface and α (λ) is the absorption coefficient of the material.

For the direct band gap semiconductors such as GaAs, α (λ) follows the relation given by [9]

$$\alpha(\lambda) = A\left(h\nu - E_g\right)^{\frac{1}{2}}$$

where constant A depends upon the material properties, E_g is the energy gap and $h\nu$ is the incident photon energy.

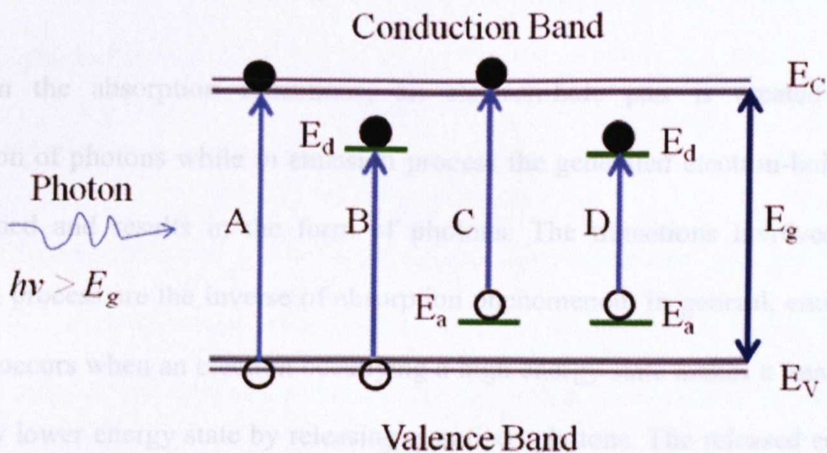

Fig.2.8 Main optical processes involved in absorption mechanism in semiconductors

In the direct optical transition, there is no involvement of phonons whereas in the indirect optical transition a phonon of energy E_p is also emitted or absorbed to keep the momentum conserved. The absorption coefficient α (λ) for the indirect band gap is given by

$$\alpha = \alpha_a + \alpha_e$$

where α_a and α_e are the absorption coefficients due to the transitions involving the absorption and emission of a phonon, respectively. These can be expressed as;

$\alpha_a = B(h\nu - E_g + E_p)^2$, for $h\nu > E_g - E_p$.

and $\alpha_e = C'(h\nu - E_g - E_p)^2$, for $h\nu > E_g + E_p$.

where, B and C are constants and their values depend upon the materials properties and temperature.

2.4.2 EMISSION PROCESSES

In the absorption transitions, an electron-hole pair is created due to absorption of photons while in emission process the generated electron-hole pair is recombined and results in the form of photons. The transitions involved in the emission process are the inverse of absorption phenomenon. In general, emission of photons occurs when an electron occupying a high energy state makes a transition to an empty lower energy state by releasing quantized photons. The released energy in the form of electromagnetic radiation is the difference of two energy states to keep the momentum conserved. The transitions due to emission of light in semiconductors are known as radiative transitions. Some important radiative transitions are given below.

i) BAND-TO-BAND TRANSITIONS

In a band-to-band recombination transition a free electron in the conduction band and a free hole in the valence band thermalise and accumulate at the conduction and valence band extrema where they tend to recombine radiatively with high

probability if the semiconductor has a direct band gap. For example GaAs, a direct gap material, is a strong emitter of light and important material for the light emitting diodes (LEDs).

Indirect band-to-band transitions can occur from all occupied states in the conduction band to all empty states in the valence band. This is, of course, subject to the condition that the momentum is conserved. Thus phonons must be emitted in such transitions. The probability of the radiative transitions is very small in indirect band gap semiconductors. This is due to the fact that most of the energy during such process is released in terms of phonons and goes into crystal in the form of heat instead of emission of photons. That is why indirect gap materials are not considered to be efficient light emitters.

ii) FREE EXCITON EMISSION

A free electron and a hole under a Coulombic interaction which binds them together into a quasi-particle is known as exciton. An exciton does not form any localized state and it can move throughout the crystal. An exciton in the crystal possesses two forms of energies which are translational kinetic energy and Coulombic interaction energy.

For a radiative recombination process, excitons are annihilated and photons with momentum equal to the momentum of the exciton are emitted. The energy of photon emitted in this process from direct-gap semiconductor is given by [10].

$$h\nu \approx E_g - E_x$$

where E_x is the energy of the exciton.

For the free exciton radiative recombination in an indirect-gap semiconductor, the energy of emitted photon is given by

$$h\nu \approx E_g - E_x - E_p$$

where E_p is the energy of phonons.

iii) BOUND-EXCITON EMISSION

An impurity atom in the crystal can attract an exciton via van der Waals interaction. This interaction lowers the exciton energy [11]. This difference of energy is released in the form of photons. The neutral impurities are very efficient at trapping excitons at low temperature to form a bound-exciton. The energy of the emitted photons in this process is less than that of the free exciton.

The bound-exciton can form complexes with neutral donor and acceptor, and ionized donor and acceptor. An exciton (X) bound to ionized donor (D^+), ionized accepter (A^-), neutral donor (D^0) and neutral accepter (A^0) are commonly denoted by (D^+, X), (A^-, X), (D^0, X) and (A^0, X) respectively in the literature [12].

iv) DONOR-ACCEPTOR PAIR TRANSITIONS

Compensated semiconductors may contain both donors and acceptors. These are called compensated because under equilibrium condition, some of the electrons from donors will be captured (compensated) by acceptors. So consequently both ionized-donors (D^+) and ionized-acceptors (A^-) exist in the compensated semiconductor.

The optical excitation can create electrons and holes in the conduction and valence bands respectively. These electrons and holes can be trapped by ionized-donors (D^+) and ionized-acceptors (A^-) to produce neutral donor (D^0) and acceptor (A^0). When returning to the equilibrium condition, electrons at neutral donors will radiatively recombine with holes at neutral acceptors. This is known as donor-acceptor pair transition (or DAP transition). It can be expressed as

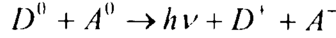

$$D^0 + A^0 \rightarrow h\nu + D^+ + A^-$$

The energy of the emitted photon is given by

$$h\nu = E_g - (E_A + E_D) + \frac{q^2}{\varepsilon r_{da}}$$

where E_g, E_A and E_D are the band gap energy, acceptor and donor binding energies, respectively. The last term in the equation is due the Coloumbic interaction between ionized donors and acceptors which are separated by a distance r_{da}. ε is the dielectric constant of the material.

Since acceptor and donor are substitutional so r_{da} is a discrete radii. If r_{da} is very large due to distant donor and acceptor, the Coulombic interaction is smaller so the last term of the above equation becomes negligible. The energy of the emitted photon is therefore given by

$$h\nu = E_g - (E_A + E_D)$$

v) FREE -TO- BOUND TRANSITIONS

Band-to-band transitions tend to dominate at higher temperatures where all the shallow donors and acceptors are ionized. At sufficiently low temperatures, carriers are frozen on the impurities. On photoexcitation, free electrons can recombine radiatively (sometimes non-radiatively) with holes trapped on acceptor levels. These transitions are known as free-to-bound transitions. The energy of the emitted photon in this process is given by

$$h\nu \approx E_g - E_A - E_P$$

where E_A is the energy of acceptor level and E_P is the energy of phonon released into the crystal to keep the momentum conserved.

2.5 DILUTE NITRIDE MATERIALS

Epitaxial growth of the dilute nitride semiconductor materials has been demonstrated in 1990s [13-15]. This was the first introduction of a new family of III-V semiconductors with uncommon physical properties favorable to technological applications like solar cells, long wavelength lasers, terahertz emitters, optical amplifiers, and temperature-insensitive semiconductor band gap [16-20].

Semiconductor alloys are usually formed by substituting the host atom by some other atoms of same valency. Whereas when isovalent impurity atoms are incorporated, they produce weak perturbation in the host crystal band structure. If the isovalent impurity atoms and the host atoms have different properties such as atomic radii, electronegativity etc, then they can change the host crystal band structure significantly.

For example when an impurity atom such as indium (In) substitutes Ga or phosphorus (P) substitutes As in GaAs material, they do not make big changes in the band structure of the GaAs. Whereas nitrogen (N), one of such isovalent impurities for the host crystal such as GaAs, can change the band structure of the GaAs drastically. For example when N is incorporated into GaAs it forms a single GaAsN crystal. The GaAs energy gap decreases by approximately 0.1eV for each percent of N in the alloy. The incorporation of N atoms can therefore be used to tune the energy gap of GaAs for desirable wavelength emission [21]. The general reason for the reduction in the band gap and other associated effects is the presence of N-related localized states near the conduction band edge which result from a significant local potential produced due to large differences in atom size and electronegativity of N

atoms and host anions [22]. Atomic properties of some elemental semiconductors are shown in Table 2.1 [23]

TABLE 2.1 Properties of elemental semiconductors

Element	Atomic Mass	Covalent Radius	Electronegativity
Ga	69.72	0.135 nm	1.81
In	114.82	0.144 nm	1.78
N	14.007	0.070 nm	3.04
As	74.92	0.118 nm	2.18
Sb	121.75	0.136 nm	2.05
Bi	208.98	0.145 nm	2.02
P	30.97376	0.106 nm	2.19

2.5.1 DEVIATION FROM VIRTUAL CRYSTAL APPROXIMATION

Virtual crystal approximation (VCA) is used to predict a number of fundamental characteristics of alloys based on binary compound materials. It works best to approximate the structural parameters such as lattice constant, compressibility factors, and deformation potentials in alloys. However, VCA cannot account for the one important parameter: a deviation of band edge energies from a linear dependence on composition. Since this deviation is usually small, it is represented by quadratic

coefficient, b, which is referred to as the bowing coefficient. For example by including this factor, the gap energy of an $AB_{1-x}C_x$ semiconductor is given by

$$E_{g,ABC}(x) = x \cdot E_{g,AB} + (1-x) \cdot E_{g,AC} - b \cdot x \cdot (1-x)$$

where 'b' is the bowing coefficient.

The bowing coefficient and other effects such as alloy scattering are due to the atomic scale disorder which includes lattice relaxation to keep bond lengths proportional to lattice mismatch and, difference in electronegativity owing to the charge density variations.

Due to these variations, a large deviation from linearity (Vegard's law) can be expected from dilute nitride alloys. For example the bowing coefficient for GaAsN is about one order of magnitude higher than the other alloys such as AlGaAs. The giant bowing of the bandgap of the GaAsN unlike the conventional III-V alloy is sketched in Fig. 1.1 of Chapter 1. The energy gap of cubic GaN is 3.3 eV, therefore, VCA predicts that the energy gap of $GaAs_{1-x}N_x$ should increase from 1.424 eV by 0.19 meV per each percent of N. However, Weyer *et al.* [24] and Kondow *et al.* [25] reported that instead of increasing the band gap of GaAsN it is reduced surprisingly by 120 meV per percent of N. On the basis of this result, Vurgaftman *et al.* [26] have suggested to correct the bowing coefficient by 10-20 eV for this large deviation. This shows that the properties of GaAsN are different to what have been expected from VCA model. Shan *et al.* [27] have first proposed a model that has been used extensively to explain the characteristics of GaAsN. This is known as the band anticrossing model (BAC).

2.5.2 THE BAND ANTICROSSING MODEL

This is an empirical model which considers the interaction between two bands. The first band is nitrogen related resonant state in the conduction band of the GaAs and the second one is the conduction band minima of the GaAs. The resonant state is the energy level created by isolated nitrogen impurity atom which can be observed by applying hydrostatic pressure on the GaAsN sample. The applied pressure can drop this level into the energy gap of the GaAs where it attracts opposite charge carriers to form the exciton states. Photoluminescence experiments can then detect this level due to its decay function [28]. It is suggested by Shan *et al.* [27] that at higher concentration of nitrogen such as 0.5%N, the density of states of these N resonant levels becomes significant to transform into a band which repels the conduction band of the GaAs. Therefore two bands are created in GaAsN material. The first one is the low energy bonding state E_- which corresponds to the conduction band edge of the GaAs and the second one is the antibonding state E_+ which creates the new conduction band state in the energy gap of the GaAs. These two states interact and repel each other. The energy difference between them increases with increasing N concentration. Fig. 2.9 shows the anticrossing behavior between the N-related state (E_N) and conduction band edge (E_{CB}) of the GaAs. The N-related states are spread over the reciprocal space with constant energy because of its localised nature. These two energy states are represented in Fig. 2.9 by dotted lines.

According to the band anticrossing model, the energy of these two states resulting from their interaction is given by

$$E_{\pm} = \frac{1}{2}\left(E_N + E_{CB} \pm \sqrt{\left(E_N - E_{CB}\right)^2 + 4V_{CB,N}^2} \right)$$

where $E_{CB}(k)$ and E_N are the energies of the conduction band edge and nitrogen state, respectively. $V_{CB,N}$ is the coupling parameter describing the strength of interaction between the bands. The dependence of E_+ and E_- with concentration can be modeled by adjusting the interaction parameter which is given by

$$V_{CB,N} = Cx^{1/2}$$

where C is a constant whose value depends upon the semiconductor host and x is the nitrogen fraction in the alloy.

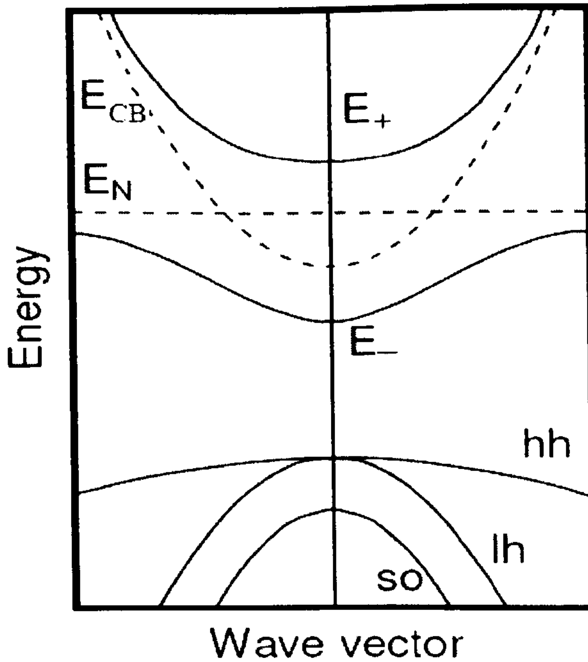

Fig.2.9 Schematic diagram of band anticrossing model of GaAsN

The shortcoming of the band anticrossing model is that it is considered to work for single isovalent impurity level and conduction band edge interaction and, it does not consider the broadening of the energy levels or splitting of L-conduction

band extrema. In spite of all its shortcomings, it has been a popular and most cited model in dilute nitride literature due to its simplicity and satisfactory fit to many characteristics of the alloy.

2.5.3 SOME IMPORTANT PROPERTIES OF GaAsN

Dilute nitride semiconductors have shown unusual properties such as a large band reduction, change of doping type, enhancement of the effective mass, low charge carrier mobility and small lifetime of the charge carriers. Some of these properties which are reported in literature are given below.

A divergent set of values of the effective mass of the electron ranging from $m_e^* \sim 0.8m_o$ to $0.1m_o$ has been reported in dilute nitrides materials [29-34] (m_o is the mass of the electron at rest).

The degradation of mobility of electrons and holes in the dilute nitride materials is expected due to enhanced effective mass (GaAs: $m_e^* \sim 0.0663m_o$) and large alloy scattering. A strong degradation of hole mobilty has been oberved in both molecular beam epitaxy (MBE) and metal organic chemical vapour deposition (MOCVD) grown GaAsN samples [35]. Similarly the enhancement of the electron effective mass leads to a decrease in mobilty of the electron [36].

Lifetime of the charge carrier is an important parameter for the light emission devices. Carrier lifetime is also found to be smaller in the dilute nitride materials due to high defect density. Lifetime of the carriers less than 1ns at room temperature in GaAsN with one percent nitrogen have been reported [37].

Undoped dilute nitrides materials grown by MBE or by MOCVD are generally p-type [38]. On annealing the sample, Kurtz *et al.* [39] have observed the conversion of the type of conductivity. They have attributed this transformation of conductivity type to nitrogen-hydrogen defects which were formed upon annealing.

2.6 DILUTE BISMIDE MATERIALS

GaAsBi is an interesting material due to its remarkable properties such as large bandgap reduction (~90 meV per % of Bi), strong enhancement of the spin-orbit splitting energy [40] and, potential applications such as terahertz emitters and detectors, spintonics.

K. Oe *et al.* have first grown dilute bismide materials epitaxially by MOCVD [41] and then later it was grown by MBE [42-43]. Bi is the heaviest element in group-V. Bi atom has relatively larger atomic radius and low electronegativity than that of As atom. This is in contrast to the small size and high electronegativity of nitrogen (the lightest group V element) as compared to As. Due to this large size difference between Bi and As atoms, a compressive strain is developed around the atom.

In the GaAsBi band structure, the large variation of atomic potential creates a localized level near the valence band maxima of GaAs that attracts the holes from the valence band. Bi atoms localized potential and the surrounding lattice relaxation disturb the GaAs electronic band structure considerably which in turn bring diverse qualitative effects that are similar to those observed in GaAsN material system. In GaAsBi material, shallow energy states appear near the valence band maxima in

contrast to the GaAsN material where these shallow energy states appear near the conduction band minima. These energy states behave like shallow donors [44] and interact with the valence band as expected from virtual crystal approximation (VCA). The effect of the interaction between the donor-like energy states and valence band charge carriers leads to large bowing of the energy bands.

The incorporation of Bi in GaAs reduce the band gap of GaAs about 88 meV for 1% Bi [44]. This effect can be exploited to tune the energy gap of GaAs in a similar fashion to the case of N incorporation in GaAs for electronic and optoelectronic applications.

2.7 BISMUTH INCORPORATION ON HIGH INDEX GaAs PLANES

An important degree of freedom in the epitaxy of III-V GaAs semiconductors is the growth of layers on high Miller index surfaces, *i.e.* surfaces oriented differently from the usual (100) orientation. The growth of epitaxial layers on high-index planes represents a step forward in semiconductor material engineering, as it offers an additional degree of freedom to develop applications with improved properties with respect to the conventional-(100) grown devices. The interest in non-(100) semiconductor structures is manifold and concerns growth, impurity incorporation, electronic properties, lasing performance, and piezoelectric effects. For example, the use of non-(100) substrates has allowed the fabrication of ultrahigh mobility two-dimensional hole gases in GaAs/AlGaAs heterostructures, high-performance InAs/GaAs quantum dot (QD) lasers, InGaAs/GaAs QDs with

enhanced piezoelectric effects, and GaMnAs epilayers with modified Mn incorporation and magnetic anisotropies [45-48].

It has been observed that when GaAsBi is grown by MBE on (311)*B* GaAs substrates an increased Bi incorporation, leading to reduced band gaps, are achieved in comparison to the conventional (100) orientation [49].

2.8 CHARACTERISATION METHODS

There are several techniques which are used to investigate the structural, electrical and optical properties of semiconductor materials. Investigation of deep level defects and imperfections in semiconductor materials space charge techniques such as conventional deep level transient spectroscopy (DLTS) and Laplace DLTS are usually employed using devices such as p-n junction diodes, Schottky diodes and metal-insulator-semiconductor structures.

For the determination of semiconductor materials structural and optical properties, there are various techniques which are commonly used such as transmission electron microscopy (TEM), high resolution x-ray diffraction (HRXRD), absorption spectroscopy, photomodulated transmission spectroscopy (PT), and photoluminescence (PL). The detailed description of the techniques used in this study is given in Chapter 4.

REFERENCES

[1] D. Wood, Optoelectronic semiconductor devices, Prentice Hall publishers (1994).

[2] H. Unlu, Solid State Electronics, 35, 1343 (1992).

[3] Y. P. Varshni, Physica Vol. 34, 149 (1967).

[4] S. Wang, S. Holmes, T. Le, R. Stradling, I. Ferguson, and A. De Oliveira, Semicond. Sci. Technol., 7, 767 (1992)].

[5] L. Pauling, J. Americam Chem. Sci., 54, 3570 (1932).

[6] R. L. Anderson, Germanium-Gallium Arsenide Heterojunction, IBM J. Res. Dev. 4(3), 283 (1960).

[7] L. Vegard, Die Konstitution Der Mischkristalle Und Die Raumfüllung Der Atome, Zeitschrift Für Physik, 5, 17 (1921).

[8] A. R. Denton and N W Ashcroft, Phys. Rev. A, 43, 3161 (1991).

[9] J. M. Essick and R. T. Mather, Am. J. Phys. 61, 7 (1993).

[10] F. Askary and P.Y. Yu, Solid State Commun., 47, 241 (1983).

[11] S. A. Ding, S. R. Barman, K. Horn, H.Yang, B. Yang, O. Brandt and K. Ploog, Appl. Phys. Lett., 70 2407 (1997).

[12] G. D. Gilliland, Materials Science and Engineering, R18, 99 (1997).

[13] M. Weyers, M. Sato, and H. Ando, Japn. J. Appl. Phys., 31, L853, Pt 2 (1992).

[14] M. Kondow, K. Uomi, A. Niwa, T. Kitatani, S. Watahiki and Y. Yazawa, Japn. J. Appl. Phys., 35, 1273 (1996).

[15] M. Kondow, K. Uomi, T. Kitatani, S. Watahiki and Y. Yazawa, J. Cryst. Growth, 164, 175 (1996).

[16] S. R. Kurtz, A. A. Allerman, E. D. Jones, J. M. Gee, J. J. Banas, and B. E. Hammons, Appl. Phys. Lett., 74, 729 (1999).

[17] J. Wei, F. Xia, C. Li, and S. R. Forrest, IEEE Photonics Tech. Lett., 4, 597 (2002).

[18] GDR-E-2008 THz Workshop, 25-26.09 (2008), Paris, France.

[19] P. J. A. Thijs, L.F. Tiemeijer, K.I. Kuindersma, J. J. M. Binsma, T. Van Dongem, IEEE J. Quantum Electron. 27, 1426 (1991).

[20] I. Suemune, K. Uesugi, and W. Walukiewicz, Appl. Phys. Lett., 77, 3021 (2000).

[21] P. Skierbiszewski, P. Perlin, P. Wisniewski, and T. Suski, phys. Rev. B, 65, 035207 (2001).

[22] H. P. Hjalmarson, P. Vogl, D.J. Wolford and J. D. Dow, Phys. Rev. Lett., 44, 810 (1980).

[23] J. J. Gersten and F.W. Smith, 'The physics and chemistry of materials', Wiley Interscience, New York, USA, (2001).

[24] M. Weyers, M. Sata and H. Ando, Japn. J. Appl. Phys., 31, L853 (1992).

[25] M. Kondow, K. Uomi, K. Hosomi and T. Mozume, Japn. J. Appl. Phys., 33, 1056 (1994).

[26] I. Vurgaftman, J. Meyer and L. R. Ram-Mohan, J. Appl. Phys., 89, 5815 (2001).

[27] W. Shan, W. Walukiewicz, J. W. Ager, E. E. Haller, J. F. Geisz, D. J. Friedman, J. M. Olson and S. R. Kurtz, Phys. Rev. Lett., 82,1221 (1999).

[28] X. Liu, M. -E. Pistol and L. Samuelson, Phys. Rev. B , 42, 7504 (1990).

[29] M. Hetterich, M. D. Dawson, A. Yu. Egorov, D. Berklau and H. Riechert, Appl. Phys. Lett., 76, 1030 (2000).

[30] Z. Pan, L. H. Li, Y. W. Lin, B. Q. Sun, D. S. Jiang and W. K. Ge, Appl. Phys. Lett., 78, 2217 (2001).

[31] R. Mouillet, L. A. de Vaulchier, E. Deleporte, Y. Guldner, L. Travers and J. C. Harmand, Solid State Common, 126, 333 (2003).

[32] M. Kondow, S. Fujisaki, S. Shirakata, T. Ikari and T. Kitatani, 'International Symposium on Compound Semiconductors', San Diego, CA, pp. 76 (2003).

[33] C. Skierbiszewski, Semicond. Sci. Technol., 17, 803 (2002).

[34] J. B. Heroux, X. Yang and W. I. Wang, J. Appl. Phys., 92, 4361 (2002).

[35] A. J. Ptak, S. W. Johnston, S. Kurtz, D. J. Friedman and W. K. Metzger, J. Cryst. Growth, 251, 392 (2003).

[36] C. Skierbiszewski, P. Perlin, P. Wisniewski, T. Suski, W. Walukiewicz, W. Shan, J. W. Ager, E. E. Haller, J. F. Geisz and D. J. Friedman, Phys. Status Solidi B, 216, 135 (1999).

[37] R. K. Ahrenkiel, S. W. Johnston, B. M. Keyes and D. J. Friedman, Appl. Phys. Lett., 77, 3794 (2000).

[38] J. F. Geisz and D. J. Friedman, Semicond. Sci. Technol., 17, 769 (2002).

[39] S. Kurtz, J. F. Geisz, D. J. Friedman, W. K Metzger, R. R. King and N. H. Karam, J. Appl. Phys., 95, 2505 (2004).

[40] K. Alberi, O. D. Dubon, W. Walukiewicz, K. M. Yu, K. Bertulis, and A. Krotkus, Appl. Phys. Lett., 91, 051909 (2007).

[41] K. Oe and H. Okamoto, Jpn. J. Appl. Phys. 37, L1283 (1998).

[42] S. Tixier, M. Adamcyk, T. Tiedje, S. Francoeur, A. Mascarenhas, P. Wei and F. Schiettekatte, Appl. Phys. Lett., 82, 2245 (2003).

[43] M. Yoshida, S. Murata, A. Chayahara, Y. Horino, J. Saraie and K. Oe, Jpn. J. Appl. Phys., 42, L1235 (2003).

[44] S. Francoeur M.-J. Seong, A. Mascarenhas, S. Tixier, M. Adamcyk and T. Tiedje, Appl. Phys.Lett. 82, 3874 (2003).

[45] M. Henini, P. J. Rodgers, P. A. Crump, B. L. Gallagher, and G. Hill, Appl. Phys. Lett., 65, 2054 (1994).

[46] A. Polimeni, M. Henini, A. Patanè, L. Eaves, P. C. Main, and G. Hill, Appl. Phys. Lett., 73, 1415 (1998).

[47] A. Patanè, A. Levin, A. Polimeni, F. Schindler, P. C. Main, L. Eaves, and M. Henini, Appl. Phys. Lett., 77, 2979 (2000).

[48] K. Y. Wang, K. W. Edmonds, L. X. Zhao, M. Sawicki, R. P. Campion, B. L. Gallagher, and C. T. Foxon, Phys. Rev. B 72, 115207 (2005).

[49] M. Henini, J. Ibáñez, M. Schmidbauer, M. Shafi, S. V. Novikov, L. Turyanska, S. I. Molina, D. L. Sales, M. F. Chisholm and J. Misiewicz, Appl. Phys. Lett., 91, 251909 (2007).

DEFECTS IN SEMICONDUCTORS AND THEIR PROPERTIES

This chapter describes the crystal imperfections present in semiconductor materials due to lattice disruption and to foreign impurities. The role of impurities as trapping or recombination-generation centers is discussed. The theory of deep levels and their carrier kinetics processes are explained on the basis of Shockley-Read-Hall theory [1, 2]. The presence of defects in dilute nitrides and dilute bismides and their properties are highlighted. A brief description of hydrogen irradiation and annealing effects is also reported.

3.1 CLASSIFICATION OF DEFECTS

The repetition of a basic unit cell along the three crystallographic orientations builds a perfect crystal structure. However, no crystal possesses such periodicity and there are different kinds of imperfections present in all crystals. These imperfections are known as crystal defects. In terms of spatial arrangement of atoms, crystal defects can be due to lattice irregularities and foreign impurity atoms incorporation.

An impurity atom which is different from the host atoms is called foreign impurity. A foreign atom can find the path into the single crystal by two ways. It can

either be incorporated unintentionally (e.g. carbon in GaAs during the MBE growth of GaAs) or it can be introduced deliberately to achieve some special properties of the materials (e.g. intentional incorporation of Si or Be in MBE grown GaAs to change its conductivity).

Crystal lattice defects can be classified according to their dimensions into three major categories: point defects, line defects and planar defects.

3.1.1 POINT DEFECTS

The defects, whose physical dimensions are of the order of atomic size, are known as point defects. A point defect can cause an interruption in the lattice periodicity. It may be found in different forms such as a vacancy, an interstitial, or a substitutional point defect. In interstitial and substitutional sites, the deviation of host crystal potential creates a local electric potential at the defect site. Therefore, these defects develop energy levels within the band gap of the material and will affect its properties. Some of the most important compositional and structural point defects in the crystalline semiconductors are described below.

(i) Vacancies

A vacancy is an unoccupied lattice site, which is due to a missing atom in a crystalline structure, as depicted in Fig.3.1.

(ii) Interstitial defect

If an atom does not occupy a regular crystal site but a site between regular ones, it is referred to as an interstitial defect. An impurity or foreign atom and a host atom that occupy an irregular site are known as foreign interstitial and self-

interstitial, respectively as shown in Fig.3.2. In order for an atom to stay at an interstitial site, it must have sufficiently low energy there.

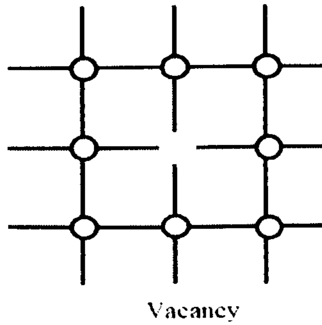

Fig.3. 1 Illustration of point defect: a vacancy in crystalline semiconductors.

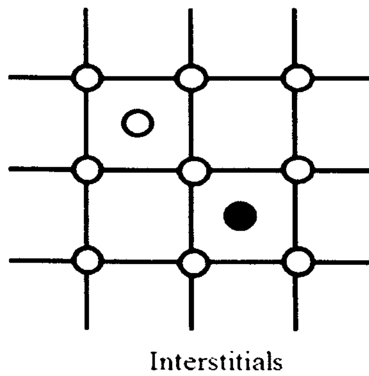

Fig.3.2 Illustration of point defect: Self Interstitial and foreign impurity interstitial (solid circle) defects in crystalline semiconductors.

(iii) Substitutional Impurity

When the host atom is replaced by some other foreign impurity atom, it is referred to as a substitutional impurity. Fig. 3. 3 shows an example of substitutional impurity atom on a As site. As a rule, impurity atoms that are chemically similar to atoms of the host crystal are incorporated substitutionally.

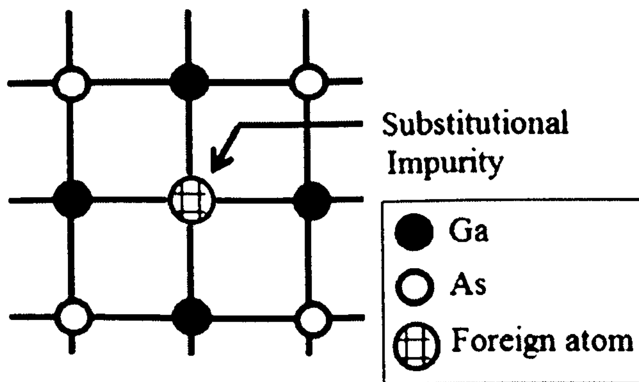

Fig.3.3 Schematic representation of substitutional defect in a crystal of GaAs.

(iv) Antisites

A special kind of substitutional defect occurs when a host atom occupies the site of another host atom. Such point perturbations are called antisite defects. For example in the case of GaAs, a Ga atom may be located at an As-site thus called an As antisite defect, and an As atom may occupy a Ga-site referred to Ga antisite defect as illustrated in Fig. 3.4 (a, b).

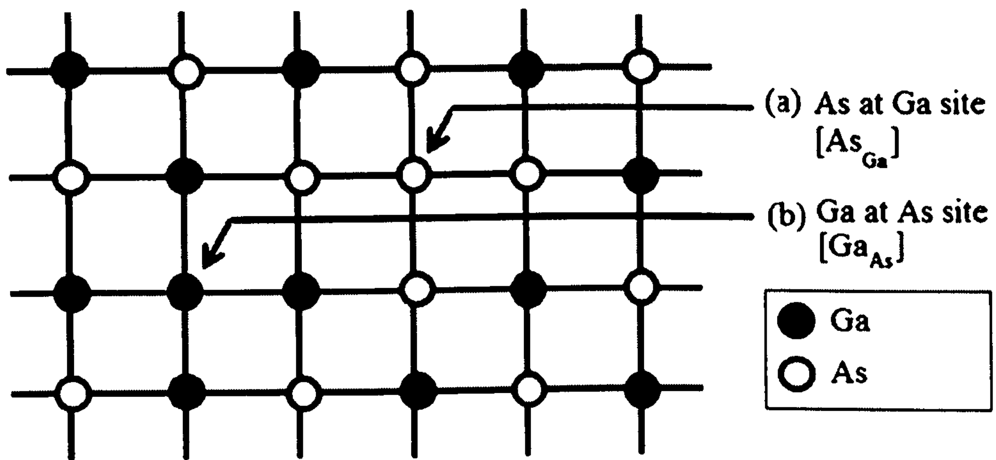

Fig.3.4 Schematic representation of (a) As antisite and (b) Ga antisite defects in a crystal of GaAs.

3.1.1.1 COMPLEXES OF THE POINT DEFECTS

Similar to the atoms bound in molecules, point perturbations may also be bounded to each other. They are called point perturbation complexes. The bonding can occur between various point perturbations. It may be between chemically identical or different impurity atoms, between impurity atoms and point defects, and among point defects themselves. Some brief description is given below.

(i) Donor-acceptor pairs

In the case of an ionised donor and an ionised acceptor, the lowering of total energy through the formation of a bound complex of associates is particularly obvious. The two point perturbations are differently charged and attract each other

through electrostatic forces. This leads to the formation of donor-acceptor pairs, in which the donor and acceptor atoms occupy neighbouring sites in the crystal.

(ii) Split-Interstitial

Split-interstitial is formed by replacing one atom from its regular site by the same pair of atoms in the interstitial positions in the crystal structure [see Fig. 3.5 (a)].

(iii) Frenkel Pair

If in a crystal, an atom moves from a regular site to an interstitial site and leaves behind a vacancy a defect pair is formed in this process that consists of a self-interstitial and a vacancy. It is known as a Frenkel defect or Frenkel pair as illustrated in Fig.3.5 (b).

(iv) Vacancy- Impurity

Vacancies also form complexes with inadvertent or deliberately introduced impurities in semiconductors as depicted in Fig.3.5 (c).

(v) Impurity Pair

Foreign atoms on interstitial sites may pair with themselves or with other impurity atom on the substitutional sites forming substitutional-interstitial pair. Fig. 3.5 (d) shows the defect pair formed by an impurity at a substitutional site with impurity atom at an interstitial site.

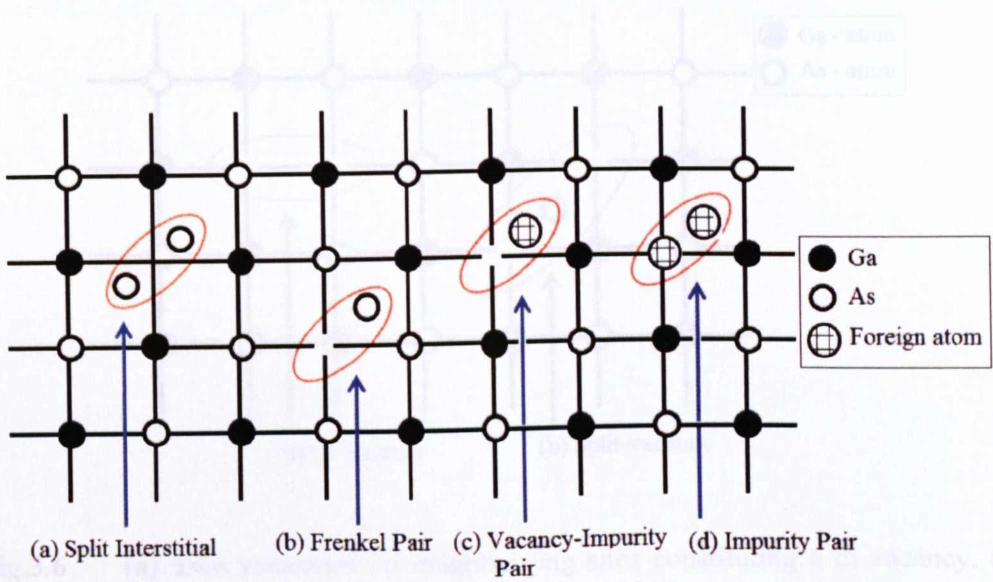

Fig.3.5 Illustration of different types of defect pairs (a) Split-interstitial, (b) Coupling of a vacancy with closest interstitial-a Frenkel pair, (c) Vacancy-impurity pair and (d) impurity-impurity pair.

(vi) Di- and multi-vacancies

The two vacancies on neighbouring sites in a crystal lattice form a vacancy pair known as di-vacancy as shown in Fig.3.6 (a). Analogous statements hold for the association of more than two vacancies, which are called multi-vacancies.

(vii) Split Vacancy

If two vacancies are separated by an interstitial atom, the complex defect is known as split vacancy as illustrated in Fig.3.6 (b).

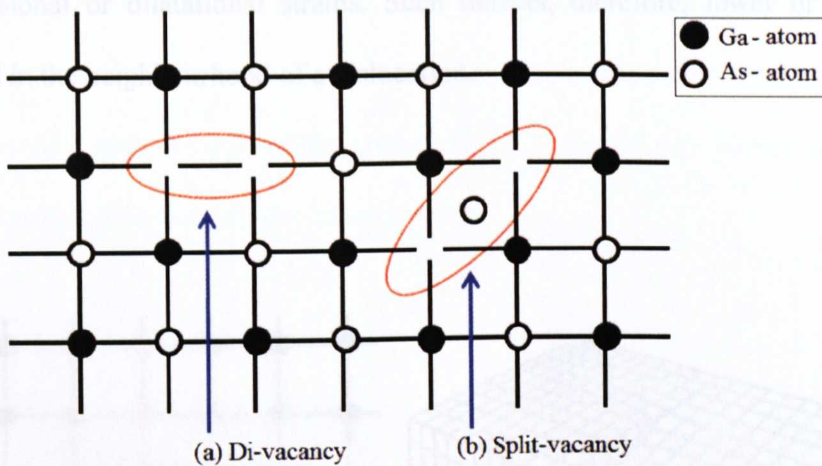

Fig.3.6 **(a)** Two vacancies on neighbouring sites constituting a di-vacancy, **(b)** Two vacancies are separated by an interstitial- Split vacancy.

(viii) Aggregates

If the complexes formed by point perturbations become larger and reach mesoscopic size, one refers to them as aggregates.

3.1.2 LINE DEFECTS

In a case where a whole row of atoms is displaced from their regular position in a crystal is called a line defect. This kind of imperfection is also known as dislocation which is the most common structural defect in semiconductors. There are two main dislocations, namely, edge dislocation and screw dislocation. The insertion of an extra half plane of atoms into the regular crystal is called edge dislocation as illustrated in Fig. 3.7 (a). If one part of the crystal is displaced with respect to other part then this type of defect is called screw dislocation as shown in Fig. 3.7 (b).

Due to the line defects, the material around the dislocation line has compressional or dilatational strains. Such defects, therefore, lower or raise the potential in the neighbourhood of a dislocation.

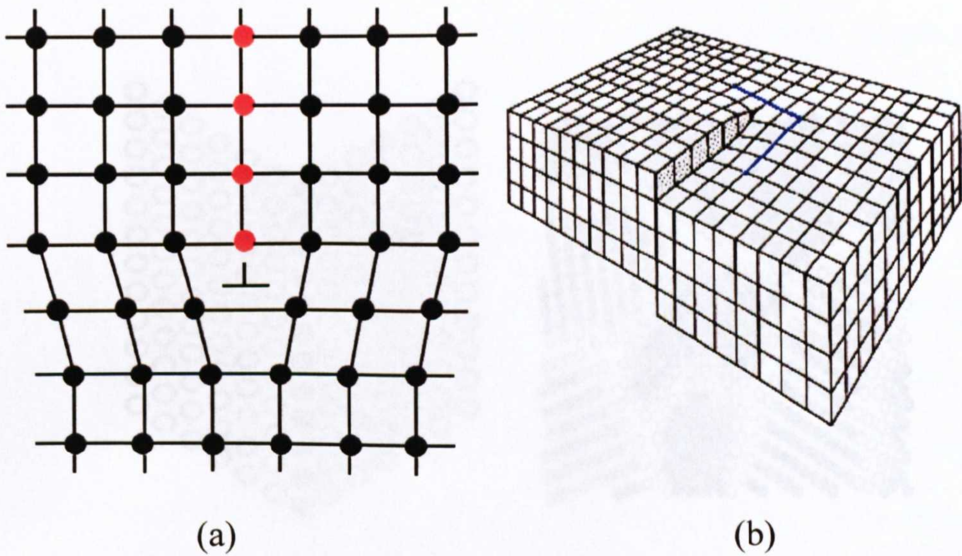

Fig.3.7 Line defects **(a)** Edge dislocation and **(b)** Screw dislocation

3.1.3 PLANAR DEFECTS

The planar defects correspond to a misplaced plane of atoms or boundaries of different orientation in a crystal. Stacking faults, twin boundaries and grain boundaries are examples of planar defects.

A change or interruption in the stacking sequence of the atomic planes produces stacking faults. A Grain boundary within a polycrystalline material separates regions of different crystalline orientation which are called grains. A grain

boundary whose lattice structures are mirror images of each other in the plane of the boundary is known as twin boundary. The influence of these defects is usually realised at the boundaries, which are charged and can attract compensating charges in the adjacent space charge of the crystal. Fig. 3.8 (a) and (b) illustrates the twin boundaries and grain boundaries respectively.

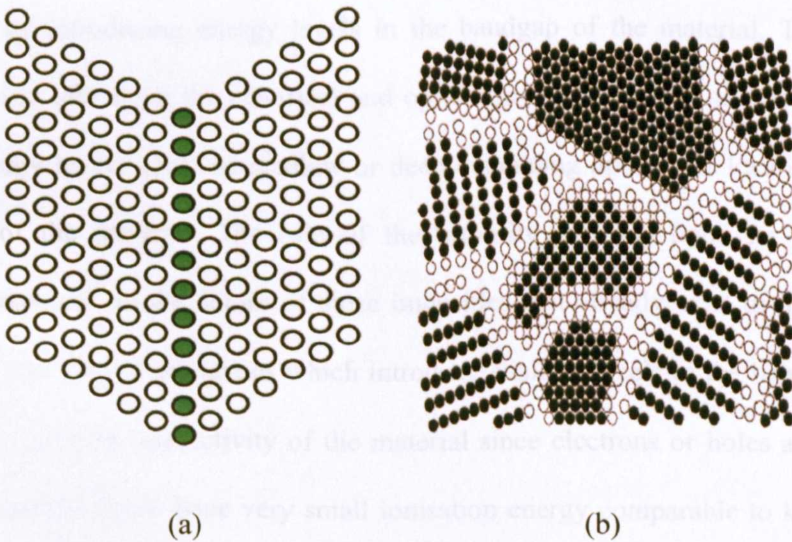

Fig.3.8 Illustration of planar defects **(a)** Twin boundaries **(b)** Solid circles represent atoms forming crystal grains and open circles are representing the atoms at crystal grain boundaries.

3.2 ROLE OF IMPURITIES IN SEMICONDUCTORS

There are usually two ways for a foreign impurity to accommodate itself inside the host lattice. It may either find an interstitial lattice site or it may substitute a host atom by replacing it. Substitutional impurities in elemental semiconductors may be divided into two types according to their position in the periodic table with respect to host atom. The first type is known as isovalent impurity which belongs to

the same column as the host element in the periodic table. The second type is donor or acceptor substitutional impurity that belongs to the right or left column of the host atom. For the case of compound semiconductors the same impurity can act as donor or accepter depending on which host atom is displaced by the impurity atom. This kind of impurity atom is known as amphoteric. A typical example is silicon in GaAs.

Any kind of impurity can play a very important role in semiconductor materials by introducing energy levels in the bandgap of the material. These can have specific effects on the electrical and optical properties of the semiconductors. These energy levels could be shallow or deep depending upon their location in the bandgap of the material. The role of the impurity depends upon its type and concentration and on the nature of those impurities that already exist in the crystal structure. The foreign impurities which introduce shallow levels in the bandgap can affect the electrical conductivity of the material since electrons or holes associated with the shallow levels have very small ionisation energy comparable to kT (0.025 eV at 300K, k is Boltzmann's constant). This means that they can be thermally ionised at room temperature and consequently they will increase the electrical conductivity of the material. For example a foreign impurity such as Si or Be incorporated in a pure GaAs material can change the electrical conductivity over many orders of magnitude with respect to intrinsic GaAs. These Si and Be impurities in GaAs in fact introduce shallow levels near the conduction and valence band and make the pure GaAs n-type (electrons are majority carriers) or p-type (holes are majority carriers), respectively . Shallow energy levels associated with Si and Be impurities in Si- and Be- doped GaAs are called shallow donors and shallow acceptors, respectively.

The control of the incorporation of shallow impurities is the key for controlling the carrier concentration that can make the semiconductor very useful for technological applications. A simple example of inhomogeneous semiconductors is a p-n junction which has a region doped with acceptors adjacent to a region doped with donors. One important property of the p-n junction is that when a positive bias is applied to the p-region and negative bias to the n-region current flows from the p region to the n region (the junction is forward biased). Virtually no current flows when the polarity of the applied voltages are reversed (the junction is reverse biased). This asymmetry of the current flow makes the p-n junction act as a rectifier of AC (alternating current) circuits. A solid state transistor which acts as a signal amplifier is of the same kind with two junctions consisting of three consecutive regions, p-n-p or n-p-n. Similarly a solid state three junctions p-n-p-n structure known as thyristor is a valuable device in power circuit applications. Under other conditions a p-n junction emits radiation or light at different wavelengths.

On the other hand deep levels do not contribute to the conduction mechanism like shallow levels and have some other role in controlling certain properties of the semiconductors. They are usually >100 meV away from the conduction and valence band. Fig. 3.9 illustrates the shallow and deep levels within the band gap of the host material. Deep levels can be incorporated deliberately or unintentionally during the growth process. They could be foreign impurities or inherent crystal imperfections. These energy levels can play an important role in the optical and electrical properties of the materials. They can for example act as non-radiative recombination centers, hindering the emission of photons and consequently have a strong influence on the optical quality of the material which is required to make lasers, and other optical and photonic devices.

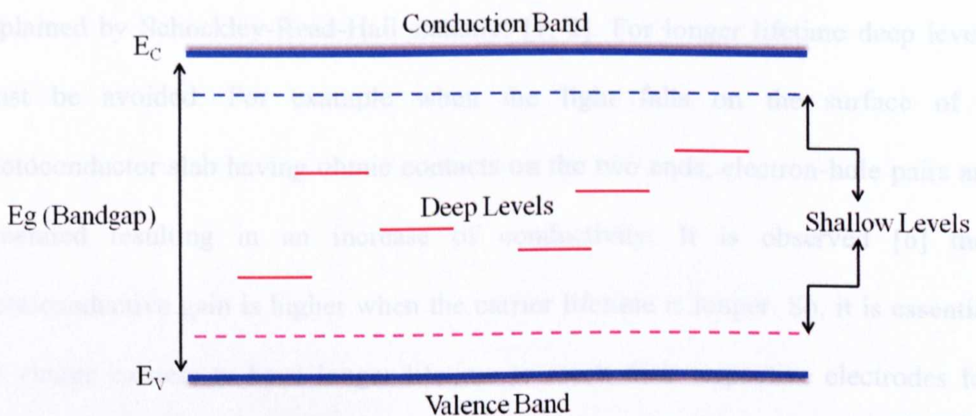

Fig.3.9 A simple band diagram of a semiconductor indicating the shallow and deep levels in the forbidden gap.

The recombination rate approaches a maximum as the energy level of the recombination center approaches midgap. Thus the most effective recombination centers are those which are located near the middle of the semiconductor band gap [3]. The large energy dissipated during the process is accomplished by a cascade process involving the successive emission of single phonons as the electron cascades down through the excited states of the center. This energy loss in the cascade process was proposed by Lax [4] in his work while measuring the capture cross-sections of electrons in semiconductors. The capture cross-section of a trap center is defined as a measure of how close the carrier has come to the recombination center to be captured [5].

Lifetime of the charge carriers is of significant importance and affects the performance of high speed switching devices. The presence of deep level impurities

in the semiconductor materials can control the lifetime of charge carriers as explained by Schockley-Read-Hall statistics [1, 2]. For longer lifetime deep levels must be avoided. For example when the light falls on the surface of a photoconductor slab having ohmic contacts on the two ends, electron-hole pairs are generated resulting in an increase of conductivity. It is observed [6] that photoconductive gain is higher when the carrier lifetime is longer. So, it is essential for charge carriers to have longer lifetime to reach their respective electrodes for collection excluding any substantial loss.

The radiative recombinations are the basis for emitting light from semiconductors. In this respect and for the manufacturing of light emitting diodes (LEDs) direct bandgap materials have a distinct advantage over indirect gap materials. However, an isovalent impurity introduced in the indirect band gap semiconductors can give the possibility to make LED diodes. A well-known example is substitutional nitrogen in GaP, which has been widely used for producing green LEDs. Similarly a Zn-O donor-acceptor complex pair in GaP introduces a 0.8eV deep level that can act as a radiative recombination center emitting light in the red spectrum [7].

3.3 DEFECTS AND THEIR CARRIER KINETICS

3.3.1 SHALLOW LEVELS: DONORS AND ACCEPTORS

The donor or acceptor impurity levels appear near the conduction or valence band edges in the semiconductor forbidden gap. They can provide electron to conduction band or hole to the valence band, respectively, depending upon the temperature condition. At very low temperature, electrons or holes stick with their

respective lattice sites. Near room temperature, the donors or acceptors are ionised and make the electrons or holes free to reside in the conduction or valence band. For simplicity let us consider the donor states case. The ions interact with free electrons with a Coulombic attraction. The attractive potential is given by

$$U(r) = \frac{-q^2}{4\pi r\varepsilon} \qquad 3.1$$

where q is the charge of carrier, r is the separation between two charge carriers and ε is dielectric constant of material.

This is similar to an electron in a hydrogen atom problem but with the electron having a different mass called the effective mass (m*). With this new mass the potential is reduced by a factor $\varepsilon_0 / \varepsilon$. The effective mass can be derived from the (E, k) relationship and is given by

$$\frac{1}{m^*} = \frac{4\pi^2}{h^2}\left(\frac{d^2E}{dk^2}\right).$$

The solution to this problem is given by

$$E_D = E_C - 13.6\left(\frac{m^*}{m_o}\right)\left(\frac{\varepsilon_0}{\varepsilon}\right)^2 eV \qquad 3.2$$

where E_C, E_D and ε_0 are the conduction band energy, donor level energy and relative dielectric constant, respectively.

To this particular case a good approximation for the Fermi level and electron/hole density relationship is provided by Joyce-Dixon [8].

$$E_F = E_C + k_B T\left[\left(\ln\frac{n}{N_C} + \frac{1}{\sqrt{8}}\left(\frac{n}{N_C}\right)\right)\right] eV \qquad \text{for n-type material} \qquad 3.3$$

$$E_F = E_V - k_B T\left[\left(\ln\frac{p}{N_V} + \frac{1}{\sqrt{8}}\left(\frac{p}{N_V}\right)\right)\right] eV \qquad \text{for p-type material}$$

where n, p and k_B are number of electrons in the conduction band, number of holes in the valence band and Boltzmann constant. The terms N_C and N_V are known as effective density of states in conduction and valence bands.

$$N_c = 2\left(\frac{2\pi\, m_e^* k_B T}{h^2}\right)^{3/2} \qquad N_v = 2\left(\frac{2\pi\, m_h^* k_B T}{h^2}\right)^{3/2}$$

3.3.2 DEEP LEVEL KINETICS

The energy states with energies more than 0.1 eV from the conduction or valence bands are usually referred to in literature as trap centers, recombination-generation centers and deep levels. These terms have precise meanings such that a state is a trap center or a recombination-generation center depending upon the doping conditions, capture cross-section and temperature. The emission and capture rates determine the occupancy of a center at equilibrium.

A defect center is defined as a trap center if a charge carrier captured by the center stays there until it is forced to emit into the band from where it came. An electron trap captures an electron from the conduction band and then re-emits it to the conduction band. This may happen for an empty center when the capture rate of an electron from the conduction band is much larger than the emission of hole to the

valence band. For a filled center this occurs when the emission rate of an electron is much larger than the capture rate of holes.

A center is called a generation center when empty it emits a hole to the valence band and when filled it emits an electron to the conduction band. On the other hand a center is called a recombination center when empty it captures an electron from the conduction band and when filled it captures a hole from the conduction band.

3.3.2.1 SHOCKLEY-READ-HALL THEORY

In the carrier recombination process there are two ways by which an electron and a hole can recombine. An electron from the conduction band can recombine with a hole in the valence band known as band to band recombination or direct recombination and if there exists a deep level the electron has a choice to recombine with the hole through the deep level known as indirect recombination as shown in Fig. 3.10 (a). A very successful theory for kinetics of charge carriers through intermediate centers (deep levels) has been worked out by Shockley, Read [1] and Hall [2] independently. According to this theory, four basic emission and capture processes can occur across a deep level of energy E_T as illustrated in Fig. 3.10 (b).

First Process: Emission of electrons from a deep level to conduction band.

The rate of electron emission 'R_e' is described by

$$R_e = e_n n_T \tag{3.4}$$

where 'e_n' is a proportionality constant and defined as the electron emission rate and n_T is the density of filled traps.

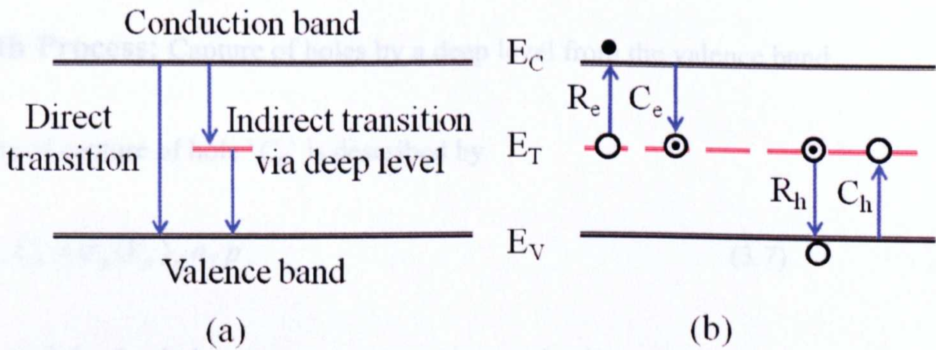

Fig.3.10 (a) Schematic diagrams of a band-to-band recombination (direct transition) and recombination through a deep level (indirect transition via an intermediate level E_T). (b) Illustration of four emission and capture processes of charge carriers (holes and electrons).

Second Process: Capture of electrons by a deep level from conduction band.

The rate of capture of electrons 'C_e' is described by

$$C_e = \sigma_n \langle V_n \rangle_{th} p_T n \tag{3.5}$$

where 'n' is the number of electrons in the conduction band, 'p_T' the concentration of empty deep states, 'σ_n' is the capture cross section and $<V_n>_{th}$ the average thermal velocity of the electrons. Essentially an electron with this thermal velocity must come within an area σ_n of the trap to be captured.

Third Process: Emission of holes from a deep level into valence band.

The rate of hole emission 'R_h' is described by

$$R_h = e_p p_T \tag{3.6}$$

where 'e_p' is the hole emission rate.

Fourth Process: Capture of holes by a deep level from the valence band.

The rate of capture of hole 'C_h' is described by

$$C_h = \sigma_p \langle V_p \rangle_{th} n_T p \tag{3.7}$$

where 'σ_p' is the hole capture cross-section and $\langle V_p \rangle_{th}$ is the average thermal velocity of the holes and 'p' the density of holes in the valence band, respectively.

The net rate of electrons leaving the conduction band is given by

$$\frac{-dn}{dt} = \sigma_n \langle V_n \rangle_{th} p_T n - e_n n_T \tag{3.8}$$

and the net rate of holes leaving the valence band is

$$\frac{-dp}{dt} = \sigma_p \langle V_p \rangle_{th} n_T p - e_p p_T \tag{3.9}$$

Thus the rate at which the density of filled traps increases is

$$\frac{dn_T}{dt} = R_e - C_e - R_h + C_h \tag{3.10}$$

$$\frac{dn_T}{dt} = \frac{-dn}{dt} + \frac{dp}{dt}$$

Utilising equations (3.8) & (3.9) in the above equation we have

$$\frac{dn_T}{dt} = \sigma_n \langle V_n \rangle_{th} p_T n - e_n n_T - \sigma_p \langle V_p \rangle_{th} n_T p - e_p p_T$$

If the total density of deep states

$$N_t = n_t + p_t$$

or $$p_t = N_t - n_t$$

So above equation becomes

$$\frac{dn_t}{dt} = \sigma_n \langle V_n \rangle_{th} n(N_t - n_t) - e_n n_t - \sigma_p \langle V_p \rangle_{th} n_t p + e_p (N_t - n_t)$$

$$\frac{dn_t}{dt} = N_t (\sigma_n \langle V_n \rangle_{th} n + e_p) - n_t (\sigma_n \langle V_n \rangle_{th} n + e_n + \sigma_p \langle V_p \rangle_{th} p + e_p)$$

or $$\frac{dn_t}{dt} = (c_n + e_p) N_t - (c_n + c_p + e_n + e_p) n_t \qquad (3.11)$$

where $c_n = \sigma_n < V_n >_{th} n$, $c_p = \sigma_p < V_p >_{th} p$ are capture coefficients of electrons and holes, respectively. These describe the rate of capturing electrons and holes. Equations (3.8), (3.9), and (3.11) are kinetic equations which completely describe the electron and hole densities in the conduction and valence bands as well as in deep levels at any time [9].

For steady state: $$\frac{dn_t}{dt} = 0$$

Equation (3.11) becomes $(c_n + e_p) N_T = (c_n + c_p + e_n + e_p) n_T$ (3.12)

Now the principle of detailed balance is a result of microscopic reversibility of electron kinetics, chemical, and other reactions. It is prerequisite for the establishment of thermal equilibrium which requires that forward and reverse reaction rates are identical for every single possible reaction path. The detailed

balance principle is used extensively in semiconductor statistics. Blakemore [10], Roosbroeck and Shockley [11] derived the formulae concerning the carrier lifetime for the intrinsic radiative recombinations. This approach was extended to extrinsic radiative processes by Sclar and Burstein [12].

The rates of creation and annihilation of free carriers in a semiconductor at thermal equilibrium are equal and this condition is termed as the detailed balance principle. According to the detailed balance principle;

$$R_e = C_e$$

$$R_h = C_h$$

i.e. $$e_n n_t = \sigma_n < V_n >_{th} p_t n \qquad (3.13)$$

$$e_p p_T = \sigma_p < V_p >_{th} n_T p \qquad (3.14)$$

Total density of deep levels is given by

$$N_t = n_t + p_t = N_T f + N_t (1 - f) \qquad (3.15)$$

where 'f' is the fermi-Dirac distribution function which gives the probability of an electron occupying the energy level 'E_T'.

From equation (3.15)

$$n_t = N_T f \qquad (3.16)$$

$$p_T = N_T (1 - f) \qquad (3.17)$$

The fermi-Dirac distribution function is given by

$$f = \left(\frac{1}{1 + \exp \frac{E_T - E_F}{k_B T}} \right) \tag{3.18}$$

Here E_T, E_F, k_B *and* T are energy of deep level, energy of fermi level, Boltzman constant and temperature respectively.

By using equations (3.16), (3.17), (3.18) and (3.13)

$$e_n N_T f = \sigma_n < V_n >_{th} n N_T (1 - f)$$

$$e_n = \sigma_n < V_n >_{th} n \exp\left(\frac{E_T - E_F}{k_B T} \right) \tag{3.19}$$

where "n" is the electron density, which is given by

$$n = n_i \exp\left(\frac{E_F - E_i}{k_B T} \right) = N_c \exp\left(-\frac{E_c - E_F}{k_B T} \right) \tag{3.20}$$

where $n_i = N_c \exp\left(\frac{E_i - E_c}{k_B T} \right)$ and N_c is the density of states in the conduction band.

By substituting equation (3.20) into (3.19)

$$e_n = \sigma_n < V_n >_{th} N_c \exp\left(-\frac{E_c - E_T}{k_B T} \right) \tag{3.21}$$

Similarly using equation (3.14) and $p = N_v \exp\left(-\frac{E_F - E_v}{k_B T} \right)$

$$e_p = \sigma_p < V_p >_{th} N_V \exp\left(-\frac{E_T - E_v}{k_B T} \right) \tag{3.22}$$

where N_c, N_v, $<V_n>_{th}$, $<V_p>_{th}$ are the density of states in the conduction band, density of states in the valence band, thermal velocity of electrons and thermal velocity of holes, respectively and given by the following equations.

$$N_c = 2\left(\frac{2\pi\, m_e^* k_B T}{h^2}\right)^{3/2}, \quad N_v = 2\left(\frac{2\pi\, m_h^* k_B T}{h^2}\right)^{3/2}, \quad <V_n>_{th} = \left(\frac{3k_B T}{m_e^*}\right)^{1/2},$$

$$<V_p>_{th} = \left(\frac{3k_B T}{m_h^*}\right)^{1/2}$$

where m_e*, m_h* are effective masses of electrons and holes.

If these values are substituted in corresponding equations (3.21) & (3.22) and all constant values are replaced by a single constant 'A'

then we get $e_n = A\,T^2\sigma_n \exp\left(-\frac{E_C - E_T}{k_B T}\right)$

where, $A = 2\left(\frac{2\pi m_e^* k_B}{h^2}\right)^{3/2}\left(\frac{3k_B}{m_e^*}\right)^{1/2}$

$$e_p = A\,T^2\sigma_p \exp\left(-\frac{E_T - E_V}{kT}\right)$$

or, $e_p = A\,T^2 N_p \exp\{-(E_T - E_V)\}$

The Arrhenius plot of $\log\left(\frac{e_{n,p}}{T^2}\right)$ versus $\left(\frac{1}{T}\right)$ yields a straight line and slope of this line gives the activation energy of the deep level which is the most important parameter that indicates the position of the deep level in the forbidden gap.

3.4 DEFECTS IN DILUTE NITRIDE SEMICONDUCTORS

Nitrogen incorporates in the GaAs lattice by replacing As atoms substitutionally and creates localised energy states near the conduction band edge which leads to an enormous bowing of the bandgap [13] that affects the electrical and optical properties of the materials [14]. However, it also occupies the non-substitutional sites in the lattice of GaAs which facilitates the formation of various defects that can degrade the quality of the crystal leading to a decrease in the optical efficiency [15] and carrier lifetime [16, 17].

Several kinds of point defects such as N-interstitials, As-antisites and Ga-vacancies in dilute nitrides have been reported in the literature. From thermodynamic calculations, Zhang and Wei [18] have showed the presence of substitutional N [Fig.3.11(a)], N–N split interstitial [Fig.3.11(b)] that can form a midgap electron state and Ga vacancies [Fig.3.11(c)] which were reported to be in the MBE and MOVPE-grown material [19]. Some of the nitrogen related defects in GaAs and their properties are given below.

(i) The presence of nitrogen interstitials in GaAs has been evident by nuclear reaction analysis (NRA) and Rutherford Backscattering Spectrometry (RBS) channeling studies [20- 22]. Energetically active defects due to nitrogen interstitial and their complexes such as (N-As) and (N-N) split interstitials have also been reported by several groups [23, 24]. First principle studies show that split interstitials emerge as lowest energy configurations. According to the calculations the formation energy for N-N and As-N defects are similar because the changes in the bond lengths N-N, and As-N are similar but N-N possess less strain on the crystal than that of As-N due to their chemical potential difference [25, 26].

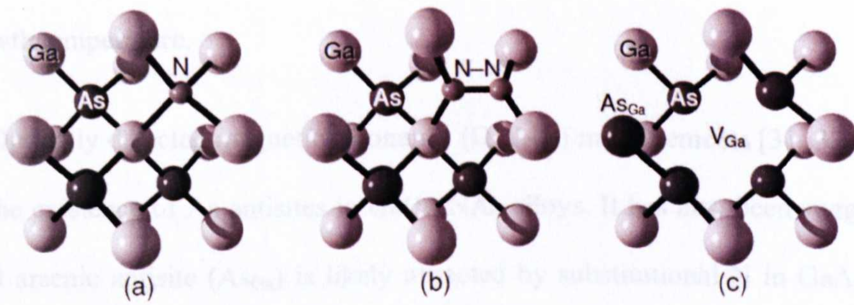

Fig.3.11 Illustration of (a) substitutional N, (b) N–N split interstitial, and (c) Ga vacancy and As antisite (after Zhang and Wei [18]).

Another study reported on N-interstitials in dilute nitride materials by W. J. Fan *et al.* [27] shows that most of the N interstitials form N–As complex and N–N complex in a very small number. T. Ahlgren *et al.* [28] studied the concentration of N interstitials in GaAsN and found that substitutional N increases with the increase of N contents in GaAsN. However, for N concentration in the range 0.7% to 3% the N interstitials remains constant to a value 2.3×10^{19} cm^{-3}. They concluded that these could be among the most important non-radiative recombination centers which are usually responsible for the decrease in optical efficiency of nitride materials.

(ii) Another important defect state in dilute nitride materials is the Ga vacancy. It is also found in GaAs materials as an isolated Ga vacancy or as a vacancy-Ga complex. Positron annihilation spectroscopy measurements have established the formation of Ga vacancies in Ga(In)NAs alloys [29, 30] and shown that the defect concentration increases with the increase of N content in the alloy. Li. W. Pessa *et al.* [29] have attributed the defects creation during MBE growth to the energetic N

ions from the radio frequency plasma source and also to low adatom mobility at the low growth temperature.

(iii) Optically detected magnetic resonance (ODMR) measurements [31, 32] have shown the existence of As antisites in Ga(In)NAs alloys. It has also been suggested [18] that arsenic antisite (As_{Ga}) is likely attracted by substitutional N in GaAs and forms a complex (N_{As}–As_{Ga}) which is an efficient non-radiative center.

(iv) Space charge techniques such as deep level transient spectroscopy (DLTS) have been considered very powerful techniques for the characterization of electrically active defects in semiconductors. For example, P. Krispin *et al.* [33] have reported the study of deep levels in dilute nitrides. They have found several hole traps denoted by HK1-HK5 in MBE grown p-type GaAsN samples. Trap level HK1 (0.16 eV) was found to be highest at the interface of GaAsN/GaAs. HK2 (0.39 eV) and HK5 (0.69 eV) are similar to the traps found in the GaAs grown by liquid phase epitaxy (LPE) and were assigned to Ga_{As} (Ga on As site). HK3 (0.35 eV) level has been assigned to copper impurities form N cell and HK4 (0.45 – 0.55 eV) has been considered to be due to iron impurities.

P. Kripsin *et al.* [34] have also examined N-related electron traps in Si-doped GaAsN samples. Two electron traps were identified at 0.8 eV and 1.1 eV above the valence band edge. They have tentatively been assigned to (N-N) and (As-N) split interstitials, respectively. Both (N-N) and (As-N) split interstitials have theoretically been predicted to create compression strain in the crystal [35]. (N-N) split interstitial defect has been predicted to trap both holes and electrons.

3.4.1 EFFECTS OF THERMAL ANNEALING

Thermal annealing of semiconductors shows various effects on the electrical, optical and structural properties of the materials. There is an extensive study of annealing effects on improvement of PL emission and point defects evolution in dilute nitride semiconductor materials.

Thermal annealing can have several effects including (1) the introduction of new defects in the band gap of the semiconductor materials (2) the decrease of the concentration of the existing defects and (3) the complete removal of the existing defects. For example, deep levels denoted by M1, M3 and M4 in Ref. [36] are commonly present in Si-doped MBE grown GaAs as identified by Lang [36]. After annealing, a decrease in the concentration of defects M1 and M4 along with a complete removal of defect M3 have been reported. Rapid thermal annealing of GaAs samples at 800 ^{0}C for 15 minutes has been found to introduced the well known electron trap level EL2 [37].

In a DLTS study of MOCVD grown p-type GaAsN, rapid thermal annealing at 600 ^{0}C to 900 ^{0}C for 30 sec generated six new deep levels which are stable at 900 ^{0}C [38] but on the other hand the existing interstitial N–As complex and other non-radiative defects were found to be effectively removed by thermal annealing [39].

Annealing effects on the optical properties of dilute nitride materials have been observed by several groups and an increase in the PL signal intensity after annealing has been reported. This improvement of the PL efficiency is commonly attributed to the annihilation of point defects in the dilute nitride materials. For example, P. Uusimaa [40] has investigated the annealing effects on PL intensity and found that PL intensity increases with the increase of annealing temperature up to

750 ^{0}C. Similarly Rao *et al.* [41] have seen higher PL intensity with sharper PL line-widths after post-growth heat treatments at 650 ^{0}C. They have suggested this enhancement in the PL properties is due to the complete annihilation of non-radiative point defect (N-H complex).

3.4.2 EFFECTS OF HYDROGEN IRRADIATION

Hydrogen irradiation produces remarkable effects on the electronic properties of semiconductors. Since the hydrogen atom has a high chemical reactivity, it makes bonds with other lattice atoms and neutralises the dangling bonds. This has the effect of eliminating non-radiative recombination centres including shallow and deep levels from the bandgap of the semiconductor materials [42].

The study related to hydrogen-nitrogen interaction has been reported by many researchers [43-50]. When hydrogen is incorporated in dilute nitride alloys it can exists as an interstitial (H-H) molecule, a single-hydrogen atom (monoatomic), or two-hydrogen atoms (diatomic) having high chemical activity so that they can make a bond with nitrogen atoms. However, the nature of interaction of the hydrogen-nitrogen atoms is still an answerable question. In an investigation of InGaAsN using Hall experiment, Xin *et al.* [51] have suggested that H atom could act like a donor atom and it can makes the material slightly n-type. Whereas some other studies have shown that it can act as a N passivating agent [52] that can neutralise the N atom by making di-hydrogen complexes with N.

Janotti *et al.* [53] have studied the atomic structure and stability of different hydrogen-nitrogen configurations by using first-principle total-energy calculations method. They have demonstrated theoretically that the mono-atomic H behaves like a donor in GaAsN for all the H-related energy states. However, it is not agreed with

theory [54] about the role of mono-atomic H in conventional semiconductors such as GaAs where single hydrogen atom can act as a donor or acceptor depending upon the relative Fermi level position. For the other configuration which involves two H atoms (di-atomic hydrogen) and a N atom, they have found that H_2^*-N complex is more stable than other existing H-H interstitial molecules. In addition, $H2^*$-N complex has been considered to be responsible for the reversal of band gap reduction in GaAsN materials [53].

The H atom can make a complex with lattice defects present in the crystal. For example, theoretical calculations [55] show that the presence of N atom in GaAs favour the formation of Ga vacancies (V_{Ga}) in GaAsN materials. These V_{Ga} are anticipated to interact with the H atom to form a (N–H–V_{Ga}) complex in the dilute nitride materials. The increase of V_{Ga}-related complexes has been experimentally demonstrated by J. Toivonen *et. al.* [56] in MOVPE grown GaAsN layers.

3.5 DEFECTS IN DILUTE BISMIDE SEMICONDUCTORS

Dilute bismide alloys are very important because of three interesting properties. Firstly it disturbs the valence band maxima of GaAs instead of affecting the conduction band which is vital for electron mobility. Secondly, for the same alloy concentration, Bi redshifts the bandgap of GaAs more than four times as compared to Sb or In. The large reduction of the band gap of the GaAs due to the incorporation of Bi is of great interest for devices operating in the long wavelength region [57, 58]. The substitution of As by Bi in GaAs develops a compressive strain due to the large difference in the radii of Bi and As atoms. The localised potential of Bi and the surrounding lattice relaxation change the electronic band structure of GaAs considerably. The incorporation of highly lattice mismatched impurity (Bi)

also creates structural defects that could deteriorate the crystal quality of GaAs. In addition, due to tendency of the Bi to surface-segregate under normal GaAs growth temperature [59], the incorporation of Bi in GaAs requires reduced temperature growth that itself leads to the formation of defects which can act as non-radiative recombination centers. However, the large difference of atomic potentials and electronegativity have produced localised states close to the valence band maxima of GaAs which can act as trapping centers for the bound holes that could reduce the non-radiative centers.

The investigations about the defect states in dilute bismide materials have not been reported comprehensively. However, the spatial distribution of Bi atoms in the bismide alloy studied by G. Giatto *et al.* [60] has shown that at 1.9% Bi, Bi distributed randomly, whereas at 2.4%Bi, it makes pairs and clusters that affects the electronic and optical properties of this material system. Some of the bismuth related defects in GaAs and properties are given below.

(i) The most important effect of Bi in GaAsBi is that the band of GaAs decreases drastically by incorporating a few percent of Bi in GaAs.

(ii) M. Kunzer *et al.* [61] have reported the presence of antisite defects in GaAsBi layers. In their studies of defects identification by using electron spin resonance (ESR) technique they have observed that a substantial amount of Bi, about 10%, have occupied the Ga site rather than substituting As in the crystal. This has the effect of increasing the resistivity and carrier trapping rate in the GaAsBi material.

(iii) A sequence of stacking faults along the interface of GaAs/GaAsBi have been observed in the high resolution transmission microscopic (HRTEM) studies, reported by J. F. Rodrigo *et al.* [62].

(iv) Time-resolved terahertz spectroscopy measurements have been performed on dilute GaAs bismide and nitride alloys by D. G. Cooke *et al.* [63]. They determined the electron mobility for $GaAs_{1-x}N_x$ (x=0.84) and $GaAs_{1-x}Bi_y$ (y=0.84%) epi-layers. Their experiments reveals the electron mobility of 2800 cm^2 /V s at a carrier density of 2.7×10^{18} cm^{-3} for bismide layers and 920 cm^2 /V s at a carrier density of 1.9×10^{18} cm^{-3} for dilute nitride layers. So in terms of electron mobility, the Bi incorporation in GaAs does not decrease the electron mobility significantly as compared to that of GaAsN materials.

(v) The band gap of the GaAsBi have been investigated and found to be temperature insensitive by using photoluminescence (PL) [64, 65], and photoreflectance (PR) measurements [66].

(vi) Photoluminescence (PL) and electroluminescence (EL) studies at room temperature by Lewis *et al.* [67] on p-i-n GaAsBi structure show that the PL peaks are blue shifted relative to the EL peaks which might be due to shallow localized states in the bismide alloy. This is because of the fact that Bi tends to behave as an impurity rather than an alloying element.

3.5.1 EFFECTS OF THERMAL ANNEALING

Thermal annealing has been used as an efficient solution to improve the physical properties of epitaxial semiconductor materials. The presence of structural

defects such as stacking faults, point defects such as antisites and non-radiative recombination centers have been proposed in GaAsBi layers. Whereas, post-growth thermal annealing studies of GaAsBi layers have shown the improvement in the luminescence intensity.

Rodrigo *et. al.* [62] have reported the influence of thermal annealing on the structural and optical properties of the GaAsBi layers grown by MBE. They have found that after annealing at 473 K for 3 hours, the mosaic structure of the layer has disappeared, the presence of the defects reduced significantly and PL intensity has improved.

In another study, I. Moussa *et al.* [68] have used high resolution x-ray diffraction (HRXRD) to investigate the effect of annealing on the crystalline structure of GaAsBi. They have reported that above an annealing temperature of 750 °C the structure stability degraded significantly. However, they have observed a clear increase in the PL intensity after thermal annealing and suggested 700 °C the optimal annealing temperature for GaAsBi alloy.

REFERENCES

[1] W. Shockley and W. T. Read, Phys. Rev. 87, 835 (1952).

[2] R.N. Hall, Phys. Rev. 87, 387 (1952).

[3] J. S. Yuan and Juin J. Liou, Semiconductor device physics and simulation, published by Plenum press, New Yark, 1998.

[4] M. Lax, Phys. Rev. 119, 1502 (1960).

[5] H. F. Wolf, Semiconductors, Wiley-Interscience, 1971

[6] T. S. Moss, G. J. Burrel and B. Ellis, Semiconductor Opto-Electronics, Butterworth, London, 1973.

[7] J. S. Jayson, R. Z. Bachrach, P. D. Dapkus, and N. E. Schumaker, Phys. Rev. B 6, 2357 (1972).

[8] W. B. Joyce and R. W. Dixon, Appl. Phys.Lett., 31, 354 (1977).

[9] H.G. Grimmeiss and C. Overn, J. Phys. E. Sci. Instruments, 14, 1032 (1981).

[10] J. S. Blakemore, Semiconductor Statistics, Pergamon Press, Oxford, New York (1962).

[11] Von Roosbroeck and W.Shockely, J. Phys. C. 17, 6521 (1954).

[12] N.Sclar and E.Burstein, Phys. Rev., 98, 1757 (1955).

[13] L. Bellaiche, S. H. Wei and A. Zunger, Phys. Rev. B 54, 17 568 (1996).

[14] S.A. Ding, S. R. Barman, K. Horn, H.Yang, B. Yang, O. Brandt and K. Ploog, Appl. Phys. Lett., 70 2407 (1997).

15] I. A. Buyanova, W. M. Chen, BMonemar, H. P. Xin, and C. W. Tu, Appl. Phys. Lett., 75, 3781 (1999).

[16] S. R. Kurtz, A. A. Allerman, C. H. Seager, R. M. Seig and E. D. Jones, Appl. Phys. Lett., 77, 400 (2000).

[17] A. Fleeck, B. J. Robinson and D. A. Thompson, Appl. Phys. Lett., 78, 1694 (2001).

[18] Wei, S. B. Zhang and Su-Huai, Phys. Rev. Lett., 86, 1789 (2001).

[19] W. Li, M. Pessa, T. Ahlgren, and J. Dekker, Appl. Phys. Lett., 79, 1094 (2001).

[20] S. G. Spruytte, C. W. Colden, J. S. Harris, W. Wampler, P. Krispin, K. Ploog and M. C. Larson, J. Appl. Phys., 89, 4401 (2001).

[21] W. Li, M. Pessa, T. Ahlgren and J. Decker, Appl. Phys. Lett., 79, 1094 (2001).

[22] T. Ahlgren, E. Vainonen-Ahlgren, J. Likonen, W. Li and M. Pessa, Appl. Phys. Lett., 80, 2314 (2002).

[23] P. Carrier, Su-Huai Wei, S. B. Zhang, and Sarah Kurtz, Phys. Rev. B 71, 165212 (2005).

[24] J. E. Lowther, S. K. Estreicher, and H. Temkin, Appl. Phys. Lett., **79**, 200 (2001).

[25] E. Arola, J. Ojanen, H-.P. Kosma and T.T. Rantala, Phys. Rev. B 72, 045222 (2005).

[26] K. Laaksonen, H-.P. Kosma, T. T. Rantala and R. M. Nieminen, Cond. Matter, 20, 235231 (2008).

[27] W. J. Fan, S. F. Yoon, T. K. Ng, S. Z. Wang, and W. K. Loke, R. Liu and A. Wee, Appl. Phys. Lett., 80, 4136 (2001).

[28] T. Ahlgren, E. Vainonen-Ahlgren, J. Likonen, W. Li and M. Pessa, Appl. Phys. Lett., 80, 2314 (2002).

[29] W. Li, M. Pessa, T. Ahlgren and J. Decker, Appl. Phys. Lett., 79, 1094 (2001).

[30] J. Toivonen, T. Hakkarainen, M. Sopanen, H. Lipsanen, J. Oila and K. Saarinen, Appl. Phys. Lett., 82, 40 (2003).

[31] N. Q. Thinh, I. A. Buyanova, P. N. Hai, W. M. Chen, H. P. Xin and C. W. Tu, Phys. Rev. B, 63, 033203 (2001).

[32] N. Q. Thinh, I. A. Buyanova, W. M. Chen, H. P. Xin and C. W. Tu, Appl. Phys. Lett., 79, 3089 (2001).

[33] P. Krispin, S. G. Spruytte, J. S. Harris and K. H. Ploog, J. Appl. Phys., 89, 6294, (2001).

[34] P. Krispin, V. Gambin, J. S. Harris and K. H. Ploog, J. Appl. Phys., 93, 6095, (2003).

[35] B. Q. Sun, D. S. Jiang, Z. Pan, L. H. Li and R. H. Wu, J. Cryst. Growth, 227-228 (2001).

[36] D. V. Lang, A. Y. Cho, A. C. Gossard, M. Ilegems and W. Wiegmann, J. Appl. Phys., 47, 2558 (1976).

[37] Akio Kitagawa, Akira Usami, Takao Wada, Yutaka Tokuda, Hiroyuki Kano, J. Appl. Phys., 65, 606 (1989).

[38] Qiang Gao, Hark Hoe Tan, Chennupati Jagadish, and Prakash N. K. Deenapanray, Jpn. J. Appl. Phys., 42, 6827 (2003).

[39] S. Z. Wang, S.F. Yoon, W.K. Loke, C.Y. Liu and S. Yuan, J. Crys. Growth 255, 258 (2003).

[40] Petri Melanen Pekka Savolainen Petteri Uusimaa Wei Li, Jani Turpeinen and Markus Pessa, Appl. Phys. Lett., 78, 91, (2001).

[41] E. V. K. Rao, A. Ougazzaden, Y. Le Bellego, and M. Juhel, Appl. Phys. Lett., 72, 1409 (1998).

[42] A. Amore Bonapasta, F. Filippone, P. Giannozzi, M. Capizzi and A. Polimeni, Phys. Rev. Lett., 89, 216401 (2002).

[43] A. Polimeni, G. Baldassarri, M. Bissiri, M. Capizzi, M. Fischer, M. Reinhardt, and A. Forchel, Phys. Rev. B 63, 201304(R) (2001).

[44] A. Polimeni, M. Bissiri, M. Felici, M. Capizzi, I. A. Buyanova, W. M. Chen, H. P. Xin, and C. W. Tu, Phys. Rev. B 67, 201303(R) (2003).

[45] A. Polimeni, A. Baldassarri Hoeger von Hoegersthal, F. Masia, A. Frova, M. Capizzi, S. Sanna, V. Fiorentini, P. J. Klar, and W. Stolz, Phys. Rev. B 69, 41201 (2004).

[46] A. Polimeni, G. Ciatto, L. Ortega, F. Jiang, F. Boscherini, F. Filippone, A. Amore Bonapasta, M. Stavola, and M. Capizzi, Phys. Rev. B 68, 085204 (2003).

[47] P. J. Klar, H. Grüning, M. Güngerich, W. Heimbrodt, J. Koch, T. Torunski, W. Stolz, A. Polimeni, and M. Capizzi, Phys. Rev. B 67, 121206 (2003).

[48] I. A. Buyanova, M. Izadifard, I. G. Ivanov, J. Birch, W. M. Chen, M. Felici, A. Polimeni, M. Capizzi, Y. G. Hong, H. P. Xin, and C. W. Tu, Phys. Rev. B 70, 245215 (2004).

[49] M. Bissiri, G. Baldassarri, A. Polimeni, M. Capizzi, D. Gollub, M. Fischer, M. Reinhardt, and A. Forchel, Phys. Rev. B 66, 033311 (2002).

[50] F. Jiang, Michael Stavola, M. Capizzi, A. Polimeni, A. Amore Bonapasta, and F. Filippone, Phys. Rev. B 69, 041309 (2004).

[51] H. P. Xin, C. W. Tu, and M. Geva, Appl. Phys. Lett., 75, 1416 (1999).

[52] A. Amore Bonapasta, F. Filippone, P. Giannozzi, M. Capizzi and A. Polimeni, Phys. Rev. Lett., 89, 216401 (2002).

[53] A. Janotti, S. B. Zhang, Su-Huai Wei and C. G. Van de Walle, 89, 086403 (2002).

[54] S. K. Estreicher, Mater. Sci. Eng. Rep. 14, 319 (1995).

[55] A. Jannoti, S. H. Wei, S. B. Zhang, S. Kurtz and C. G. Van de Walle, Phys. Rev. B, 67, 161201 (2001).

[56] J. Toivonen, T. Hakkarainen, M. Sopanen, H. Lipsanen, J. Oila and K. Saarinen, Appl. Phys. Lett., 82, 40 (2003).

[57] S. Tixier, M. Adamcyk, T. Tiedje, S. Francoeur, A. Mascarenhas, P. Wei, and F. Schiettekatte, Appl. Phys. Lett., 82, 2245 (2003).

[58] Y. Tominaga, Y. Kinoshita, K. Oe, and M. Yoshimoto, Appl. Phys. Lett., 93, 131915 (2008).

[59] E. C. Young, M. B. Whitwick, T. Tiedje and D.A. Beaton, phys. stat. sol. (c) 0002 (2003).

[60] G. Ciatto, E. C. Young, F. Glas, J. Chen, R. Alonso Mori, and T. Tiedje, Phys. Rev. B 78, 035325 (2008).

[61] M. Kunzer, W. Jost, U. Kaufmann, H. M. Hobgood and R.N. Thomas, Phys. Rev. B 48, 4437 (1993).

[62] J.F. Rodrigo, D.L. Sales, M. Shafi, M. Henini, L. Turyanska, S. Novikov and S. I. Molina, Applied Surface Science, 256, 5688 (2010).

[63] D. G. Cooke, E.C. Young, F.A. Hegmann and T. Tiedje, Appl. Phys. Lett., 89, 122103 (2006).

[64] K. Oe and H. Okamoto, Jpn. J. Appl. Phys., Part 2 37, L1283 (1998).

[65] K. Oe, Jpn. J. Appl. Phys., Part 1 41, 2801 (2002).

[66] J. Yoshida, T. Kita, O. Wada, and K. Oe, Jpn. J. Appl. Phys., Part 1 42, 371 (2003).

[67] R. B. Lewis, D. A. Beaton, X. Lu and T. Tiedje, J. Cryst. Growth, 311, 1872 (2009).

[68] I. Moussa , H. Fitouri , Z. Chine , A. Rebey and B. El Jani, Semicond. Sci. Technol. 23, 125034 (2008).

CHAPTER 4

EXPERIMENTAL TECHNIQUES

This chapter describes the electrical [conventional deep level transient spectroscopy (DLTS); Laplace DLTS (LDLTS)], and optical [Photoluminescence (PL) spectroscopy; optical transmission spectroscopy] characterisation techniques used to investigate the semiconductor samples presented in this thesis. The hardware and software required to implement these methods are also presented. The conventional DLTS and LDLTS are space-charge capacitance techniques and function in the space charge region of a p-n junction or Schottky diode. The properties of Schottky diodes, which were utilised to study deep traps, will be discussed. PL is one of the very useful optical spectroscopy tools to investigate optical dynamical processes occurring in semiconductor materials.

4.1 SCHOTTKY DIODES: PROPERTIES AND CHARACTERISATION

4.1.1 ENERGY BAND DIAGRAM

A Schottky junction can be obtained by making contact between a metal with a work function (Φ_m) and an n-type semiconductor of electron affinity (χ_n) and work function (Φ_s) assuming no interfacial layer exists ($\Phi_m > \Phi_s$). The positions of the Fermi levels in the semiconductor and metal are different when isolated. However,

when they are brought into contact electrons move from semiconductor to metal until the Fermi levels equilibrate. Uncompensated donor ions are therefore left behind in the space charge region situated in the semiconductor. The energy band diagram of a Schottky junction shown in Fig. 4.1 is sketched with the requirements of constant Fermi level and vacuum level in the thermodynamic equilibrium condition.

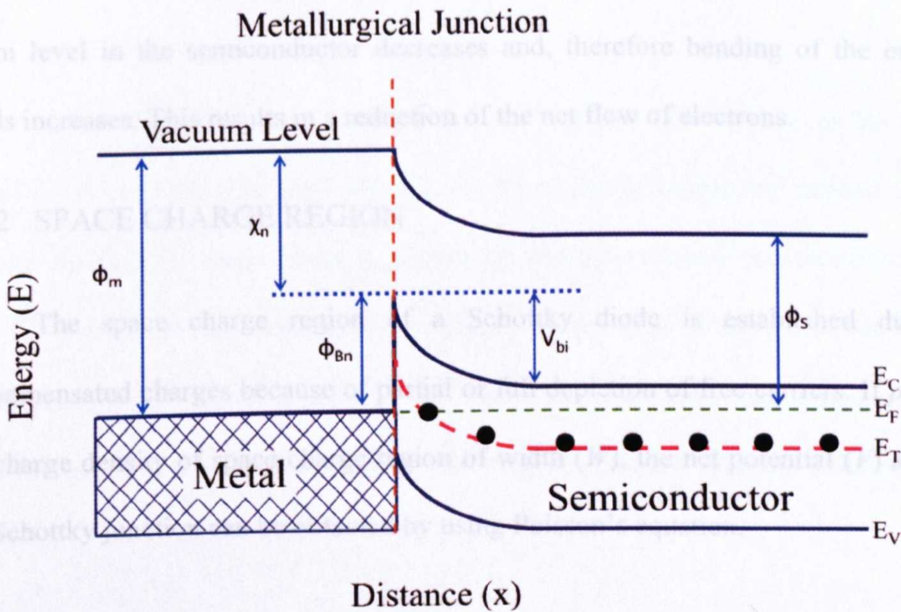

Fig.4.1 Energy band diagram of Schottky junction.

For an ideal Schottky junction, the Schottky barrier (Φ_{Bn}) from metal to semiconductor and the built-in potential (V_{bi}) from the semiconductor to metal are given by $\Phi_{Bn} = \Phi_m - \chi_n$ and $V_{bi} = \Phi_m - \Phi_s$, respectively.

When an external voltage is applied across the junction it changes the flow of electrons across the junction. The junction is reverse biased when a negative voltage

(V_R) is applied to the metal with respect to the semiconductor and the junction is said to be forward biased when a positive voltage (V_F) is applied to the metal. In the case of forward biased junction, the total potential across the junction is decreased to (V_{bi} - V_F). The Fermi level in the semiconductor rises with respect to that of the metal so that the energy band bending is reduced which allows an increase of the net flow of electrons from semiconductor to metal. On the other hand when the junction is reverse biased, the total potential across the junction is increased to ($V_{bi} + V_R$). The Fermi level in the semiconductor decreases and, therefore bending of the energy bands increases. This results in a reduction of the net flow of electrons.

4.1.2 SPACE CHARGE REGION

The space charge region of a Schottky diode is established due to uncompensated charges because of partial or full depletion of free carriers. If $\rho(x)$ is the charge density of space charge region of width (W), the net potential (V) across the Schottky junction can be obtained by using Poisson's equation.

$$V = \frac{1}{\varepsilon_s}\int_0^W x\,\rho(x)\,dx \qquad (4.1)$$

where ε_s is the dielectric constant of semiconductor and x is the distance from the junction into the semiconductor.

If $\rho(x)$ is uniform in the space charge region as given by $\rho(x) = -qN_d$, equation (4.1) reduces to:

$$W = \left(2\varepsilon_s \frac{V}{qN_d}\right)^{1/2} \qquad (4.2)$$

where N_d is the density of donor ions in the space charge region.

Equation (4.2) gives the relationship between the width of the space charge region and the total potential across the Schottky junction.

For the forward bias and reverse bias conditions, equation (4.2) can be rewritten as:

Forward bias: $$W = \left(2\varepsilon \frac{(V_{bi} - V_F)}{qN_d} \right)^{1/2}$$

Reverse bias: $$W = \left(2\varepsilon \frac{(V_{bi} + V_R)}{qN_d} \right)^{1/2}$$

In the ideal case, it is assumed that there are no free carriers in the space charge region and the boundary between the space charge region and neutral region is very sharp. This assumption is known as depletion region approximation. In reality, there exists a small transition region around this boundary which is not completely free from mobile carriers [1]. This small transition region is known as Debye length. The empirical formula for the width (L_D) of this region is give by

$$L_D = \sqrt{\frac{\varepsilon_s k_B T}{q^2 N_d}} \qquad (4.3)$$

where k_B is the Boltzmann's constant and T is the temperature in Kelvin.

Depletion region approximation is reasonably satisfied when the space charge region is much larger than the Debye length. For instance, under reverse bias when the space charge region becomes reasonably larger, this is convincingly a good approximation [1].

4.1.3 CAPACITANCE ASSOCIATED WITH SPACE CHARGE REGION

Differential capacitance associated with space charge region of a Schottky junction can be expressed as

$$C' = \frac{dQ}{dV_R} \tag{4.6}$$

Where dQ is the charge in the space charge region when a reverse bias dV_R is applied.

The differential capacitance is related to the width of the space charge region by the expression:

$$C' = \frac{A\varepsilon_s}{W} \tag{4.7}$$

Equation (4.7) is similar to the expression for the parallel plate capacitor of area A and separation W between plates.

Thus, the capacitance of a reverse biased junction using equations (4.7) and (4.2) can be written as:

$$C' = \frac{dQ}{dV_R} = \frac{A}{2}\left(\frac{2\varepsilon_s qN_d}{V_{bi} + V_R}\right)^{1/2} \tag{4.8}$$

Equation (4.8) shows that as the applied reverse bias is increased the capacitance of the diode decreases.

The capacitance-voltage characteristics of a Schottky junction allow the measurement of the background doping concentration and doping concentration profile of the semiconductor. The plot of $1/C^2$ versus V_R results in a straight line and the slope of this line gives the doping concentration whilst the intercept at $1/C^2 = 0$ yields the built-in-voltage across the junction.

4.2 DEEP LEVEL TRANSIENT SPECTROSCOPY (DLTS)

Almost all defects characterization techniques available to date are based on the measurement of space charge region variations with the applied pulse biases. The basic principle of the DLTS is to perturb the occupancy of a trap by applying a variable reverse bias to the Schottky diode. Lang [2] in 1974 introduced a method which allows the measurement of the capacitance changes associated with space charge region. This measurement as a function of time allows the carriers emission process from the deep levels. This can be then used to determine different parameters associated with the defect.

To understand the principle and operation of the DLTS technique, one must have some basic knowledge of the capacitance transients arising from the space charge region of a Schottky diode.

4.2.1 CAPACITANCE TRANSIENTS

Consider a schottky diode formed on the n-type semiconductor with uniform donor density N_d. For simplicity let us assume that the electron trap located at energy E_T in the bandgap with a uniform density N_T. A pulse with fixed repetition frequency is applied to the diode. The pulse with width t_P repeats between reverse bias V_R and filling bias V_P (where $V_P < V_R$). Fig. 4.2 (a) shows the diode under steady state condition, V_R is applied to the sample such that all the traps are empty of charge and there is no net flow of the charge carriers in the space charge region. When the reverse bias V_R decreases to V_P for a short interval of time by a bias pulse as shown in Fig. 4.2 (b), the space charge region width decreases. As a result of the decrease in the space charge region, the electrons from the conduction band will flow to the

region that was previously depleted of carriers and the traps within this region will capture these electrons.

Assuming there is only filling of the traps and no emission of charge carriers during the bias V_P, from the Kinetics of capture process (equation (3.11) Chapter 3), the rate equation for the density of filled traps is given by

$$\frac{dn_T}{dt} = c_n\left(N_T - n_T\right) \tag{4.9}$$

Where n_T is density of filled traps and c_n is the capture coefficient of electrons, and it is defined as

$$c_n = \sigma_n < V_n >_{th} n \tag{4.10}$$

where $<V_n>_{th}$ is the mean thermal velocity of the electron, σ_n is the carrier capture cross-section and $n = N_d - N_T \approx N_d$ is the effective doping concentration.

If the duration of the bias pulse is long enough, then all the trap levels will be filled by electrons i.e. $n_T = N_T$. By the end of the pulse, the sample is returned to the quiescent reverse bias 'V_R' as shown in Fig. 4.2 (c) and the depletion region is again depleted of free carriers. The filled levels start to emit electrons so that the concentration of the filled trap 'n_T' will vary again and this variation can be expressed from the kinetics of emission process by the following rate equation.

$$\frac{dn_T}{dt} = e_p N_T - n_T\left(e_p + e_n\right) \tag{4.11}$$

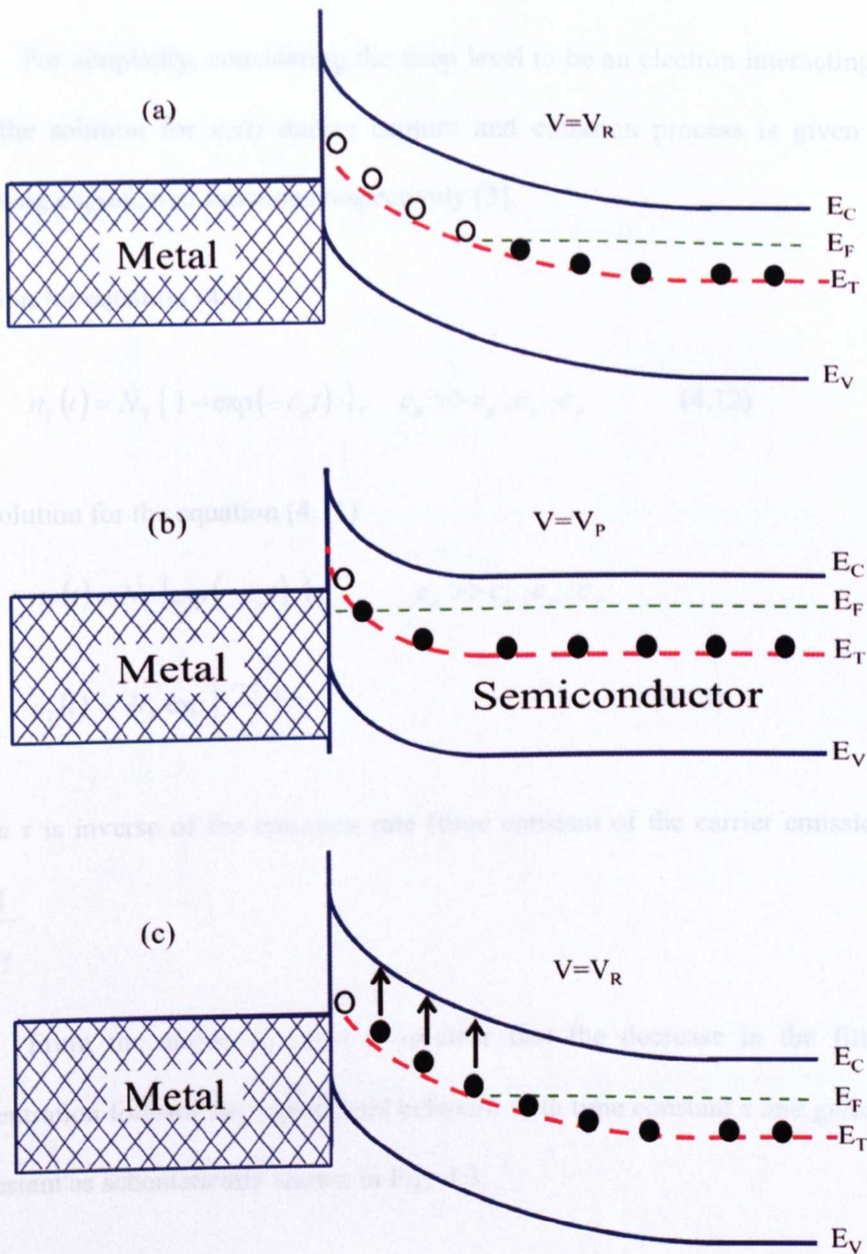

Fig.4.2 Energy band diagram of Schottky diode with electron trap E_T with a uniform density N_T. **(a)** the junction at steady reverse bias V_R (traps are emptied) **(b)** the junction at applied bias V_P (carrier filling of the traps) **(c)** the junction at applied quiescent bias V_R (emission of carriers).

For simplicity, considering the deep level to be an electron interacting centre then the solution for $n_T(t)$ during capture and emission process is given by the following exponential functions respectively [3].

Solution for equation (4.9)

$$n_t(t) = N_t\{1 - \exp(-c_n t)\}, \quad c_n >> e_n, e_p, c_p \qquad (4.12)$$

and solution for the equation (4.11)

$$n_t(t) = N_t\{\exp(-e_n t)\}, \qquad e_n >> c_n, e_p, c_p$$

or $$n_T(t) = N_T \exp\left(\frac{-t}{\tau}\right) \qquad (4.13)$$

where τ is inverse of the emission rate (time constant of the carrier emission): i.e. $\tau = \frac{1}{e_n}$.

From the above equation it is clear that the decrease in the filled trap concentration follows the exponential behavior with time constant τ and gives rise to a transient as schematically shown in Fig. 4.3.

Since it is difficult to measure the change in the concentration of the filled traps with time directly, so the simplest indirect method is to monitor the capacitance changes of a junction associated with the concentration variations.

So by including the contribution of the filled traps $n_T(t)$ in the space charge region, equation (4.8) is given as

$$C = \frac{dQ}{dV_R} = \frac{A}{2}\left(\frac{2\varepsilon_s qN_d^*}{V_{bi} + V_R}\right)^{1/2} \qquad (4.14)$$

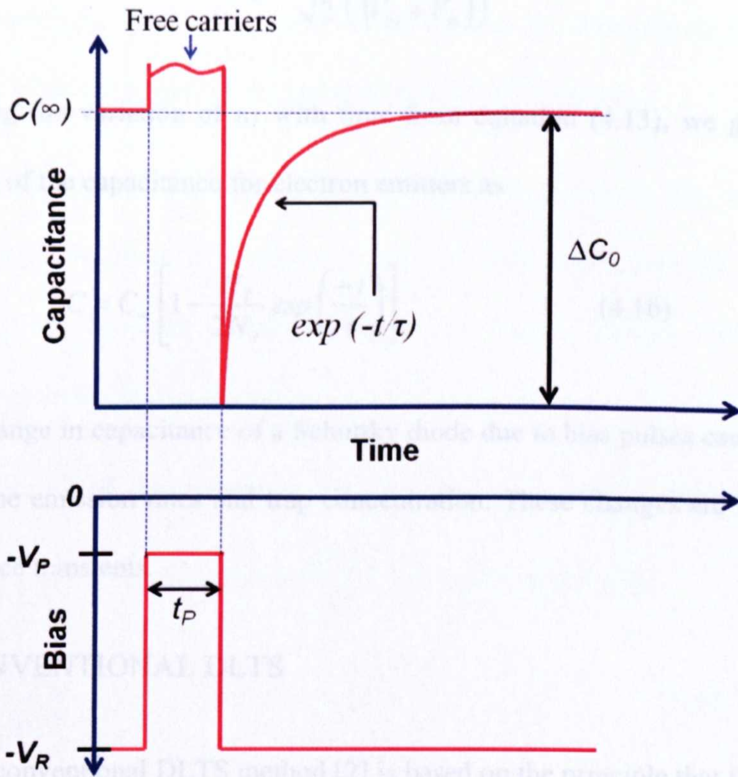

Fig.4.3 Capacitance transient response of a Schottky diode by applying a reverse bias pulse.

where $N_d^* = N_d - n_T$.

For $n_T << N_d$, equation (4.14) can be expanded and we get the expression for the capacitance as [3]

$$C = C_\infty \left(1 - \frac{n_T}{2N_d}\right) \qquad (4.15)$$

where C_∞ is the steady state capacitance at reverse bias 'V_R' and is given by

$$C_r = \frac{A}{\sqrt{2}}\left(\frac{\varepsilon_s qN_d}{(V_{bi}+V_R)}\right)^{1/2}$$

By including the variation of n_T with time from equation (4.13), we get the time dependence of the capacitance for electron emitters as

$$C = C_r\left[1-\frac{N_T}{2N_d}exp\left(\frac{-t}{\tau}\right)\right] \qquad (4.16)$$

Thus the change in capacitance of a Schottky diode due to bias pulses can be used to determine the emission rates and trap concentration. These changes are in the form of capacitance transients.

4.2.2 CONVENTIONAL DLTS

The conventional DLTS method [2] is based on the principle that the junction capacitance is sampled at two different times t_1 and t_2 ($t_2>t_1$) during the carrier emission process. The difference in capacitance $[C(t_1)-C(t_2)] = \Delta C$ is at a certain temperature T is the output signal (S) of the conventional DLTS technique. Using equation (4.16), the DLTS signal (S) is given by

$$\Delta C(t) = C(t_2) - C(t_1) = \Delta C_o\left[exp\left(\frac{-t_1}{\tau}\right) - exp\left(\frac{-t_2}{\tau}\right)\right]$$

$$\text{or}\quad S(T) = \Delta C_0\left[\exp\left(\frac{-t_1}{\tau}\right) - \exp\left(\frac{-t_2}{\tau}\right)\right] \qquad (4.17)$$

where ΔC_o is the maximum change in capacitance and given by

$$\Delta C_o = \frac{C_r N_T}{2N_d}$$

The emission rates of the carriers also depend upon the temperature of the diode and therefore, the DLTS signal (S) changes as the temperature (T) changes. Equation (4.17) is the output of the conventional DLTS system.

The realization of the idea of DLTS method is shown in Fig. 4.4 (a). The DLTS signal (S) is small for $\tau \ll (t_1\text{-}t_2)$ and $\tau \gg (t_1\text{-}t_2)$. Whereas, the intensity of DLTS signal (S) becomes significant when $\tau \sim (t_1\text{-}t_2)$. Thus, a DLTS peak is constructed as shown in Fig. 4.4 (a).

The value of the maximum DLTS signal S_{max} can be determined from equation (4.17) by using the relation $\dfrac{dS(T)}{d\tau} = 0$ which is given by

$$\tau_{max} = \left(\frac{t_2 - t_1}{\ln\left(t_2 / t_1\right)} \right), \qquad (\text{for } \tau = \tau_{max}) \qquad (4.18)$$

Equation (4.18) is called rate window. The value of the rate window can be changed by choosing different values of t_1 and t_2. Different rate windows correspond to different peak positions with respect to temperature in the DLTS spectra as shown in Fig. 4.4 (b). Thus the activation energy of the trap can be determined by measuring the emission rates as a function of temperature using different rate windows and then plotting them in the Arrhenius plot as shown in Fig. 4.4 (c).

Moreover, equations (4.17) and (4.18) show that the peak height of the DLTS signals is independent of the absolute value of t_1 and t_2 rather it depends upon their ratio. Further, S_{max} is proportional to ΔC_0, therefore, to the trap concentration N_T. Hence the DLTS peak height can directly give the trap concentration.

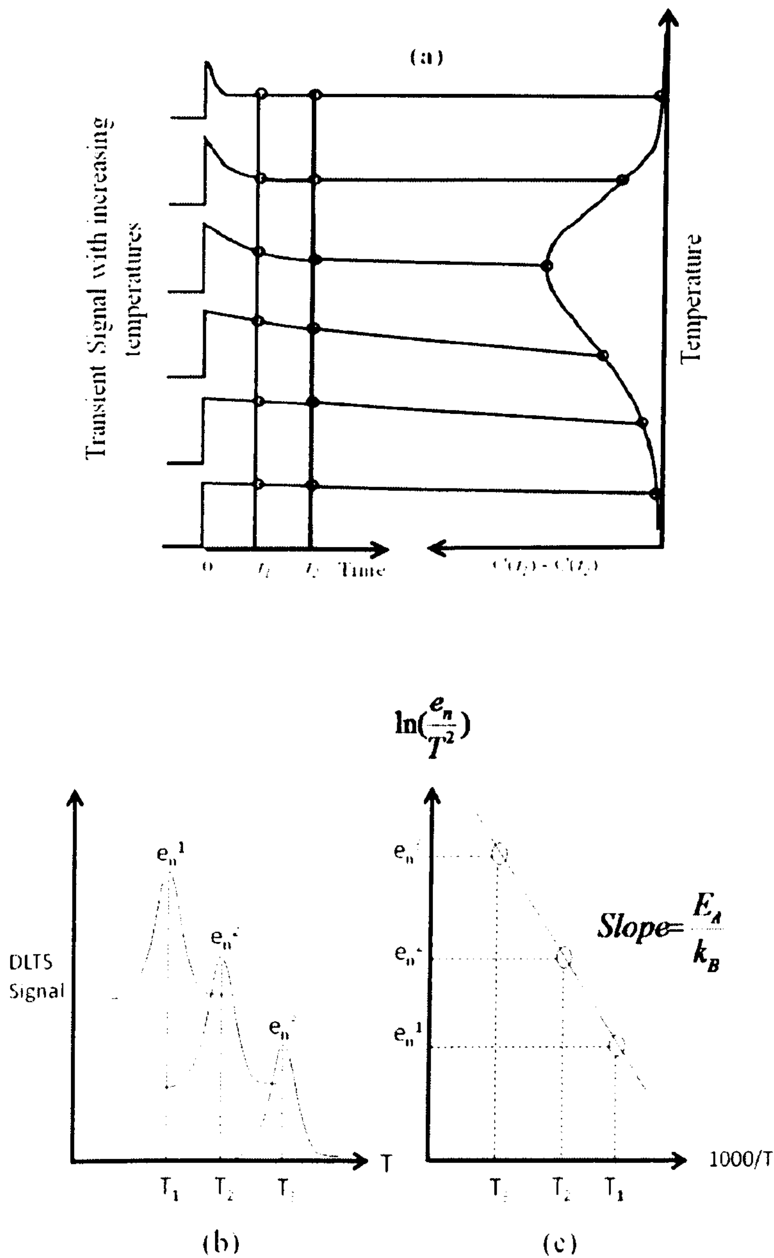

Fig.4.4 (a) Schematic diagram illustrating the formation of DLTS spectra. (b) DLTS spectra taken at different rate windows. (c) The emission rates versus temperature are plotted in the Arrhenius plot to determine the activation energy of the trap.

4.2.3 LAPLACE DLTS SPECTROSCOPY

Although the DLTS method is widely used in studying deep level impurities and defects in semiconductors, it is not entirely free from problems. One of them is accurate temperature measurement in the thermal scanning technique [4], where the temperature of the diode is continuously increased or decreased. Lang *et al.* [4] pointed out that the thermally scanned techniques are less accurate for determining the activation energies than the isothermal transient techniques. Secondly, the time constant resolution of the standard DLTS is too poor for studying the fine structure during the emission process. For example, even for a perfect defect with no complicated factors, standard DLTS produces a spectrum of broad peak and any variation in the time constant during the emission from the defect center contributes in further broadening of the peak [5]. Thus, the resolved structure is not achievable unless the time constants are well separated. Laplace DLTS spectroscopy is the advanced version of DLTS technique in which these concerns are addressed and improvements in resolution have been made.

Laplace DLTS spectroscopy is an isothermal technique in which the sample is held at a constant temperature. This will allow digitising the analog transient output of the capacitance meter using digital schemes and averaging many digitised transients acquired during the emission process in order to increase the signal to noise ratio.

All of the assessable time constants are determined from the obtained wave form by the software which is based on the Laplace transformation scheme [6].

The mathematical approach, which has been utilised for the quantitative description of the capacitance transients, is given by

$$f(t) = \int_0^{\infty} F(s)\, e^{-st}\, ds \qquad (4.19)$$

where f(t) is the recorded transient and F(s) represents the spectral function.

The mathematical representation of the capacitance transient given in the equation (4.19) is the Laplace transforms of the true spectral function F(s). The capacitance transient acquired by the Laplace DLTS is shown in Fig. 4.5 (a). Thus, to find out the real spectrum of the emission rates F(s) present in the transient, it is therefore essential to exploit an appropriate algorithm that efficiently performs an inverse Laplace transform on the recorded transient *f(t)*.

To do so three main algorithm routines known as FLOG, CONTIN and FTIKREG have been used in Laplace DLTS technique [6]. The result of such procedure is a spectrum of delta-like peaks for the mono- and multi-exponential transients as illustrated in Fig. 4.5 (b). The parallel use of the three numerical routines raise the confidence level in the spectra obtained. The high resolution of the Laplace DLTS technique is shown in Fig. 4.6 which illustrates a comparison of standard DLTS spectra (inset of Fig. 4.6) and Laplace DLTS spectra obtained from the same (Si: Au, H) sample [7].Standard DLTS gives a broad featureless spectrum whilst Laplace DLTS resolves the spectrum into two peaks.

4.2.4 DLTS APPLICATIONS

Capacitance transient spectroscopy is considered to be a very powerful tool for determining important properties of electrically active deep levels, as described in the following sections.

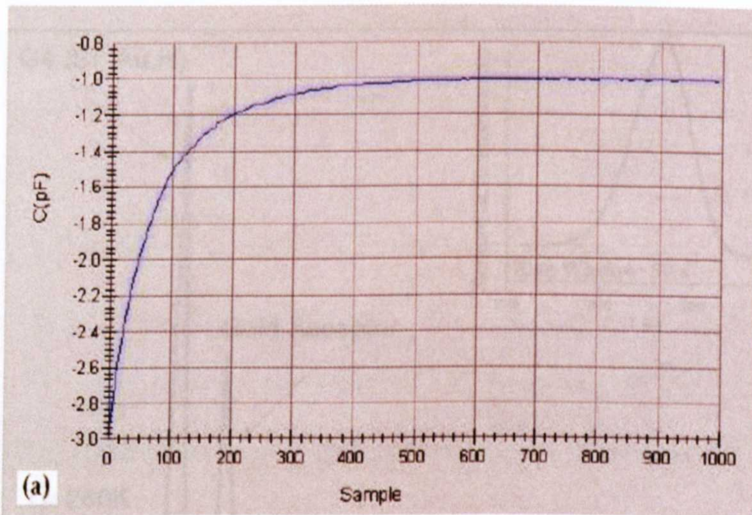

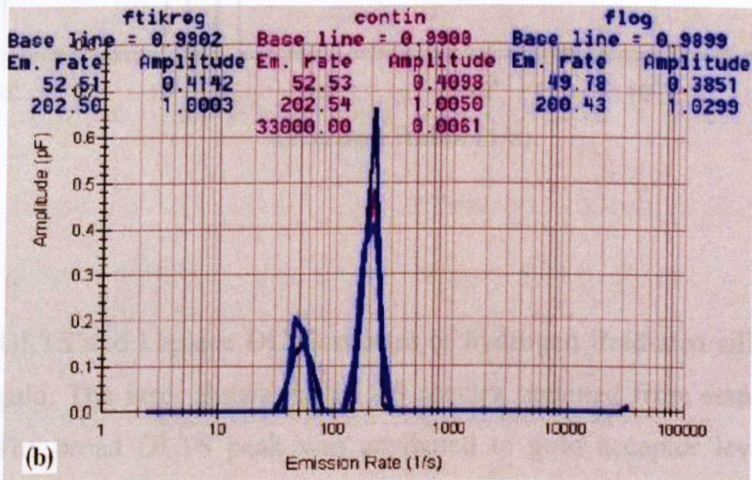

Fig.4.5 The illustration of the capacitance transient obtained from LDTS software.(b) the corresponding spectra determined from the capacitance transient with the use of three numerical routines.

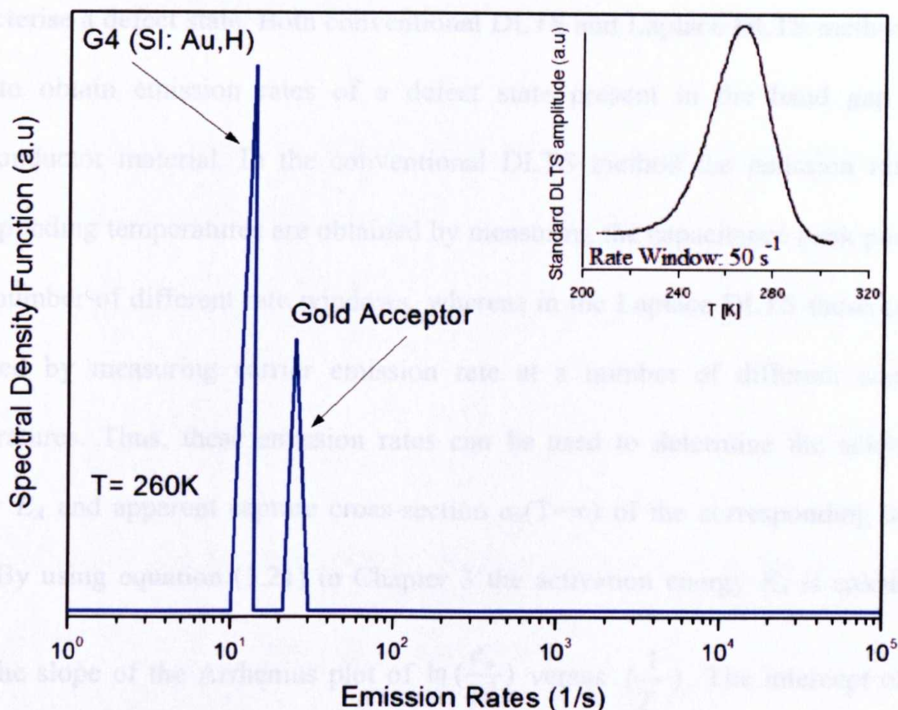

Fig.4.6 DLTS and Laplace DLTS spectra of hydrogen irradiated silicon sample containing gold. The inset shows the DLTS spectra obtained from standard DLTS technique. The broad DLTS peak was attributed to gold acceptor level G4. The Laplace DLTS resolved the spectra into two peaks which were attributed to gold acceptor and gold-hydrogen level in Ref. [7].

4.2.4.1 EMISSION RATE SIGNATURES

Emission rates are basic fingerprints that can be assigned uniquely to characterise a defect state. Both conventional DLTS and Laplace DLTS methods are used to obtain emission rates of a defect state present in the band gap of a semiconductor material. In the conventional DLTS method the emission rates at corresponding temperatures are obtained by measuring the capacitance peak position for a number of different rate windows, whereas in the Laplace DLTS these can be obtained by measuring carrier emission rate at a number of different constant temperatures. Thus, these emission rates can be used to determine the activation energy E_A and apparent capture cross-section $\sigma_n(T=\infty)$ of the corresponding defect state. By using equation (3.21) in Chapter 3 the activation energy E_A is calculated from the slope of the Arrhenius plot of $\ln(\frac{e_n}{T^2})$ versus $(\frac{1}{T})$. The intercept of the Arrhenius plot gives the value of the apparent capture cross-section $\sigma_n(\infty)$, assuming that σ_n is temperature independent. Direct measurements of σ_n, which is not based on the emission of the carriers rather based on the trapping of the carriers by the defect center, are explained below.

4.2.4.2 CAPTURE CROSS-SECTION MEASUREMENTS

The direct capture cross-section of a defect centre can be measured by using the filling-pulse method. In this process, measurements are carried out by reducing the filling pulse width (t_P) that causes the incomplete filling of the trap. This leads to a direct analysis of the capture process. The amplitude $S(t_P)$ of the DLTS peak varies with the different applied pulse widths (t_P). Thus, from the capture

kinetics, the peak height (S) is related to the filling pulse width (t_p) through the following equation [8].

$$1 - \frac{S(t_p)}{S(\infty)} = \exp\left(\frac{-t_p}{\tau_c}\right) \quad (4.20)$$

where, $S(\infty)$ is the saturated or maximum peak amplitude corresponding to the complete filling of the trap with carriers.

Capture cross-section σ_n of a defect centre is given by the following relation [8].

$$\sigma_n = \frac{1}{\tau_c \langle V_n \rangle_{th} n} \quad (4.21)$$

where $\langle V_n \rangle_{th}$ is the thermal velocity of the carrier and n is the free carrier concentration. The value of the capture time constant $\frac{1}{\tau_c}$ can be determined from the slope of the graph of $\ln\left(1 - \frac{S(t_p)}{S(\infty)}\right)$ versus t_p using equation (4.20) and then σ_n can be obtained by using equation (4.21).

One of the characteristic of the capture cross section is its dependence on temperature. However, it can be temperature independent. In a case where σ_n is thermally activated, it is found to follow the behaviour expressed by [9].

$$\sigma_n(T) = \sigma_\infty \exp\left(\frac{-E_\sigma}{k_B T}\right) \quad (4.22)$$

where E_σ is the energy barrier to capturing the electrons and σ_∞ is the apparent value of the capture cross-section which is obtained from the intercept of the Arrhenius plot.

4.2.4.3 TRAP CONCENTRATION

Total change in the capacitance yields the total amount of traps whose occupancy was changed during the filling. As discussed earlier in section 4.2.2 that the DLTS signal S is proportional to the magnitude of the capacitance transient ΔC_o. Assuming all the traps have been filled i.e. $n_T = N_T$, equation (4.15) can be rewritten as [2].

$$\Delta C_o = C_\infty\left(1 - \frac{N_T}{2N_d}\right) - C_\infty$$

For $N_T << N_d$. $$\frac{\Delta C_o}{C_\infty} = \frac{N_T}{2N_d} \quad (4.23)$$

where C_∞ is the steady state capacitance of the diode at reverse bias (V_R), N_d is the doping concentration of shallow levels and N_T is the trap concentration. Thus, DLTS peak amplitude gives a direct measure of the trap concentration.

4.3 SYSTEM HARDWARE IMPLEMENTATION

This section describes the hardware required to implement a flexible conventional DLTS and Laplace DLTS system. A computer with a data acquisition card (i.e. analog to digital signal converter) provides overall system control via GPIB interface to all equipments of the system including capacitance meter, current-voltage meter, pulse generator and the cryostat temperature controller. The block diagram and photograph of the DLTS system is shown in Fig. 4.7 (a, b). The overall DLTS/ Laplace DLTS system is capable of operating over the temperature range of 10K to 450 K.

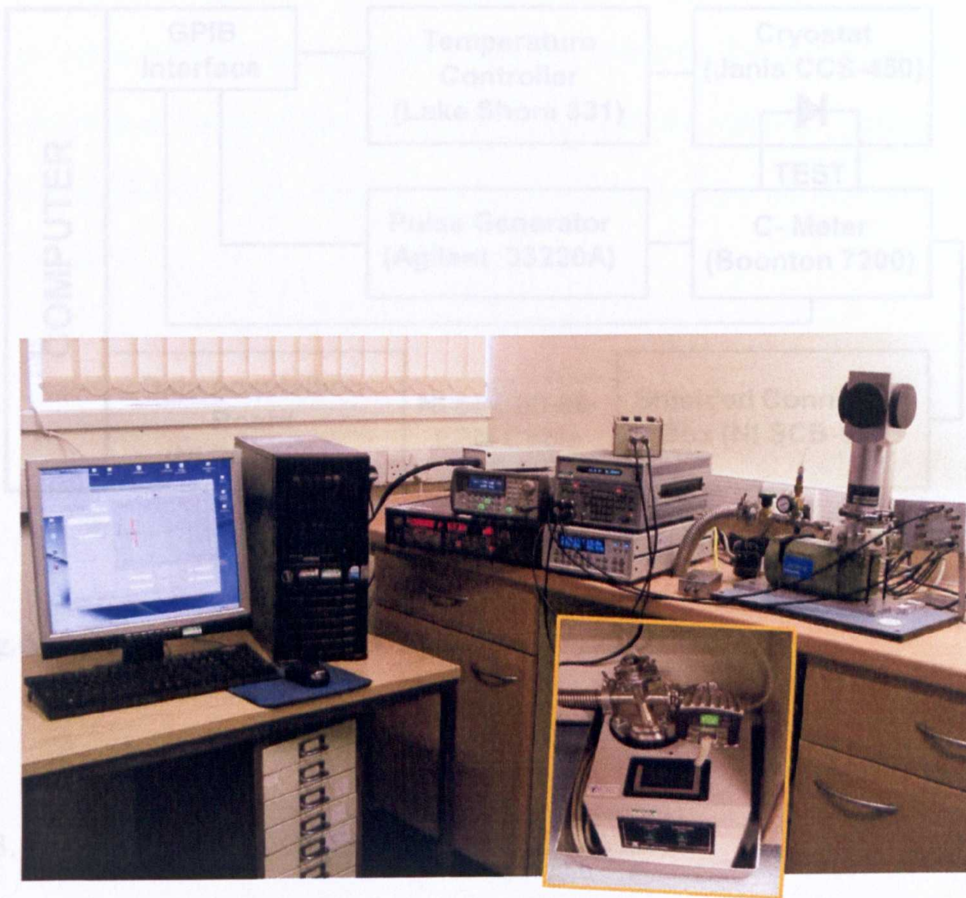

Fig.4. 7 (a) Photograph of the DLTS apparatus.

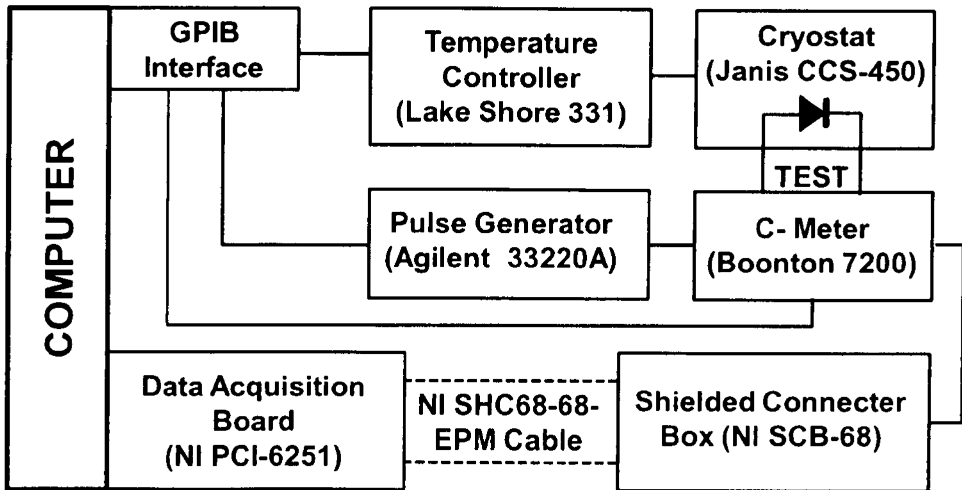

Fig.4.7(b) Schematic diagram of DLTS system.

4.3.1 DESCRIPTION OF SYSTEM HARDWARE

4.3.1.1 SIGNAL SOURCE

A Boonton capacitance meter, model 7200, has been used to measure the capacitance transients that emanate from the test sample. It offers much better signal to noise ratio (S/N) in comparison to the more conventional Boonton model 72BD. It has a response time of ~120μs which makes this apparatus very suitable for DLTS measurements. The sampling frequency for measuring the capacitance transients is 1MHz. It is experienced that for the capacitance spectroscopy measurements an optimum S/N ratio is achieved using a test signal level of 100 mV rms.

Model 7200 has test and differential connections along with bias voltage inputs and a d.c output proportional to the magnitude of differential capacitance. It has the ability to zero stray capacitance of cables and test fixtures by using the Zero

function. The measurement can also be normalized by connecting an external compensating capacitor-bridge to the differential terminals. The GPIB interface of the capacitance meter offers an option to operate via computer control. The capacitance meter is also used to perform standard capacitance-voltage (C-V) measurements.

4.3.1.2 CURRENT-VOLTAGE SOURCE-METER

A current-voltage source-meter, model Keithley 236, has been used for the current-voltage (I-V) measurements. This apparatus offers a source voltage and source current in the range 100μV-110V and 100fA-100mA, respectively. It can measure voltages and currents in the range 10μV-110V and 10fA-100mA with a good sensitivity of ±10μV and 10fA, respectively. This range and sensitivity allows the precise I-V measurements of semiconductor materials.

The I-V unit is fully programmable and is capable of sourcing and measuring voltage or current simultaneously. It has the option to be controlled manually or through a computer via GPIB interface.

4.3.1.3 PULSE GENERATOR

As discussed earlier, the DLTS measurements require bias pulses to perturb the occupancy of the electron/ hole traps by successively filling or emptying them with carriers using repetitive voltage pulses. The pulse generator is used to make changes in the sample bias as a means of filling and emptying the traps in a controlled manner. A pulse generator, model Agilent 33220A, has been used to generate a required train of pulses for DLTS measurements.

It can generate pulses with pulse duration (t_P) from 20 ns to 990 ms with an output voltage having amplitude of 10 mV. The Agilent 33220A pulse generator has the option to be controlled remotely through a computer with the use of standard GPIB-interface.

4.3.1.4 CRYOSTAT AND TEMPERATURE CONTROLLER

Since thermally stimulated emission of carriers from energy levels depends on the temperature, one of the significant factors in the DLTS measurement procedure is to monitor the temperature of the sample accurately. Generally, difficulties can arise due to the scanning nature of the DLTS technique where a slow but continuous increase/decrease in specimen temperature occurs during the capacitance measurements. In LDLTS where the measurements are carried out under isothermal condition a good stability of the specimen temperature is achieved.

A state-of-the-art cryostat (model Janis CCS-450) with an associated temperature controller (model Lake Shore 331) has been employed for the DLTS and LDLTS system.

The cryostat system contains a cold finger with the sample holder on its top, radiation shield, lightweight aluminium vacuum shroud, electrical feedthrough ports for sample contacts and thermal sensors. The cryostat operates with a compressor which makes the flow of helium gas (He) continuous through a high efficiency flexible six feet cryogen transfer line. It is based on close-cycle refrigeration principle. The Model CC-450 allows scanning of temperature in the range from 10K to 450K with ±1K. The Lake Shore 331 temperature controller allows a precise control over sample temperature which is an essential requirement for conventional

DLTS and Laplace DLTS measurements. This cooling system can also be controlled via GPIB-interface.

4.3.1.5 DATA ACQUISITION BLOCK

This is the vital element of the conventional DLTS/Laplace DLTS system. A National Instruments (NI) data acquisition (DAQ) card (model PCI-6251) has been utilised for collection and processing the capacitance transient data. The NI PCI-6251 is a high-speed multifunction DAQ signal card optimised for superior accuracy at fast sampling rates. It is 16-bit with maximum sampling frequency of 200 kHz. The DAQ offers ± 10.0V input/output voltages. These PCI-based boards offer a simple, seamless bridge between the computer and the GPIB instruments.

Capacitance transient data is collected through the DAQ with a suitable shielded input/output 68-pin terminal board (NI SCB-68), which is connected with a matching shielded cable (NI SHC68-68EPM).

4.3.1.6 COMPUTER INTERFACE

The general-purpose interface bus (GPIB), which is also known as IEEE 488 bus, has provided a standard high-speed interface for communication between instruments and controllers. All the equipments including capacitance meter, current-voltage source meter, pulse generator and temperature controller are connected to the computer by means of GPIB cables.

4.4 SYSTEM SOFTWARE

A detailed software program to collect DLTS and Laplace DLTS data and to control each equipment remotely has been developed by Prof. L. Dobaczewski *et al.*, Institute of Physics Polish Academy of Sciences, Warsaw, Poland and Prof. A. R.

Peaker *et. al.*, University of Manchester. UK under the project "Copernicus Project CI [10]. The software mainly runs in two modes of operations namely conventional DLTS and Laplace Transient processing mode. The software is known as Laplace Transient Processing software.

The conventional DLTS mode of operation is mainly based on the rate window concept as discussed earlier in section 4.2.2. The realisation of the rate window concept is actually done by using different weighting functions to determine the transient signal time constants which are proportional to emission rates of the charge carriers. The Laplace DLTS mode of operation is achieved by applying algorithms that contain three mathematical routines as mentioned in section 4.2.3.

4.4.1 CONVENTIONAL DLTS MEASUREMENT MODE

In this mode the software offers three type of different routines namely TrapView version 4.0, Multiple rate windows and Exponential Fitting. All these routines are based on the rate window concept. To measure the capacitance transients, each routine runs in a different way. A brief description about these routines is given below.

4.4.1.1 TRAPVIEW VERSION 4.0

This mode of operation gives the option to choose one pair of rate windows from the default of a set of three pairs. This mode of operation allows the acquisition of the DLTS spectra over pre-programmable temperature ranges where the traps manifest themselves. This is very advantageous in the sense that data is collected only in the temperature ranges of interest, and consequently a great deal of time and memory is saved [10].

4.4.1.2 MULTIPLE RATE WINDOWS

In this mode of operation, the software employs nine different rate windows to collect data of the capacitance transients by scanning the temperature in a predetermined range. The values of the rate windows used in this procedure to obtain conventional DLTS spectra are 5, 10, 20, 50, 100, 200, 500, 1000, and 2000 Hz [10]. Thus, Muti-rate windows mode has the advantage of obtaining nine different DLTS spectra at different rate windows in one temperature scan.

4.4.1.3 EXPONENTIAL FITTING

This is the most sophisticated conventional DLTS measurement mode because it provides a large amount of information. In this one scan mode of operation, a number of rate windows (emission rates) can be obtained that allows the determination of the trap activation energy from Arrhenius plots with great accuracy. In addition, the whole transient scan be analysed by on-the-fly exponential fitting calculations. One of the main advantages of this mode is that the capacitance transients can be analysed by fitting one exponential, two exponentials and three exponentials curve-fittings procedures. This mode of DLTS operation also offers an option to measure sample capacitance as a function of temperature simultaneously along with conventional DLTS measurements [10].

4.4.2 LAPLACE TRANSIENT PROCESSING MODE

Laplace DLTS is an isothermal technique which measures the capacitance transient signals at a fixed temperature. The Laplace DLTS data is acquired by specifying the number of capacitance transients to be measured at a fixed

temperature. This mode allows the averaging of the transient signals which helps improve the signal to noise (S/N) ratio as discussed in section 4.2.3.

It is worth pointing out that few initial data points of the transients are ignored because of the recovery time of the capacitance meter. The whole transient data is then analysed using the three different mathematical routines discussed in section 4.2.3 to determine the Laplace DLTS peaks [10].

4.4.3 EXPERIMENTAL DATA BASE

The acquired data is stored using Microsoft Access Jet database engine version 3.7 which is linked with the Laplace software. The data files are processed using standard techniques.

4.5 PHOTOLUMINESCENCE

Photoluminescence (PL) spectroscopy is a powerful technique to characterise the optical behaviour of semiconductor materials. In general, luminescence describes the emission of light from a semiconductor on supplying energy.

Among the optical techniques used for the characterization of semiconductors, PL is the most extensively used technique. In the PL technique, light is incident onto a sample, where it is absorbed and gives excess energy into the material in a process called photo-excitation and then one observes the radiations emitted by the semiconductor material after non-equilibrium condition is established via the photo-excitation. The intensity and spectral content of these emitted

radiations are then utilised to determine the information about various important material properties.

The photo-excitation process causes the electrons to move into permissible excited states and returning of these electrons to their equilibrium states releases the energy in the form of light. The energy of the emitted light is proportional to the difference in energy levels between the two electron states involved in the transition between the excited state and the equilibrium state. This is called a radiative process. When the de-excitation of electrons emits no light, the process is called non-radiative and energy involved in this transition is dissipated in the form of heat into the material.

The return to equilibrium is also known as recombination that can involve both radiative and non-radiative processes. Fig. 4.8 (a) shows the photo-excitation of an electron from the valence into the conduction band and then the non-equilibrium electron tends to relax back into the equilibrium state as illustrated in Fig. 4.8 (b). The energy released during intraband relaxation transfers to the crystal lattice. Finally, the electron recombines with the hole, which was created due to its transfer to excited states, results in the emission of light (E_{PL}) as shown in Fig. 4.8 (c).

PL spectroscopy can be used to determine some of the important parameters of semiconductor materials. For example, it can be used to determine the bandgap of semiconductor, to detect the impurity level or defect centres and to assess the material's quality.

PL has the advantage that it can be used for the materials where Schottky junction fabrication is difficult or impossible. The preparation of PL samples is relatively easy. Another advantage of the PL is that the luminescence can be

investigated at different areas on the sample surface. Among other features, it is a contactless technique, thus, non-destructive in nature.

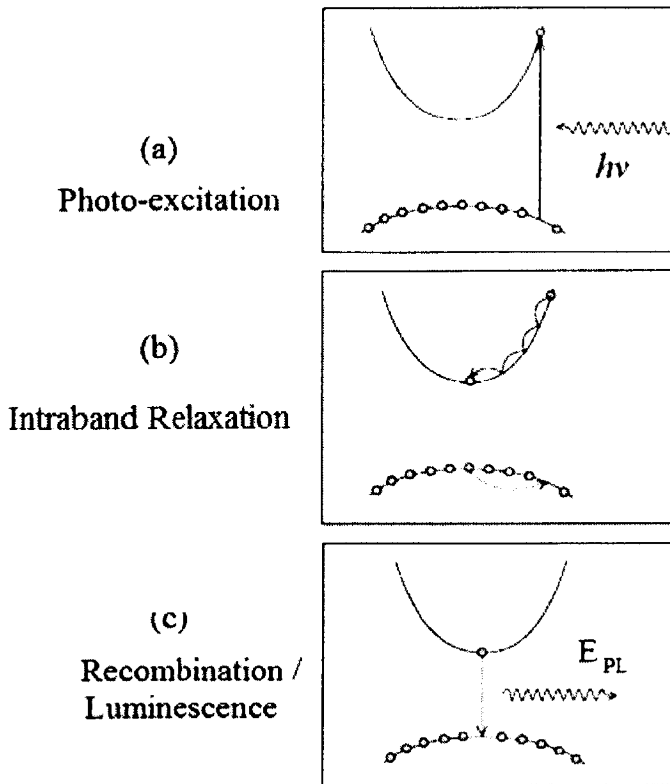

Fig.4.8 Schematic illustration of the basic processes involved in a typical luminescence emission from optically excited semiconductors.

4.6 SYSTEM HARDWARE IMPLEMENTATION

This section describes the hardware required to implement a PL system which is interfaced with the computer. The PL system is capable to operate over the temperature range 10K-350K. The photograph and block diagram of the PL system is shown in the Fig. 4.9 and 4.10, respectively. Some of the important elements of the PL system are described below.

4.6.1 DESCRIPTION OF SYSTEM HARDWARE

4.6.1.1 SPECTROMETER

The main element of the photoluminescence experimental setup is a spectrometer. The iHR 550 spectrometer used in this study was purchased from Horiba Jobin Yvon. It has a focal length of 550mm and aperture of f/6.4. It offers a motorised grating turret which has the capacity to hold three different gratings. Gratings with following specifications; 1200 grooves/ mm blazed at 500nm, 600 grooves/mm blazed at 2000 nm and grating with 300 grooves/mm blazed at 3000 nm are used. The entry and exit slits are adjustable from 0.1mm to 2mm. Spectrometer is capable of scanning with a speed of 160nm/sec. The iHR 550 allows minimum step size of 0.025nm. It also offers a motorized internal filter wheel with capacity to accommodate six different filters which are placed just after the entry slit inside the spectrometer.

4.6.1.2 LASERS, LIGHT CHOPPER AND OPTICS

The PL setup is equipped with excitation sources consisting of blue, green and red lasers. The power of the laser incident on the sample can be tuned manually

by using a density filter. A mechanical light chopper is utilised to chop the laser light. It has two chopping frequencies, 90 Hz and 120Hz. A band-pass filter is implemented in the path of the laser light to stop the unwanted higher order lines of the laser light. Optics including lenses and reflectors which are utilised to focus the light onto the sample and to focus the PL signal on the entry slit of the spectrometer are shown in Fig.4.10

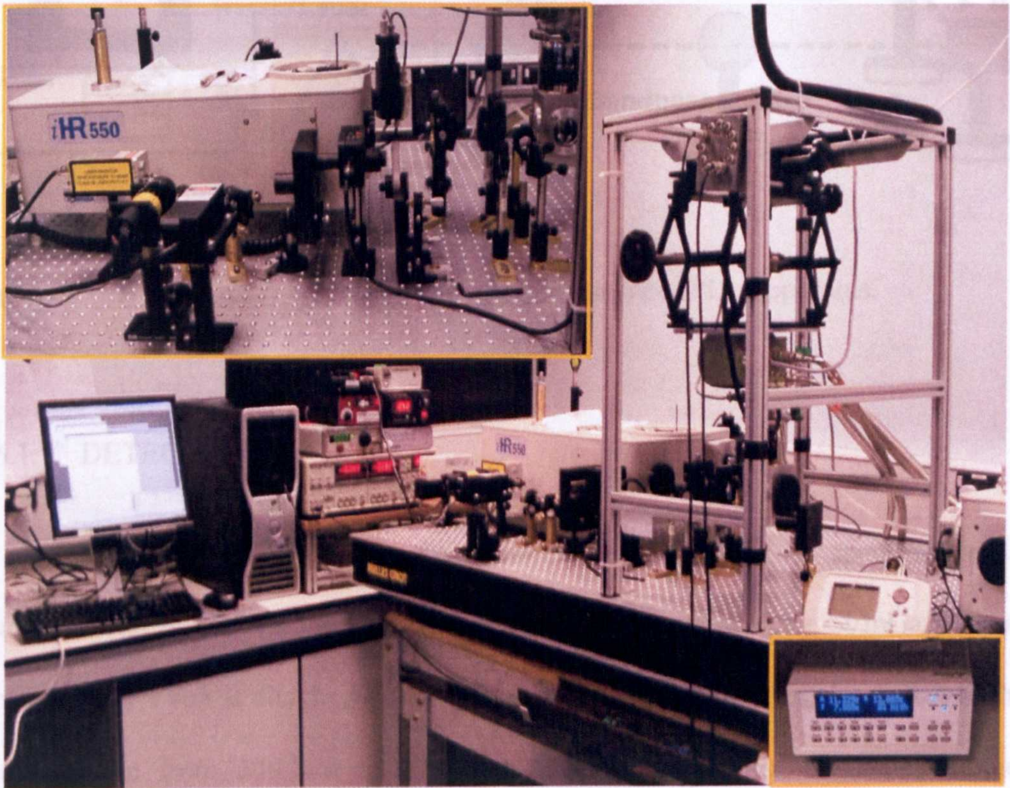

Fig.4.9 Photograph of Photoluminescence (PL) Apparatus

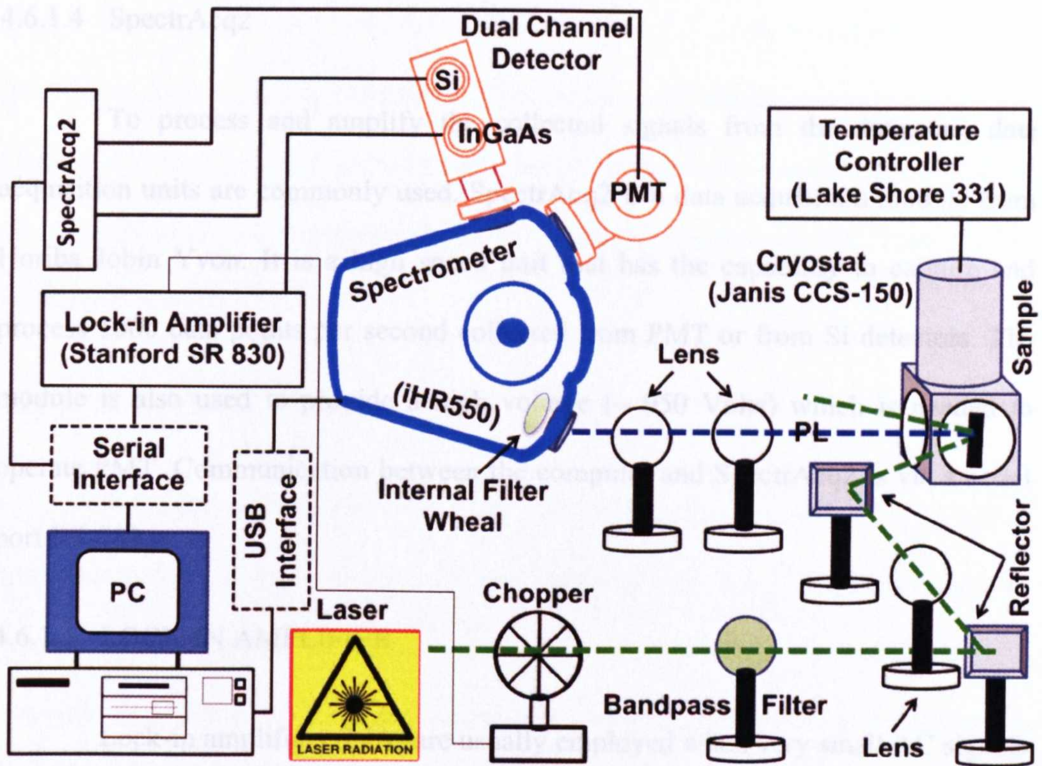

Fig.4.10 A systematic diagram of Photoluminescence (PL) Apparatus.

4.6.1.3 DETECTORS

For the detection of the photoluminescence signal, the spectrometer is equipped with two detectors. One dual channel solid state detector Si/InGaAs from Horiba Jobin Yvon is attached at the side exit of the spectrometer. It can cover the optical range from 300 nm to 1700 nm. The second detector, single channel photomultiplier tube (PMT), is placed at the front exit of the spectrometer. It can detect the light in the spectral range from 180nm to 900nm.

4.6.1.4 SpectrAcq2

To process and amplify the collected signals from the detectors, data acquisition units are commonly used. SpectrAcq2 is a data acquisition module from Horiba Jobin Yvon. It is a high speed unit that has the capability to capture and process 1000 data points per second collected from PMT or from Si detectors. The module is also used to provide a high voltage (~ 950 Volts) which is needed to operate PMT. Communication between the computer and SpectrAcq2 is via a serial port RS-232.

4.6.1.5 LOCK-IN AMPLIFIER

Lock-in amplifiers (LIA) are usually employed when very small AC signals need to be detected and any other unwanted signals have to be rectified. The LIA measurement is based on the phase sensitive detection. The phase sensitive detection basically refers to the demodulation or rectification of the noisy signal from the detector by mixing with a reference signal coming from the mechanical chopper which is used to chop the light with fixed frequency. A digital lock-in amplifier, model Stanford SR830 DSP, has been implemented in the PL setup. SR830 has the capability to measure and amplify very small signals down to few nano-volts (nV) with sensitivity of 2 nV.

4.6.1.6 CRYOSTAT AND TEMPERATURE CONTROLLER

For the temperature dependent PL measurements a state-of-the-art cryostat, model Janis CCS-150 has been used. To control the temperature of the sample, a temperature controller, model Lake Shore 331, along with cryostat have been implemented for our low temperature PL setup. The cryostat cooling system is

almost the same as discussed earlier in section 4.3.1.4. It also consists of a cold finger, radiation shield, homemade sample holder, aluminium vacuum shroud and thermal sensors. The principle of refrigeration is based on close-cycle flow of helium gas (He) through a compressor. It allows scanning the temperature from 10K to 350K.

4.6.1.7 COMPUTER INTERFACE

A computer with 120 MB RAM, 200 MB hard disk, windows XP as an operating system, a high speed USB port, a serial port RS-232 is the minimum requirement for the PL apparatus interface. The spectrometer is interfaced with computer via USB port. Data acquisition box spectrAcq2 and lock-in amplifier are connected to the computer by means of serial port RS-232 and can be initialised and controlled from computer. A filter wheel fitted inside the spectrometer can also be controlled through high speed USB port.

4.6.2 SYSTEM CONTROLLING SOFTWARE

Software, named SynerJY, which has been supplied by Horiba Jobin Yvon is used to control each equipment of the PL system remotely. The software facilitates the selection of suitable grating, detector and entry/exit slit widths etc. Different parameters which are required to perform the PL measurement can be entered through software. The software is flexible in terms of recording and processing data simultaneously. The software can drive the turret containing three gratings, slits, and shutters. It also has control over the entrance and exit mirrors to select detector at axial and side positions. A filter wheel having different colour filters situated inside the spectrometer can also be controlled using the software.

REFERENCES

[1] S. M. Sze and Kwok K. Ng, 'Physics of Semiconductor Devices' 3rd edition published by John Wiley & Sons, Inc. (2007).

[2] D. V. Lang, J.Appl. Phys. 45, 3023 (1974).

[3] D. K. Schroder, Semiconductor material and device characterisation' 2nd edition published by John Wiley & Sons, Inc. (1998)

[4] D. V. Lang, 'Topics in Applied Physics-Thermally Stimulated Relaxation in Solids', Vol.37, edited by P. Braunlich, Soringer Verlag, New York, (1979).

[5] L. Dobaczewski, P. Kaczor, I. D. Hawkins and A.R. Peaker, J. Applied. Phys. 76, 1 (1994).

[6] L. Dobaczewski, A.R. Peaker and K. B. Nielsen, J. Applied. Phys. 96, 4689 (2004).

[7] P. Deixler, J. Terry, I. D. Hawkins, J. H. Evans-Freeman, A. R. Peaker, L. Rubaldo, D. K. Maude, J.-C. Portal, L. Dobaczewski, K. B. Nielsen, A. N. Larsen, and A. Mesli, Appl. Phys. Lett., 73, 3126 (1998).

[8] Akbar Ali, M. Shafi and Abdul Majid, Phys. Scr., 74, 450 (2006).

[9] C. H. Henry and D. V. Lang, Phys Rev.B15, 989 (1977).

[10] Laplace DLTS Software manual at http://www.laplacedlts.eu/

CHAPTER 5

EXPERIMENTAL DETAILS

This chapter presents the experimental details pertaining to the work reported in this thesis. It includes the description of the conditions and processing procedure for the preparation of samples used in this study. The details of equipment and measurements carried out for the characterisation of semiconductor materials, GaAsN and GaAsBi, are also given.

5.1 SAMPLES

Samples of two different kinds of materials, dilute nitrides and bismides, have been used in this study. Dilute nitride samples are annealed in a systematic way at different temperatures to observe the effects of annealing on the electrical properties of these materials. As-grown dilute nitride samples are also hydrogenated and investigated. The dilute bismide layers are also annealed and characterised. The detailed description of the samples is given below.

5.1.1 DILUTE NITRIDE SAMPLES

Epitaxial layers of silicon-doped (n-type) GaAsN with different N concentrations (N= 0% to 1.2%) are grown by molecular beam epitaxy (MBE) with

growth rate of 1μm per hour at a growth temperature of 500°C on epi-ready GaAs substrates heavily doped with Si (electron concentration $n=2x10^{18}$ cm^{-3}). The five samples investigated in this work are labeled as Vn1256 (N=0%), Vn667 (N=0.2%), Vn666 (N=0.4%), Vn669 (N=0.8%) and Vn668 (N=1.2%). The growth details of the GaAsN epitaxial layers are also given in Table 5.1.

The epitaxial layers were processed into circular mesas of various diameters ranging from 0.25mm to 1mm using photolithography and wet chemical etching techniques. Fig. 5.1 (a) shows the diode structure which consists of the following layers in order of growth from the substrate: (i) a 0.1 micron thick buffer layer of GaAs doped at $n = 2x10^{18}cm^{-3}$; (ii) 1 micron of GaAsN, $n = 3x10^{16}$ cm^{-3}. Schottky devices are fabricated and mounted on a TO5 header as depicted in Fig. 5.1 (b) for the conventional and Laplace DLTS measurements. Ge/Au/Ni/Au were first evaporated and alloyed to form Ohmic contacts to the bottom of the n^+ GaAs substrate. Schottky contacts were then formed by evaporation of Ti/Au on top of the doped epilayer.

Samples were annealed in a rapid thermal annealer (RTA) in a N_2 ambient. Post growth annealing was performed on each GaAsN sample (N= 0.2% to 1.2%) from 500°C to 800°C for 60s. After post growth annealing, Schottky junctions were formed in the same manner as described above.

Hydrogenation has also been performed on the as-grown GaAsN samples. Hydrogen irradiation of GaAsN layers was carried out in collaboration with a group at Department of Physics and INFM, Università di Roma "La Sapienza" Piazzale Aldo Moro 2, 00185 Roma, Italy. A Kaufman source has been utilised to obtain an energetic beam of hydrogen ions. The samples were hydrogenated by using an ion

beam irradiation with a dose $d_H = 1.3 \times 10^{19}$ ions/cm^2 at 300 ^{0}C. Schottky junctions were obtained by carrying out the processing steps in a similar fashion as discussed above. A through DLTS study on the dilute nitride as-grown, annealed and hydrogenated samples has been carried out. The details of the measurements are given in following section 5.2.

TABLE 5.1 Growth parameters for dilute GaAsN epilayers

$GaAs_{1-x}N_x$ epi-layers grown on (100) n^+-GaAs substrates					
Sample	**Growth T (°C)**	**N_2 (SCCM)**	**x (%)**	**Si doping (cm^{-3})**	**Layer thickness (μm)**
Vn667	~500	0.1	0.2	3×10^{16}	1
Vn666	~500	0.2	0.4	3×10^{16}	1
Vn669	~500	0.35	0.8	3×10^{16}	1
Vn668	~500	0.65	1.2	3×10^{16}	1
Vn1256	~500	0	**0**	3×10^{16}	1

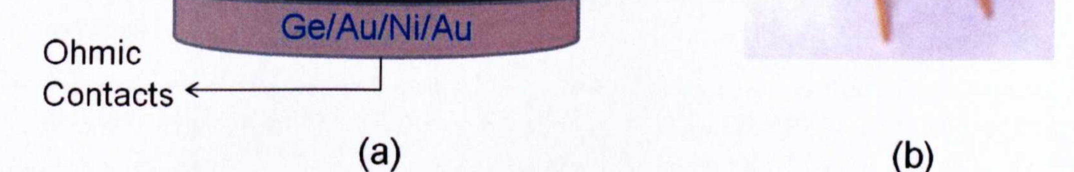

Fig.5. 1 **(a)** Schematic diagram of the GaAsN Schottky diode. **(b)** Diodes mounted on a TO5 header showing circular mesas of various diameters.

5.1.2 DILUTE BISMIDE SAMPLES

Undoped GaAsBi layers were grown by MBE on semi-insulating (100) and (311)B GaAs substrates at a growth temperature of ~350°C with a growth rate of 1 monolayer per second using different As to Ga flux ratios. Atomic Ga and Bi were used as group-III and group-V sources, respectively, while As in the form of dimmers (As_2) was produced by using a two-zone purpose made cell. The beam equivalent pressure for Ga and Bi was ~9×10^{-7}, 1.2×10^{-7} Torr, respectively. As_2 flux was varied from $1.2\text{x}10^{-5}$ to $6\text{x}10^{-6}$ Torr. The growth details of the GaAsBi epitaxial layers are also given in Table 5.2. The near stochiometric condition was achieved

with an As overpressure of 8.0×10^{-6} Torr and 1.0 10^{-5} Torr for growth of GaAsBi layers on (100) and (311)B GaAs substrates, respectively, as indicated in Table 5.2.

Fig. 5.2 shows the GaAsBi layer structure grown on (100) and (311)B GaAs substrates. The nominal thickness of the GaAsBi epilayers is 1 μm. To investigate the effect of annealing on the optical and structural properties of these layers annealing heat treatment were carried out at 200°C for 3hours under N_2 gas conditions in a tubular furnace.

Fig.5. 2 Schematic diagram of GaAsBi layer on (100) and (311)B GaAs substrates.

TABLE 5.2 Growth parameters for dilute GaAsBi epilayers

GaAsBi layer grown on (100) substrates				
Sample	**Ms-819**	**Ms-821**	**Ms-820**	**Ms-822**
Growth T (°C)	~350	~350	~350	~350
As (Torr)	$\sim 1.2 \times 10^{-5}$	$\sim 1.0 \times 10^{-5}$	$\sim 8.0 \times 10^{-6}$	$\sim 6.0 \times 10^{-6}$
Bi (Torr)	$\sim 1.2 \times 10^{-7}$	$\sim 1.2 \times 10^{-7}$	$\sim 1.2 \times 10^{-7}$	$\sim 1.2 \times 10^{-7}$
			This is the region of near-stochiometric growth	
GaAsBi layer grown on (311)B substrates				
Sample	Ms-823	Ms-825	Ms-824	Ms-826
Growth T (°C)	~350	~350	~350	~350
As (Torr)	$\sim 1.2 \times 10^{-5}$	$\sim 1.0 \times 10^{-5}$	$\sim 8.0 \times 10^{-6}$	$\sim 6.0 \times 10^{-6}$
Bi (Torr)	$\sim 1.2 \times 10^{-7}$	$\sim 1.2 \times 10^{-7}$	$\sim 1.2 \times 10^{-7}$	$\sim 1.2 \times 10^{-7}$
		This is the region of near-stochiometric growth		

GaAsBi epilayers grown at different As_2 overpressures have been studied using different techniques such as conventional absorption spectroscopy, photoluminescence and high resolution x-ray diffraction technique. Since GaAsBi epi-layers are undoped, grown on semi-insulating substrates, DLTS study can not be carried out on these layers due to their highly resistive character. The details of the measurements are given in following section.

5.2 MEASUREMENT DETAILS

The following sections give some key details of the measurement carried out for the study presented in this thesis.

5.2.1 CURRENT-VOLTAGE MEASUREMENTS

After the fabrication of the Schottky diodes, the first step is to measure their current-voltage (I-V) characteristics which provide the immediate information about the quality and suitability of diodes for further DLTS and LDLTS measurements. A figure of merit for the samples for DLTS measurements is a very low reverse current (~1μA). I-V measurements were carried out with a Keithley 236 electrometer. The current is measured in the voltage range from -4 V to +1 V with voltage steps of 0.1 V. The experimental values of reverse current at -4 V in all the samples selected for DLTS measurements are in the range from 10^{-9} to 10^{-5}A at room temperature.

5.2.2 CAPACITANCE-VOLTAGE MEASUREMENTS

Capacitance-voltage (C-V) measurements on a diode yield the background doping concentration and doping profile. These parameters are important and used in

the analysis of DLTS measurements. C-V measurements have been performed on all the Schottky diodes using the Boonton 7200 capacitance meter.

5.2.3 DLTS MEASUREMENTS

A series of conventional and Laplace DLTS measurements for varying rate windows were carried out. The details of the conventional and Laplace DLTS are covered in chapter 4. The measurements of the emission rates were performed by applying a suitable train of pulses with width t_P that repeats between reverse bias V_R and filling bias V_P (where $V_P < V_R$) with fixed repetition frequency. The temperature of the sample was fixed during the Laplace DLTS measurements while it was increased slowly with a rate of 2K per minute during the conventional DLTS measurements. A variable temperature, from 10K to 450K, cryostat with a specially designed sample holder that can accommodate a TO5 header to carry out the DLTS measurements. The data of the emission rates, corresponding to a number of peaks in the conventional DLTS spectra, were obtained by using a number of conventional DLTS scans at different rate windows. For those peaks which appeared broader in the conventional DLTS spectra and may be due to the contribution of more than one energy levels, Laplace DLTS measurements were carried to resolve each peak. The emission rates data of the resolved peaks were obtained by using a number of Laplace DLTS scans at different fixed temperatures. Direct capture cross-section measurements have been carried out as described in section 4.2.4.2 of Chapter 4.

5.2.4 OPTICAL ABSORPTION MEASUREMENTS

Optical absorption measurements have been performed to determine the bandgap of the samples. A beam of white light generated with a 100W tungsten

halogen lamp is incident on the sample via an optical fiber. The sample is placed in the cryostat in such a way that the light beam is incident normal to the surface of the sample. A fraction of the incident beam is reflected and a part of the beam is absorbed. Whereas, the other portion of the incident beam is transmitted. Two lenses are used to collect and focus the transmitted beam onto the entry slit of the iHR550 spectrometer. It is then detected by the Si detector. Optical measurements for the band gap determination and analysis have been performed on GaAsBi and GaAs control samples.

5.2.5 PHOTOLUMINESCENCE MEASUREMENTS

The PL spectroscopy technique is a contactless and non-destructive method that is commonly used to probe the electronic structure of semiconductor materials. Low temperature photoluminescence measurements have been performed using two systems. The first one operates at $T \geq 10$ K as described in sections 4.5 and 4.6 and the second one is an in-house system which can cool down to helium temperatures.

In the closed-loop cryogenic PL system the excitation light was generated using a solid state green laser having $\lambda = 532$ nm. In the helium gas flow in-house PL system, the 514.5nm green line excitation was generated from an Ar laser. Both systems use similar apparatus for collecting the PL signal as described below.

Laser light passes through a chopper which is operated at 90 Hz. A reference signal from the chopper is fed to the reference input of the SR 830 lock-in amplifier. Next the light passes through the band pass filter (315-750nm) to eliminate the higher order harmonic lines which are present in our green laser. A mirror then deflects the light onto another 2nd mirror through a focusing lens. The laser light then

falls onto the sample which is placed inside the cryostat. The incident of light on the sample is established with such an angle that the laser light is deflected off-axis with respect to entrance slit of the spectrometer. The luminescence from the sample is focused onto the spectrometer entrance slit by using two lenses. A line filter is placed just inside the spectrometer to eliminate the laser light. The filtered signal is dispersed by the diffraction grating and then detected by the dual color Si/InGaAs detector. The signal from the detector is then fed into a lock-in amplifier to improve the signal-to-noise ratio using the chopper frequency as reference signal. Finally, PL spectrum is recorded in the computer. PL measurements have been carried out in the temperature range from 10 K to 350K.

5.2.6 HIGH RESOLUTION X-RAY DIFFRACTION MEASUREMENTS

X-ray diffraction, a non-destructive structural technique, is an ideal tool for the determination of chemical composition in semiconductors. High-resolution x-ray diffraction (HRXRD) measurements were carried out in collaboration with the group of Dr M.Schmidbauer at Leibniz Institute for Crystal Growth, Berlin, Germany. 004 and 311 symmetrical reflections were optimized for GaAsBi layers grown on (100) and (311)*B* GaAs substrates, respectively. A double-crystal diffractometer equipped with a parabolic (focusing) multilayer mirror was used. The x-rays are produced using the $K\alpha_1$ transition of copper (λ=0.1540508 nm), and are monochromated with a four-bounce Ge 220 Bartels monochromator.

CHAPTER 6

DEEP LEVELS IN GaAsN GROWN BY MOLECULAR BEAM EPITAXY

6.1 INTRODUCTION

Dilute III-V nitrides are relatively a quite new material system and it attracts a great deal of attention due to its anomalous properties. These are very promising materials for many technological applications like solar cells [1], long wavelength lasers [2], terahertz emitters [3], optical amplifiers [4], and temperature-insensitive semiconductor band gap [5].

The incorporation of nitrogen decreases the bandgap of GaAs about 100meV per percent of N and therefore allows tuning the emission wavelength in the near-infrared region. However, the incorporation of nitrogen introduces deep defect levels in the material energy band gap. These defect levels have severe effects on the material's optical and electronic properties. For example, the presence of non-radiative recombination defect centres in dilute nitride materials can degrade the optical efficiency of the material [6]. These defect centres also decrease the lifetime of the charge carriers [7, 8] and therefore affects the charge transport properties. A well-known non-radiative electron trap EL3 with activation energies from 0.5 to 0.55 eV is most commonly considered to be responsible for the carrier non-radiative-

recombination in dilute GaAsN epitaxial films. Another midgap EL2-like deep level with thermal activation energies from 0.7 eV to 0.8 eV that could have strong influence on the properties of dilute GaAsN epitaxial films has been reported [9-11] and assigned to nitrogen dimmers (N-N on arsenic site). Zhang *et. al.* [12] show that nitrogen related defects in GaAsN layers have different properties depending on the amount of nitrogen incorporated in the GaAs lattice. Due to the obvious interest in GaAsN as an optical material, this work studies the effect of nitrogen on the creation of electrically active deep level defects in MBE grown GaAsN layers with low nitrogen concentrations (0.2% - 1.2%) using DLTS and high resolution Laplace DLTS techniques. The details of the samples used in this investigation and their preparation are given in chapter 5.

The major objective of this study is to provide feedback information to optimise the growth conditions in order to improve the quality of the material and understand the effect of deep states on the performance of future devices based on dilute GaAs nitrides. Some of the information about the nitrogen related defect published in the literature is given in section 3.4 of chapter 3.

6.2 RESULTS

6.2.1 CURRENT-VOLTAGE (I-V) AND CAPACITANCE-VOLTAGE (C-V) CHARACTERISTICS

The procedure to determine the current-voltage (I-V) characteristics of the diodes has been described in chapter 5. Current-voltage (I-V) measurements have been carried out to check the suitability of the diodes for further electrical characterisation. The GaAsN diodes containing nitrogen (N= 0, 0.2, 0.4, 0.8 and

1.2%) thus tested and those exhibit low leakage current (~ 5 μA for voltages up to – 4 Volts) have been selected for further DLTS and LDLTS measurements. Typical I-V characteristics of the Schottky diodes having different nitrogen contents are shown in Fig. 6.1.

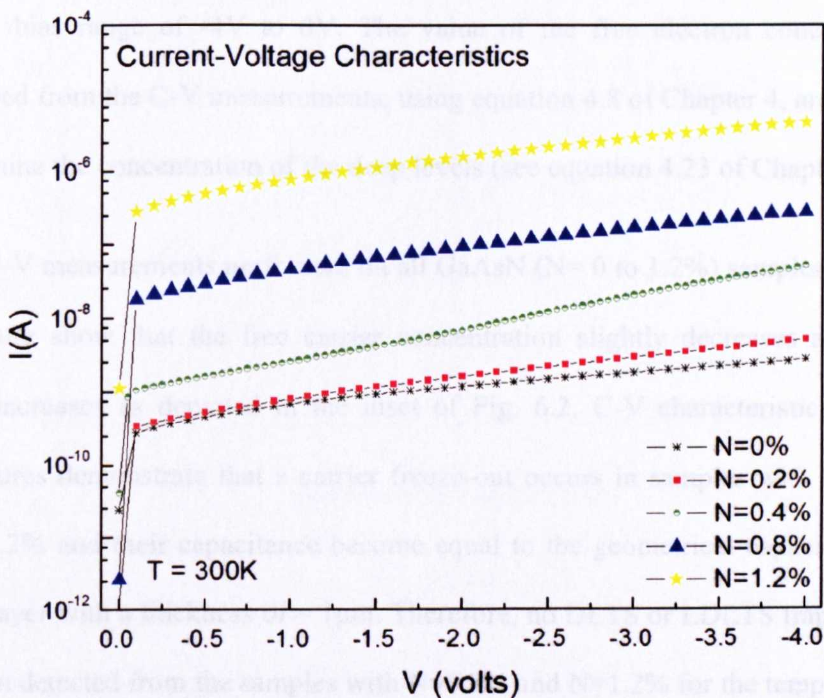

Fig.6.1 Current-voltage characteristics of selected Schottky diodes containing different nitrogen contents.

Capacitance-voltage (C-V) measurements were also performed on all the samples in order to determine the background doping concentration. The reverse bias V_R was varied in the range from 0 to -4 volts and the corresponding capacitance was recorded. Fig. 6.2 shows a typical $1/C^2$ versus reverse bias voltage plot obtained from the (C-V) data of a GaAsN sample (N=1.2%). Shallow level doping concentrations for all samples were derived from the slope of the plot of $1/C^2$ versus V_R. The linear best-fit through the data points shows the uniform doping density over the bias range of -4V to 0V. The value of the free electron concentration determined from the C-V measurements, using equation 4.8 of Chapter 4, are utilised to determine the concentration of the deep levels (see equation 4.23 of Chapter 4).

C-V measurements performed on all GaAsN (N= 0 to 1.2%) samples at room temperature show that the free carrier concentration slightly decreases as the N content increases as depicted in the inset of Fig. 6.2. C-V characteristics at low temperatures demonstrate that a carrier freeze-out occurs in samples with N=0.8% and N=1.2% and their capacitance become equal to the geometrical capacitance of GaAsN layer with a thickness of ~ 1μm. Therefore, no DLTS or LDLTS trap signals have been detected from the samples with N=0.8% and N=1.2% for the temperatures up to 120 K and 160 K, respectively.

As discussed in section 2.5 of Chapter 2, the localised energy levels associated with the N appears near to the conduction band edge and their interaction moves the conduction band edge down into bandgap of the GaAsN. The reduction of the bandgap is due to the splitting of the conduction band into two bands having high and low energy states and this splitting depends up on the N composition. For the GaAsN layers with higher N content the conduction bands splitting is larger so the

electrons need relatively higher energy to participate into the conduction mechanism. It could be the reason that at low temperatures carriers freeze-out have been observed only in the samples containing high N composition.

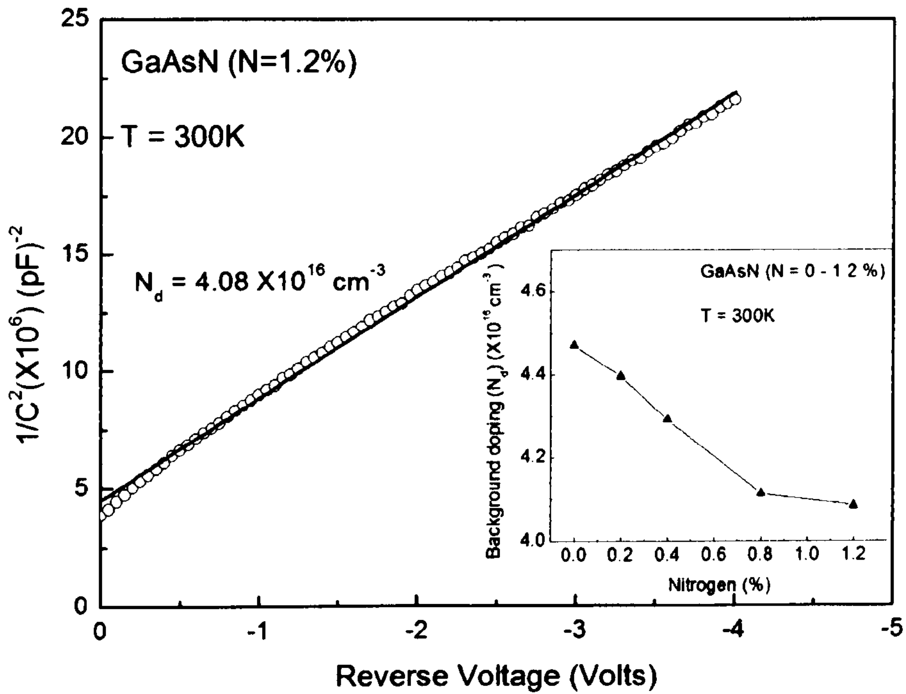

Fig.6.2 The plot of the junction capacitance of GaAsN (N = 0.2%) Schottky diode in the form of $1/C^2$ as a function of reverse bias voltage. The doping concentration is determined from the slope of best fit of $1/C^2$ versus V_R. The inset shows the background concentration obtained from samples having different nitrogen contents.

6.2.2 DLTS MEASUREMENTS

After performing the routine I-V and C-V characterisation, suitable diodes were selected for DLTS and LDLTS experiments. The samples were mounted in an 8K closed-cycle helium-cryostat and DLTS spectra were obtained using a reverse bias of -4V with a 1ms pulse duration which was found sufficient to fill the traps. The sampling rate window was 50 s^{-1}. The measurements were taken at temperatures covering the range 10K-400K. In addition, high resolution isothermal spectroscopic LDLTS experiments were performed in which the temperature was maintained constant within 0.1K by the digital temperature controller. Fig.6.3 shows a typical DLTS scan obtained from a set of five samples (silicon-doped GaAsN Schottky diodes) containing different nitrogen compositions (N= 0% to 1.2%). LDLTS increases the energy resolution of conventional DLTS by more than an order of magnitude. For example, trace D of Fig.6.3 shows the DLTS spectra of the sample with the highest nitrogen composition (N=1.2%) where very broad features are apparent and span over a wide temperature range (~160-350K). This broad feature of the standard DLTS signal was resolved by LDLTS as shown in Fig. 6.4, which is a clear demonstration of the high resolution of this technique.

DLTS scans reveal the presence of seven (A_1 to A_7), four (B1 to B4), four (C1 to C4) and three (D1 to D3) peaks associated with electrically active defect states in GaAsN samples containing nitrogen N=0.2%, N=0.4%, N=0.8% and N=1.2%, respectively.

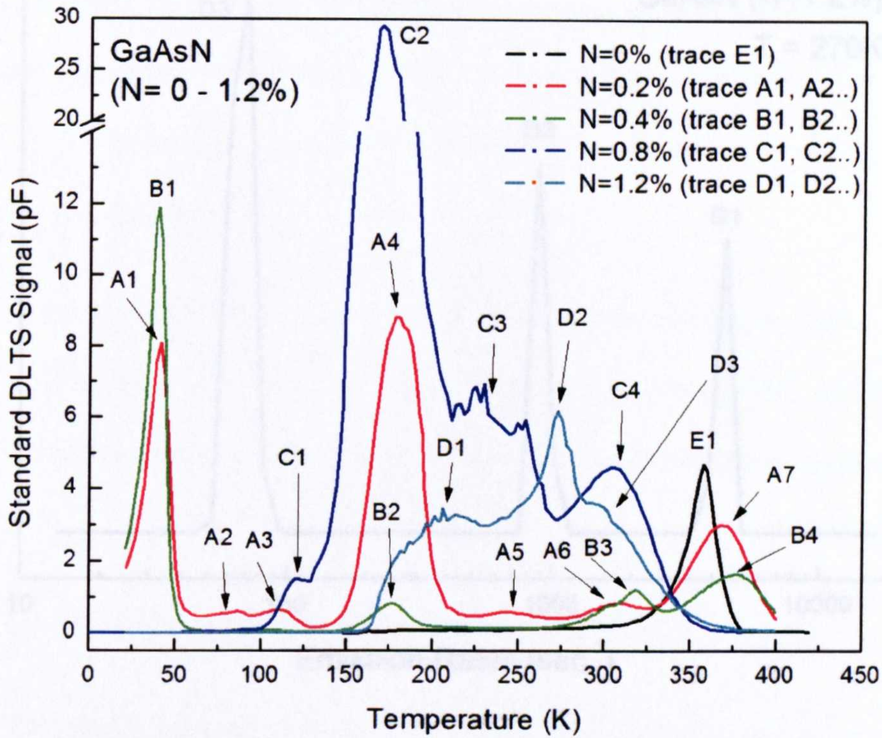

Fig.6.3 Standard DLTS Spectra of n-type MBE-grown GaAsN Schottky diodes with varying nitrogen compositions from 0 to 1.2%. The DLTS scans were taken using a rate window of 50 s^{-1}, an applied reverse-bias V_R = -4 V with a pulse height V_P = -0.5 V and duration of 1ms.

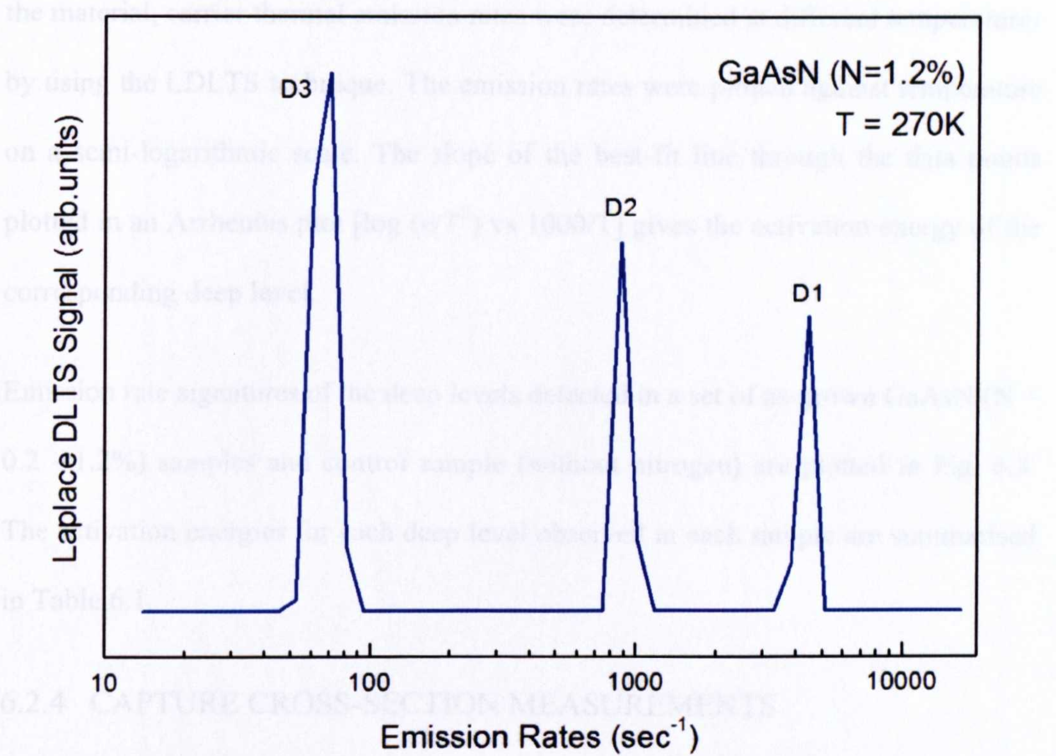

Fig.6.4 Laplace DLTS spectra of the sample with N=1.2% taken at 270K. The experimental conditions used were similar to those used for the standard DLTS scans.

6.2.3 THERMAL EMISSION RATES

To identify the energy location of these defect states within the band gap of the material, carrier thermal emission rates were determined at different temperatures by using the LDLTS technique. The emission rates were plotted against temperature on a semi-logarithmic scale. The slope of the best-fit line through the data points plotted in an Arrhenius plot [log (e/T^2) vs 1000/T] gives the activation energy of the corresponding deep level.

Emission rate signatures of the deep levels detected in a set of as-grown GaAsN (N = 0.2 - 1.2%) samples and control sample (without nitrogen) are plotted in Fig. 6.5. The activation energies for each deep level observed in each sample are summarised in Table 6.1.

6.2.4 CAPTURE CROSS-SECTION MEASUREMENTS

The direct capture cross-sections were determined for the deep levels detected in the GaAsN layers with N 0% to 1.2%. The measurements were carried out at fixed temperature by reducing the filling pulse width (t_p) as described in section 4.2.4.2 of Chapter 4. Assuming the capture cross-sections are temperature-independent, the value of capture cross-section of each trap have been determined from the slope of the best-fit line through the data points plotted in an Arrhenius plot [log $(1-S(t_p)/S(\infty)$ versus t_p] as shown in Fig. 6.6.

6.2.5 TRAP CONCENTRATION

The DLTS peak gives a direct measure of the trap concentration which is determined by using equation (4.2.3) given in section 4.2.4.3 of chapter 4. The

concentrations thus found for the detected defects states are summarized in Table 6.1.

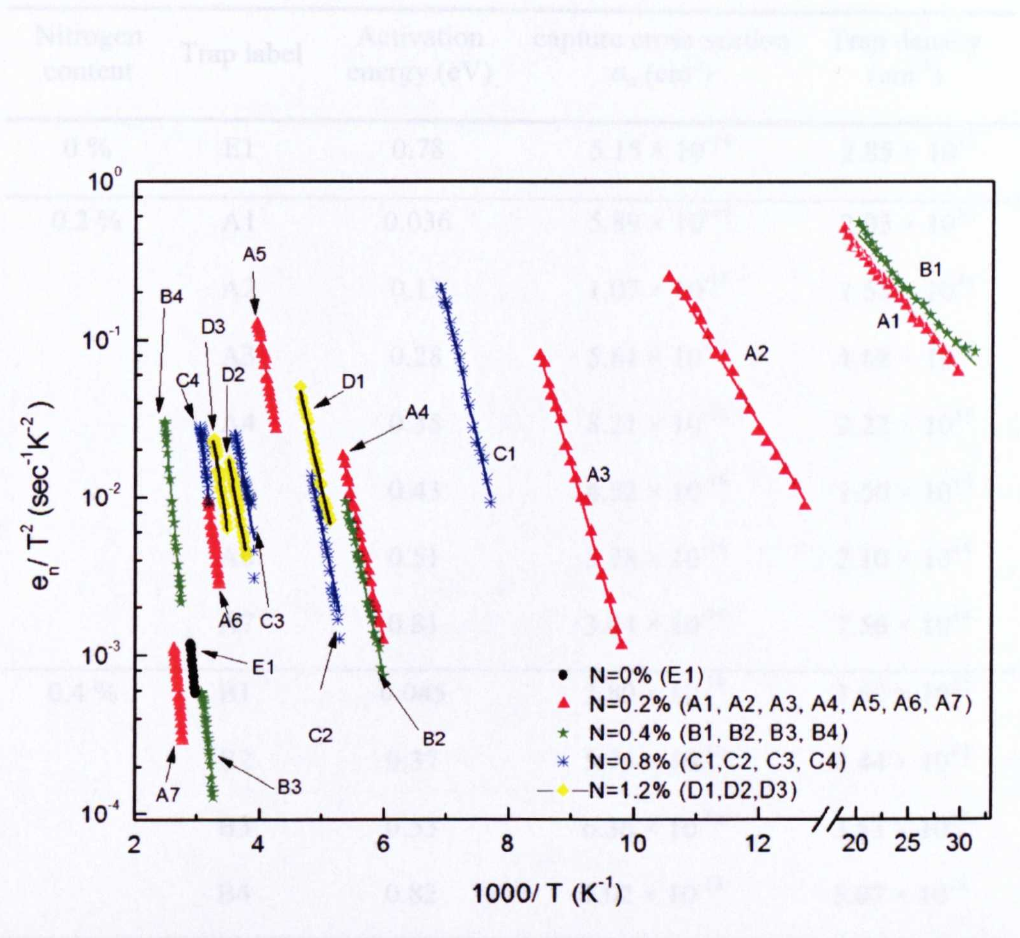

Fig.6.5 Arrhenius plots are derived from the thermal emission rates obtained from five samples having N (0 to 1.2%). Filled symbols are data points, while lines through the symbols are the least-squares fits to the data.

TABLE 6.1: Typical parameters derived from DLTS and LDLTS measurements

Nitrogen content	Trap label	Activation energy (eV)	capture cross-section σ_n (cm^2)	Trap density (cm^{-3})
0 %	E1	0.78	5.15×10^{-14}	2.85×10^{15}
0.2 %	A1	0.036	5.89×10^{-19}	2.03×10^{15}
	A2	0.13	1.07×10^{-18}	1.53×10^{14}
	A3	0.28	5.61×10^{-17}	1.68×10^{14}
	A4	0.35	8.21×10^{-16}	2.22×10^{15}
	A5	0.43	4.52×10^{-16}	1.50×10^{14}
	A6	0.51	5.28×10^{-16}	2.10×10^{14}
	A7	0.81	3.64×10^{-14}	7.56×10^{14}
0.4 %	B1	0.045	2.80×10^{-18}	3.60×10^{15}
	B2	0.37	5.75×10^{-16}	2.44×10^{14}
	B3	0.53	6.36×10^{-16}	3.52×10^{14}
	B4	0.82	1.02×10^{-14}	5.07×10^{14}
0.8 %	C1	0.34	2.63×10^{-16}	1.86×10^{14}
	C2	0.38	4.24×10^{-16}	3.51×10^{15}
	C3	0.44	7.41×10^{-16}	6.97×10^{14}
	C4	0.55	5.51×10^{-16}	5.82×10^{14}
1.2 %	D1	0.35	2.43×10^{-16}	5.57×10^{14}
	D2	0.43	5.09×10^{-16}	9.97×10^{14}
	D3	0.50	5.78×10^{-16}	5.74×10^{14}

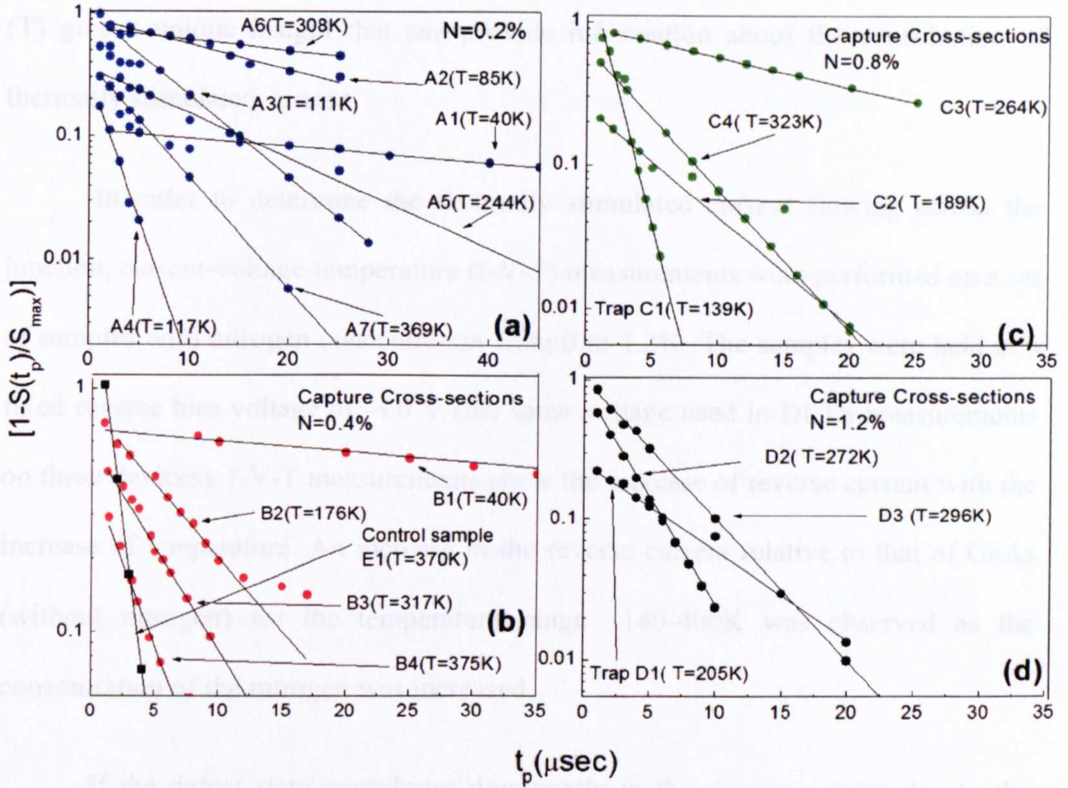

Fig.6. 6 Electron capture cross-sections of traps detected in GaAsN (N=0% to 1.2%) samples. S represents the DLTS peak height at constant temperature, at a particular pulse width (t_p) and S_{max} is the saturated peak height of the DLTS signal. Straight lines are least-square fit through data points.

6.2.6 CURRENT-VOLTAGE-TEMPERATURE (I-V-T) CHARACTERISTICS

The reverse current measurements at constant voltage by varying temperature (T) give a unique insight that can provide information about the contribution of thermally stimulated current.

In order to determine the thermally stimulated current flowing across the junction, current-voltage-temperature (I-V-T) measurements were performed on a set of samples with nitrogen concentration from 0 to 1.2%. The samples were held at a fixed reverse bias voltage of -4.0 V (the same voltage used in DLTS measurements on these devices). I-V-T measurements show the increase of reverse current with the increase of temperature. An increase in the reverse current relative to that of GaAs (without nitrogen) for the temperature range ~140-400K was observed as the concentration of the nitrogen was increased.

If the defect state contributes dominantly to the reverse current due to the generation of the carriers from the defect state then it follows the relation given by [13, 14].

$$I_R(T) = I_r \; exp\left(\frac{-E_A}{kT}\right)$$

where, I_r is the saturation limit of current at high temperature, I_R is the reverse current, E_A is the activation energy of the defect state, k is the Boltzmann constant and T is the measurement temperature.

The slope of the straight line through the data points obtained from the Arrhenius plot of ln($|I_R|$) versus inverse of temperature using above equation gives

the activation energy of the defect state responsible for the generation of carriers [15]. Therefore, the measured values of reverse current at constant voltage of -4.0 V were plotted as a function of inverse of measurement temperature as shown in Fig. 6.7. The activation energies determined from the slope of the least square fit through data points of I-V-T measurements are 0.78, 0.77, 0.81, 0.57 and 0.52eV for the GaAsN samples having nitrogen 0, 0.2, 0.4, 0.8 and 1.2%, respectively.

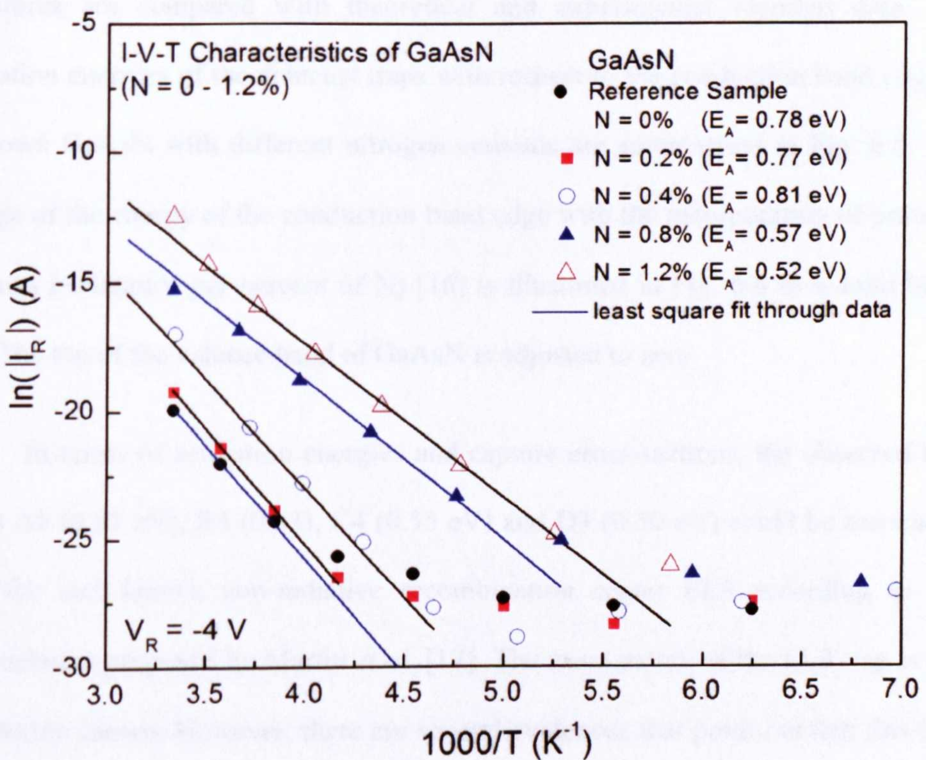

Fig.6.7 Illustration of thermally stimulated current flowing across the junctions of the Schottky diodes having different N contents, measured at -4 V. Activation energies (E_A) are obtained from the linear parts of the Arrhenius plots between reverse current (I_R) and inverse of the temperature.

6.3 DISSCUSSION

6.3.6 DLTS AND LDLTS ANALYSIS

DLTS and LDLTS measurements reveal several electron emitting defect states as illustrated in Fig. 6.3 and Fig. 6.4. The activation energies and capture cross-sections of each trap were determined from their thermal emission rates and capture rates, respectively. In order to identify these traps their emission rate signatures are compared with theoretical and experimental reported data. The activation energies of the detected traps with respect to the conduction band edge of as-grown GaAsN with different nitrogen contents are summarised in Fig. 6.8. The change of the energy of the conduction band edge with the incorporation of nitrogen in GaAs (~100meV per percent of N) [16] is illustrated in Fig. 6.8 as a solid black line. The top of the valence band of GaAsN is adjusted to zero.

In terms of activation energies and capture cross-sections, the observed trap levels A6 (0.51 eV), B3 (0.53), C4 (0.55 eV) and D3 (0.50 eV) could be associated with the well-known non-radiative recombination center EL3 according to the nomenclature proposed by Martin *et al.* [17]. The exact nature of the EL3 trap is not completely known. However, there are several evidences that point out that this trap is related to the off-center substitutional oxygen in As sites in GaAs material as discussed in Ref. [18, 19]. In the samples studied in this thesis the oxygen might originate from the nitrogen plasma RF source used to grow the GaAsN layers as suggested by Polyakov *et al.* [11]. However, Polyakov *et al.* have also observed this EL3 related center in GaAs control samples. Its presence was attributed to the strong background of oxygen in their growth system. Contrary to this work, no EL3-like was detected in our control samples.

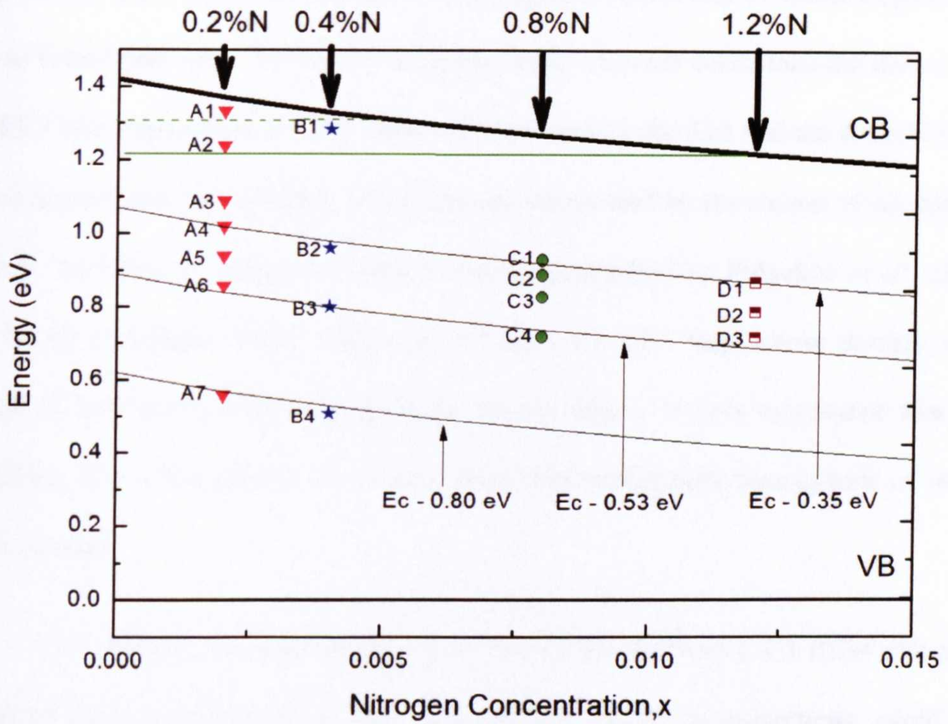

Fig.6.8 The energy location of the electron emitting trap levels below the conduction band of GaAsN epilayers. Nitrogen composition dependence of the band gap energy for GaAs is redrawn from Ref [16]. The top of the GaAs valence band is set to zero. The traps energies are plotted with respect to the conduction band edge GaAsN with different N compositions.

This suggests that the MBE system used to grow our layers has no memory effect for oxygen contamination. To shed further light on the origin of the EL3-like trap, Polyakov *et al.* investigated the effect of the growth conditions of GaAsN epilayers. It was found that when the GaAsN is grown under As-rich conditions the density of the EL3-like trap decreases [11]. This was explained by the fact that the formation of As vacancies and incorporation of oxygen are suppressed by the excess of As during growth. In addition, InGaAsN epilayers were investigated by Polyakov *et al.* using the DLTS technique. Their study also revealed the EL3 trap whose density was found to increase dramatically with In incorporation. It was concluded that In facilitates the incorporation of oxygen from the background atmosphere of their MBE system.

The electron emitting levels A4 (0.35 eV), B2 (0.37 eV), C1 (0.34 eV) and D1 (0.35 eV), with almost the same energies and capture cross-sections, could be due to the same defect. The activation energies of these traps are very close to that of the well-known EL6 trap [17]. EL6 is one of the three main recombination trap centers in GaAs grown under As-rich conditions by different techniques such as Horizontal Bridgman (HB), Liquid Encapsulated Czochralski (LEC) and Vapor Phase Epitaxy (VPE). The other two are EL2 and EL3. The origin of EL6 in HB, LEC and VPE GaAs has been assigned to point defects or impurity complexes containing Ga vacancies [20]. The possible structures of this trap suggested in Ref. 20 are Si_{Ga}-V_{Ga} and V_{Ga}-V_{As}. Its existence in the GaAsN layers has been also reported by Polyakov *et al.* [21]. Their DLTS investigation of MOCVD $GaAs_{0.65}N_{0.35}$ layers, with relatively thinner thicknesses (0.5 micron), observed the presence of a trap with similar activation energy that has a higher accumulation at the interface. They attributed this level to the interface states that originate from the lattice

mismatch between the GaAs buffer layer and the GaAsN epilayer. In another study of Be-doped GaAsN heterostructures by Krispin *et al.* [22] a trap level with similar activation energy (0.32 eV) has been reported, which was attributed to a donor-like interfacial level rather than an acceptor-like trap. However, the argument that these traps form at the interface because of the strain relaxation has been ruled out by Jenn-Fang *et al.* [23]. Their XRD data and theoretical simulations show strong evidence that the strain relaxation is not the origin of this trap (0.35 eV). It is clear that further complementary techniques such as paramagnetic resonance (EPR) are required to probe further the source of this trap. Despite its unknown defect structure this trap is common in GaAsN grown by different epitaxial methods [22,23, this work].

It is well known that the substitutional nitrogen (N_{As}) causes tensile strain in the GaAsN layers. The theoretical study by Zhang *et al.* [12] shows that the formation of N complexes such as As-N [$(AsN)_{As}$] and N-N [$(NN)_{As}$] split interstitial defects on single As-site compensate partially this tensile strain in GaAsN layers grown on GaAs substrates. However, the minimization of the strain is mainly due to the formation of the defect complexe $(AsN)_{As}$, which creates compressive strain, because $(NN)_{As}$ generates less tensile strain than (N_{As}). They predicted that in the dilute N limit the N-related complexes (N-N) and (N-As) split interstitials are associated with defect states at 0.66 eV and 0.42 eV below the conduction band edge, respectively. Deep levels labeled as A5 (0.43 eV), C2 (0.38 eV), C3 (0.44 eV) and D2 (0.43 eV) observed in the samples having different nitrogen compositions are in a reasonable agreement with the Zhang [12] predictions. Therefore, traps A5, C2, C3 and D2 could be assigned to N-As split interstitial complexes at As sites $(AsN)_{As}$. A similar N-related electron trap in MBE grown InGaAsN films with activation of

0.41 eV has been assigned to N-As defect complex by Xie *et al.* [24]. This is a further evidence that this defect is due to $(AsN)_{As}$.

The electron trap A3 (0.28 eV) was detected only in the sample containing 0.2% nitrogen. In terms of activation energy Krispin *et al.* [25, 26] have observed a similar electron trap at 0.29 eV, 0.27 eV, 0.25 eV in MBE GaAsN samples with N≤0.1%, N=0.5% and N=3%, respectively. The origin of these traps has been assigned to N-N split interstitial at As-site in accordance with the theoretical prediction given by Zhang *et al.* [12]. A similar N-N split interstitial defect with activation energy 0.25eV in GaInAsN has also been reported by Kurtz *et al.* [27]. The trap A3 (0.28 eV) is therefore identified as due to nitrogen split interstitials defect complexes.

The DLTS and LDLTS measurements on the reference sample (without nitrogen) displayed the presence of only one electron level, E1, with activation energy of 0.78 eV and capture cross-section of 5.15×10^{-14} cm^{2}. The origin of this trap could not be identified with previously reported traps in MBE grown GaAs. However, as our samples are grown at 500 ^{0}C which is comparatively lower than the standard growth temperature of 580-600 ^{0}C , this centre is likely to be associated with the intrinsic defect (0.65 eV), As_{Ga}, observed by D.C.Look *et al.* [29] in MBE GaAs samples grown at temperatures (400 ^{0}C) well below the standard 580-600^{0}C temperature window. This confirms that the 0.78 eV trap is not due to nitrogen either intentionally [9, 11] or unintentionally [10] incorporated in n-type GaAsN. In addition, this trap is strongly influenced by the nitrogen since its concentration decreases dramatically from 2.85×10^{15} cm^{-3} to 0 with the increase of the nitrogen content from 0% to 1.2%.

Since the midgap electron trap EL2 controls the semi-insulating properties of GaAs as it compensates the residual acceptors, it is one of the most extensively studied defects in semiconductors due to its fascinating properties [30-31]. Although the EL2 trap is present in VPE [28] and MOCVD [32] it is not known to be in MBE grown GaAs epitaxial layers. However, it can be created in MBE Si-doped GaAs by rapid thermal annealing [33] and irradiation in LPE GaAs [34]. It is also possible to annihilate it by broad band illumination of light (~1μm) at low temperature and cannot be optically stimulated afterwards [30].

Besides the appearance of EL2-like trap in the reference sample, DLTS scan shows its presence also in samples with N=0.2% and N=0.4% labeled as A7 and B4 with activation energies of 0.81 eV and 0.82 eV from the conduction band edge of GaAsN, respectively. This midgap level is absent in samples with higher nitrogen contents of 0.8% and 1.2%. This fundamental experimental observation of the annihilation of the reported EL2-like trap in GaAsN needs further investigation using other techniques in order to understand the role of nitogen in eliminating completely this deep electron level. One tentative explanation is that if this EL2-like trap is related to the famous antisite As_{Ga} the nitrogen could form a complex by an exchange mechanism between As_{Ga} and N_{As}. Theoretical investigation [12] of the As_{Ga}-N_{As} pair suggests that isolated As_{Ga} is infrequent at high nitrogen concentrations. The reduction of As_{Ga} at higher nitrogen compositions could explain the disappearance of this level in samples with 0.8% and 1.2%.

In the GaAsN layers having nitrogen contents in the range from 0.2% - 0.4% additional shallow levels [A1 (0.036 eV), A2 (0.13eV), B1 (0.045eV)] were detected in addition to the deep electron emitting level of energy ~0.8 eV. This infers that

these shallow levels are introduced by the nitrogen incorporation in the host material GaAs. Theoretical study by Li *et al.* [35] has predicted that the formation of Si_{Ga}-N_{As} is energetically favourable in GaAsN alloys. It was suggested that this complex has a higher activation energy than the silicon donor on a gallium site (Si_{Ga}). From this argument one can suggest that these shallow electron traps with such small activation energies could be assigned to a Si-N complex. The presence of Si-N complexes in GaAsN:Si films was considered by Y. Jin *et al.* [36] to be the dominant factor of the decrease in the free carrier concentration and mobitity, as determined by Hall effect, with increasing nitrogen incorporation up to 2%. This increase of the Si-N complexes with nitrogen content is not observed in this investigation. In fact the Si-N complexes are not detected in samples with 0.8% and 1.2% nitrogen but deeper defects are observed. In the light of these findings and as tentative explaination one can propose that nitrogen is forming defects with a more complex nature involving Si_{Ga} and N interstitials.

As far as the literature is concerned no DLTS observation of these shallow traps has been reported. This is due to the fact that most of the DLTS experiments are carried out at temperatures greater than 77K. The process of filling and emptying shallow traps cannot take place at these temperatures. This is a major limitation to explore shallow defects because the traps are completely empty of charge carriers. In order to probe the shallow levels, the DLTS system used in this study has been set up to operate at temperatures 8K and above.

6.3.7 CURRENT-VOLTAGE-TEMPERATURE ANALYSIS

The relationship of the reverse current in the reverse-biased devices as a function of temperature has been investigated in order to determine the dominant

electron traps that contribute to the leakage current. It is well known that the leakage current has a significant influence on the performance of modern electronic devices. The I-V-T characteristics in Fig. 6.7 clearly show a trend of an increase of the leakage current with the incorporation of N. This behaviour could be tentatively explained by an increase in the concentration of N-related defects. These can act as channels which facilitate further the flow of the reverse current.

The activation energies of thermally stimulated traps determined from the Arrhenius plots of reverse current versus 1/T are 0.78, 0.77, 0.81, 0.57 and 0.52eV for the GaAsN samples having nitrogen 0%, 0.2%, 0.4%, 0.8% and 1.2%, respectively. The values of the thermal activation energies of the traps in GaAsN layers with nitrogen 0.8% and 1.2% are almost the same as those determined by DLTS for the traps labeled as C4 and D3, and assigned to the well-known recombination center EL3. Whereas, in terms of activation energies, the defects detected in samples with N=0%, N= 0.2%, N=0.4% using I-V-T are similar to E1, A7 and B4 observed in DLTS measurements. These traps were attributed to EL2-like defect center.

The I-V-T measurements indicate that the EL3 and EL2-like trap levels are the main defect centers responsible for the generation of reverse current in the GaAsN epilayers investigated in this study.

6.4 CONCLUSIONS

We have studied a set of MBE grown dilute GaAsN epitaxial layers containing low nitrogen concentration (0.2% to 1.2%). The DLTS measurements revealed several deep defect levels in the band gap of GaAsN. From the careful comparison of our observed DLTS data with the results published in the literature, it is concluded that the well-known trap level EL3 (0.50-0.55 eV) present in all four samples. The I-V-T measurements reveal that EL3-like deep level is the main trap in samples with N≥0.8%, which is responsible for the leakge current across the Schottky junctions. The comparison of thermal emission and capture rate signatures with the reported data also shows that $(N\text{-}As)_{spl}$ split interstitial, nitrogen-split interstitial defect and EL6-like (0.35 eV) defect levels are also present in our samples depending on the nitrogen composition.

It was established for the first time that the annihilation of the EL2-like (0.78 eV) electron trap is attributed to the higher incorporation of nitrogen in MBE grown GaAs. An amount of N=0.8% was sufficient for the complete elimination of this trap, which was found to be the prevailing centre responsible for the reverse generation current in samples with N≤0.4%. In addition, newer shallow centers are detected in samples with N≤0.4%. These shallow levels which are absent in samples with N>0.4% are assigned to Si-N complexes.

REFERENCES

[1] S. R. Kurtz, A. A. Allerman, E. D. Jones, J. M. Gee, J. J. Banas, and B. E. Hammons, Appl. Phys. Lett., 74, 729 (1999).

[2] Jian Wei, F. Xia, C. Li and S. R. Forrest, IEEE Photonics Tech. Lett. 14, 597 (2002).

[3] GDR-E-2008 THz Workshop, 25-26.09.2008, Paris, France.

[4] Peter J. A. Thijs, Luuk F. Tiemeijier, P. I. Kuindersma, J. J. M. Binsma and T. Van Dongen, IEEE J. Quantum Electron. 27, 1426 (1991).

[5] I. Suemune, K. Uesugi, and W. Walukiewicz, Appl. Phys. Lett., 77, 3021 (2000).

[6] I. A. Buyanova, W. M. Chen, B. Monemar, H. P. Xin and C. W. Tu, Appl. Phys. Lett., 75, 3781 (1999).

[7] S. R. Kurtz, A. A. Allerman, C. H. Seager, R. M. Sieg and E. D. Jones, Appl. Phys. Lett., 77, 400 (2000).

[8] A. Fleck, B. J. Robinson, and D. A. Thompson, Appl. Phys.Lett., 78,1694 (2001).

[9] S. Dhara, N. Halder, J. Kumar and B. M. Arora, Appl. Phys. Lett., 85, 964 (2004).

[10] Jenn-Fang Chen, Ru-Shang Hsiao, Ming-Ta Hsieh, Wen-Di Huang, P. S. Guo, Wei-I Lee, Shih-Chang Lee and Chi-Ling Lee, Jap. J. Appl. Phys., 44, 7507 (2005).

[11] A.Y. Polyakov,N.B. Smirnov, A.V. Govorkov, Andrei E. Botchkarev, Nicole N. Nelson, M.M.E. Fahmi, James A. Griffin, Arif Khan, S. Noor Mohammad, D.K. Johnstone, V.T. Bublik, K.D. Chsherbatchev, M.I. Voronova and V.S. Kasatochkin, Solid State Elect. 46, 2155 (2002).

[12] S. B. Zhang and Su-Huai., Phys. Rev. Lett., 86, 1789 (2001).

[13] E. J. Miller, E. T. Yu, P. Waltereit and J. S. Speck, Appl. Phys. Lett., 84, 535 (2004).

[14] D.K.Schroder, IEEE Trans. Electron Devices ED-29, 1336 (1982).

[15] R. J. Kaplar, A. R. Arehart, S. A. Ringel, A. A. Allerman, R. M. Sieg, and S. R. Kurtz, J. Appl. Phys., 90, 3405 (2001).

[16] K. Uesugi, N. Morooka, and I. Suemune, Appl. Phys. Lett., 74, 9 (1999).

[17] G. M. Martin, A. Mitonneau, and A. Mircea, Electron. Lett. 13, 191 (1977).

[18] A. Wohlrab, B. Gründig-Wendrock, M. Jurisch, F.-M. Kiessling and J. R. Niklas, Eur. Phys. J. Appl. Phys., 27, 223 (2004).

[19] M. Skowronski, Mat Sci Forum, 83–87, 377 (1992).

[20] Zhao-Qiang Fang, T. E. Schlesinger, and A. G. Milnes, J. Appl. Phys., 61, 5741 (1987).

[21] A.Y. Polyakov, Solid State Elect. 46, 2141 (2002).

[22] P. Krispin, S. G. Spruytte and J. S. Harris and K. H. Ploog, J. Appl. Phys.,88, 4153 (2000).

[23] J. F. CHEN, R. HSIAO, M. T. HSIEH, W. D. HUANG, P. S. GUO, W. LEE, S. C. LEE and Chi-Ling LEE, J. J. Appl. Phys., 44, No. 10, 7507 (2005).

[24] S. Y. Xie, S. F. Yoon and S. Z. Wang, J. Appl. Phys., 97, 073702 (2005).

[25] P. Krispin, S. G. Spruytte, J. S. Harris and K. H. Ploog, J. Appl. Phys., 80, 2120 (2002).

[26] P. Krispin, V. Gambin, J. S. Harris and K. H. Ploog, J. Appl. Phys., 93, 6095 (2003).

[27] S. R. Kurtz, S. Johnston and H. M. Branz, Appl. Phys. Lett., 86, 113506 (2005).

[28] M. D. Miller, G. H. Olsen and M. Ettenberg, Appl. Phys. Lett., 31, 538 (1977).

[29] D. C. Look and z.Q.Fang, Phys. Rev. Lett., 70, 465 (1993).

[30] G. M. Martin, J. P. Farges, G. Jacob, and J. P. Hallais, J. Appl. Phys., 51, 2840 (1980).

[31] D. Kabiraj and Subhasis Ghosh, Appl. Phys. Lett., 87, 252118 (2005).

[32] M. O. Watanabe, A. Tanaka, T. Nakanisi and Y. Zohta, Jap. J. Appl. Phys., 20, L429 (1981).

[33] A. Kitagawa, A. Usami, Takao Wada, J. Appl. Phys., 61, 1215 (1987).

[34] P. N. Brunkov, V. S. Kalinovsky, V. G. Nikitin and M. M. Sobolev, Semicond. Sci. Technol. 7, 1237 (1992).

[35] J. Li, P. Carrier, S. H. Wei, S. S. Li, and J. B. Xia, Phys. Rev. Lett., 96, 035505 (2006).

[36] Y. Jin, Y. He, H. Cheng, R. M. Jock, T. Dannecker, M. Reason, A. M. Mintairov, C. Kurdak, J. L. Merz and R. S. Goldman, 95, 092109 (2009).

CHAPTER 7

EFFECTS OF THERMAL ANNEALING ON THE DEEP LEVELS IN GaAsN

7.1 INTRODUCTION

In general, defects and impurities deteriorate the optical and electrical properties of semiconductor materials. In order to recover these qualities it is common practice to subject the material to appropriate thermal treatment. There are two defect mechanisms which can occur upon the annealing procedure, namely, diffusion and disassociation of the traps. In the diffusion process when the annealing temperature is increased, the defect could migrate towards the surface or grain boundaries. In addition, the defect capability to diffuse through the crystal is determined by its charge state. The defects can be trapped by other impurities, for example recombination of an interstitial with a vacancy. In the dissociation process the intricate defects can break-up into separate defect complexes upon annealing.

Post-growth thermal annealing experiments have shown that an improvement of the electrical and optical quality is possible [1, 2] presumably due to the removal of some defect states [3]. There have been several studies reported in the literature about the annealing behavior of dilute nitride semiconductor materials. A brief

survey about the improvements in material's quality and transport properties after annealing is given below.

Jin *et al.* [4] have observed a substantial improvement in free carrier concentration and mobility after the post-growth annealing treatment of n-type GaAsN layers up to 800 ^{0}C. Using Hall effect experiments, a thermally activated increase in the free carrier concentration have been observed for temperatures above 150K. They attributed this increase of both carrier mobility and free carrier concentration to the elimination of the N-related defect states by post-growth annealing.

Studies of defects in GaAs/GaAsN by Krispin *et al.* [5, 6] have shown that the donor-like defect levels accumulated at the GaAs-on-GaAsN interface are responsible for the carrier depletion in as-grown heterostructures and their concentration rise remarkably in thicker GaAsN layers. From the electrical depth profiling measurements, it was suggested that these interfacial defect states can be removed by post-growth thermal annealing for 60s at 760 ^{0}C with a GaAs proximity cap under N_2 atmosphere.

In a DLTS study of MOCVD grown p-type GaAsN [7], rapid thermal annealing in the temperature range 600 ^{0}C - 900 ^{0}C for 30 sec generated six new deep levels. Most of them have been found to be thermally stable at 900 ^{0}C with some variations in their concentration. However, interstitial N–As complex and other non-radiative defects detected in the as-grown material have been found to be effectively removed by thermal annealing [8].

X-Ray Diffraction (XRD) and Deep-Level Transient Fourier Spectroscopy (DLTFS) studies to investigate the thermal annealing behaviour of GaInNAs have

been reported by Rangel-Kuoppa *et al.* [9]. They used two types of samples grown by molecular beam epitaxy (MBE): one medium doped with Si (2×10^{16} cm^{-3}) and one heavily doped with Si (1×10^{18} cm^{-3}). For the medium doped as-grown sample one main electron trap with activation energy of 0.976eV was detected, whereas for the heavily doped sample one main electron trap with activation energy of 0.35eV has been reported. Their thermal annealing measurements have shown that the density of these two electron traps decreases as the annealing temperature increases. However, depending on the annealing temperature, four more deep centres appeared in the medium doped samples. The XRD study did not show any structural change for the heavily doped sample, but it did for the medium doped sample only for the annealing temperature of 700 ^{0}C. It was suggested that the presence of Si strongly eliminates the creation of electron traps.

Ramstainer *et al.* [10] have investigated N-related defects in diluted GaAsN samples grown by solid-source MBE. They observed two additional peaks at 409 cm^{-1} and 427 cm^{-1} in addition to GaAs-related peak in their Raman Resonance spectroscopy measurements. The integrated intensity of the peaks was found to be related to N concentration. They assigned the Raman local vibrational modes at 409 cm^{-1} and 427 cm^{-1} to the N dimers on Ga site $(NN)_{Ga}$ and As site $(NN)_{As}$, respectively. Their intensity was found to be reduced by thermal annealing at 800 ^{0}C.

Toivonen *et al.* [11] have also observed defect complexes containing Ga vacancies in GaAsN epilayers which can behave as non-radiative centers. They used the positron annihilation spectroscopy to investigate GaAsN/GaAs epilayers, and found that GaAsN layers contain defect complexes involving Ga vacancies. Their

concentration increases rapidly up to 10^{18} cm^{-3} with increasing N and decreases after annealing at 700 °C.

An investigation of the effect of rapid thermal annealing on optical properties of undoped GaAsN/GaAs multi-quantum wells (MQWs) was carried out by Buyanova *et al.* [12]. A reasonable increase in the PL intensity and a substantial decrease in the PL linewidth were observed. Their magnetic resonance studies revealed a significant reduction in the concentration of non-radiative defects after the heat treatment with halogen lamps in a flowing N_2 ambient at 850 °C for 10s. They suggested that the reduction of the non-radiative defects after heat treatment leads to an improvement in the optical quality of GaAsN/GaAs MQWs.

The incorporation of impurities can create defect states that can hinder the luminescence intensity. For example, hydrogen impurities might be incorporated during the growth of samples by MOCVD or by gas-source MBE. These could reduce the light emission from the samples [13-15]. Thermal annealing treatment in this regard can in principle improve the luminescence by reducing the density of defect states. Rao *et al.* [16] have studied GaAsN epilayers using PL and secondary ion mass spectrometry (SIMS) techniques. From PL measurements, they have seen higher PL intensity with smaller line-widths after post-growth heat treatments for 15min at 650 ^{0}C. On the basis of their SIMS data they have inferred that this enhancement in the PL properties is due to the annihilation of defects associated with N-H complexes in GaAsN epilayers. In another investigation of defects in GaAsN epilayers and GaAs/GaAsN MQWs, which has been carried out by using optically detected magnetic resonance techniques, Thinh *at el.* [17] have studied the formation of two non-radiative defects (an As_{Ga}-related complex and an unknown). A

remarkable improvement in the efficiency of the light emission was achieved after post-growth annealing at 850 °C for 10s. This was considered to be possibly due to the decrease in the concentration of these non-radiative defects.

In addition to the enhancement of the luminescence from the nitride materials upon annealing, a shift in the PL emission has also been observed by several researchers. Wang *et al.* [18] have reported PL experiments on GaAsN samples that reveal the existence of a red-shift in the PL peak energy after thermal annealing. Their observations have shown that the PL from GaAsN does not originate from band-to-band transitions, but rather from localized state excitonic recombinations. Furthermore it was found that the interstitial N–As complex and the defects related to the broad energy-tail in the low-energy side of the PL spectrum could be effectively removed by the thermal annealing process. Another example of the redshift of PL emission is demonstrated by the work of Francoeur *et al.* [19]. Their PL measurements showed a redshift in the luminescence peak detected in MOCVD grown InGaAsN layers after annealing at 650 °C for 5 minutes. A shift of 15 meV in a sample containing 0.7% N was observed. From the XRD measurement they attributed this redshift to the increase of nitrogen incorporation.

Several other annealing studies of nitride materials reported in the literature show a blue shift of the PL emission upon thermal annealing. Kudrawiec *et al.* [20], E. Tournie *et al.* [21] and M. Kondow *et al.* [22]). Tournie *et al.* performed PL and x-ray diffraction experiments on Ga(In)NAs quantum wells and investigated the influence of post-growth annealing on their optical and structural properties. A blue shift in the PL emission was reported and was attributed to the internal atomic rearrangement in the InGaAsN well layer. Similarly the annealing induced blue-shift

in InGaAsN materials observed by Kondow *et al.* has also been suggested to be mainly due to the atoms rearrangement in the material. Whereas the work of Li *et al.* [23], Damimano *et al.* [24], Kim *et al.* [25] and Albrecht *et al.* [26] attributed the blue shift of PL emission to the N diffusion.

As demonstrated by several researchers the defect sates have a great influence on the electrical and optical properties of the materials. It is therefore of paramount importance to perform electrical measurements to investigate such defect states and gather the knowledge of the annealing effects on these defect states. In the study reported in this thesis, the effects of thermal annealing on the defects observed in as-grown GaAsN (N= 0.2 – 1.2%) have been investigated.

7.2 RESULTS

7.2.1 CURRENT-VOLTAGE (I-V) AND CAPACITANCE-VOLTAGE (C-V) CHARACTERISTICS

I-V measurements were performed on the as-grown and annealed samples to check their suitability for the DLTS and Lapalce DLTS measurements. The samples having low leakage current (~ 3 μA at – 4 Volts) have been selected for further electrical investigations. The C-V data were found to fit the $1/C^2$ - V_R relationship as discussed in section 4.1.3 of Chapter 4. The background concentration has been determined from least square fit through data points in the plot of $1/C^2$ versus V_R. The values of the background concentrations obtained from the C-V measurements were used to determine the density of the traps detected in DLTS measurements.

7.2.2 DLTS MEASUREMENTS

DLTS and LDLTS measurements have been performed on as-grown GaAsN layer, and layers annealed at different temperatures using a reverse bias of -4V with a 1ms pulse duration. The sampling rate window was 50 s^{-1} and the temperature was scanned from 10 to 400K for the standard DLTS measurements. For the LDLTS measurements, the temperature was maintained constant within 0.1K by utilising the temperature controller.

Four sets of GaAsN samples have been investigated in this study. Each set contains an as-grown $GaAs_{1-x}N_x$ sample with x=0.2%, 0.4%, 0.8% and 1.2% and samples with the same N composition annealed at 500 °C, 600 °C, 700 °C and 800 °C. Typical standard DLTS spectra obtained from each as-grown GaAsN and annealed sample refereed to here as set one, set two, set three and set four are shown in Figs. 7.1, 7.2, 7.3 and 7.4, respectively. The traces (a), (b), (c), (d) and (e) correspond to as-grown GaAsN and annealed GaAsN samples at 500 °C, 600 °C, 700 °C and 800 °C, respectively. The DLTS spectra have been offset intentionally for better clarity of the evolution and/or annihilation of the defects in the annealed samples.

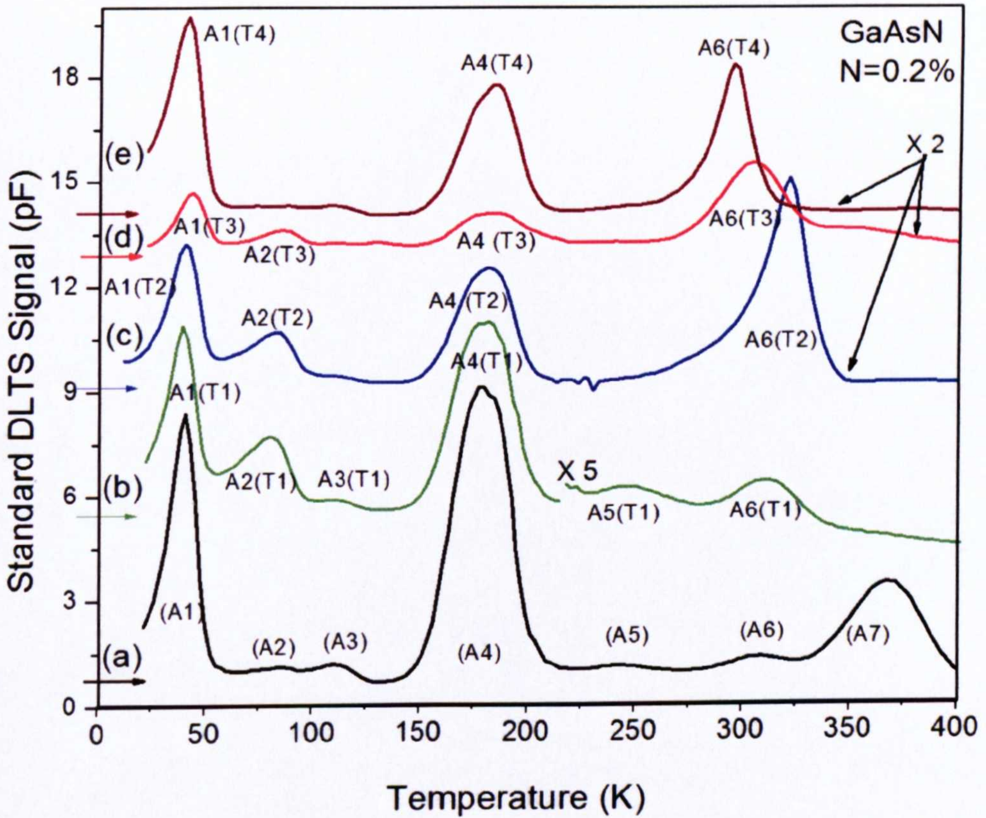

Fig.7. 1 Standard DLTS spectra from **(a)** the as-grown GaAsN (N = 0.2%) layer, and the layers annealed at **(b)** T1=500 °C, **(c)** T2=600 °C, **(d)** T3=700 °C and **(e)** T4=800 °C. Rapid thermal annealing was carried out for 1min. The spectra were taken using a reverse bias of -4V with a 1ms pulse duration and the sampling rate window was 50 s^{-1}. The spectra have been offset intentionally for clarity. The horizontal arrows indicate the zero level of the spectrum.

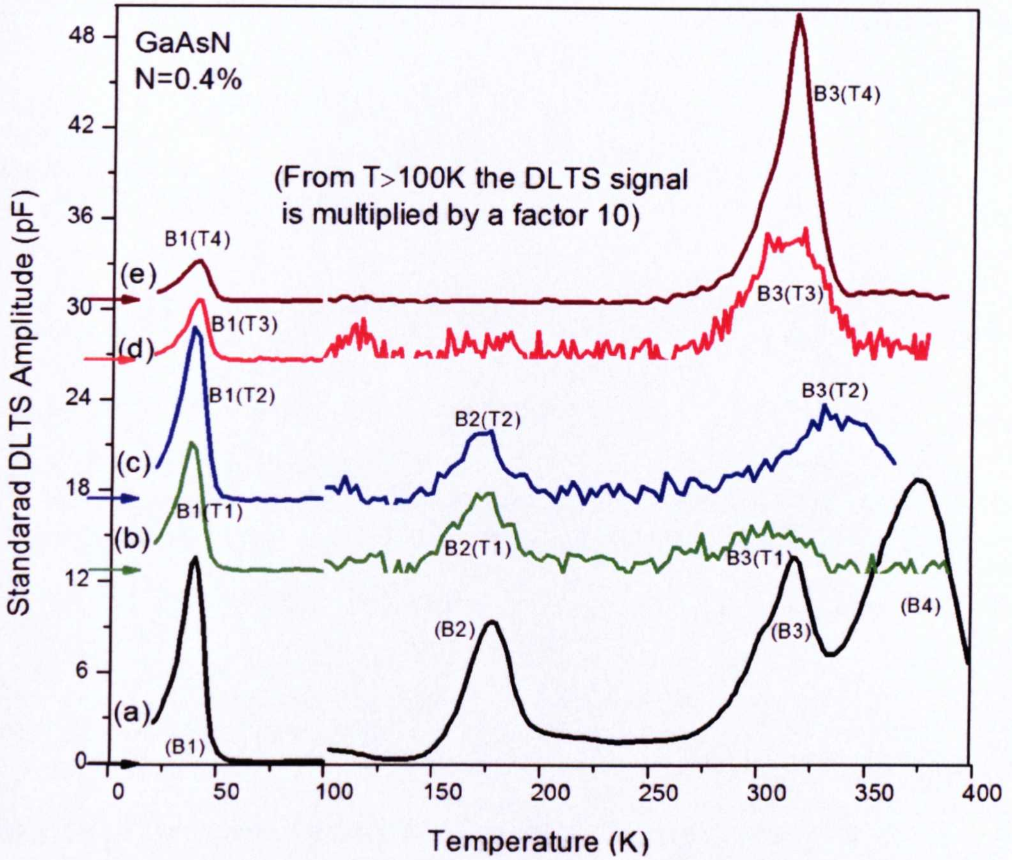

Fig.7. 2 DLTS spectra from **(a)** the as-grown GaAsN (N = 0.4%) layer, and the layers annealed at **(b)** T1=500 °C, **(c)** T2=600 °C, **(d)** T3=700 °C and **(e)** T4=800 °C. Rapid thermal annealing was carried out for 1min. The spectra were taken using a reverse bias of -4V with a 1ms pulse duration and the sampling rate window was 50 s^{-1}. The spectra have been offset intentionally for clarity. The horizontal arrows indicate the zero level of the spectrum.

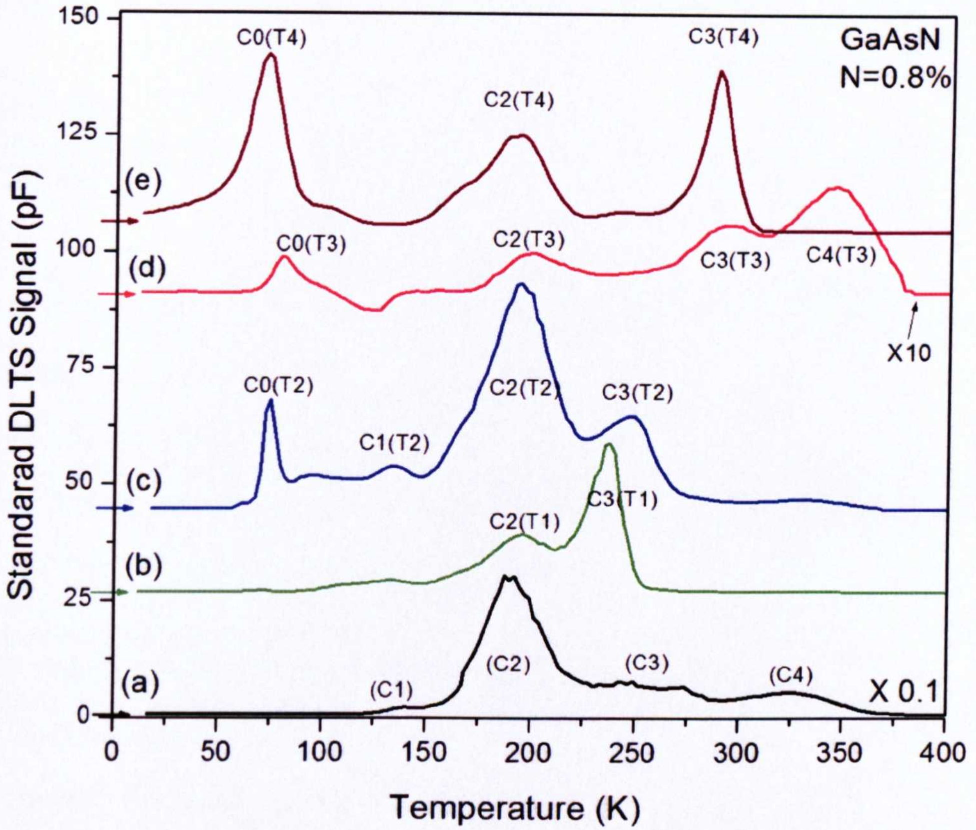

Fig.7. 3 Standard DLTS spectra from (a) the as-grown GaAsN (N = 0.8%) layer, and the layers annealed at **(b)** T1=500 °C, **(c)** T2=600 °C, **(d)** T3=700 °C and **(e)** T4=800 °C. Rapid thermal annealing was carried out for 1min. The spectra were taken using a reverse bias of -4V with a 1ms pulse duration and the sampling rate window was 50 s^{-1}. The spectra have been offset intentionally for clarity. The horizontal arrows indicate the zero level of the spectrum.

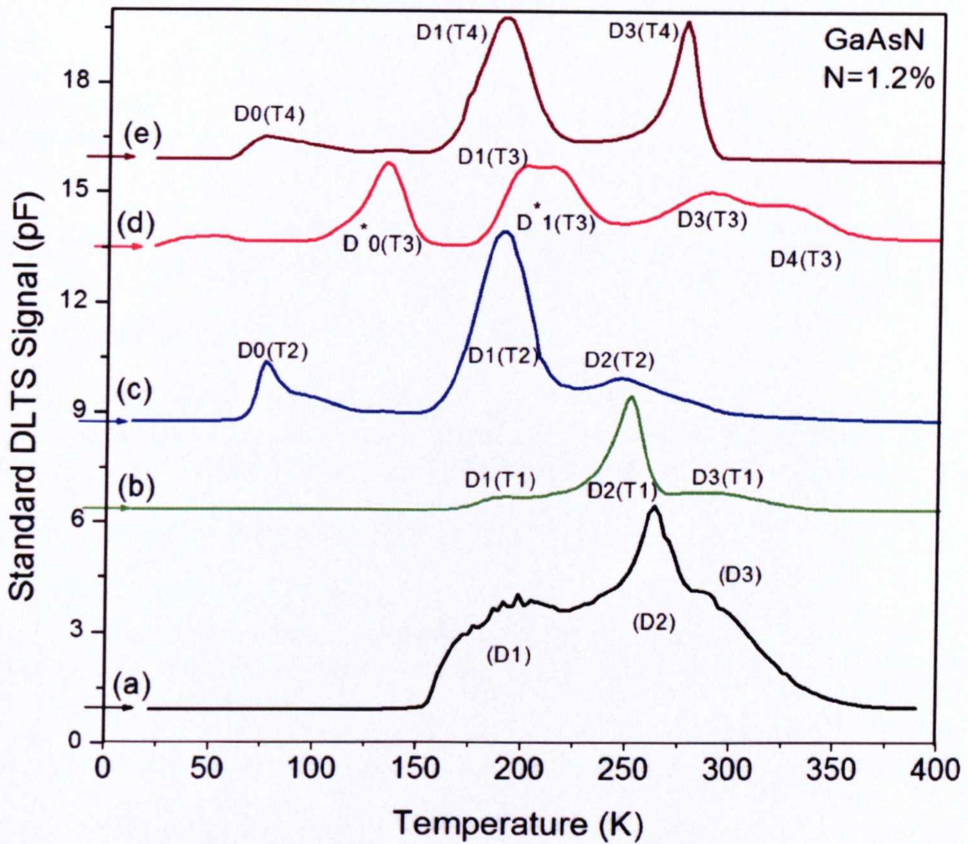

Fig.7. 4 Standard DLTS spectra from **(a)** the as-grown GaAsN (N = 1.2%) layer, and the layers annealed at **(b)** T1=500 °C, **(c)** T2=600 °C, **(d)** T3=700 °C and **(e)** T4=800 °C. Rapid thermal annealing was carried out for 1min. The spectra were taken using a reverse bias of -4V with a 1ms pulse duration and the sampling rate window was 50 s^{-1}. The spectra have been offset intentionally for clarity. The horizontal arrows indicate the zero level of the spectrum.

7.2.2.1 DLTS RESULTS OF GaAsN WITH N=0.2%

Fig. 7.1 shows typical DLTS spectra obtained from the as-grown and annealed GaAsN samples containing 0.2% nitrogen. The as-grown sample exhibit seven peaks, labeled A1-A7, detected in the DLTS spectra. These are related to electron emitting defect states as discussed in Chapter 6. The DLTS spectra obtained from the GaAsN layer annealed at 500 ^{0}C, 600 ^{0}C, 700 ^{0}C and 800 ^{0}C show six electron traps [labeled A1(T1) – A6(T1)], four electron traps [labeled A1(T2), A2(T2), A4(T2) and A6(T2)], four electron traps [labeled A1(T3), A2(T3), A4(T3) and A6(T3)] and three electron traps [labeled A1(T4), A4(T4) and A6(T4)], respectively. The emission rate data for all the deep levels has been obtained by utilising high resolution Laplace DLTS technique in the temperature range from 10K to 400K. The emission rates were plotted against temperature on the semi-logarithmic scale. The slope of the best-fit line through the data points plotted in an Arrhenius plot [log (e/T^2) vs 1000/T] gives the activation energy of the corresponding deep level. Emission rate signatures of each trap are plotted in Fig. 7.5. Assuming capture cross section σ_n is temperature-independent, σ_n for each trap has also been calculated from the slope of the respective Arrhenius plots [log $(1-S(t_p)/S(\infty)$ versus t_p] as described in section 4.2.4.2 of Chapter 4. The values of activation energies and σ_n for each trap are given in Table 7.1.

7.2.2.2 DLTS RESULTS OF GaAsN WITH N=0.4%

DLTS spectra of the as-grown and annealed GaAsN samples containing 0.4% nitrogen is depicted in Fig. 7.2. As seen, four electron emission peaks labeled as B1, B2, B3 and B4 are observed in the as-grown sample.

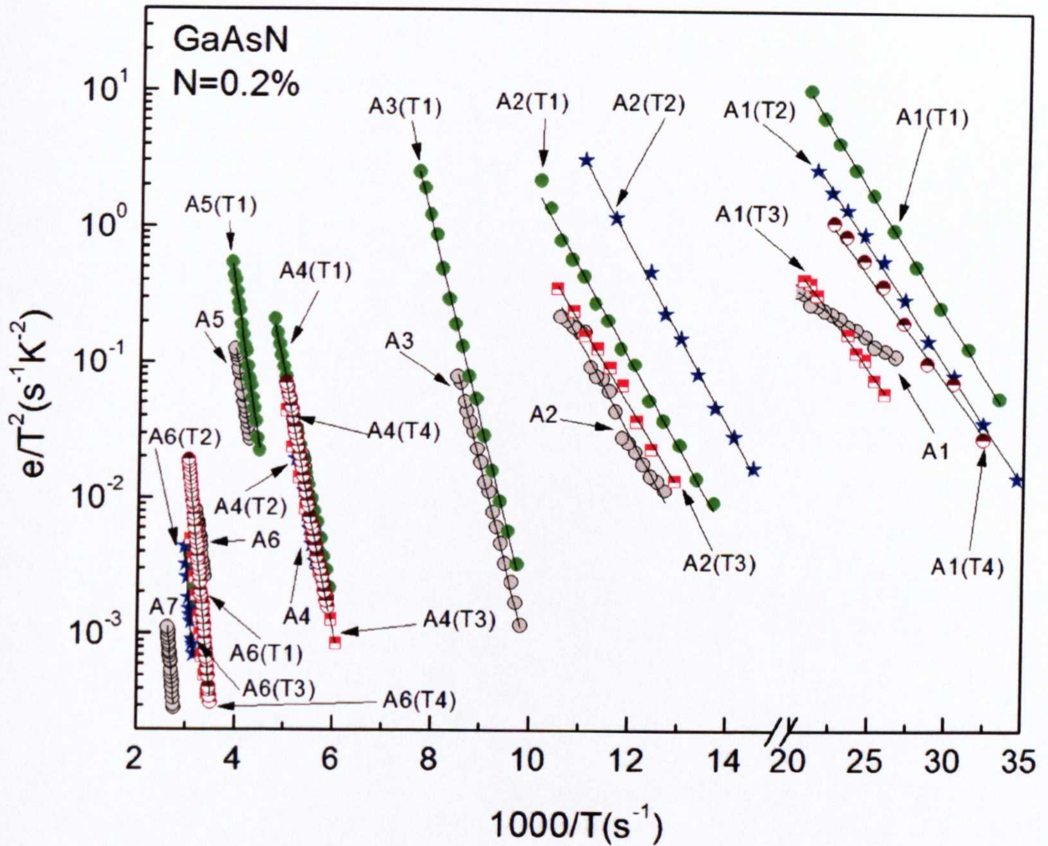

Fig.7. 5 Arrhenius plots derived from the thermal emission rates for the as-grown GaAsN (N = 0.2%) and annealed samples. The traps detected in the as-grown and annealed samples at temperature Tn (n=1-4) are labeled as follows: as-grown sample (no annealing) A1-A7; A(T1) for T1=500 °C; A(T2) for T2=600 °C; A(T3) for T3=700 °C and A(T4) for T4=800 °C. The labeling adopted (A1, A2, A3…….) is used to distinguish the traps from one another). The annealing time was 1 min.

TABLE 7.1. Trap parameters obtained from standard DLTS and Laplace DLTS data analysis for the as-grown and annealed GaAsN (N = 0.2%) samples.

Nitrogen (0.2 %)	Trap label	Activation Energy (eV)	Capture cross-section σ_n (cm^2)	Trap density (cm^{-3})
As-grown	A1	0.036	5.89×10^{-19}	2.03×10^{15}
	A2	0.13	1.07×10^{-18}	1.53×10^{14}
	A3	0.28	5.61×10^{-17}	1.68×10^{14}
	A4	0.35	8.21×10^{-16}	2.22×10^{15}
	A5	0.43	4.52×10^{-16}	1.50×10^{14}
	A6	0.51	5.28×10^{-16}	2.10×10^{14}
	A7	0.81	3.64×10^{-14}	7.56×10^{14}
Anneal 500^{0}C	A1(T1)	0.056	4.71×10^{-19}	1.69×10^{15}
	A2(T1)	0.12	2.01×10^{-18}	6.88×10^{14}
	A3(T1)	0.27	5.77×10^{-17}	1.23×10^{14}
	A4(T1)	0.32	7.31×10^{-16}	1.72×10^{15}
	A5(T1)	0.46	1.45×10^{-16}	9.10×10^{13}
	A6(T1)	0.51	3.12×10^{-16}	9.87×10^{13}
Anneal 600^{0}C	A1(T2)	0.051	7.72×10^{-19}	5.27×10^{14}
	A2(T2)	0.13	1.67×10^{-18}	1.84×10^{14}
	A4(T2)	0.36	3.03×10^{-16}	4.24×10^{14}
	A6(T2)	0.53	6.25×10^{-16}	7.65×10^{14}
Anneal 700^{0}C	A1(T3)	0.057	1.95×10^{-19}	4.73×10^{14}
	A2(T3)	0.118	2.06×10^{-18}	1.50×10^{14}
	A4(T3)	0.33	2.87×10^{-16}	2.94×10^{14}
	A6(T3)	0.55	6.02×10^{-16}	6.05×10^{14}
Anneal 800^{0}C	A1(T4)	0.053	5.13×10^{-19}	1.71×10^{15}
	A4(T4)	0.37	4.38×10^{-16}	1.12×10^{15}
	A6(T4)	0.55	6.15×10^{-16}	1.29×10^{15}

After annealing the samples at 500 °C, 600 °C, 700 °C and 800 °C, DLTS measurements reveal three traps [labeled B1(T1), B2(T1) and B3(T1)], three traps [labeled B1(T2), B2(T2) and B4(T2)], two traps [labeled B1(T3) and B3(T3)] and two traps [labeled B1(T4) and B3(T4)], respectively. The Arrhenius plot of the thermal emission rates versus the temperature is shown in Fig. 7.6. The activation energies of each trap were determined from the slope and intercept of the Arrhenius plots.

The capture cross-section were determined from the slope of the respective Arrhenius plots between $\log(1-S(t_p)/S(\infty)$ and pulse width (t_p) as described in section 4.2.4.2 of Chapter 4. The values of the activation energies and capture cross-sections are given in Table 7.2.

7.2.2.3 DLTS RESULTS OF GaAsN WITH N=0.8%

DLTS measurements on as-grown GaAsN and layers annealed at 500 °C, 600 °C, 700 °C and 800 °C samples having 0.8% nitrogen are illustrated in Fig. 7.3. DLTS spectra obtained from as-grown sample reveal four electron emission peaks labeled as C1, C2, C3 and C4. After the annealing of the samples at 500 °C, 600 °C, 700 °C and 800 °C, DLTS measurements reveal two traps [labeled C2(T1) and C3(T1)], four traps [labeled C0(T2), C1(T2), C2(T2) and C3(T2)], four traps [labeled C0(T3), C2(T3), C3(T3) and C4(T3)] and three traps [labeled C0(T4), C2(T4) and C3(T4)], respectively. As mentioned above, the emission rates are plotted in the Arrhenius plots shown in Fig. 7.7. The activation energies and capture cross-sections obtained from the Arrhenius plots of thermal emission rates and capture rates are given in Table 7.3.

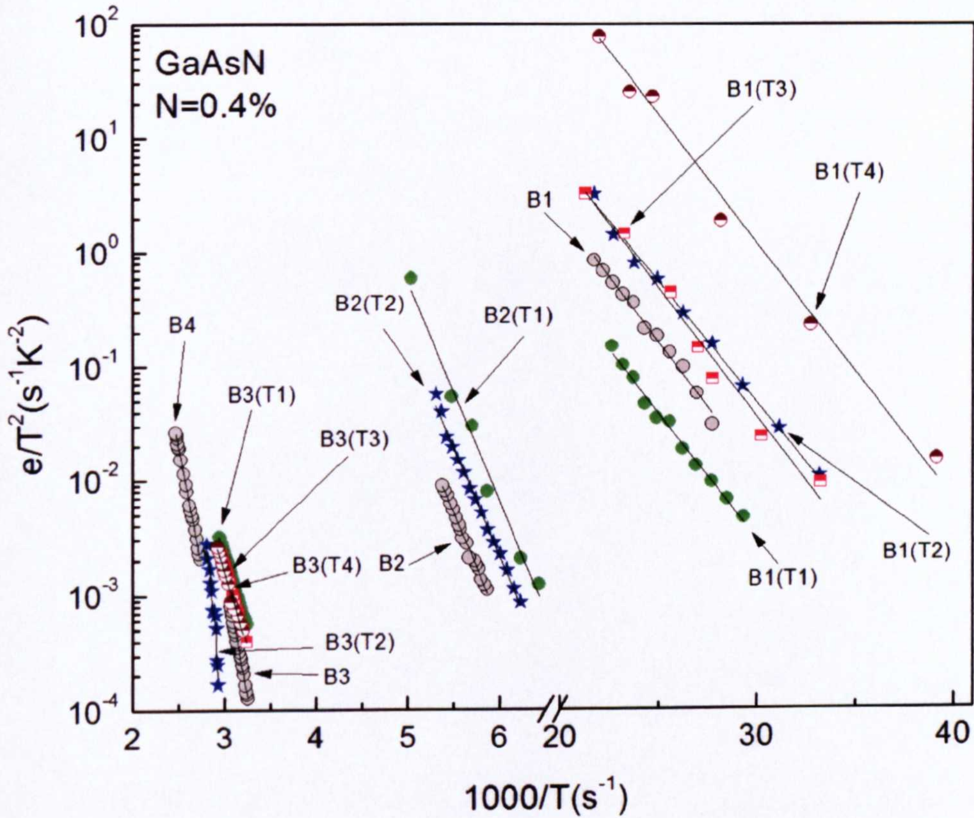

Fig.7. 6 Arrhenius plots derived from the thermal emission rates for the as-grown GaAsN (N = 0.4%) and annealed samples. The traps detected in the as-grown and annealed samples at temperature Tn (n=1-4) are labeled as follows: as-grown sample (no annealing) B1-B4; B(T1) for T1=500 °C; B(T2) for T2=600 °C; B(T3) for T3=700 °C and B(T4) for T4=800 °C. The labeling adopted (B1, B2, B3…) is used to distinguish the traps from one another). The annealing time was 1 min.

TABLE 7.2. Trap parameters obtained from standard DLTS and Laplace DLTS data analysis for the as-grown and annealed GaAsN (N = 0.4%) samples.

Nitrogen (0.4 %)	Trap label	Activation Energy (eV)	Capture cross-section σ_n (cm^2)	Trap density (cm^{-3})
As-grown	B1	0.045	2.80×10^{-18}	3.60×10^{15}
	B2	0.37	5.75×10^{-16}	2.44×10^{14}
	B3	0.53	6.36×10^{-16}	3.52×10^{14}
	B4	0.82	1.02×10^{-14}	5.07×10^{14}
Anneal 500^{0}C	B1(T1)	0.044	1.87×10^{-18}	2.98×10^{15}
	B2(T1)	0.36	4.21×10^{-16}	1.66×10^{14}
	B3(T1)	0.54	5.53×10^{-16}	8.54×10^{13}
Anneal 600^{0}C	B1(T2)	0.042	2.13×10^{-18}	2.86×10^{15}
	B2(T2)	0.35	3.78×10^{-16}	1.12×10^{14}
	B3(T2)	0.55	6.26×10^{-16}	1.55×10^{14}
Anneal 700^{0}C	B1(T3)	0.045	1.21×10^{-18}	1.74×10^{15}
	B3(T3)	0.51	5.93×10^{-16}	3.26×10^{14}
Anneal 800^{0}C	B1(T4)	0.044	2.56×10^{-18}	1.21×10^{15}
	B3(T4)	0.50	8.04×10^{-16}	6.95×10^{14}

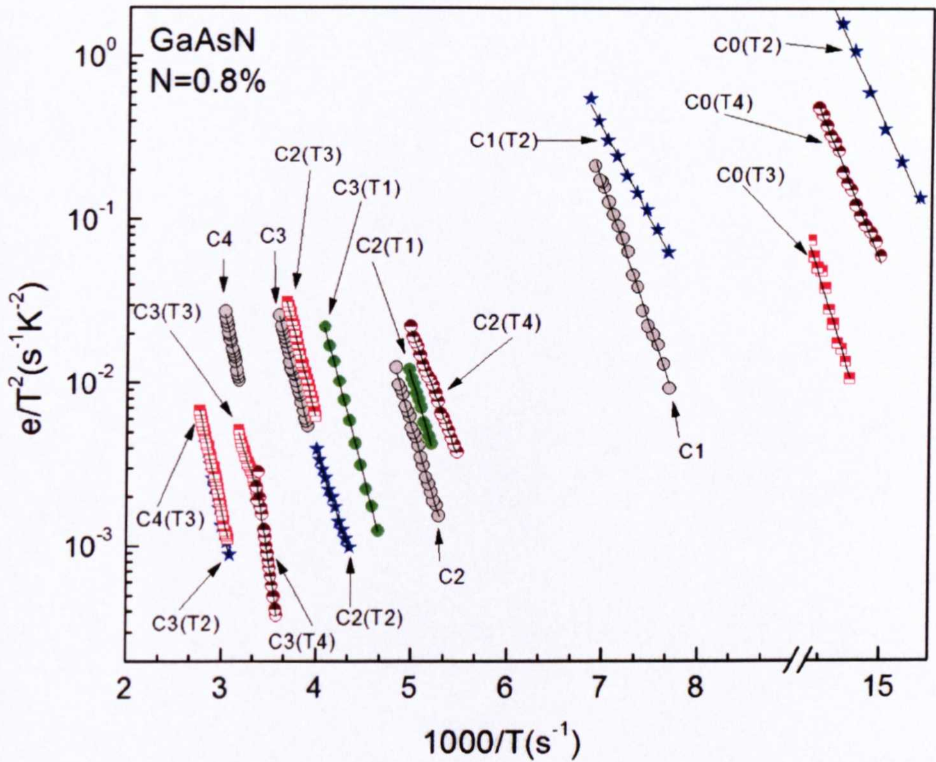

Fig.7. 7 Arrhenius plots derived from the thermal emission rates for the as-grown GaAsN (N = 0.8%) and annealed samples. The traps detected in the as-grown and annealed samples at temperature Tn (n=1-4) are labeled as follows: as-grown sample (no annealing) C1-C4; C(T1) for T1=500 °C; C(T2) for T2=600 °C; C(T3) for T3=700 °C and C(T4) for T4=800 °C. The labeling adopted (C1, C2, C3…) is used to distinguish the traps from one another). The annealing time was 1 min.

TABLE 7.3. Trap parameters obtained from standard DLTS and Laplace DLTS data analysis for the as-grown and annealed GaAsN (N = 0.8%) samples.

Nitrogen (0.8 %)	Trap label	Activation Energy (eV)	Capture cross-section σ_n (cm^2)	Trap density (cm^{-3})
As-grown	C1	0.34	2.63×10^{-16}	1.86×10^{14}
	C2	0.38	4.24×10^{-16}	3.51×10^{15}
	C3	0.44	7.41×10^{-16}	6.97×10^{14}
	C4	0.55	5.51×10^{-16}	5.82×10^{14}
Anneal 500^0C	C2(T1)	0.37	2.29×10^{-16}	5.05×10^{14}
	C3(T1)	0.45	6.67×10^{-16}	1.28×10^{15}
Anneal 600^0C	C0(T2)	0.11	1.81×10^{-18}	4.24×10^{14}
	C1(T2)	0.25	2.11×10^{-17}	1.71×10^{14}
	C2(T2)	0.35	3.12×10^{-16}	9.84×10^{14}
	C3(T2)	0.51	5.34×10^{-16}	3.67×10^{14}
Anneal 700^0C	C0(T3)	0.12	1.59×10^{-18}	2.84×10^{13}
	C2(T3)	0.35	2.51×10^{-16}	3.20×10^{13}
	C3(T3)	0.45	4.24×10^{-16}	5.43×10^{13}
	C4(T3)	0.53	5.13×10^{-16}	8.61×10^{13}
Anneal 800^0C	C0(T4)	0.13	3.24×10^{-18}	4.54×10^{15}
	C2(T4)	0.32	4.53×10^{-16}	2.10×10^{15}
	C3(T4)	0.56	6.71×10^{-16}	9.91×10^{14}

7.2.2.4 DLTS RESULTS OF GaAsN WITH N=1.2%

Fig. 7.4 shows the DLTS spectra obtained from the as-grown GaAsN layer containing 1.2% nitrogen and layers annealed at 500 °C, 600 °C, 700 °C and 800 °C. The DLTS spectra of the as-grown (N=1.2%) sample shows electron emission peaks with relatively broad features. High resolution Laplace DLTS resolved the broad features and three peaks related to electron emission have been detected. These are labeled as D1, D2 and D3. Similarly, a number of deep levels are observed after the thermal treatment of the samples: three for T1=500 °C [labeled D1(T1), D2(T1) and D3(T1)], three for T2=600 °C [labeled D0(T2), D1(T2), and D2(T2)], five for T3= 700 °C [labeled D^*0(T3), D1(T3), D^*1(T3), D3(T3) and D4(T3)] and, three for T4= 800 °C [labeled D0(T4), D1(T4) and D3(T4)]. The emission rate data for all these levels has been obtained in the usual way as explained previously. Arrhenius plots constructed from these data are plotted in Fig. 7.8. The energy location of all these deep levels in the bandgap of the GaAsN samples and their capture cross-sections have been determined from the Arrhenius plots as mentioned in above section. These are given in Table. 7.4.

7.2.2.5 TRAP CONCENTRATION

The concentrations of the detected deep levels in as-grown GaAsN layer and, layers annealed at 500 °C, 600 °C, 700 °C and 800 °C, for each set of samples having N = 0.2%, 0.4%, 0.8% and 1.2% have been determined from the respective peak height in the standard DLTS spectra using the standard formula, $\Delta C/C = N_T / 2N_D$ as outlined in Chapter 4. The concentration values obtained for each trap in all the samples in each set are given in Table 7.1, 7.2, 7.3 and Table 7.4, respectively.

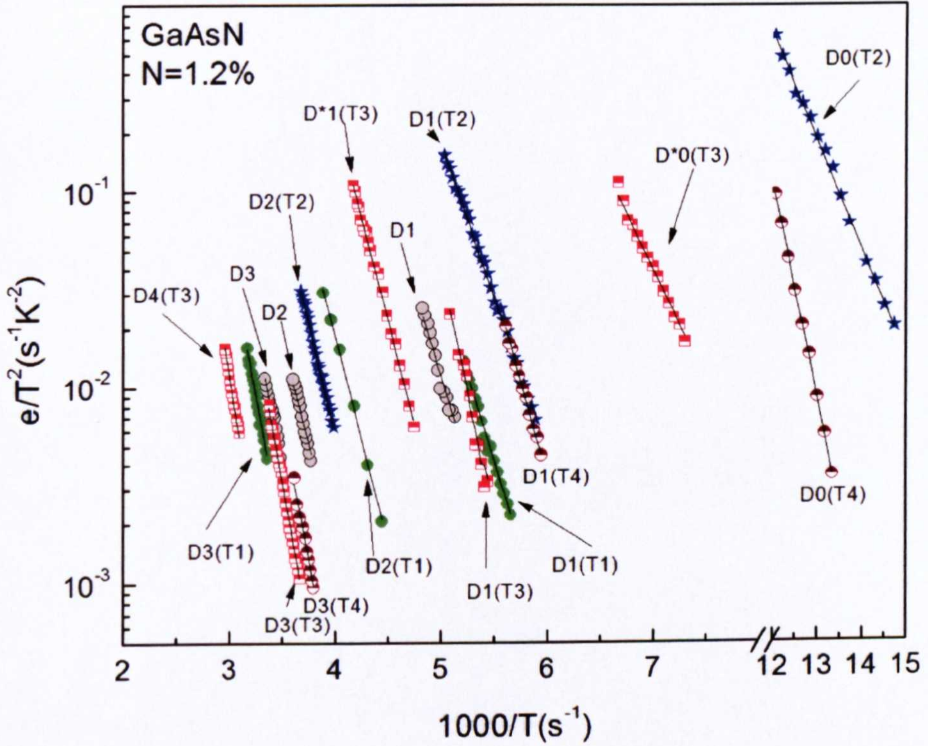

Fig.7. 8 Arrhenius plots derived from the thermal emission rates for the as-grown GaAsN (N = 0.4%) and annealed samples. The traps detected in the as-grown and annealed samples at temperature Tn (n=1-4) are labeled as follows: as-grown sample (no annealing) D1-D4; D(T1) for T1=500 °C; D(T2) for T2=600 °C; D(T3) for T3=700 °C and D(T4) for T4=800 °C. The labeling adopted (D1, D2, D3…) is used to distinguish the traps from one another). The annealing time was 1 min.

TABLE 7.4. Trap parameters obtained from Standard DLTS and Laplace DLTS data analysis for the as-grown and annealed GaAsN (N = 1.2%) samples.

Nitrogen (1.2 %)	Trap label	Activation Energy (eV)	Capture cross-section σ_n (cm^2)	Trap density (cm^{-3})
As-grown	D1	0.35	2.43×10^{-16}	5.57×10^{14}
	D2	0.43	5.09×10^{-16}	9.97×10^{14}
	D3	0.50	5.78×10^{-16}	5.74×10^{14}
Anneal 500^0C	D1(T1)	0.34	1.07×10^{-16}	5.50×10^{13}
	D2(T1)	0.43	3.16×10^{-16}	4.72×10^{14}
	D3(T1)	0.51	3.91×10^{-16}	7.33×10^{13}
Anneal 600^0C	D0(T2)	0.13	1.91×10^{-18}	2.70×10^{14}
	D1(T2)	0.32	4.71×10^{-16}	8.72×10^{14}
	D2(T2)	0.45	3.28×10^{-16}	1.97×10^{14}
Anneal 700^0C	D^*0(T3)	0.22	1.15×10^{-17}	4.53×10^{14}
	D1(T3)	0.35	2.41×10^{-16}	4.38×10^{14}
	D^*1(T3)	0.38	3.94×10^{-16}	4.30×10^{14}
	D3(T3)	0.53	5.36×10^{-16}	2.97×10^{14}
	D4(T3)	0.60	8.79×10^{-16}	2.13×10^{14}
Anneal 800^0C	D0(T4)	0.12	9.91×10^{-19}	1.31×10^{14}
	D1(T4)	0.38	5.94×10^{-16}	8.21×10^{14}
	D3(T4)	0. 53	7.63×10^{-16}	8.12×10^{14}

7.3 DISCUSSION

7.3.1 GaAsN WITH N=0.2%

From the DLTS spectra shown in Fig. 7.1, the DLTS peak around 37K that appear in the as-grown sample is also present in all the annealed samples. From the thermal emission rate and capture rate signatures the activation energy and capture cross-section of this electron trap, labeled as A1 in the as-grown spectra and, A1(T1), A1(T2), A1(T3) and A1(T4) for the samples annealed at 500 °C, 600 °C, 700 °C and 800 °C, respectively, are in the range of (0.036-0.057) eV and (1.95 – 5.89) $\times$ 10^{-19} cm^2, respectively. The values of the activation energy for this trap show that it is much greater than the activation energy of the hydrogen-like shallow donors in GaAs, which are typically 0.005-0.006eV. Peak A2 which appears in the as-grown sample around 80K is also observed in samples annealed at 500 °C, 600 °C and 700 °C but it is annihilated in the sample annealed at 800 °C. Its concentration increases from 1.53 to 3.00 $\times$ 10^{14} cm^{-3} with heat treatment from 500 °C to 700 °C and becomes zero after 800 °C. The activation energy and capture cross-section values are found to be in the range of (0.11 – 0.13) eV and (1.07 – 2.01) $\times$ 10^{-18} cm^2, respectively. Since the control sample (without N) has shown no such deep levels as discussed in Chapter 6, and their existence only appear with the incorporation of N in the GaAs, one can infer that these donor-like centers are related to N-induced defect levels. The actual nature of these traps is not known but they might be due to Si-N complexes. In this regard, the study of Jin *et al.* [4] supports the existence of Si-N complexes. This suggestion was made based on the study of the transport properties of GaAsN alloys in which the free carrier concentration was found to decrease with the increase of the N content. Similarly, theoretical calculation by Li *et*

al. [31] predicted that the binding of N with Si is energetically favorable and the complex formations push the Si-donor level deep into the bandgap of the GaAsN. Our experimental results support their arguments, and therefore, on the basis of the studies in references [4, 27] the defect states at energies from 0.036eV to 0.13eV below the conduction band edge are associated with the Si-N complexes which are deep donor-like states that can act as carrier trapping centers. Annealing from 500 °C to 800 °C does not have a major effect on trap A1 but it does on the level A2 when annealed at 800 °C.

Electron emitting level A3 in the as-grown sample is also detected in the sample annealed at 500 °C. However, it is annihilated in the samples treated from 600 °C to 800 °C. The density of trap A3 decreases from 1.68 to 1.23×10^{14} cm^{-3} when annealed at 500 °C and becomes zero upon annealing between 600-800 °C. The activation energy and capture cross-section of trap A3 and its counterpart A3(T1) are found to be 0.28eV and 5.61×10^{-17} cm^2 and, 0.27eV and 5.77×10^{-17} cm^2, respectively. These values are comparable to those of the reported trap (0.25eV) in GaAsN samples with higher nitrogen (3%) mole fraction [28]. This trap has been attributed to a nitrogen-split interstitial defect on an As site. Rangel-Kuoppa *et al.* [29] have also seen a similar trap in their annealing study of MBE-grown GaInNAs samples. They suggested that the trap, which appeared after annealing at 750 °C, with activation energy of 0.25eV might be due to As-interstitial or As-antisite.

DLTS peaks labeled as A4(T1), A4(T2), A4(T3) and A4(T4) observed in the samples annealed at 500 °C, 600 °C, 700 °C and 800 °C, respectively are the counterpart of the trap A4 (0.35eV) detected in the as-grown GaAsN layer as illustrated by their thermal emission rates in Fig. 7.5. The thermal activation energy

and capture cross-section are found to be in the range 0.32 – 0.37eV and 2.87 – 8.21 $\times 10^{-16}$ cm^2, respectively (Table 7.1). Variations in the density of this defect have been observed on annealing the sample from 500 ^oC to 800 ^oC. It decreases from 2.22 $\times 10^{15}$ cm^{-3} in as-grown sample to 5.88 $\times 10^{14}$ cm^{-3} in samples annealed at temperatures up to 700 ^oC and then increases to a value of 1.12 $\times 10^{15}$ cm^{-3} after annealing at 800 ^oC. This trap is similar to EL6 defect in GaAs [30] commonly considered as V_{Ga}-As_i complex. Polyakov *et al.* [31] have observed a related trap in their study on GaAs, GaAsN and GaInAsN samples. They observed that the intensity of the peak related to this trap decreases when nitrogen is incorporated in GaAs, i.e. GaAsN. A further decrease was reported for the quarternary GaInAsN alloy. This infers that this defect state is intrinsic to GaAs. The decrease of its concentration with the incorporation of N indicates that the N atoms are making a complex with this trap level. Krispin *et al.* [5] have also observed a similar trap level in p-type GaAsN samples and attributed it to an interfacial defect. Jenn-Fang *et al.* [32] investigated the thickness dependence transport properties of MOCVD- grown GaAsN and reported` an analogous defect state which was also assigned to an interfacial defect state. With regards to the annealing behavior of this defect state, annealing up to 800 ^oC appears to have very little impact on the defect concentration.

The thermal emission rate signatures of trap A5 (0.43eV) observed in the as-grown and of A5(T1) (0.46eV) detected in the sample annealed at 500 ^oC, with a slight difference in their activation energies, show that these defects could have the same origin. However, after annealing at 500 ^oC a small decrease in the trap density occurs from 1.50 $\times 10^{14}$ cm^{-3} to 9.10 $\times 10^{13}$ cm^{-3}. Annealing at temperatures of 600 ^oC and above annihilated this trap. Polyakov *et al.* [31] have reported a trap of comparable characteristics in GaAsN samples, and associated it to EL5 in GaAs. It is

worth noting that Rangel-Kuoppa *et al.* [29] have also observed a trap with nearly the same activation energy (0.40eV) in GaInAsN layers when annealed at 700 °C. It was suggested that this might be due to a dislocation caused by the movement of N from its substitutional position.

DLTS peak A6 measured in the as-grown sample around 300K is also present in the annealed samples. Its activation energy and capture cross-section are in the range of 0.49 - 0.55 eV and 3.12 – 6.25 × 10^{-16} cm^2, respectively. Its concentration increases from 2.10 × 10^{14} cm^{-3} to 1.29 × 10^{15} cm^{-3} upon annealing up to 800 °C. In terms of energy location it could be related to the well-known non-radiative recombination center EL3 [30] which is considered to be due to off-center substitutional oxygen atom at an As site. In a similar study, Polyakov *et al.* [31] have associated this level found in GaAsN to EL3 trap.

Trap A7 which is detected at ~375K in the as-grown sample was annihilated after 500 °C heat treatment. This trap is also present in the control sample (N = 0). Its concentration is found to decrease dramatically from 7.56 × 10^{14} cm^{-3} to zero after a 500 °C thermal anneal. It is presumed that this deep level is due to some point defect or point defect-impurity complex. From the capture cross-section value and its energy location (0.81eV), this peak A7 is similar to the extensively studied trap EL2 [30] which is usually assigned to As anitsite (As_{Ga}) [33]. A comparable midgap electron trap present at 0.7 eV in GaAsN layers grown by liquid phase epitaxy (LPE) has been reported by Dhar *et al.* [34]. They found that this trap originates from the incorporation of nitrogen and tentatively assigned it to (N–N) defects at As sites. Kaplar *et al.* [35], Rangel-Kuoppa *et al.* [29] and Polyakov *et al.* [31] have also observed a related trap with a slight difference in activation energy in Sn-doped

InGaAsN, Si-doped GaInAsN and Si-doped GaAsN samples, respectively. Rangel-Kuoppa *et al.* [29] and Polyakov *et al.* [31] have assigned this trap to EL2. In comparison with literature it is also concluded that trap A7 could be related to the well-known trap EL2.

7.3.2 GaAsN WITH N=0.4%

The effect of rapid thermal annealing treatment on the deep levels detected in as-grown GaAsN containing 0.4% nitrogen is illustrated in the DLTS spectra shown in Fig. 7.2.

The trap level that manifests itself at the low temperature range is consistent in all the samples: B1 in as-grown material and B1(T1), B1(T2), B1(T3) and B1(T4) in annealed samples at 500 ^{o}C, 600 ^{o}C, 700 ^{o}C and 800 ^{o}C, respectively. However, its concentration decreases from 3.60×10^{14} cm^{-3} in the as-grown layer to 1.21×10^{14} cm^{-3} in the 800 ^{o}C annealed layer. This result demonstrates that this trap is fairly stable in GaAsN (N = 0.4%) layer since the heat treatment up to 800 ^{o}C does not affect it significantly. Thermal emission rates and capture cross section measurements yield activation energies and capture cross-sections in the range 0.042-0.045eV and $1.21 - 2.80 \times 10^{-18}$ cm^2, respectively. The emission rate signatures shows that this trap is most probably of the same nature as the one observed in GaAsN layers with N = 0.2% and is therefore related to the Si-N complexes as discussed in section 7.3.1.

Trap level B2 (0.37eV) remains stable in the samples heat treated up to 600 ^{o}C and then it is eliminated for annealing temperatures $\geq$700 ^{o}C. The concentration of the this trap decreases from 2.44×10^{14} cm^{-3} to 1.12×10^{14} cm^{-3} upon annealing at 600 ^{o}C. The thermal emission rates of this trap are found to be similar to that of A4

present in the as-grown sample having 0.2% nitrogen and have been assigned to the well-known EL6 level as explained in Chapter 6.

Electron trap level B3 (0.53eV) which is present in non-annealed GaAsN layers (N=0.4%) is found to be stable upon annealing up to 800 °C. Its appearance with slight difference in activation energy has also been recognized in as-grown and annealed samples containing 0.2% nitrogen as discussed in the previous section. The variations in the carrier concentration of this trap upon annealing has been observed and found to be in the range of (1.12 - 6.35) × 10^{14} cm^{-3}. Since the temperature and its energy location, and capture cross-section are similar to those of A6 in GaAsN with N=0.2% and EL3 [30], it can be related to trap EL3.

Heat treatment of the as-grown sample with N=0.4% has been able to eradicate the deeper trap B4(0.82 eV) as evidenced by the DLTS spectra shown in Fig. 7.2. The reduction in the concentration of similar trap in GaInAsN layers after annealing was also reported by Rangel-Kuoppa *et al.* [29]. They have identified the trap as point defects-impurity complex. Its content reduction was associated with the decrease of this complex upon annealing.

7.3.3 GaAsN WITH N=0.8%

The DLTS spectra obtained from the as-grown and annealed samples containing 0.8% nitrogen are shown in Fig. 7.3. Electron emitting level C1 detected in the as-grown samples is found to be unstable. It was observed only in samples annealed at 600 °C and cannot be detected in samples heat treated at higher temperatures. The activation energy, capture cross-section and trap density are given in Table 7.3. Their emission and capture rates suggest that this could be related to the

nitrogen-split interstitial defect on As site as reported by Krispin *et al.* [28] for a similar defect state. After the heat treatment of 600 °C, 700 °C and 800 °C, a new trap labeled as C0(T2), C0(T3) and C0(T4) has been observed, respectively. Its concentration has an unusual behaviour; it decreases from 4.24×10^{14} cm^{-3} in as-grown layers to 2.84×10^{13} cm^{-3} in 700 °C annealed samples and increases to 4.54×10^{15} cm^{-3} upon annealing at 800 °C. The energy location of these traps (0.11-0.13eV) suggests that it could be related to Si-N complexes [4, 27] as discussed in the previous section.

The existence of trap C2 (0.38eV) in the as-grown and annealed samples, labeled as C2(T1), C2(T2), C2(T3), C2(T4) and C2(T4), has been observed. Emission and capture rates of this trap are similar to the well-know center EL6 (0.35eV) [30]. It is worth pointing out that the density of this trap (see Table 7.3) changes with annealing temperature. The trap level C3 (0.44eV) was found to be stable up to the annealing temperature of 800 °C. Its thermal emission signature is comparable to that of A5 (0.43eV) observed in the as-grown GaAsN with N=0.2%. As discussed in section 7.3.1, it could be assigned to a nitrogen related defect center. Polyakov *et al.* [31] have also observed a trap with equivalent characteristics and was suggested to be related to defect state EL5 (0.42eV) in GaAs. Trap center C4 detected in the as-grown samples disappeared in samples annealed at 500 °C, 600 °C and 800 °C but it was present in the samples annealed at 700 °C. This unusual behaviour with the rapid thermal anneal is not well understood. The trap density was found to decrease from 5.82×10^{14} cm^{-3}in as-grown layers to 8.61×10^{13} cm^{-3} in 700 °C heat treated layers. In order to identify the trap C4 the emission and capture rate signatures of this trap were compared with the reported data in the literature which shows that it could be related to the well-known EL3 (0.55eV) [31].

7.3.4 GaAsN WITH N=1.2%

Fig. 7.4 shows the DLTS spectra of GaAsN sample containing 1.2% nitrogen. Trap D1 observed in the as-grown sample has also been detected in the annealed samples. The activation energy and capture cross-section for this trap are found to be in the range of 0.32 – 0.38 eV and 1.07 – 5.49 × 10^{-16} cm^2, respectively. Variations in the concentration of this trap as a function of annealing temperature are noticed which are given in Table 7.4. The comparison of the thermal emission rates of this trap with those of EL6 [31] suggest that the deep levels, D1 (0.35eV), D1(T1) (0.34eV), D1(T2) (0.32eV), D1(T3) (0.35eV) and D1(T4) (0.38eV) could also be assigned tentatively to EL6 (0.35eV). Another electron emitting trap, D^*1(T3) (0.37eV), which overlapped with peak D1(T3), has been resolved by high resolution Laplace DLTS. Its emission rate signature has only been observed in the sample annealed at 700 °C. The energy location and capture cross section of this trap suggest that this trap has also the same origin as that of D1(T3). After annealing the samples at 600 °C and 800 °C, new traps D0(T2) (0.13eV) and D0(T4) (0.12eV) around 75K were detected, respectively. These were not present in the as-grown samples. The thermal emission rates of these traps are similar to the traps A2(0.13eV) observed in the as-grown GaAsN having 0.2% nitrogen. As we discussed earlier in section 7.3.1, these shallow energy traps could be related to the Si-N complexes. A similar electron trap with slightly different activation energy ET1(0.19eV) is reported by Xie *et al.* [36]. They have detected this electron trap as a minority carrier in p-type Be-doped InGaAsN layers. The trap ET1(0.19eV) emerged after annealing the samples at 750 °C for 1 min. They assigned this trap to the continuous distribution of point defects located just below the edge of the conduction band. A similar continuous distribution

of point defects with activation energy ~ 0.20 eV near the conduction band edge has also been reported by Kaplar *et al.* [35].

The evolution of another electron emitting trap, $D^{*}0(T3)$ (0.22eV), has been observed only in the samples annealed at 700 °C. By considering the activation energy and capture cross-section, one could suggest that they have similar origin as A2, or E1 (0.20eV) [35]. An analogous trap with activation energy of 0.20eV has been documented by Khan *et al.* [37] in their studies of InGaAsN. They have assigned this trap to N-related level.

Trap D2 which is present in the as-grown and annealed samples at 500 °C and 600 °C has been exterminated at 700 °C and 800 °C. Its concentration is found to decrease from 9.97×10^{14} cm^{-3} to 1.97×10^{14} cm^{-3} after the heat treatment of 600 °C for 1 min. The energy and capture cross-section revealed from the Arrhenius plots are in the range of 0.43-0.45eV and $3.16 - 5.09 \times 10^{-16}$ cm^{2}, respectively. According to the reported theoretical [38] and experimental work [28] on GaAsN materials this deep centre can be assigned to the N-related defects as discussed in Chapter 6.

Deep level D3 shows an unstable behaviour in the annealed samples. It is first annihilated in the samples annealed at 600 °C, and then it emerges again in the other samples annealed at 700 °C and 800 °C. The energy and capture cross-section of this trap is in the range of 0.50-0.53eV and $(3.91\text{-}7.63) \times 10^{-16}$ cm^{2}, respectively. This trap has the same emission rates as those of EL3 as discussed in section 7.3.1. Defect level D4(T3) (0.60eV) has been emerged after annealing at 700 °C. The origin of this trap is not known. However, a similar trap with activation energy 0.59 eV has been observed in the investigation of InGaAsN films [39]. On the basis of SIMS measurements it was assigned to oxygen-related defect centre. In another

study of defect levels, Rangel-Kuoppa *et al.* [29] have also seen a similar trap having activation energy of 0.59eV in GaInNAs epilayers. They have also suggested this trap to be related to oxygen.

7.4 CONCLUSIONS

In summary, the thermal annealing behaviour of defects present in the as-grown Si-doped GaAsN layers containing nitrogen concentration in the range 0.2 – 1.2% has been investigated by DLTS and Laplace DLTS techniques. Seven defect states were observed in the as-grown GaAsN (N=0.2%) samples. Heat treatment of these samples at different annealing temperatures annihilated some of the traps. At least four of the traps were annihilated after annealing upto 800 °C. Similarly, annealing the layers containing N = 0.4% have also shown the annihilation of some of the defect states revealed in the as-grown samples. On the contrary to the above samples with low nitrogen concentrations, layers containing N = 0.8 and 1.2% both creation and annihilation of some of the traps have been observed upon annealing.

DLTS and LDLTS studies of the annealed samples show that the EL3-like trap (0.5 – 0.55 eV), which was suspected to be the main center responsible for the generation of leakage current, still present in all GaAsN layers with some variations in its concentration.

The defect state having an activation energy in the range of 0.77 – 0.82 eV found in the reference (N = 0%) and as-grown GaAsN (N = 0.2 - 0.4%) samples was annealed out. The comparison with literature suggests that it might be related to the native arsenic antisite (As_{Ga}) such as EL2 in GaAs.

Another defect state having an activation energy in the range of 0.3 – 0.37 eV manifests itself in most of the as-grown GaAsN (N = 0.2 – 1.2%) and annealed samples. The thermal emission rate signatures of this trap suggest that it is very close to the GaAs native defect EL6.

The nitrogen related defect with activation energy ~ 0.44 eV has also been observed in some as-grown and annealed samples. A variation in its density has been seen upon annealing.

Some new shallow traps with energies ranging from 0.036 to 0.13 eV have also been detected in both as-grown and annealed samples which are scarcely reported in the literature.

REFERENCES

[1] D. J. Friedman, J.F. Geisz, S. Kurtz, and J.M. Olson, J. Cryst. Growth 195, 409 (1998).

[2] S. G. Spruytte, C. W. Coldren, J. S. Harris, W. Wampler, P. Krispin, K. Ploog and M. C. Larson, J. Appl. Phys., 89, 4401 (2001).

[3] L. Grenouillet, C. Bru-Chevallier, G. Guillot, P. Gilet, P. Ballet, P. Duvaut, G. Rolland, and A. Million, J. Appl. Phys., 91, 5902 (2002).

[4] Y. Jin, Y. He, H. Cheng, R. M. Jock, T. Dannecker, M. Reason, A. M. Mintairov, C. Kurdak, J. L. Merz, and R. S. Goldman, Appl. Phys. Lett., 95, 092109 (2009).

[5] P. Krispin, S. G. Spruytte and J. S. Harris and K. H. Ploog, J. Appl. Phys.,88, 4153 (2000).

[6] P. Krispin, S. G. Spruytte and J. S. Harris and K. H. Ploog, J. Appl. Phys.,89, 6294 (2001).

[7] Qiang Gao, Hark Hoe Tan, Chennupati Jagadish, and Prakash N. K. Deenapanray, Jpn. J. Appl. Phys., 42, 6827 (2003).

[8] S. Z. Wang, S.F. Yoon, W.K. Loke, C.Y. Liu and S. Yuan, J. Crys. Growth 255, 258 (2003).

[9] V. T. Rangel-Kuoppa and J. Dekker, Physica Scripta., Vol. T114, 12 (2004).

[10] M. Ramsteiner, D. S. Jiang, J. S. Harris, and K. H. Ploog. Appl. Phys. Lett., 84, 1859 (2004).

[11] J. Toivonen, T. Hakkarainen, M. Sopanen, H. Lipsanen, J. Oila and K. Saarinen, Appl. Phys. Lett., 82, 40 (2003).

[12] I. A. Buyanova, G. Pozina, P. N. Hai, N. Q. Thinh, J. P. Bergman, W. M. Chen, H. P. Xin and C. W. Tu, Appl. Phys. Lett., 77, 2325 (2000).

[13] H. Saito, T. Makimoto and N. Kobayashi, J.Cryst.Growth 195, 416(1998).

[14] H. P. Xin, C. W. Tu, and M. Geva, Appl. Phys. Lett., 75, 1416 (1999).

[15] J. F. Geisz, D. J. Friedman, J. M. Olson, S. R. Kurtz, and B. M. Keyes, J. Cryst. Growth, 195, 401 (1998).

[16] E. V. K. Rao, A. Ougazzaden, Y. Le Bellego, and M. Juhel, Appl. Phys. Lett., 72, 1409 (1998).

[17] N. Q. Thinh, I. A. anova, W. M. Chena, H. P. Xin, and C. W. Tu, Appl. Phys. Lett., 79, 3089 (2001).

[18] S. Z. Wang, S. F. Yoon, W. K. Loke, C.Y. Liu and S. Yuan, J. Cryst. Growth, 255, 258 (2003).

[19] S. Francoeur, G. Sivaraman and H. Temkin, Appl. Phys. Lett., 72, 1857 (1998).

[20] R. Kudrawiec, J. Misiewicz, E.-M. Pavelescu, J. Konttinen, and M. Pessa, IEE. Proc.-Optoelectron., 151, 323 (2004).

[21] E. Tournie, M.-A. Pinault, and A. Guzman, Appl. Phys. Lett., 80, 4148 (2002).

[22] Takeshi Kitatani Masahiko Kondow and Sho Shirakata, J. Phys. Cond. Matter, 16, (2004).

[23] Wei Li, Jani Turpeinen and Markus Pessa, Appl. Phys. Lett., 78, 91 (2001).

[24] B. Damilano, J. Barjon, J.-Y. Duboz, J. Massies A. Hierro, J.-M. Ulloa, and E. Calleja, Appl. Phys. Lett., 86, 071105 (2005).

[25] T. S. Kim, J. Y. Park, T. V. Cuong, H. G. Kim, H. J. Lee, E. K. Suh, and C. H. Hong, J. Cryst. Growth, 267, 412 (2004).

[26] M. Albrecht, T. Remmele V. Grillo, H. P. Strunk, A. Yu. Egorov, Gh. Dumitras, and H. Riechert, Appl. Phys. Lett., 81, 2719 (2002).

[27] J. B. Li, P. Carrier, S. H. Wei, S. S. Li and J. B. Xia, Phys. Rev. Lett., 96, 035505 (2006).

[28] P. Krispin, V. Gambin, J. S. Harris, and K. H. Ploog, J. Appl. Phys., 93, 6095 (2003).

[29] V. T. Rangel-Kuoppa and J. Dekker, Materials Sci. and Eng. B, 129, 222 (2006).

[30] G. M. Martin, A. Mitonneau, and A. Mircea, Electron, Lett. 13, 191 (1977).

[31] A. Y. Polyakov, N. B. Smirnov, A. V. Govorkov, Andrei E. Botchkarev, Nicole N. Nelson, M. M. E. Fahmi, James A. Griffin, Arif Khan, S. Noor Mohammad, D. K. Johnstone, V. T. Bublik, K. D. Chsherbatchev, M. I. Voronova and V. S. Kasatochkin, Solid-State Electron, 46, 2155 (2002).

[32] Jenn-Fang CHEN, Ru-Shang HSIAO, Ming-Ta HSIEH, Wen-Di HUANG, P. S. GUO, Wei-I LEE, Shih-Chang LEE and Chi-Ling LEE, J. J. Appl. Phys., 44, No. 10, 7507 (2005).

[33] R.R. Sumathi, M. Udhayasankar, J. Kumar, P. Magudapathy and K. G. M. Nair, Physica B, 308, 1209 (2001).

[34] S. Dhar, N. Halder, J. Kumar and B. M. Arora, Appl. Phys. Lett., 85, 964 (2004).

[35] R. J. Kaplar, A. R. Arehart, S. A. Ringel, A. A. Allerman, R. M. Sieg, and S. R. Kurtz, J. Appl. Phys., 90, 3405 (2001).

[36] S. Y. Xie, S. F. Yoon and S. Z. Wang, J. Appl. Phys., 97, 073702 (2005).

[37] Aurangzeb Khan, Sarah R. Kurtz, S. Prasad, S. W. Johnston, and Jihua Gou, Appl. Phys. Lett., 90, 243509 (2007).

[38] S. B. Zhang and Su-Huai Wei, Phys. Rev. Lett., 86, 1789 (2001).

[39] A. Balcioglu, R. K. Ahrenkiel, and D. J. Friedman, Appl. Phys. Lett., 76, 2397 (2000).

CHAPTER 8

EFFECTS OF HYDROGEN IRRADIATION ON DEEP LEVELS IN GaAsN

8.1 INTRODUCTION

Hydrogen is the most common elements in nature. It exhibits high chemical activity and diffusivity in semiconductors. Hydrogen can be easily incorporated in most of the semiconductor materials during the growth process either unintentionally or intentionally. This is due to the fact that the growth techniques, such as metal-organic chemical vapor deposition (MOCVD), laser ablation, and sputtering (H_2 environment), contain a large amount of hydrogen in their growth environment. The molecular beam epitaxy (MBE) is usually considered to be almost free from contaminants. However, desorption of hydrogen from the stainless steel MBE chamber could lead to hydrogen incorporation in the films. Thus, based on these facts, hydrogen is an unavoidable and commonly found impurity in semiconductor materials.

The effect of hydrogen on shallow impurities is well documented. In 1954, Mollwo *et al.* [1] have first studied the hydrogen irradiation of ZnO. Their results

revealed a remarkable increase in the n-type conductivity of the material. Later in 1980, Haller *et al.* [2, 3] observed the electrically active copper (Cu) impurities in Ge. It was established that Cu can be completely passivated by hydrogen, and the formation of $Cu\text{-}H_3$ has been proposed as the resulting neutral species. The study of metal-oxide-semiconductor (MOS) transistors by Sah *et al.* [4] demonstrated the hydrogen passivation of shallow boron dopant impurities in p-type silicon. They proposed that interstitial hydrogen acts as a donor in Si and compensates the boron acceptors. The behaviour of hydrogen as a donor in boron-doped silicon (p-type) have also been confirmed by Pankove *et al.* [5]. Another study of phosphorus (P) doped Si by Johnson *et al.* [6] revealed that hydrogen can also passivate P donors and thus behaves as an acceptor in *n*-type materials. In addition, it was found that the electron mobility increases. According to the above studies, hydrogen has an opposite behaviour to the prevailing conductivity of the material, i.e. it can act as a donor and an acceptor in p-type and n-type materials, respectively. This amphoteric behaviour in silicon was confirmed by different researchers using different experimental techniques [7–10].

In III-V semiconductors such as GaAs, hydrogen has a similar effect as the one described above in silicon. For example, the infrared absorption spectroscopy measurements of hydrogenated carbon-doped p-type GaAs shows that the hydrogen form complexes with carbon acceptors (H-C) which lead to the passivation of these shallow impurity levels [11]. In the Si-doped n-type GaAs samples, Chevallier *et al.* [12, 13, 14] have observed the passivation of Si donors by hydrogen exposure. By using hydrogen diffusion and electrical measurements, they argued that the decrease and increase of the free electron concentration and mobility, respectively, can be attributed to the transformation of active Si donors into electrically neutral hydrogen-

silicon related complexes. The existence of Si-H complexes in GaAs was confirmed by high resolution Fourier transform spectroscopy.

Incorporation of a few percent of nitrogen impurities in GaAs can lower the bandgap of GaAs drastically as explained in Chapter 6. This has profound effects on the electronic and optical properties of GaAsN. Hydrogen irradiation of these novel materials opens up a new field of interest because when hydrogen is incorporated into GaAsN, a complete reversal of the drastic bandgap reduction caused by N is observed. This suggests a strong mutual passivation between hydrogen and nitrogen in diluted III-V nitride alloys [15]. In fact, the study of the atomic structure and various hydrogen-related configurations in GaAsN, using first-principle total-energy calculations, has shown that monoatomic hydrogen (single hydrogen atom) can only act as donor in both p- and n-type dilute nitride materials (Janotti *et al.* [16]). The role of hydrogen in dilute GaAsN is therefore different from the one in conventional semiconductors where hydrogen has an amphoteric behaviour depending on the conductivity type of the material. A more detailed description of the role of hydrogen in GaAsN is given in section 3.4.2 of Chapter 3. Some of the findings, regarding the interaction between the hydrogen and nitrogen in the dilute nitride GaAs reported in literature, are given in the following section.

Photoluminescence (PL) studies of the hydrogenated-GaAsN by Polimeni and co-workers [17,18,19] showed that the increasing dose of hydrogen shifts the fundamental transition towards the GaAs band gap value. It was observed that hydrogen fully passivates the N-related lines that appear in the PL spectra of dilute GaAsN thin films. This provides a direct evidence of the interactions between nitrogen and hydrogen in reducing nitrogen related defects. It was also found that

hydrogenation recovers the bandgap and shape of the conduction band edge of the host material GaAs. This was reported to be due to the electron effective mass [20]. Magneto-PL studies by Masia *et al.* and Polimeni *et al.* [21, 22] confirmed that the effective mass of electrons decreases back to essentially the GaAs value. The X-ray diffraction (XRD) measurements also show the shifts of the lattice constant of GaAsN back to the lattice parameter of GaAs [23]. In another study of hydrogenation of GaAsN, Simone *et al.* [24] explained the coupling of hydrogen with nitrogen through first-principles calculations. It was suggested that the formation of di-hydrogen (two hydrogen atoms) – complexes with nitrogen are mainly responsible for the complete recovery of the GaAs properties like bandgap, lattice constant and electron effective mass.

In addition, hydrogen has the tendency to make complexes with the crystal lattice defects as well as with other deep levels. There is a strong motivation to reduce the concentration of deep level impurities and defects which can affect tremendously the optical and electronic performances of semiconductor materials-based devices. In this regard, hydrogen irradiation could play an important role in the operation of modern optoelectronic and electronic devices by neutralizing the effect of deep levels. Indeed, a remarkable reduction in the number of deep levels and defect concentration after hydrogenation in several semiconductors such as Si, Ge, GaP, GaAs, and AlGaAs has been reported [25]. Regarding the dilute nitride GaAs, a PL study of p-type GaAsN/GaAs heterostructures by Bissiri *et al.*[26] showed that nitrogen related radiative-recombination complex centers are fully quenched upon hydrogenation. This finding provides evidence for strong interaction between H and N complexes. In spite of all this knowledge on hydrogen passivation of impurities

and defects, the exact mechanism involved in their reduction or annihilation is not fully understood and need further exploration.

In this work, the effect of hydrogenation on the deep levels in as-grown GaAsN is investigated by using DLTS and LDLTS techniques. To our knowledge, no DLTS investigations of deep levels in hydrogenated dilute nitride GaAs have been reported in the literature.

8.2 RESULTS

8.2.1 CURRENT-VOLTAGE (I-V) AND CAPACITANCE-VOLTAGE (C-V) CHARACTERISTICS

I-V measurements were performed on the as-grown and hydrogenated GaAsN samples to check their suitability for the DLTS and Lapalce DLTS measurements as shown in Fig. 8.1. The samples with low leakage current have been selected for further electrical investigations. The C-V measurement data have found to fit the $1/C^2$ - V_R relationship as discussed in section 4.1.3 of Chapter 4. The value of the shallow level concentration determined from the C-V measurements have been utilised to determine the density of traps detected in DLTS measurements. No remarkable changes in the I-V and C-V characteristics of the hydrogenated GaAsN samples have been observed.

8.2.2 DLTS MEASUREMENTS

DLTS and Laplace DLTS measurements have been carried out on three sets of samples. Each set comprises control (without nitrogen), as-grown and hydrogenated

$GaAs_{1-x}N_x$ samples with x=0.2%, 0.4% and 0.8%. Details about the hydrogen irradiation of the samples are given in Chapter 5. The DLTS spectra were acquired with the application of a reverse bias of -4 V, a filling pulse of height -0.5 V with duration of 1 msec and using a sampling rate window of 50 s^{-1}.

The DLTS results of the control and as-grown GaAsN samples have been presented in Chapter 6, and are included here in order to examine the effects of hydrogen irradiation on the deep levels detected in the as-grown samples.

Fig. 8.2 shows typical DLTS spectra obtained from the first set of samples having a nitrogen content of 0.2%. A standard DLTS spectrum of the control sample (without nitrogen) is also depicted in Fig. 8.2 for comparison purposes. The DLTS spectra of the as-grown samples have shown the presence of seven DLTS peaks associated with electrically active defect states which were labelled as A1, A2, A3, A4, A5, A6 and A7. After the hydrogen irradiation of these samples only two DLTS peaks related to electron emitting levels labelled as AH1 and AH2 were detected. It is clear from these measurements that the annihilation of five traps is the consequence of the hydrogen irradiation.

The DLTS spectra obtained from the second set of samples with N=0.8% are illustrated in Fig. 8.3. Four DLTS peaks related to defect levels have been identified in the as-grown GaAsN (N=0.4%) samples, whilst only one peak associated to electron emitting level is detected in the hydrogenated samples. The other three defect levels were eradicated as a result of the hydrogen irradiation of these samples. The observed defect level in the hydrogenated samples is labelled as BH1.

Fig. 8.4 shows the standard DLTS and Laplace DLTS spectra (inset) obtained from the third set of samples with N=0.8%. The as-grown samples have shown the

presence of four peaks associated with electron emitting deep levels labelled as C1, C2, C3 and C4. In the hydrogenated samples three DLTS peaks are observed. High resolution Laplace DLTS (inset of the Fig. 8.4) measurements performed on these samples reveal four peaks relating to electrically active defect states. These are labelled as CH1, CH2, CH3 and CH4.

To identify the energy location of these defect states within the band gap of the material, carrier thermal emission rates were determined at different temperatures using LDLTS. The thermal emission rates were plotted against the inverse of the temperature in a semi-logarithmic plot as illustrated in Fig. 8.5, 8.6 and 8.7. The value of activation energy of each trap is derived from the slope of these Arrhenius plots. Assuming the capture cross-sections are temperature independent, their values were calculated from the from the slope of the Arrhenius plots [log $(1-S(t_p)/S(\infty)$ versus t_p] as described in section 4.2.4.2 of Chapter 4. The concentration of each trap detected in the as-grown and hydrogenated GaAsN samples is determined by using equation (4.2.3) given in section 4.2.4.3 of Chapter 4. Typical parameters of the deep levels obtained from the DLTS and LDLTS measurements are given in Table 8.1.

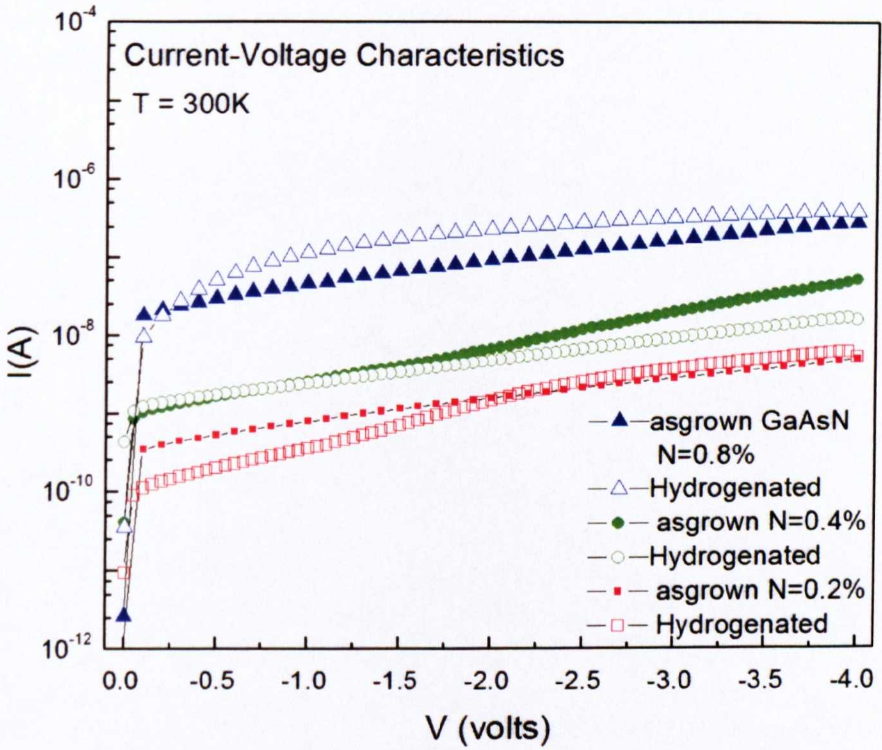

Fig.8. 1 Current-voltage characteristics of as-grown and hydrogenated GaAsN Schottky diodes containing different nitrogen contents.

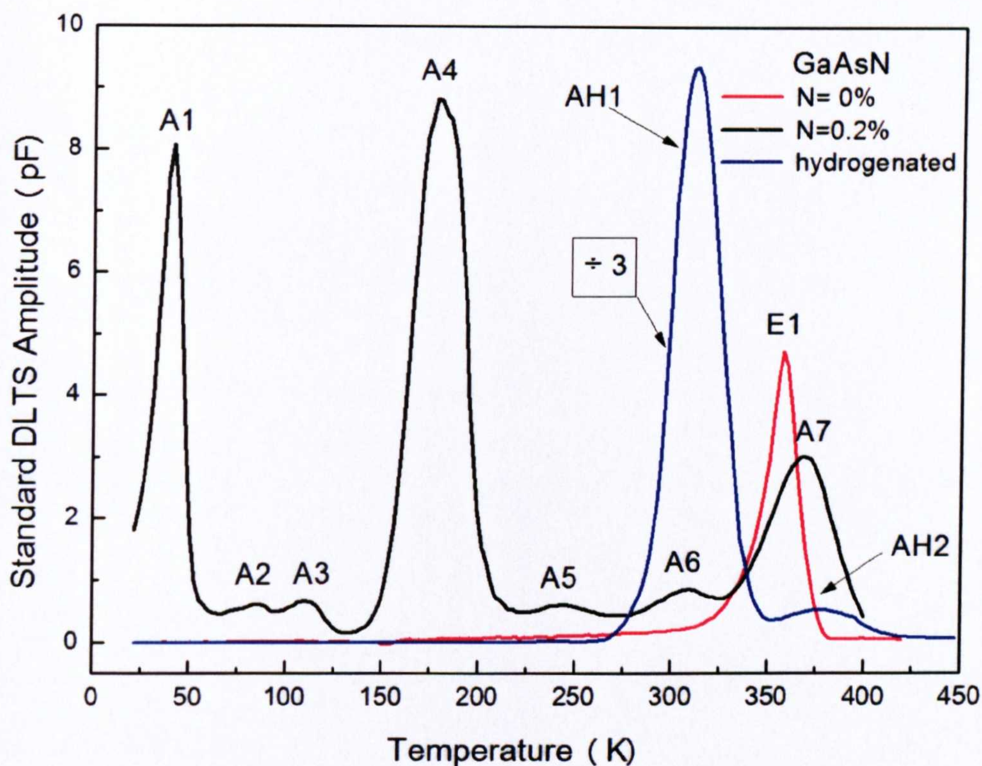

Fig.8. 2 Typical DLTS spectra of as-grown and hydrogenated GaAsN (N=0.2%) samples. For comparison purposes, the DLTS spectra of the control sample (without nitrogen) is also shown. DLTS scans were taken using a rate window of 50 s^{-1}, an applied reverse-bias V_R = -4 V with a pulse height V_P = -0.5 V and duration of 1ms.

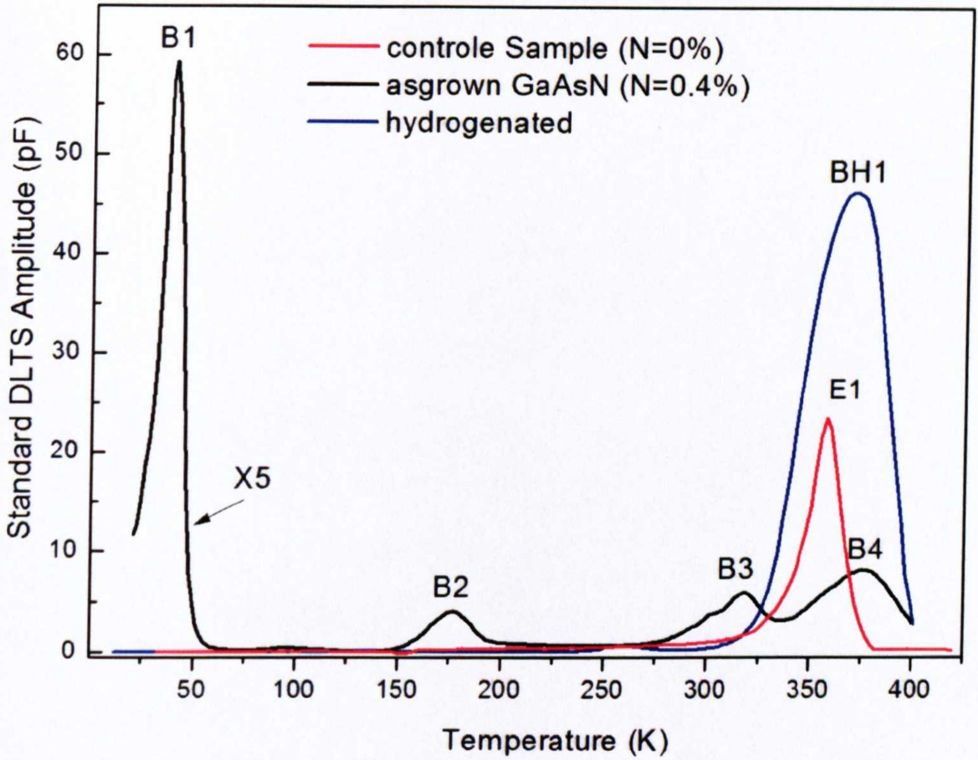

Fig.8. 3 Typical DLTS spectra of as-grown and hydrogenated GaAsN (N=0.4%) samples. For comparison purposes, the DLTS spectra of the control sample (without nitrogen) is also shown. DLTS scans were taken using a rate window of 50 s^{-1}, an applied reverse-bias V_R = -4 V with a pulse height V_P = -0.5 V and duration of 1ms.

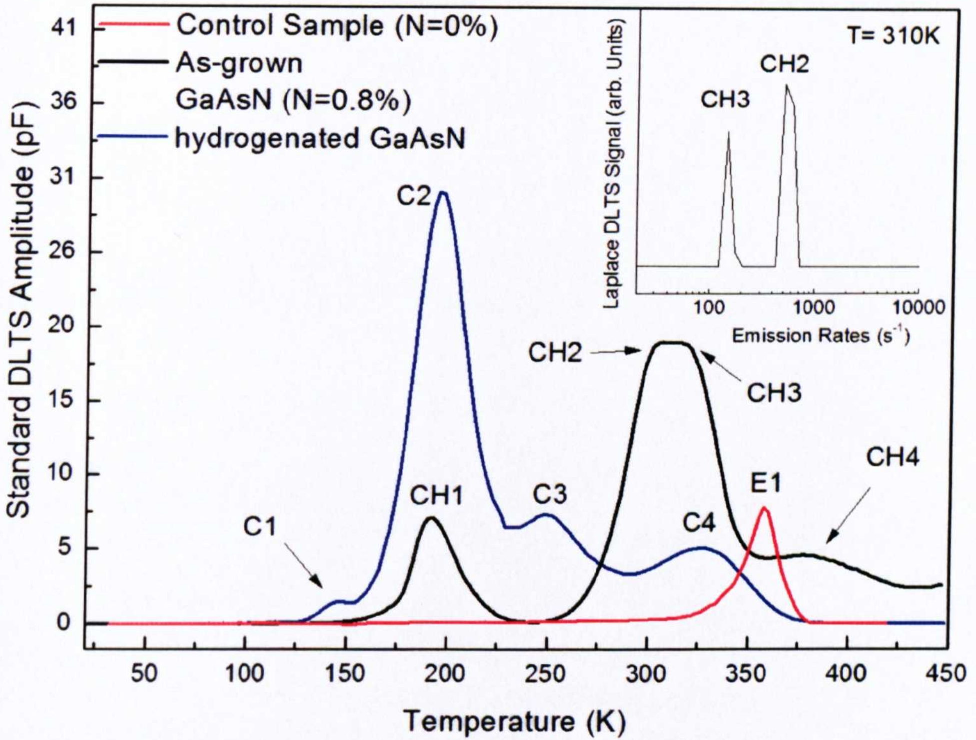

Fig.8. 4 Typical DLTS spectra of as-grown and hydrogenated GaAsN (N=0.2%) samples. For comparison purposes, the DLTS spectra of the control sample (without nitrogen) is also shown. DLTS scans were taken using a rate window of 50 s^{-1}, an applied reverse-bias V_R = -4 V with a pulse height V_P = -0.5 V and duration of 1ms. The inset shows the Laplace DLTS spectra of hydrogenated GaAsN taken at 310K similar experimental conditions as those of the standard DLTS scans.

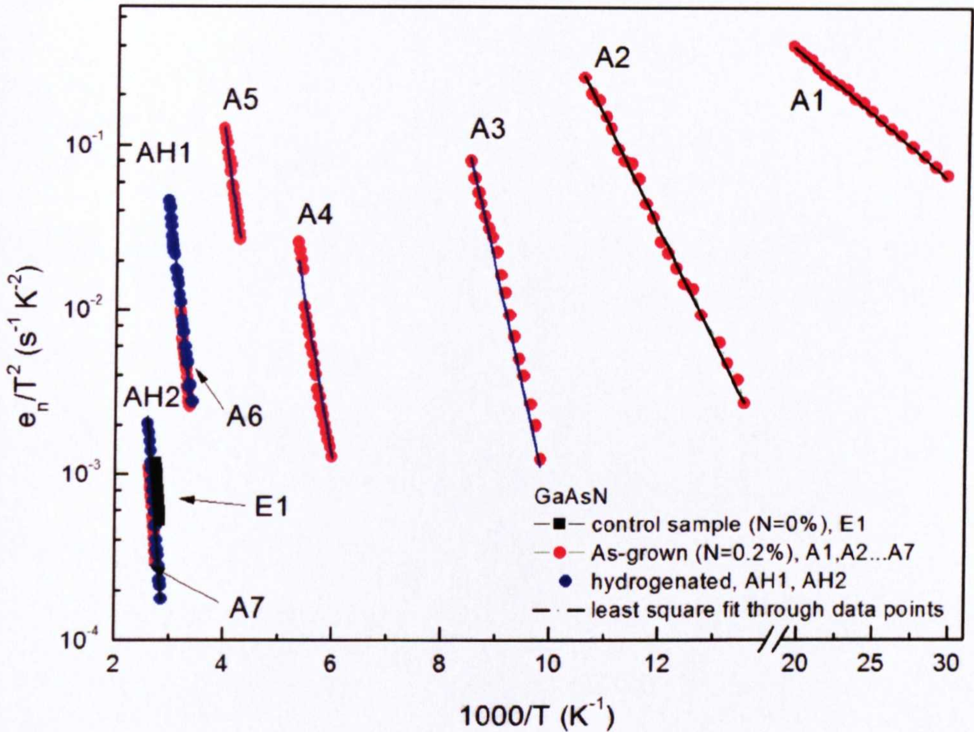

Fig.8. 5 Arrhenius plots derived from the thermal emission rates for the control (N-0%), as-grown GaAsN (N = 0.2%) and hydrogenated samples. Filled symbols are data points, while lines through the symbols are the least-squares fits to the data.

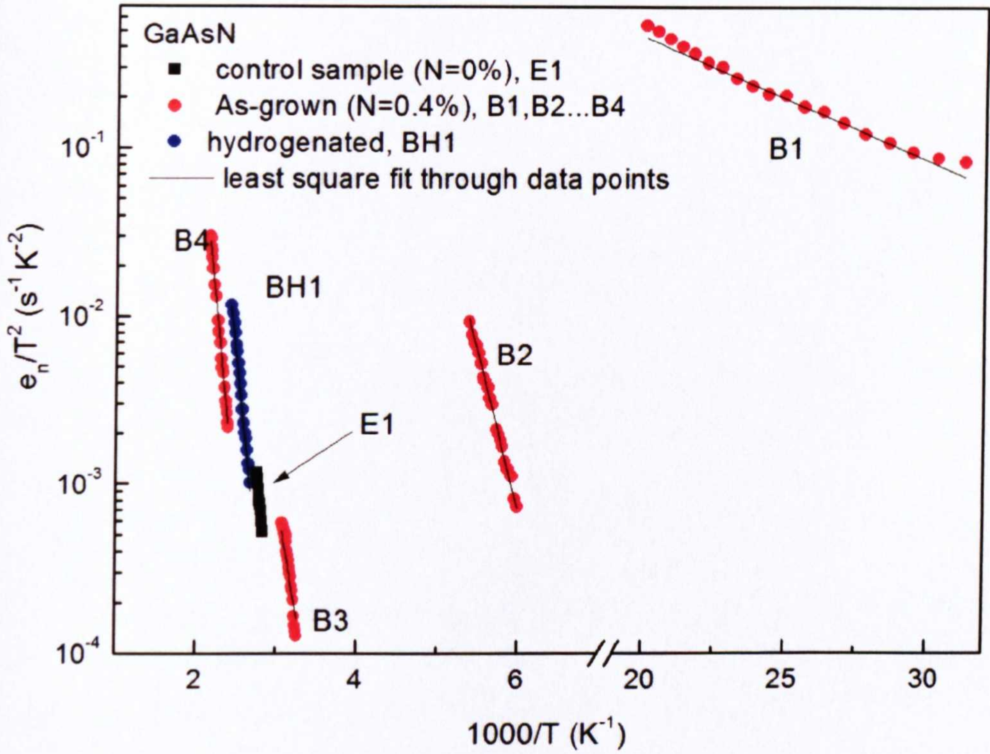

Fig.8. 6 Arrhenius plots derived from the thermal emission rates for the control (N-0%), as-grown GaAsN (N = 0.4%) and hydrogenated samples. Filled symbols are data points, while lines through the symbols are the least-squares fits to the data.

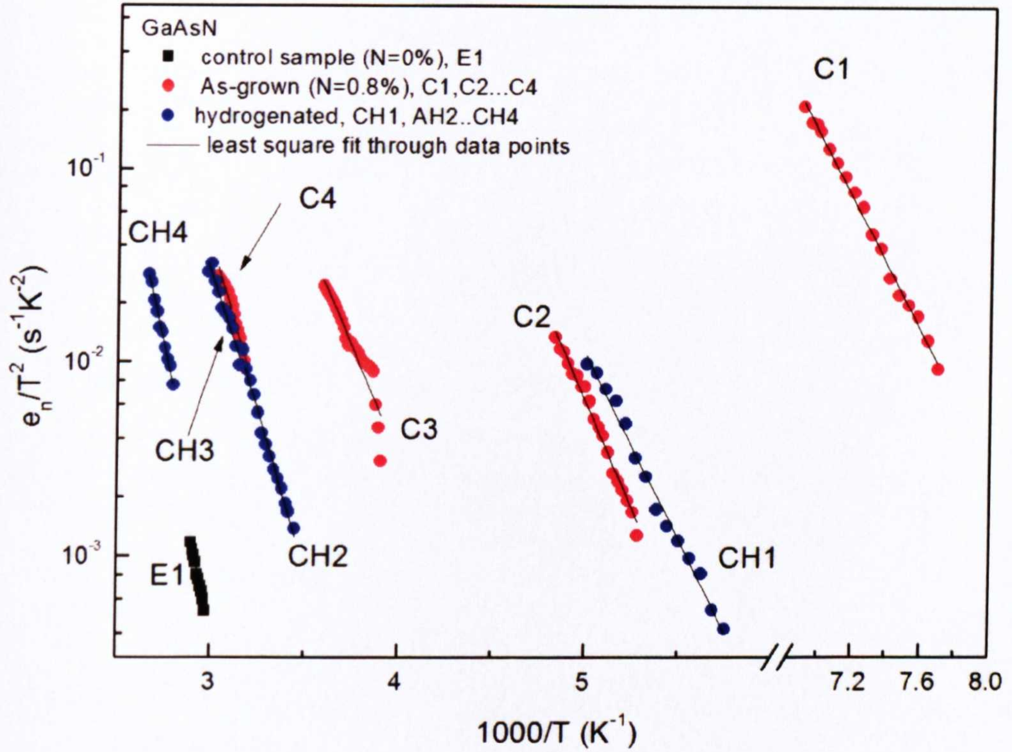

Fig.8. 7 Arrhenius plots derived from the thermal emission rates for the control (N-0%), as-grown GaAsN (N = 0.8%) and hydrogenated samples. Filled symbols are data points, while lines through the symbols are the least-squares fits to the data.

TABLE 8.1 Trap parameters obtained from Standard DLTS and Laplace DLTS data analysis for the as-grown and hydrogenated GaAsN (N = 0- 0.8%) samples.

Nitrogen	Trap Label	Activation Energy (eV)	Capture cross-section σ_n (cm^2)	Trap density (cm^{-3})
0 %	E1	0.78	5.15×10^{-14}	2.85×10^{15}
As-grown	A1	0.036	5.89×10^{-19}	2.03×10^{15}
0.2%	A2	0.13	1.07×10^{-18}	1.53×10^{14}
	A3	0.28	5.61×10^{-17}	1.68×10^{14}
	A4	0.35	8.21×10^{-16}	2.22×10^{15}
	A5	0.43	4.52×10^{-16}	1.50×10^{14}
	A6	0.51	5.28×10^{-16}	2.10×10^{14}
	A7	0.81	3.64×10^{-14}	7.56×10^{14}
Hydrogenated	AH1	0.53	4.91×10^{-16}	3.09×10^{16}
	AH2	0.82	2.53×10^{-14}	1.66×10^{15}
As-grown	B1	0.045	2.80×10^{-18}	3.60×10^{15}
0.4%	B2	0.37	5.75×10^{-16}	2.44×10^{14}
	B3	0.53	6.36×10^{-16}	3.52×10^{14}
	B4	0.82	1.02×10^{-14}	5.07×10^{14}
Hydrogenated	BH1	0.81	8.41×10^{-14}	1.36×10^{16}
As-grown	C1	0.34	2.63×10^{-16}	1.86×10^{14}
0.8%	C2	0.38	4.24×10^{-16}	3.51×10^{15}
	C3	0.44	7.41×10^{-16}	6.97×10^{14}
	C4	0.55	5.51×10^{-16}	5.82×10^{14}
Hydrogenated	CH1	0.37	2.18×10^{-16}	9.13×10^{14}
	CH2	0.61	6.20×10^{-16}	2.61×10^{15}
	CH3	0.58	5.49×10^{-16}	2.56×10^{15}
	CH4	0.82	3.57×10^{-14}	6.39×10^{14}

8.3 DISCUSSION

DLTS and LDLTS results obtained from the as-grown GaAsN (N=0.2%) samples have been discussed in Chapter 6. These showed the presence of seven electron emitting levels. After exposure to hydrogen-irradiation, the DLTS measurements reveal the presence of only two electron emitting levels labelled as AH1 and AH2. The effective elimination of five defect levels is therefore directly related the hydrogen irradiation process. As reported in the previous sections, hydrogen impurity is an amphoteric defect in GaAs which compensates both donors and acceptors [27]. However, hydrogen does not possess this property in GaAsN [28], and this could suggest that a strong passivation of nitrogen occurs instead. In this regard, Janotti *et al.* [28] have explained this unusual behaviour of hydrogen in diluted III-V nitrides. They explained that the strong bonding between nitrogen and hydrogen, and the formation of H_2^*-N complexes are the main reasons of this passivation behaviour. The H_2^*-N is a neutral complex which is responsible for the removal of defect levels from the bandgap of GaAsN. Therefore, based on this finding, most of the defect levels become electrically inactive. This could explain the annihilation of most of the electrically active deep defect levels present in the as-grown GaAsN epilayers with N=0.2% investigated in this work.

The activation energy and capture cross-section of trap level AH1 (0.53eV) is found to be similar to the one of the trap level A6 (0.51eV) in the as-grown GaAsN sample. However, the concentration of AH1 is found to be about 30 times higher than that of A6 after hydrogen irradiation. In terms of temperature and energy location of trap AH1, it could be assigned to the well-known non-radiative level EL3 which is related to the substitutional oxygen on arsenic sites [29]. The formation of EL3-like trap in hydrogenated n-type GaAs samples has also been reported by Kim *et al.* [30]

in their DLTS investigations. It was observed that the concentration of this trap increases from 2×10^{14} cm $^{-3}$ to 9×10^{14} cm $^{-3}$ when the substrate temperature was increased from 200 ^{o}C to 280 ^{o}C during the hydrogen irradiation exposure. It was suggested that the proper substrate temperature during hydrogen irradiation process is an important parameter for the effective passivation of defects in GaAs. The increasing temperature of the substrate during hydrogenation of the sample could increase the concentration of some of the defect states. The increase observed in the concentration of AH1 trap level could be explained by the fact that our samples were hydrogenated at high temperature of 300 ^{o}C.

Trap AH2 (0.82eV) in hydrogenated samples has shown comparable emission rates and capture cross-section as those of A7 (0.81eV) in as-grown GaAsN epilayers. Emission rates of both AH2 and A7 are illustrated in the Arrhenius plots shown in Fig. 8.5. Thus, these are believed to be the same defect level. The concentration of trap AH2 and A7, are 5.13×10^{14} cm^{-3} and 1.50×10^{15} cm^{-3}, respectively. The effect of hydrogen irradiation on A7 is profound since it decreases its concentration by a factor of 3. Kim *et al.* [30] have also seen a similar trap in the untreated and hydrogen treated GaAs samples. The concentration of this trap first decreased and then recovered to its original value when exposed to hydrogen irradiations at substrate temperatures from 85 ^{o}C to 280 ^{o}C. The origin of this trap has been suggested to be related to the well-known antisite (As_{Ga}) defect center EL2 as discussed in Chapter 6.

The second set of samples investigated consisted of as-grown and hydrogen treated GaAsN with N =0.4% epilayers. While four deep levels, B1 (0.045 eV), B2 (0.37 eV), B3 (0.53 eV) and B4 (0.82 eV) were detected in the untreated samples,

only one deep level at E_c - 0.81 eV , denoted as BH1, appeared dominantly in the hydrogenated samples. The B1 - B4 trap levels observed in the as-grown GaAsN (N=0.4%) samples have already been discussed in Chapter 6. The emission rate signatures and capture cross-section of BH1 are similar to those of B4 and E1 in as-grown and control samples, respectively. These are identified with EL2-like trap center [see Chapter 6]. The concentration of BH1 is found to be 1.36 × 10^{16} cm^{-3} which is about 27 times higher than that of B4 (5.07 × 10^{14} cm^{-3}). It is presumed that this could be due to the formation of complexes involving hydrogen and arsenic-antisites.

In the third set of samples having N=0.8%, deep level C1, which was detected in the as-grown samples, does not appear in the DLTS spectra of the hydrogenated samples. As depicted in Fig. 8.7, deep levels C2 and CH1 have approximately similar emission rates signatures . However, the concentration of CH1 is found to be three times smaller than that of C2. It can be tentatively assigned to N-As split interstitial complexes as discussed in chapter 6. The deep level C3 disappeared after the hydrogenation.

The Laplace DLTS spectra of the broader peak that appears in standard DLTS measurements shows that this contains at least two components related to defect states (labelled as CH2 and CH3) which are closely spaced in terms of activation energies (0.61eV and 0.59eV, respectively). Their activation energies and capture cross-sections are comparable to those of defect state C4 which is present in the as-grown samples. Whereas, the concentration of these traps are four times larger than that of C4. The nature of this defect is not known. However, it could be related to hydrogen complexes because these were absent in the as-grown sample. A similar

DLTS peak at 320K in the hydrogenated n-type GaAs has been observed by Soltanovich *et al.* [31]. They attributed this peak to the well known M3 level which is considered to be hydrogen-related defect in GaAs. The energy level of M3, as reported in the literature, varies widely in the range from E_c-0.43 eV to E_c-0.61 eV [32]. This is due to the fact that its carrier emission is dependent on the electric field.

Regarding the trap CH4, the emission rate signature and capture cross-section are very close to that of E1 in the control sample. The concentration of CH4 is found to be 4.5 times less than the concentration of E1. This trap level was not detected in the as-grown sample (N=0.8%) which infers that hydrogen irradiation is the main cause for the creation of this defect level. Variations in the concentration of the EL2-like trap (E1 in the control sample) after hydrogen irradiation have been observed in this work. [EL2] decreases for N=0.2% and then increases for N=0.4%. For N=0.8%, EL2-like trap E1 was annihilated, and then reappeared after hydrogenation. The behaviour of this trap in GaAsN has a close analogy to EL2 trap observed in n-type GaAs subjected to hydrogen exposures at different substrate temperatures [29]. To identify the exact nature of the trap, some other techniques that are sensitive to chemical species such as electron paramagnetic resonance (EPR) spectroscopy and secondary ion mass spectroscopy (SIMS) are required. This is beyond the scope of this thesis.

8.4 CONCLUSIONS

It is worth pointing out that DLTS data on hydrogenated GaAsN is lacking in the literature. Therefore, the purpose of this work was to carry out a detailed DLTS and LDLTS investigation in order to shed some light on the effect of hydrogenation on the non-radiative centres in as-grown dilute nitride GaAs epilayers containing nitrogen composition from 0.2-0.8%.

The main finding of this study is that hydrogenation of dilute GaAsN epilayers passivate most of the deep levels present in the material. However, for the samples with high N concentration (N = 0.8%) the DLTS and Laplace DLTS results demonstrated that although hydrogen can passivate some of the defect states and reduce the concentration of others it can also create new defects which could be hydrogen-related complexes.

In view of device applications involving hydrogenation these results might help in the improvement of device performance.

REFERENCES

[1] E. Mollwo, Z. Phys., 138, 478 (1954).

[2] E. E. Haller, B. Joos and L. M. Falicov, Phys. Rev. B., 21, 4729 (1980).

[3] J. M. Kahn, R. E. McMurray, E. E. Haller and L. M. Falicov, Phys. Rev. B., 36, 8001 (1987).

[4] C. T. Sah, J. Y. Sun and J. J. Tzou, Appl. Phys. Lett., 43, 204 (1983).

[5] J. I. Pankove, D. E. Carlson, J. E. Berkeyheiser and R. O. Wance, Phys. Rev. Lett., 51, 2224 (1983).

[6] N. M. Johnson, C. Herring and D. J. Chadi, Phys. Rev. B.,56, 769 (1986).

[7] M. Stavola, K. Bergman, S. J. Pearton and J Lopata, Phys. Rev. Lett., 61, 2786 (1988).

[8] B. Bech Nielsen, J. U. Anderson and S. J. Pearton, Phys. Rev. Lett., 60, 321 (1988).

[9] T. Zundel and J. Weber, Phys. Rev. B., 39, 13549 (1989).

[10] M. Stutzmann, J. Harsanyi, A. Breitschwerdt and C. P. Herrero, Appl. Phys. Lett., 52, 1667 (1988).

[11] B. Clerjaud, F. Gendron, M. Krause, and W. Ulrici, Phys. Rev. Lett., 65, 1800 (1990).

[12] J. Chevallier, W. C. Dautremont-Smith, C. W. Tu, S. J. Pearton, Appl. Phys. Lett., 47, 108 (1985).

[13] J. Chevallier, A. Jalil, R. Azoulay and A. Mircea, Mater. Sci. Forum, 10, 591 (1986).

[14] A. Jalil, J. Chevallier, R. Azoulay and A. Mircea, J. Appl. Phys., 59, 3774 (1986).

[15] Jingbo Li, Pierre Carrier, Su-Huai Wei, Shu-Shen Li and Jian-Bai Xia, Phys. Rev. Lett., 96, 035505 (2006).

[16] A. Janotti, S. B. Zhang, Su-Huai Wei and C. G. Van de Walle, Optical Materials, 25, 261 (2004).

[17] A. Polimeni, G. Baldassarri H. v. H., M. Bissiri, M. Capizzi, M. Fischer, M. Reinhardt, and A. Forchel, Phys. Rev. B 63, 201304(R) (2001).

[18] G. Baldassarri H. v. H., M. Bissiri, A. Polimeni, M. Capizzi, M. Fischer, M. Reinhardt, and A. Forchel, Appl. Phys. Lett., 78, 3472 (2001).

[19] M. Bissiri, G. Baldassarri, A. Polimeni, V. Gaspari, F. Ranalli, M. Capizzi, A. Amore Bonapasta, F. Jiang, M. Stavola, D. Gollub, M. Fischer, M. Reinhardt, and A. Forchel, Phys. Rev. B 65, 235210 (2002).

[20] A. Polimeni, von Hoegersthal, M. Bissiri, M. Capizzi, A. Frova, M. Fischer, M. Reinhardt, and A. Forchel, Semicond. Sci. Technol., 17, 797 (2002).

[21] F. Masia, A. Polimeni, G. Baldassarri Ho¨ger von Ho¨gersthal, M. Bissiri, M. Capizzi, P.J. Klar, and W. Stolz, Appl. Phys. Lett., 82, 4474 (2003).

[22] A. Polimeni, G. Baldassarri Hoger von Hogersthal, F. Masia, A. Frova, M. Capizzi, S. Sanna, V. Fiorentini, P. J. Klar, and W. Stolz, Phys. Rev. B 69, 041201 R (2004).

[23] A. Polimeni, G. Ciatto, L. Ortega, F. Jiang, F. Boscherini, F. Filippone, A. Amore Bonapasta, M. Stavola, and M. Capizzi, Phys. Rev. B 68, 085204 (2003).

[24] Simone Sanna and Vincenzo Fiorentini, Phys. Rev. B 69, 125208 (2004).

[25] S. J. Pearton, J. W. Corbett and T. S. Shi, Appl. Phys. A43, 153 (1987).

[26] M. Bissiri, G. Baldassarri, A. Polimeni, V. Gaspari, F. Ranalli, M. Capizzi, A. Amore Bonapasta, F. Jiang, M. Stavola, D. Gollub, M. Fischer, M. Reinhardt, and A. Forchel, Phys. Rev. B 65, 235210 (2002).

[27] S. K. Estreicher, Mater. Sci. Eng. Rep. 14, 319 (1995).

[28] A. Janotti, S. B. Zhang, Su-Huai Wei and C. G. Van de Walle, 89, 086403 (2002).

[29] A.Y. Polyakov,N.B. Smirnov, A.V. Govorkov, Andrei E. Botchkarev, Nicole N. Nelson, M.M.E. Fahmi, James A. Griffin, Arif Khan, S. Noor Mohammad, D.K. Johnstone, V.T. Bublik, K.D. Chsherbatchev, M.I. Voronova and V.S. Kasatochkin, Solid State Elect. 46, 2155 (2002).

[30] Eun Kyu Kim, Hoon Young Chot, Hyeon So0 Kim, Suk-ki Mint and Taewhan Klm, Semicond. Sci. Technol., 7, 695497 (1992).

[31] O. A. Soltanovich, E. B. Yakimov, E. V. Erofeev, V. A. Kagadei and J. Weber, Physica B, 404, 5096 (2009).

[32] Yutaka Tokuda, Kazuhiro Kamiya and Tsugunori Okumura, J. Appl. Phys., 88, 1943 (2000).

CHAPTER 9

CHARACTERISATION OF GaAsBi EPILAYERS GROWN BY MBE ON (100) AND (311)B GaAs SUBSTRATES

In this chapter the investigation of GaAsBi epitaxial layers grown by MBE on conventional (100) and high-index planes using optical (photoluminescence and standard absorption spectroscopy) and structural (X-ray diffraction) techniques is discussed.

9.1 INTRODUCTION

The incorporation of Bi in III-V semiconductors has attracted in recent years a considerable deal of attention [1–6] due to the fact that their bandgaps can be engineered for several applications in the photonics, electronics and spintonics sector. For example, the band gap of GaAs is strongly reduced upon the addition of small amounts of Bi (~ 90 meV per percent of Bi), with a strong enhancement of the spin-orbit splitting energy [3, 4]. These remarkable properties make the Ga(In)BiAs system an attractive candidate to develop GaAs-based applications for long-wavelength optoelectronics as well as for spintronics. While the use of dilute nitrides

in device applications is currently limited because the electron mobility of these compounds is abruptly reduced due to strong N-related alloy scattering, dilute bismides might exhibit improved transport properties [6].

Tixier *et al.*[2] investigated the growth of GaAsBi epitaxial layers on (100) GaAs by molecular beam epitaxy using low group III/V ratios and low growth temperature of 380 ^{0}C. From the secondary ion mass spectroscopy (SIMS) measurements, Bi incorporation into GaAs up to 3.6% have been achieved. These growth conditions are not usually considered for the growth of other standard GaAs alloys. From Rutherford backscattering (RBS) and x-ray diffraction measurements it was shown that the lattice parameter of GaAsBi obeys Vegard's law and they evaluated a hypothetical lattice constant of zincblende GaBi alloy as $a_{GaBi} = 6.33 \pm 0.06$Å [2].

The growth of epitaxial layers on high-index planes represents a step forward in semiconductor material engineering as it offers an additional degree of freedom to develop applications with improved properties with respect to the conventional (100)-grown devices. The interest in non-(100) semiconductor structures is manifold and concerns growth, impurity incorporation, electronic properties, lasing performance, and piezoelectric effects. To mention a few examples, the use of non-(100) substrates has allowed the fabrication of ultrahigh mobility two-dimensional hole gases in GaAs/AlGaAs heterostructures, high-performance InAs/GaAs quantum dot (QD) lasers, InGaAs/GaAs QDs with enhanced piezoelectric effects, and GaMnAs epilayers with modified Mn incorporation and magnetic anisotropies [7–9]. Some details about the GaAsBi are given in sections 2.6 and 2.7 of Chapter 2, and in sections 3.5 and 3.6 of Chapter 3.

9.2 RESULTS

9.2.1 X-RAY DIFFRACTION MEASUREMENTS

High-resolution x-ray diffraction (HRXRD) is a very important tool for structural characterization of thin epitaxial films. Very useful information about the composition, thickness, and strain in the epilayers can be acquired by using XRD technique. High resolution X-Ray Diffraction study was carried out in collaboration with the group at Institute for Crystal Growth, Berlin, Germany. The HRXRD measurements were performed with a double-crystal diffractometer equipped with a parabolic (focusing) multilayer mirror. The x-rays are produced using the $K\alpha_1$ transition of copper (λ=0.1540508 nm), and are monochromated with a four-bounce Ge 220 Bartels monochromator.

The GaAsBi layers under investigation were grown by molecular beam epitaxy with constant Bi flux (1.2×10^{-7} Torr) and variable arsenic flux (1.2×10^{-5} - 6×10^{-6} Torr) to achieve GaAsBi layers under nominally stoichiometric conditions. The important growth parameters are also given in Table 9.1. HRXRD measurements were performed on GaAsBi layers grown on (100) and (311)*B* GaAs substrates after centering and optimizing the 004 and 311 symmetrical reflections.

The composition of GaAsBi ternary films on (100) and (311)*B*-oriented substrates can be determined by the x-ray reflections from the (004) and (311) planes. As the crystallographic parameters such as lattice constant and spacing between the planes of the substrate and epitaxial layer are different, an x-ray diffraction pattern as a function of angle will show at least two peaks corresponding

to the satisfied Bragg conditions for the substrate and the GaAsBi epilayer. The Bragg's law for constructive interference is given by

$$n\lambda = 2d\ sin\theta \tag{1}$$

where n is an integer, λ is the wavelength of the incident photons, d is the interplanar spacing and θ is the Bragg angle of the substrate.

Differentiation of equation (1) allow the determination of the relationship between the peak-splitting $\Delta\theta$ and interplanar spacing Δd for coherently strained epilayer [10]. This is given as

$$\frac{\Delta d}{\Delta\theta} = -\frac{n\lambda}{2\,sin\,\theta}\,cot\,\theta \tag{2}$$

From equation (1) and (2), the peak-splitting $\Delta\ \theta$ is given by

$$\Delta\theta = -\left(\frac{\Delta d}{d}\right)\frac{1}{cot\,\theta} \tag{3}$$

where $(\Delta d/d)$ is the deformation in the epilayer.

Now if we assume that the layer is in the non-relaxed state the deformation $(\Delta d/d)$ can be expressed as [11]

$$\left(\frac{\Delta d}{d}\right) = \frac{1}{P}\left(\frac{\Delta a}{a}\right) \tag{4}$$

where $(\Delta a/a)$ is the relaxed lattice mismatch between substrate and layer, and P is the distortion coefficient.

Once the mismatch strain is known, then the composition of $GaAs_{1-x}Bi_x$ can be calculated using Vegard's law [12] (see equation 5).

TABLE 9.1 Details for the growth of dilute GaAsBi epilayers

GaAsBi layer grown on (100) substrates				
Sample	**Ms-819**	**Ms-821**	**Ms-820**	**Ms-822**
Growth T (^oC)	~350	~350	~350	~350
As (Torr)	~1.2×10^{-5}	~1.0×10^{-5}	~8.0×10^{-6}	~6.0×10^{-6}
Bi (Torr)	~1.2×10^{-7}	~1.2×10^{-7}	~1.2×10^{-7}	~1.2×10^{-7}
			This is the region of near-stochiometric growth	
GaAsBi layer grown on (311)B substrates				
Sample	Ms-823	Ms-825	Ms-824	Ms-826
Growth T (^oC)	~350	~350	~350	~350
As (Torr)	~1.2×10^{-5}	~1.0×10^{-5}	~8.0×10^{-6}	~6.0×10^{-6}
Bi (Torr)	~1.2×10^{-7}	~1.2×10^{-7}	~1.2×10^{-7}	~1.2×10^{-7}
		This is the region of near-stochiometric growth		

$$a\left(GaAs_{1-x}Bi_x\right)=(1-x).\,a(GaAs)+x.\,a(GaBi) \tag{5}$$

By rearranging equation (5) the Bi-concentration, x, can be extracted using equation (6)

$$x=\frac{\Delta a\ a}{(\Delta a\ a)_{GaAs/GaBi}} \tag{6}$$

where $(\Delta a/a)_{GaAs\ GaBi} = \dfrac{a_{GaAs}-a_{GaBi}}{a_{GaAs}}$

From equation (3) and (4) we can have the following relation.

$$\left(\frac{\Delta a}{a}\right)=P\left(\frac{\Delta d}{d}\right)=-P.\Delta\theta.\cot\theta \tag{7}$$

Thus using equation (7), equation (6) for the composition x can be rewritten as

$$x=P\left(\frac{a_{GaAs}}{a_{GaBi}-a_{GaAs}}\right)\Delta\theta.\cot\theta \tag{8}$$

where θ is the Bragg angle for the GaAs substrate reflections and $\Delta\theta$ is the angle shift of the GaAsBi reflections with respect to the GaAs substrate.

We have used the study of Tixier et al. [2] which evaluate a hypothetical zincblende GaBi alloy as a_{GaBi} = 6.33 ± 0.06Å. So by using lattice parameter of the GaAs i.e. a_{GaAs} which is 5.653Å, equation (8) can be written as given below

$$x=P\left(\frac{1}{0.1197}\right)\Delta\theta.\cot\theta \tag{9}$$

The distortion coefficient P depends upon the elastic constants and on the surface orientation. For the sample grown on (100) and (111)-GaAs, P is given by [11].

$$P_{100} = \frac{C_{11}}{C_{11} + 2C_{12}} \tag{10}$$

and

$$P_{111} = \frac{C'_{11} \frac{2}{3}(2C'_{44} - C'_{11} + 2C'_{12})}{C_{11} + 2C'_{12}} \tag{11}$$

From reference [11] the value of P for the samples grown on $(311)B$, is given by

$$P_{311} = P_{100} \frac{\alpha}{54.74^{o}}(P_{111} - P_{100}) \tag{12}$$

where α is the angle between <311> and <100> directions and is equal to 25.24^{o}. The value of 54.74° in equation (12) is the angle between the <100> and <111> directions.

Given that the Bi content of our samples is low, the elastic constants of GaAs are used to calculate P. These are C_{11} = 119 GPa, C_{12} = 53.4 GPa and C_{44} = 59.6 GPa. The values obtained are P_{100}=0.527 and P_{311}=0.691.

HRXRD curves ($\omega/2\theta$ scans) obtained from two GaAsBi epilayers grown under near-stoichiometric conditions on (100) and on $(311)B$ GaAs substrates are shown in Fig. 9.1 (a) and 9.1 (b).

9.2.2 OPTICAL TRANSMISSION MEASUREMENTS

We have examined the bandgap of the GaAsBi layers by using the standard optical transmission technique. The details about the samples used in this study were described in Table 9.1. The band structure of the semiconductors controls the absorption process. For example, in the case of direct bandgap materials the

absorption coefficient increases with the square root of the incremental energy greater than the bandgap [13] as given by the following equation (13)

$$\alpha \propto \sqrt{(h\upsilon - E_g)} \qquad (13)$$

The transmission measurements as described in section 5.2.4 of Chapter 5 were performed on GaAsBi layers grown on (100) and on (311)*B*- GaAs substrates to determine the absorption coefficient. Typical spectra obtained from these epilayers are shown in Fig. 9.2 for the samples grown near-stochiometric conditions. As the interest is to investigate only the absorption in the GaAsBi epitaxial layers, the data were normalized with a transmission spectra taken from the control sample GaAs (Bi = 0%). The normalized data then were utilised to determine the absorption coefficient α for both layers grown on (100) and (311)B-GaAs. Fig. 9.3 shows the square of the absorption coefficient, α^2, for the two near stoichiometric (100) and (311)*B* GaAsBi epilayers as a function of the incident photon energy. For convenience and clarity, saturation part of the transmission data was not plotted in Fig. 9.3. A comparison of the data obtained in this study with the results reported in literature has also been performed and illustrated in the inset of the Fig.9.3.

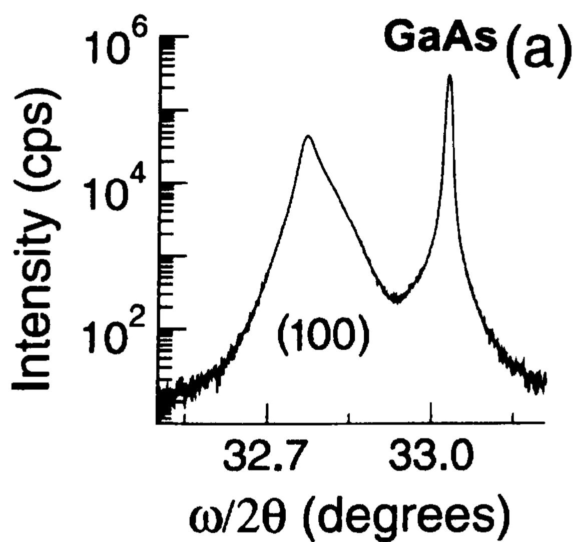

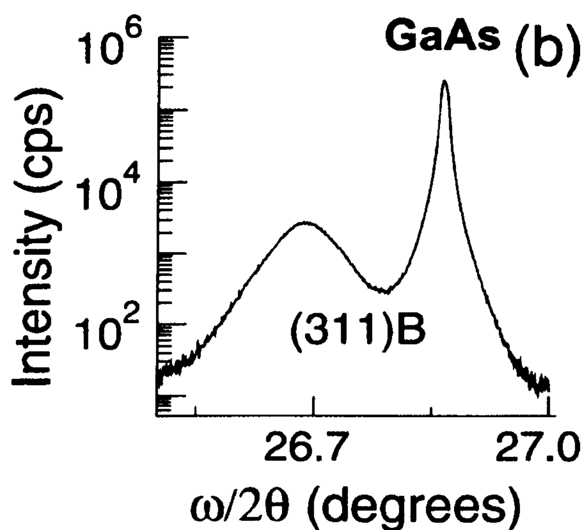

Fig.9. 1 HRXRD scans of two near-stoichiometric GaAsBi samples grown **(a)** on (100)- and **(b)** on (311)*B* GaAs substrates.

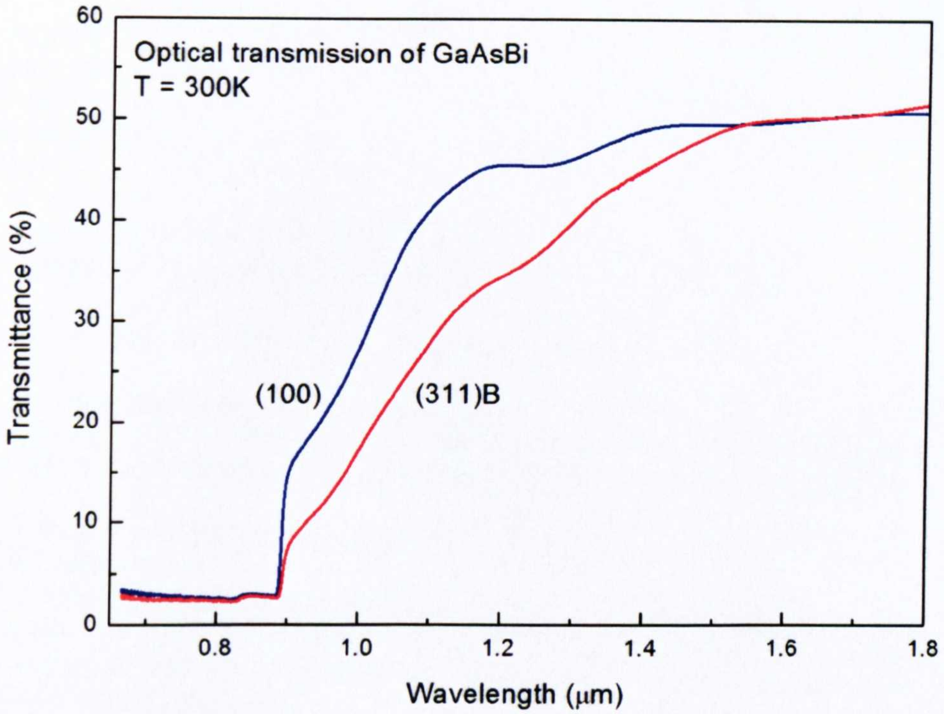

Fig.9. 2 Typical transmission spectra measured at 300K for GaAsBi layers grown near-stochiometric conditions on (100) and (311)B-GaAs substrates.

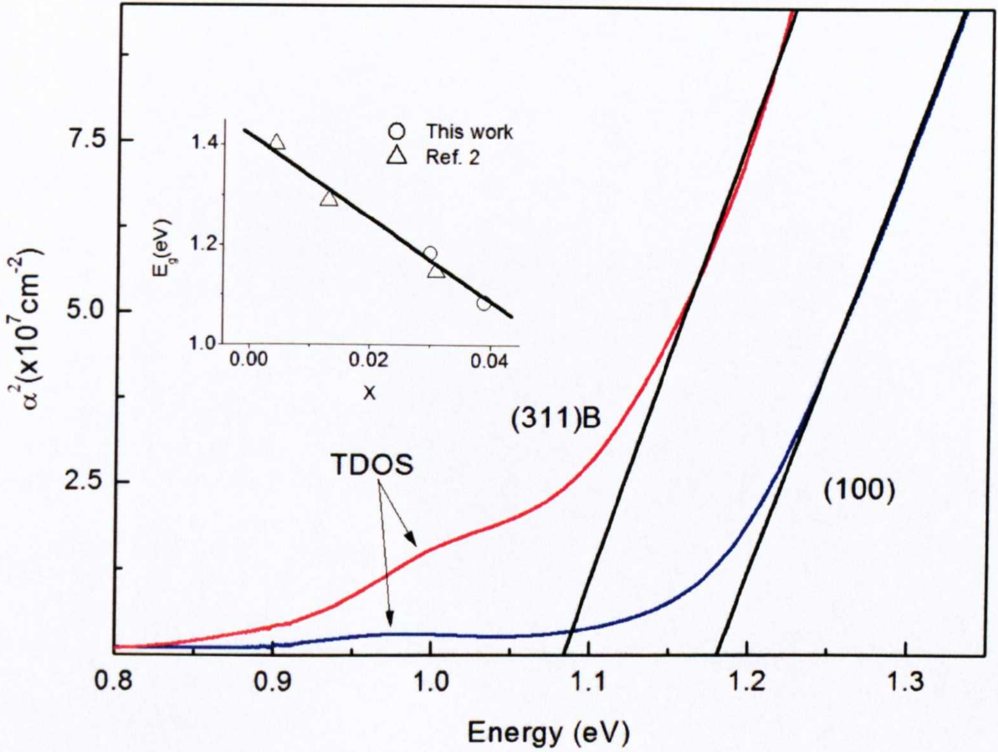

Fig.9. 3 Square of the absorption coefficient α^2 for the two near stoichiometric (100) and (311)*B* GaAsBi epilayers as a function of incident photon energy, obtained from transmission measurements at 300 K. Straight lines show an extrapolation of the linear part of α^2 to zero. Inset: Band-gap energy (E_g) vs x for these two samples, together with data from Ref. 2.

9.2.3 PL SPECTRA OF AS-GROWN AND ANNEALED GaAsBi LAYERS

In this section the photoluminescence (PL) measurements performed on GaAsBi epilayers grown on (100) and on (311)*B* GaAs substrates are reported. In addition, the PL results on the low temperature annealed samples are presented here for the first time. The growth parameters of the samples are given in Table 9.1. Full details of the growth and layer structures are given in Chapter 5. In the 10K closed-cycle PL system set up during the course of this work no signal from the GaAsBi epilayer could be detected. An in-house PL equipment operating below 10K was used to optically characterise these layers. PL spectra were recorded at a temperature of 4.5K with an excitation of 514.5nm line from an Ar laser with an excitation power of 100mW. The signal was measured using an InGaAs detector associated with a standard lock-in amplifier.

It is well-known that the optical and electronic properties of semiconductor materials are sensitive to the post-growth thermal annealing conditions such as duration of the annealing and temperature. For example, it has been reported that annealing at temperatures >400 °C can produce Mn segregation in GaAsMn magnetic semiconductors. This leads to strong structural changes of the samples [14]. Therefore, a much lower post-growth heat treatment was used to investigate, for the first time, the influence of annealing on the optical and structural properties of MBE grown GaAsBi alloys. In this study the GaAsBi layers were annealed at 200 °C for 3 hours under inert N_2 gas conditions in a tubular furnace.

Amongst all the as-grown (100) and (311)B samples shown in Table 9.1 only samples Ms822 [(100)] and Ms826 [(311)B] show a very weak GaAsBi-related PL signal. It is worth pointing out that the GaAs related peak is only detected in some

samples including Ms822 and Ms826 as shown in Fig. 9.4 (a) and (b), and Fig. 9.5 (a) and (b), respectively.

The effect of the annealing heat treatment is clearly visible when comparing the PL spectra of the as-grown and annealed samples grown on (100) and (311)*B* as shown in Fig. 9.6 and Fig. 9.7, respectively. Fig. 9.6 (a) and Fig. 9.7 (a) show a strong enhancement of the GaAsBi emission from Ms822 and Ms826 samples. In addition, a relatively weak GaAsBi emission emerges in the annealed samples labelled Ms820 [(100)] Ms824 [(311)B] as depicted in Fig. 9.6 (b) and Fig. 9.7 (b), respectively. A second post-growth anneal carried at the same conditions (200 °C for 3 hours) did not affect significantly the PL properties.

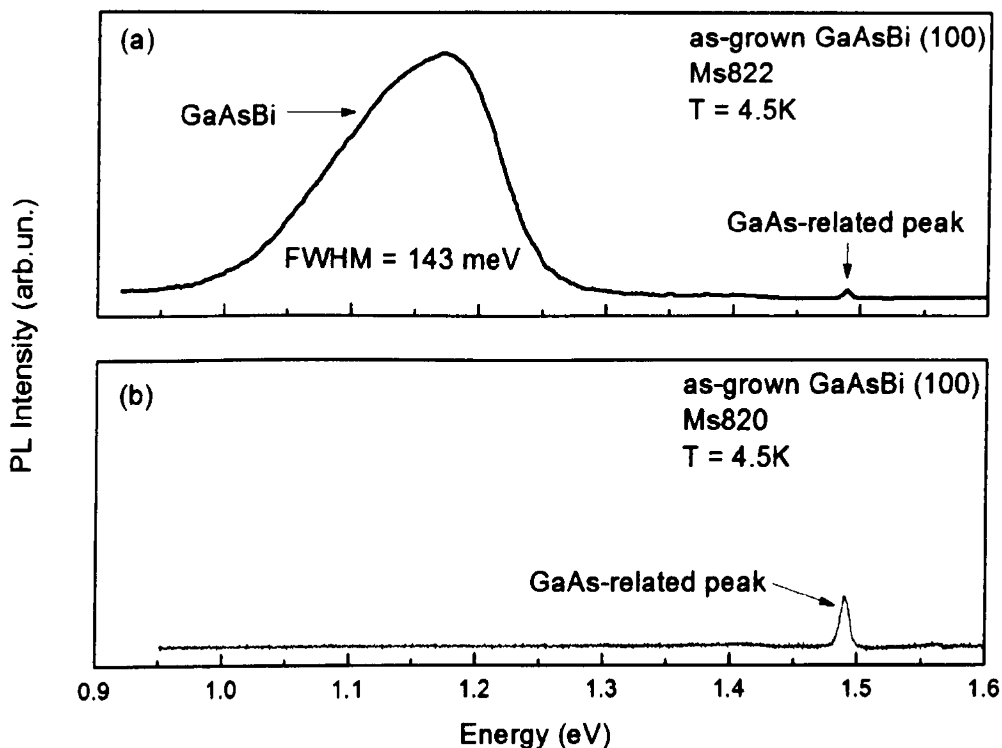

Fig.9. 4 PL spectra of as-grown GaAsBi layers grown on (100) substrates. (a) spectra of sample Ms822 showing both the GaAsBi and GaAs related emissions (b) spectra of sample Ms820 showing only a GaAs related peak.

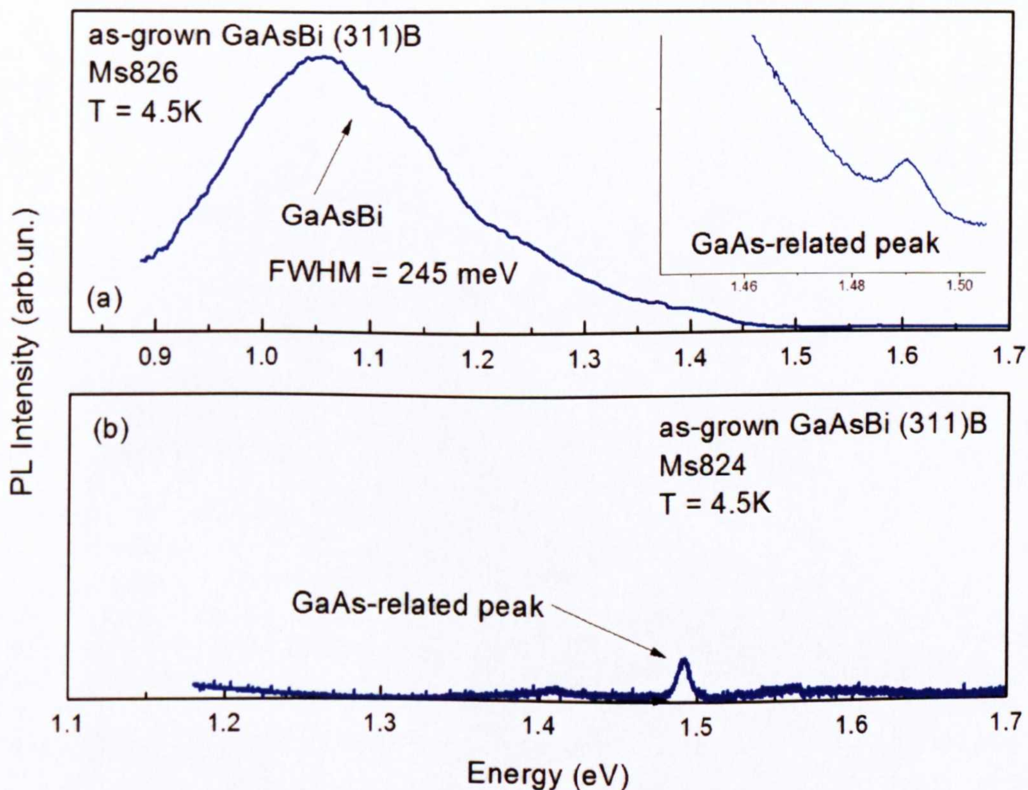

Fig.9. 5 PL spectra of GaAsBi layers grown on (311)B substrates. (a) spectra of Ms826 sample showing both the GaAsBi (main figure) and GaAs (inset) emission peaks. (b) spectra of sample Ms824 showing only the GaAs related peak.

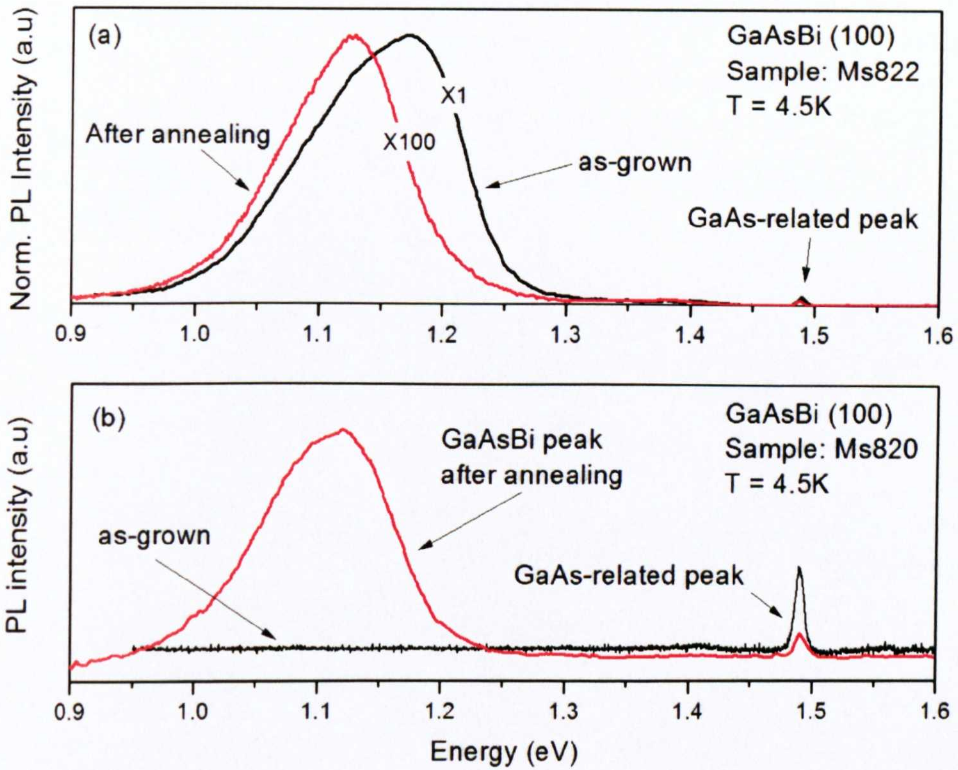

Fig.9. 6 PL spectra of annealed GaAsBi layers grown on (100) substrates. **(a)** spectra showing a significant enhancement in the intensity of the GaAsBi-related peak as compared to that of the as-grown layer. **(b)** spectra of the annealed sample Ms820 showing the appearance of GaAsBi-related peak .

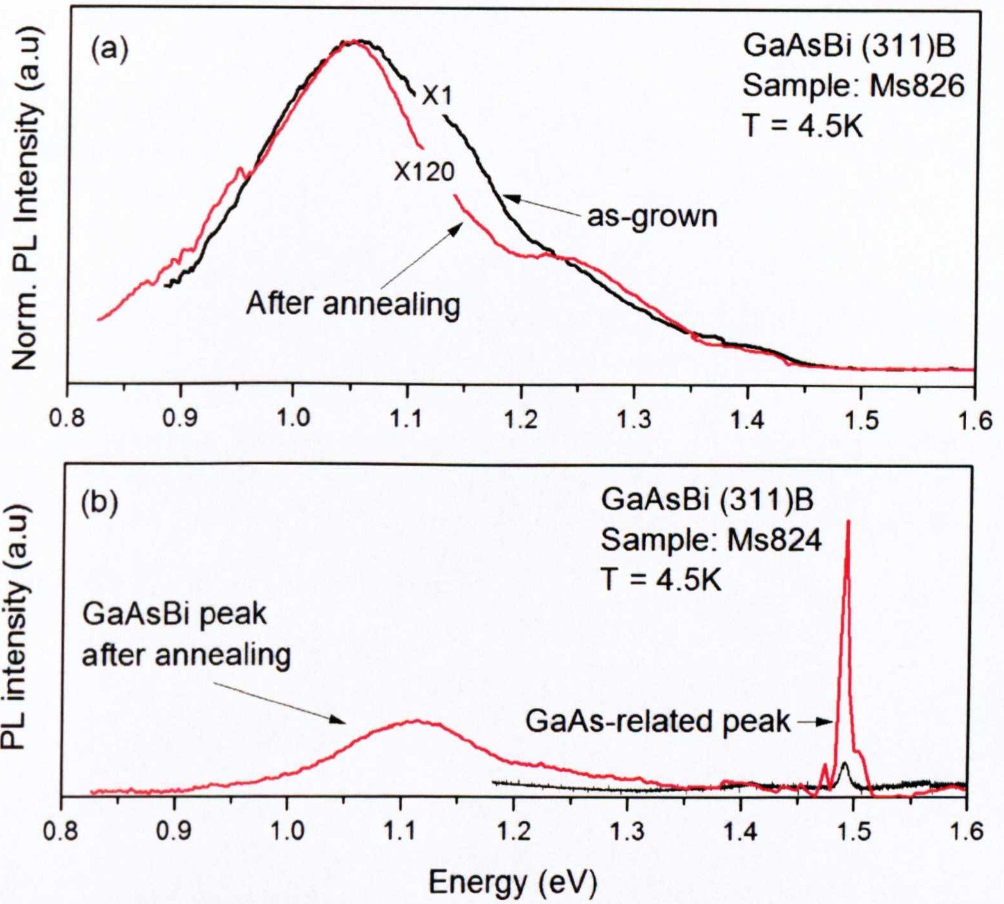

Fig.9. 7 PL spectra of annealed GaAsBi layers grown on (311)B substrates. **(a)** spectra of MS826 showing a strong increase in the intensity of the GaAsBi-related peak after annealing. **(b)** spectra of sample Ms824 showing the appearance of the GaAsBi-related peak after post-growth heat treatment.

9.3 DISCUSSION

9.3.1 HRXRD ANALYSIS

Fig. 9.1 (a) and 9.1(b) show the selected HRXRD curves ($\omega/2\theta$ scans) measured at an x-ray wavelength of λ = 1.54 Å (Cu $K\alpha_1$) from two GaAsBi epilayers grown under near-stoichiometric conditions on (100) and on (311)B GaAs substrates. In addition to the reflections arising from the GaAs substrate, a broad diffraction peak located at lower diffraction angles is also observed in the HRXRD curves. This peak can be attributed to the GaAsBi alloy [1, 2].

Similar patterns were obtained for the rest of the samples. It is interesting to note that, while the intensity of the substrate reflections is comparable for both (100) and (311)B samples as shown in [Figs. 9.1(a) and 9.1(b)], the intensity of the GaAsBi layer reflections is much lower in the case of the (311)B samples. This indicates that the (311)B GaAsBi epilayers are appreciably thinner than the (100) epilayers, which suggests that the actual growth rate is greatly reduced for the (311)B surface. Asymmetric reciprocal space maps (not included in the thesis) revealed that, within experimental accuracy, the degree of plastic relaxation in all our samples is close to zero. Thus, the GaAsBi epilayers were grown coherently on both the (100) and the (311)B GaAs substrates. However, the width of the rocking curves, together with the fact that no interference fringes appeared in any of the HRXRD scans, suggests that a substantial degree of structural disorder and/or a highly inhomogeneous Bi distribution is present in these epilayers.

The Bi concentration x of the $GaBi_xAs_{1-x}$ films were determined from the Bragg's angle of the GaAs and GaAsBi reflections as a function of the relaxed lattice

parameters of GaAs and GaBi (a_{GaAs} and a_{GaBi}) and using equation (9). The Bi content of all our (100) and (311)B $GaBi_xAs_{1-x}$ epilayers, as obtained from the HRXRD scans are plotted in Fig. 9.8. In the figure, x has been plotted as a function of the As flux used to grow the films. The As flux required for near-stoichiometric growth for both the (100) and the (311)B samples is indicated with vertical arrows in the upper axis of the graph. The figure clearly shows that for both growth directions the maximum Bi composition is achieved near stoichiometric conditions, in agreement with previous reports on MBE-grown (100)-oriented GaAsBi [1, 2]. Remarkably, the Bi content incorporated into all the (311)B epilayers, with the exception of the sample grown with the lowest As flux, is appreciably larger than that incorporated into the (100) samples. In the particular case of the (311)B epilayer grown closest to stoichiometric conditions, we observe the largest Bi concentration ($x \sim 0.04$).

Fig. 9.9 (a) shows the zincblende crystal structure in which Bi atom occupies the As site. The orientation dependence of Bi-incorporation in GaAs is not exactly known yet. However, it could be due to the surface bonding geometry of Ga and As atoms in the (100) and (311)B planes. For example, Fig. 9.9 (b) shows the simplified two-dimensional drawing of surface geometry of the (100) and (311)B planes with zincblende lattices. The microscopic surface structure of the (311)B face can be considered to be zigzag periodic bonds chain containing Ga surface atoms with two dangling bonds and As surface atoms with one dangling bond. Whereas, unlike the (311)B, the (100) plane always has As atoms with two surface dangling bonds. So, in terms of surface dangling bonds energy, (311)B is the Ga kink sites that possess high bond energies as compared to (100) directions which favours the easy trapping of

adatoms. [15]. Thus, it could be the reason of larger incorporation of Bi in (311)B than the (100) orientation.

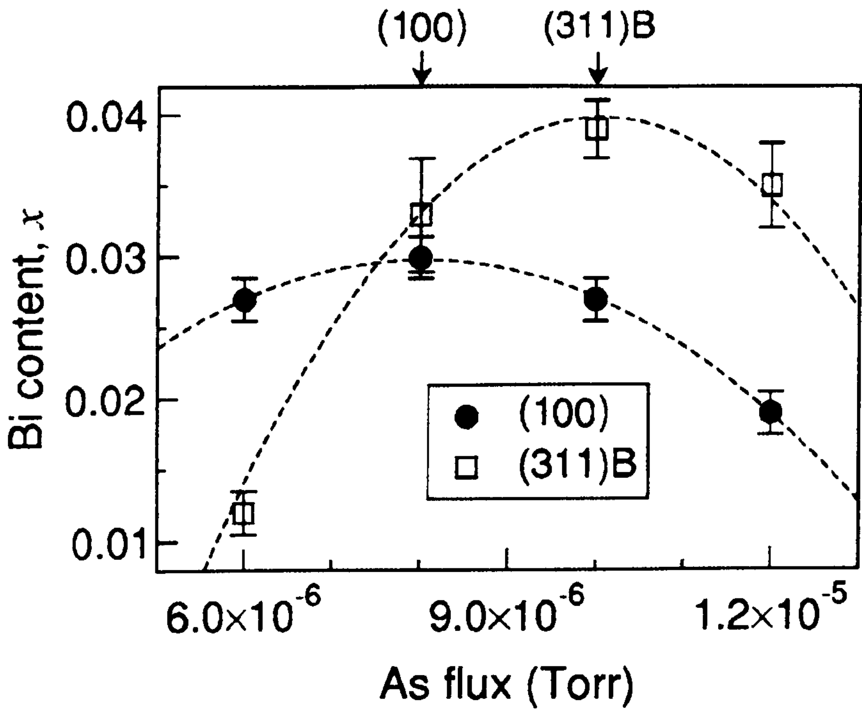

Fig.9. 8 Bi composition x of different (100) and (311)B $GaBi_xAs_{1-x}$ epilayers as a function of the As flux used for the growth. The arrows indicate the As flux for near-stoichiometric growth of (100) and (311)B GaAs.

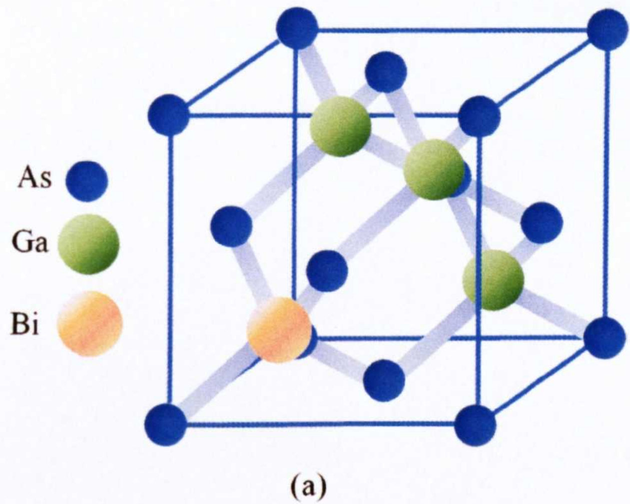

(a)

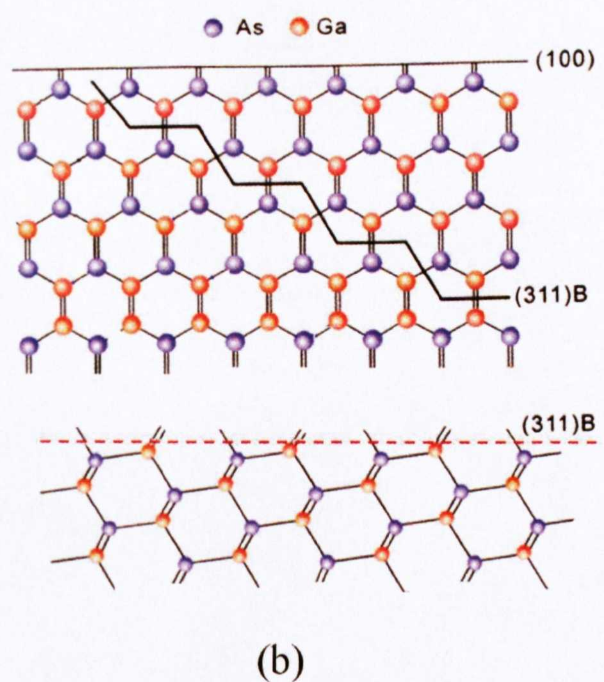

(b)

Fig.9. 9 **(a)** The crystal structure of GaAsBi **(b)** the simplified two-dimensional drawing of surface geometry of the (100) and (311)B planes.

9.3.2 ABSORPTION ANALYSIS

The larger Bi content of the (311)B epilayers gives rise to reduced band-gap energies E_g with respect to the (100) samples. Fig. 9.3 shows the square of the absorption coefficient α^2 around the band-gap edge of the (100) and (311)B samples grown near stoichiometric conditions. These curves were obtained from conventional optical transmission measurements at 300 K. For both samples, α^2 displays an almost linear dependence on photon energy E, which is a consequence of the direct band gap of GaAsBi. By extrapolating the linear part of $\alpha^2(E)$ to zero, E_g is obtained. Note that in Fig. 9.3 the $\alpha^2(E)$ curves have been obtained by taking the nominal thickness of the epilayers (1 μm). However, as discussed above, the HRXRD data indicate that the (311)B epilayer might be thinner.

While an overestimation of the sample thickness would give rise to an underestimation of α^2, this clearly does not affect the E_g values obtained from the $\alpha^2(E)$ curves. We find that for the (311)B epilayer grown near stoichiometric conditions, E_g is around 90 meV lower than for the corresponding (100) sample, as expected from the larger Bi content of the former (see Fig. 9.8; $x \sim 0.04$ versus $x \sim 0.03$).

Some departures of $\alpha^2(E)$ from the linear dependence are associated with the tail of density of states (TDOS) in the GaAsBi layers. The TDOS that appear at low energy are probably due to the defect states located near the conduction and valence bands and the strain caused by lattice mismatch [16].

For comparison purposes, we have plotted in the inset of Fig. 9.3 E_g versus x for the two stoichiometric samples, together with E_g values of MBE-grown $GaBi_xAs_{1-x}$ (x <0.04) reported in Ref. 2. The plot shows that the band gap of the (311)*B* sample is consistent with the data from the (100) epilayers, thus, confirming the higher incorporation of Bi in the (311)*B* surface. Given that the incorporation of N into GaAsN alloys has been shown to decrease when the samples are grown on *B*-type (As-rich) non-(100) substrates [17], the larger Bi content of the (311)*B* GaAsBi epilayers might seem surprising at a first sight. Note, however, that in *B*-surfaces the Ga atoms have two dangling bonds available [18], which suggests that the large Bi atom may be more easily incorporated at double dangling bond sites while the small N atom may prefer the single-dangling bond sites. The differences in morphology, symmetry, and surface reconstruction may also be responsible for the different amounts of Bi/N incorporated into the (100) and non-(100) surfaces.

9.3.3 PL ANALYSIS OF AS-GROWN AND ANNEALED GaAsBi ALLOYS

The near stoichiometric as-grown layers, Ms820 [(100)] and Ms825 [(311)B], have not demonstrated any photoluminescence emissions except a weak GaAs peak in sample Ms820 [see Fig. 9.4 (b)]. This very low photoluminescence efficiency could be due to the presence of structural defects and non-radiative recombination defect levels in the epilayers [19, 20].

In the samples (Ms822 [(100)] and Ms826) [(311)B] grown with the lowest arsenic overpressure, the GaAsBi-related PL bands are observed at 1.17 eV and 1.06 eV with full-width at half-maximum (FWHM) of 141 meV and 243 meV,

respectively. The FWHM for layers grown on (100) is nearly similar to the previously reported values [21]. However, for the case of (311)B layers the FWHM is larger than that of (100). This could be explained by more clustering of Bi in (311)B and carrier localisation at Bi pairs and clusters [22-24].

The material quality was improved dramatically for both (100) and (311)B layers by annealing at 200 °C for 3 hours (stronger PL emission and narrower linewidth). For the (100) samples (Ms822) the photoluminescence intensity increased by a factor of ~100 and the FWHM decreased by ~70 meV. A slight red shift (50 meV) of the PL peak position was observed. This is in contrast to the undesirable blue shift in the luminescence in dilute GaAsN due to the annealing effect [25-29]. In a similar study by Z Chine *et. al* [30] a red shift of 60 meV was also reported for (100) MOCVD GaAsBi layers annealed at 600 °C for 15 mins. However, they did not observe any energy shift for annealing temperatures lower than 600 °C. No tentative explanation was given to the origin of the small red-shift. The low temperature anneal technique used in this work might favour some interstitial Bi atoms to migrate to substitutional sites. This would result in more incorporation of Bi which leads to a lowering of the energy gap.

To contrary the (311)B sample, Ms826, shows no shift in the energy position of the GaAsBi-related PL peak and a comparatively smaller decrease in the PL linewidth (20 meV) after annealing. However, the PL signal intensity increased by a factor ~120 compared to ~100 for the Ms822 (100) sample.

The narrowing of the optical linewidth in both GaAsBi orientations after annealing is an indication of reduced incorporation of defects on these planes. This argument is supported by the TEM results [19] obtained from the (311)B GaAsBi

samples where the annealing treatment reveals a more homogeneous GaAsBi layer (i.e. lower defect density) after the disappearance of the mosaic structure (i.e. less grain boundaries). Although no work is reported in the literature on the annealing effect in MBE-grown GaAsBi materials it is worth mentioning that an improvement of the PL intensity has also been observed in MOCVD GaAsBi alloys heat treated at much higher temperatures (up to ~ 600 ^{o}C) [20] but with a lower order of magnitude than our MBE grown GaAsBi samples. In this context one could argue that using low temperature annealing would result in less thermal dissociation of surface defects and possibly interface defects [20]. These findings provide evidence of the role of the low temperature thermal annealing in reducing the non-radiative recombination centres.

9.4 CONCLUSIONS

(100) and (311)B GaAsBi layers grown by molecular beam epitaxy under various conditions including near stoichiometric conditions have been investigated using optical and structural techniques. The increased Bi contents, leading to reduced band gaps, are achieved when GaAsBi is grown by MBE on (311)B GaAs substrates in comparison to the conventional (100) orientation. The incorporation of Bi into the GaAsBi alloy, as determined by HRXRD is sizably larger in the (311)B epilayers than in (100) epilayers. HRXRD reveals 4% Bi-content in (311)B and 3% in (100) orientation near stoichiometric growth conditions.

The conventional optical transmission results at 300 K confirmed that the bandgap (E_g) of the (311)B epilayer grown near-stochiometric conditions is around 90 meV lower than that corresponding to (100) sample. This measurement provide further evidence that Bi incorporates more on (311)B than on (100) surfaces.

The low temperature post-growth heat treatment of the $GaAs_{1-x}Bi_x$ epitaxial alloys reveals an improvement in the structural and optical properties of these materials. The large increase in PL signal infers the reduction of the structural defects and non-radiative recombination centers.

REFERENCES

[1] K. Oe, Jpn. J. Appl. Phys., Part 1 41, 2801 (2002); M. Yoshimoto, S. Murata, A. Chayahara, Y. Horino, J. Saraie, and K. Oe, Jpn. J. Appl. Phys., Part 2 42, L1235 (2003).

[2] S. Tixier, M. Adamcyk, T. Tiedje, S. Francoeur, A. Mascarenhas, P. Wei, and F. Schiettekatte, Appl. Phys. Lett., 82, 2245 (2003).

[3] S. Francoeur, M. J. Seong, A. Mascarenhas, S. Tixier, M. Adamcyk, and T. Tiedje, Appl. Phys. Lett., 82, 3874 (2003); B. Fluegel, S. Francoeur, A. Mascarenhas, S. Tixier, E. C. Young, and T. Tiedje, Phys. Rev. Lett., 97, 067205 (2006).

[4] K. Alberi, O. D. Dubon, W. Walukiewicz, K. M. Yu, K. Bertulis, and A. Kroktus, Appl. Phys. Lett., 91, 051909 (2007).

[5] K. Bertulis, A. Kroktus, G. Aleksejenko, V. Pacebutas, R. Adomavicius, G. Molis, and S. Marcinkevicius, Appl. Phys. Lett., 88, 201112 (2006).

[6] D. G. Cooke, F. A. Hegmann, E. C. Young, and T. Tiedje, Appl. Phys. Lett., 89, 122103 (2006).

[7] M. Henini, P. J. Rodgers, P. A. Crump, B. L. Gallagher, and G. Hill, Appl. Phys. Lett., 65, 2054 (1994).

[8] A. Polimeni, M. Henini, A. Patanè, L. Eaves, P. C. Main, and G. Hill, Appl. Phys. Lett., 73, 1415 (1998); A. Patanè, A. Levin, A. Polimeni, F. Schindler, P. C. Main, L. Eaves, and M. Henini, ibid. 77, 2979 (2000).

[9] K. Y. Wang, K. W. Edmonds, L. X. Zhao, M. Sawicki, R. P. Campion, B. L. Gallagher, and C. T. Foxon, Phys. Rev. B 72, 115207 (2005).

[10] P.F. Fewster, Cond. Sci. Technol., 8, 11, 1915 (1993).

[11] J. Ibáñez, R. Kudrawiec, J. Misiewicz, M. Schmidbauer, M. Henini, and M. Hopkinson, J. Appl. Phys., 100, 093522 (2006).

[12] L. Vegard, Zeitschrift für Physik, 5, 17 (1921).

[13] J. M. Essick and R. T. Mather, Am. J. Phys, 61, 7 (1993).

[14] C. Michel, S. D. Baranovskii, P. Thomas, W. Heimbrodt, M. T. Elm, P. J. Klar, U. Wurstbauer, M. Reinwald, and W. Wegscheider, J. Appl. Phys., 102, 073712 (2007).

[15] B. Lee, S. S. Bose, M. H. Kim, A. D. Reed, G. E. Stillman, W. I. Wang and L. Vina, J. Cryst. Growth, 96, 27 (1989).

[16] R. Kudrawiec, P. Poloczek, J. Misiewicz, M. Shafi, J.Iba'n˜ez, R. H. Mari, M. Henini, M. Schmidbauer, S. V. Novikov, L. Turyanska, S. I. Molina, D. L. Sales, M. F. Chisholm, Microelectronics Journal, 40, 537 ((2009).

[17] A. Arnoult, F. Gonzalez-Posada, S. Blanc, V. Bardinal, and C. Fontaine, Physica E (Amsterdam), 23, 352 (2004).

[18] B. Lee, S. S. Bose, M. H. Kim, A. D. Reed, G. E. Stillman, W. I. Wang, L. Viña, and P. C. Colter, J. Cryst. Growth 96, 27 (1989).

[19] J.F. Rodrigo, D.L. Sales, M. Shafi, M. Henini, L. Turyanska, S. Novikov, S.I. Molina, Applied Surface Science, 256, 5688 (2010).

[20] I. Moussa, H. Fitouri, Z. Chine, A. Rebey, B. El Jani, Semicond. Sci. Technol. 23, 125034 (2008).

[21] G. Feng, K. Oe, M. Yoshimoto, Jpn. J. Appl. Phys, 32 764. (2007).

[22] S. Francoeur, S. Tixier, E. C. Young, T. Tiedje and A. Mascarenhas, Phys. Rev. B, 77, 085209 (2008).

[23] B. Fluegel, S. Francoeur, A. Mascarenhas, S. Tixier, E. C. Young and T. Tiedje, Phys. Rev. Lett., 97, 067205 (2006).

[24] G. Pettinari, A. Polimeni, M. Capizzi, J. H. Blokland, P. C. M. Christianen, J. C. Maan, E C. Young and T. Tiedje, Appl. Phys. Lett., 92, 262105 (2008).

[25] Q. D. Zhuang1, A. Krier1, and C. R. Stanley2 J. Appl. Phys., 101, 103536 (2007).

[26] P. J. Klar, H. Gruening, J. Koch, S. Schaefer, K. Volz, W. Stolz, W. Heimbrodt, A. M. Kamal Saadi, A. Lindsay, and E. P. O'Reilly, Phys. Rev. B 64, 121203 (2001).

[27] P. J. Klar, H. Gruning, L. Chen, T. Hartmann, D. Golde, M. Gungerich, W. Heimbrodt, J. Koch, K. Volz, B. Kunert, T. Torunski, W. Stolz, A. Polimeni, M. Capizzi, Gh. Dumitras, L. Geelhaar, H. Riechert, IEE Proceedings-Optoelectronics, 150, 28 (2003).

[28] S. G. Spruytte, Christopher W. Coldren, James S. Harris, William Wampler, Peter Krispin and Klaus Ploog, and Michael C. Larson, J. Appl. Phys., 89, 4401 (2001).

[29] L. Grenouillet, C. Bru-Chevallier, G. Guillot, P. Gilet, P. Ballet, P. Duvaut, G. Rolland, and A. Million, J. of Appl. Phys. 91, 5902 (2002).

[30] Z Chine1, H Fitouri, I Zaied, A Rebey and B El Jani, Semicond. Sci. Technol. 25, 065009 (2010).

CHAPTER **10**

SUMMARY AND CONCLUSIONS

This thesis encompasses work on setting up the characterisation techniques, namely deep level transient spectroscopy (DLTS) and Photoluminescence (PL) spectroscopy, which are very powerful for the electrical and optical investigation of semiconductor materials and devices. Secondly it includes the characterisation of dilute nitride (GaAsN) and dilute bismide (GaAsBi) materials. As these material systems are comparatively new, it is very important to aquire knowledge and deeper understanding about their electronic and optical properties in order to develop novel devices based on these materials electronic and optoelectronic applications. In the following, the main results and conclusions are summarised.

10.1 DLTS AND PL TECHNIQUES

Deep Level Transient Spectroscopy (DLTS) is a unique and powerful tool for studying electrically active defects that can affect the charge carrier dynamics in semiconductors. These defect states are considered to be responsible for the lifetime reduction of charge carriers, large leakage currents and non-radiative recombination or generation centres in semiconductor materials. To investigate these defects, DLTS is a widely used technique which is usually implemented on Schottky diodes or p-n junctions. Different characterising parameters such as activation energy, capture

cross-section and defect concentration in the material can be determined very accurately.

A dedicated DLTS system was setup that comprises a capacitance meter, current-voltage meter, pulse generator and cryostat temperature controller. These were interfaced to a computer via GPIB hardware for data acquisition and control. An advanced software program (named Laplace DLTS software provided by our collaborator Prof. L. Dobaczewski, Institute of Physics Polish Academy of Sciences, Warsaw, Poland) has been used. The hardware and software were made compatible and the whole system was successfully used to collect standard DLTS and Laplace DLTS data and to control each equipment remotely.

The software allows the use of two different variants of DLTS technique namely standard DLTS and Laplace DLTS. In the standard DLTS technique capacitance transients are obtained from a Schottky diode or pn junction when a suitable reverse bias pulse with certain repetition rate is applied to the sample and its temperature is slowly varied. The decay time constant of the transient is related to the emission rate of the charge carriers from the defect state. These emission rates as a function of temperature provides the information about the activation energy of the defect state involved. Laplace DLTS, known as a high resolution Laplace transform DLTS (LDLTS), on the other hand is an isothermal technique in which the capacitance transients are digitized and averaged at a fixed temperature. Emission rates of the defect state then are acquired by using a numerical method corresponding to the inverse Laplace transformation.

Photoluminescence (PL) spectroscopy is a powerful technique to characterise the optical behaviour of semiconductor materials. Among the optical techniques used

for the characterization of semiconductors, PL is the most extensively used technique. PL spectroscopy can be used to determine some of the important parameters of semiconductor materials. For example, it can be used to determine the bandgap of semiconductor, to detect the impurity level or defect centres and to provide information about the quality of materials.

A complete PL experimental setup has been successfully developed by implementing a spectrometer (model: iHR 550) equipped with excitation sources (consisting of blue, green and red lasers), a mechanical light chopper and two detectors (a dual channel solid state detector Si/InGaAs and a single channel photomultiplier tube). All the equipments are interfaced to a computer via a serial port RS-232. The PL system utilised a lock in amplifier and a data acquisition module SpectrAcq2 (model from: Horiba Jobin Yvon) for the data collection.

10.2 DEEP LEVELS IN GaAsN (N = 0 % to 1.2%)

Deep levels have been characterized in dilute GaAsN epitaxial layers containing nitrogen concentration in the range 0.2% to 1.2% grown by molecular beam epitaxy (MBE) using standard deep level transient spectroscopy (DLTS) and Laplace DLTS spectroscopy techniques. The DLTS measurements revealed several deep defect levels in the band gap of GaAsN. From the careful comparison of our observed data with the results published in literature, the well-known recombination level EL3 has been observed in every GaAsN layers having different nitrogen compositions. The thermal emission rate signatures of some of the defect states exhibited in GaAsN layers (containing different nitrogen composition) have been found to be related to $(N\text{-}As)_{spl}$ split interstitial, nitrogen-split interstitial defect and

EL6-like interfacial defect levels when compared with reported data published in the literature.

A deep level related to the famous EL2-like was detected in the control sample GaAs (N=0%). The annihilation of the EL2-like electron trap with increasing nitrogen concentration in GaAs has been observed for the first time in GaAsN layers (N = 0 to 1.2%). An amount of N=0.8% was sufficient for the complete elimination of this trap, which was found to be the prevailing centre responsible for the reverse generation current in samples with N≤0.4%. It is also reported in this thesis for the first time that some shallower defect states are present in the GaAsN layers (N= 0.2% - 0.4%) and are tentatively assigned to Si-N complexes. These shallower defect states were annihilated in samples having N>0.4%.

10.3 ANNEALING EFFECTS ON THE DEEP LEVELS IN GaAsN

The thermal annealing behavior of the as-grown Si-doped GaAsN layers containing nitrogen concentration in the range 0.2 – 1.2% have been studied by DLTS and Laplace DLTS techniques. Seven defect states were observed in the as-grown GaAsN (N=0.2%) samples. Heat treatment of these samples at different annealing temperatures annihilated some of the traps. At least four of the traps were eridicated after annealing at 800 °C. Similarly, annealing of the layers containing N = 0.4% have also shown the annihilation of some of the defect states present in the as-grown samples. On the contrary to above described samples, in the layers containing N 0.8 and 1.2% generation and/or annihilation of some of the traps have been observed. In addition to the current-voltage-temperature (I-V-T) studies, DLTS and LDLTS, have shown that EL3-like trap is the main defect state in our as-

grown and annealed samples. This suggests that such electron traps with activation energy of 0.5 – 0.55 eV are the main recombination-generation centers in GaAsN.

The defect state having an activation energy in the range 0.77 – 0.82 eV found in the reference (N = 0%) sample and in the as-grown GaAsN (N = 0.2 - 0.4%) samples was annhihilated in the annealed dilute nitride samples with 0.2% and 0.4% nitrogen composition. The comparison with literature suggests that it might be related to the native arsenic antisite (As_{Ga}) such as EL2 in GaAs. Another defect state having activation energy in the range 0.3 – 0.37 eV is detected in most of the as-grown GaAsN (N = 0.2 – 1.2%) and annealed samples. The thermal emission rates of this trap suggest that it is very close to the GaAs native defect EL6. The nitrogen related defects with activation energy ~ 0.44 eV have also been observed in some as-grown and annealed samples. It was observed that thermal annealing affects the density of the traps. Some new shallow traps with energies ranging from 0.036 to 0.13 eV have also been detected in as-grown and annealed samples which have not been previously reported in the literature.

10.4 HYDROGENATION of GaAsN

Hydrogen-irradiation has been performed on the GaAsN layers containing 0.2% 0.4% and 0.8% nitrogen contents. Standard DLTS and high resolution Laplace DLTS techniques were utilised to determine the effect of the hydrogenation on the deep levels present in the as-grown samples.

Only two defect states at 0.53 eV and 0.82 eV below the conduction band of the GaAsN sample with N= 0.2% have been found electrically active after hydrogen irradiation of the as-grown samples in which DLTS investigation revealed seven

deep levels. This finding confirms that hydrogen irradiation of GaAsN (N=0.2%) layers, reduces the defects states. The hydrogenated GaAsN samples containing 0.4% nitrogen show that three out of four electron traps detected in the as-grown layers at 0.045 eV, 0.37 eV, 0.53 eVand 0.82 eV below the conduction band disappeared and only one electron level at 0.73 eV has been detected.

The investigation of the defect states in the as-grown GaAsN layer having 0.8% nitrogen reveals the existence of four defects states. The hydrogen irradiation of these layers passivates some of the traps and reduces the concentration of the others. It also creats the new defects which could be related to hydrogen-complexes.

10.5 OPTICAL AND STRUCTURAL CHARACTERISATION OF GaAsBi ALLOYS

GaAsBi layers have been grown by MBE with constant Bi flux (1.2×10^{-7} Torr) and variable arsenic flux (1.2×10^{-5} - 6×10^{-6} Torr) to achieve GaAsBi layers under nominally stoichiometric conditions. The increased Bi contents, leading to reduced band gaps, are achieved when GaAsBi is grown on (311)B GaAs substrates in comparison to the conventional (100) orientation. The incorporation of Bi into the GaAsBi alloy, as determined by HRXRD, is sizably larger in the (311)B epilayers than in (100) epilayers. HRXRD reveals 4% Bi-contents in (311)B and 0.3% in (100) orientation for samples grown near stoichiometric conditions.

From the conventional optical transmission measurements at 300 K it was confirmed that for the (311)B epilayer grown near stoichiometric conditions E_g is around 90 meV lower than that corresponding to (100) sample grown under similar conditions.

The low temperature post-growth annealing of $GaAs_{1-x}Bi_x$ epitaxial layers deposited by MBE on (100) and (311)-GaAs substrates results in the improvement of their structural and optical properties. A large increase in PL signal infers the elimination of the structural defects and non-radiative recombination centers.

10.6 FUTURE WORK

Due to the limitation of the DLTS technique, further work must still be done to probe the exact nature of the defect states exhibited in dilute nitride GaAs materials by using some other useful techniques, such as photoluminescence (PL), electron paramagnetic resonance spectroscopy (EPRS) and secondary ion mass spectroscopy (SIMS). It would also be interesting and useful to investigate the GaAsN epilayers grown on high index planes.

Since the bismides are also new alloys like GaAs-nitrides, many aspects of their electronic and physical structure remain unknown. For example, many of the growth did not show the strong luminescence from GaAsBi layers, it requires further electrical and optical characterisation of these materials. Raman spectroscopy, transmission electron microscopy (TEM) along with XRD measurements could be very useful to get information for better understanding of these structures. The study of the defects in GaAsBi layers would also be of interest, as it can provide feedback information to optimise the growth conditions in order to improve the quality of the material and understand the effect of deep states on the performance of future devices based on these material systems.